Investigating Natural Product Glycosides as Allosteric Modulators of P2X Purinergic Receptors

Elizabeth Jayne Allum

A thesis presented for the degree of Doctor of Philosophy at the University of East Anglia, Norwich, UK

School of Pharmacy

January 2023

Abstract

Natural products have been used traditionally for thousands of years to treat a wide variety of ailments. The active compounds in *Panax ginseng,* the ginsenosides, have been shown to have numerous beneficial effects in conditions such as cancer and inflammation. Ginsenoside CK, a metabolite of the ginsenosides, has been shown to potentiate responses by the P2X7 and P2X4 purinergic ion channels. P2X ion channels are widespread throughout the body, although their potential as a novel drug target is only beginning to be explored.

Screening novel compounds at ion channels can be a time-consuming affair – to overcome this, a high-throughput screening assay was used to assess activity of natural product glycosides at multiple P2X receptors. Using this assay, activity of ginsenosides was confirmed at P2X1, P2X2, and P2X3 in addition to P2X4 and P2X7. The ginsenosides were found to potentiate responses to ATP at all P2X receptors tested, although to varying degrees, suggesting the potential for development of specific modulators for each receptor.

Next, the proposed binding pocket for the ginsenosides was explored in the P2X2 and P2X4 receptors and the degree of conservation between receptor subtypes considered. Whilst some residues, namely D318 (hP2X7 numbering) were conserved, multiple differences in proposed interactions with ginsenoside CK were uncovered. Residues around this region of the central vestibule were found to be key in determining receptor sensitivity to ATP, with mutations of residues D318 and L320 leading to enhanced sensitivity to ATP.

One particular residue, F322 in hP2X7, was found to have a key role in sensitivity of the receptor to ATP and modulation of dye uptake responses by ginsenosides. Potentiation by ginsenoside CK was retained in ion-based assays but reduced in dye uptake assays, highlighting the importance of using multiple assays to confirm findings.

Contents

List of Figures

Chapter 1

Chapter 2

Chapter 3

Chapter 4

Chapter 5

Appendices

List of Tables

Chapter 1

Chapter 3

Chapter 4

Chapter 5

Acknowledgements

They say it takes a village to raise a child, and I would certainly say the same for completing a PhD: I would not have been able to do this without the support of many, many others, for all of whom I am incredibly grateful.

Firstly, I would like to thank the BBSRC, the NRP DTP, and UEA for supporting my doctoral research. Starting this journey as a pharmacist was unusual. It has been a big learning curve to go from the pharmacy to the laboratory, but I am honoured to have been given this opportunity to further myself as a scientist. My academic journey began with UEA, and it feels fitting to have finished it (for now!) at the home of the wonderful.

Of course, I was constantly supported throughout my research by my peers in the lab: to Stefan, Lučka, Jack, and Hanna, thank you all for being my friends. Working in a lab can be isolating at times, but I never felt alone with you there to talk about everything and nothing with. I wish you all the best of successes in your future endeavours; I will be rooting for you all! And to all my friends outside the lab: I could not wish for a better group of Chumleys.

I feel so incredibly lucky to have had the supervision of Dr Leanne Stokes for not only the last almost four and a half years, but also during my MPharm research project: thank you for inspiring me to do this crazy thing all those years ago, and for believing I was capable the entire time, even when I did not. I truly believe that your supervisor can make or break your PhD experience, and I can honestly say I would not have been here looking at my completed thesis if I hadn't had your consistent support, guidance, and friendship. Thank you for replying to my endless messages and offering me reassurance when I needed it most. To you, Ian, Amber, and Fraser: I wish you all nothing but joy and happiness.

Now to my family: I could not have asked for a better group of cheerleaders than you all. Being away from home has not been easy, but I have felt your support from all the way down the A140. Thank you for always telling me how proud you are; it means more than you know. My silly orange cat Fearghas, who sadly did not make it to see the end of my journey; you still continue to bring me joy whenever I think of you. You are so very loved and missed. And my beautiful Mabel, whose paws have followed me (quite literally) every step of the way. Thank you both for being my sanctuary.

Finally, to the two most important people in my life. You both know how hard this journey has been for me, but you have been there every step of the way. To my mum, who has an unwavering belief in me in everything I do. Thank you for everything you have done for me. Even now, you're still holding my hand and guiding me as I make my way through life. And to my beloved Rob; what a ride this has been. Thank you for letting me make these mad decisions and supporting me in whatever I choose to do next. For always making me feel loved no matter what, for listening to me explain my work in terrible detail, and for getting me through these last few months. There is truly no one else I would rather do this life with than you. You make me believe I can do anything.

Watch me.
I will go to my own Sun.
And if I am burned by its fire,
I will fly on scorched wings.
- *Segovia Amil*

Chapter 1 – Introduction

1.1 Purinergic Signalling

The role of adenine-based compounds in the regulation of physiological processes was first described early in the 20th century by Drury and Szent-Györgi, whereby adenosine and what was believed to be 'adenylic acid' (also known as adenosine monophosphate or AMP) were able to modulate cardiovascular function in a range of animal studies (Drury and Szent-Györgyi, 1929). It would be some time before the term 'purinergic' was coined in 1971 by the pioneer of purinergic research, Geoffrey Burnstock, following discovery of non-adrenergic, non-cholinergic (NANC) transmission in colonic smooth muscle of the guinea pig earlier in the 1960s (Burnstock, 1971) (Burnstock et al., 1964, Burnstock et al., 1966). Before long, the characterisation of P1 (adenosine-mediated) and P2 (nucleoside di- and tri-phosphate-mediated) purinergic receptors was suggested based on their differential pharmacology (see http://garfield.library.upenn.edu/classics1990/A1990DZ17600001.pdf) (Hoult, 1979). The adenosine receptors were the first to be classified, with subtypes A_1, A_{2A}, A_{2B}, and A_3 outlined as the appropriate nomenclature for these receptors in 2001 (Fredholm et al., 2001). In due course, the first P2 purinergic receptors were cloned in 1993: these were the P2Y1 receptor found in the chick brain and the P2Y2 receptor found in mouse neuroblastomas (Webb et al., 1993, Lustig et al., 1993). Soon after in 1994, the first P2X receptors, P2X1 and P2X2, were cloned by Valera *et al* and Brake *et al* respectively (Valera et al., 1994, Brake et al., 1994, Kaczmarek-Hájek et al., 2012). Ultimately, Abbracchio and Burnstock suggested the contemporary classification of purinergic receptors in 1994, leading us to what is used today: P2Y receptors are G-protein coupled receptors activated by an array of purinergic ligands, and P2X receptors are ligand-gated ion channels activated primarily by ATP (Abbracchio and Burnstock, 1994). At present, there are four adenosine receptors (A_1, A_{2A}, A_{2B}, and A_3), eight P2Y receptors (P2Y1, P2Y2, P2Y4, P2Y6, P2Y11, P2Y12, P2Y13, and P2Y14), and seven P2X receptors (P2X1, P2X2, P2X3, P2X4, P2X5, P2X6, and P2X7) (Burnstock, 2007) **(Figure 1.1**).

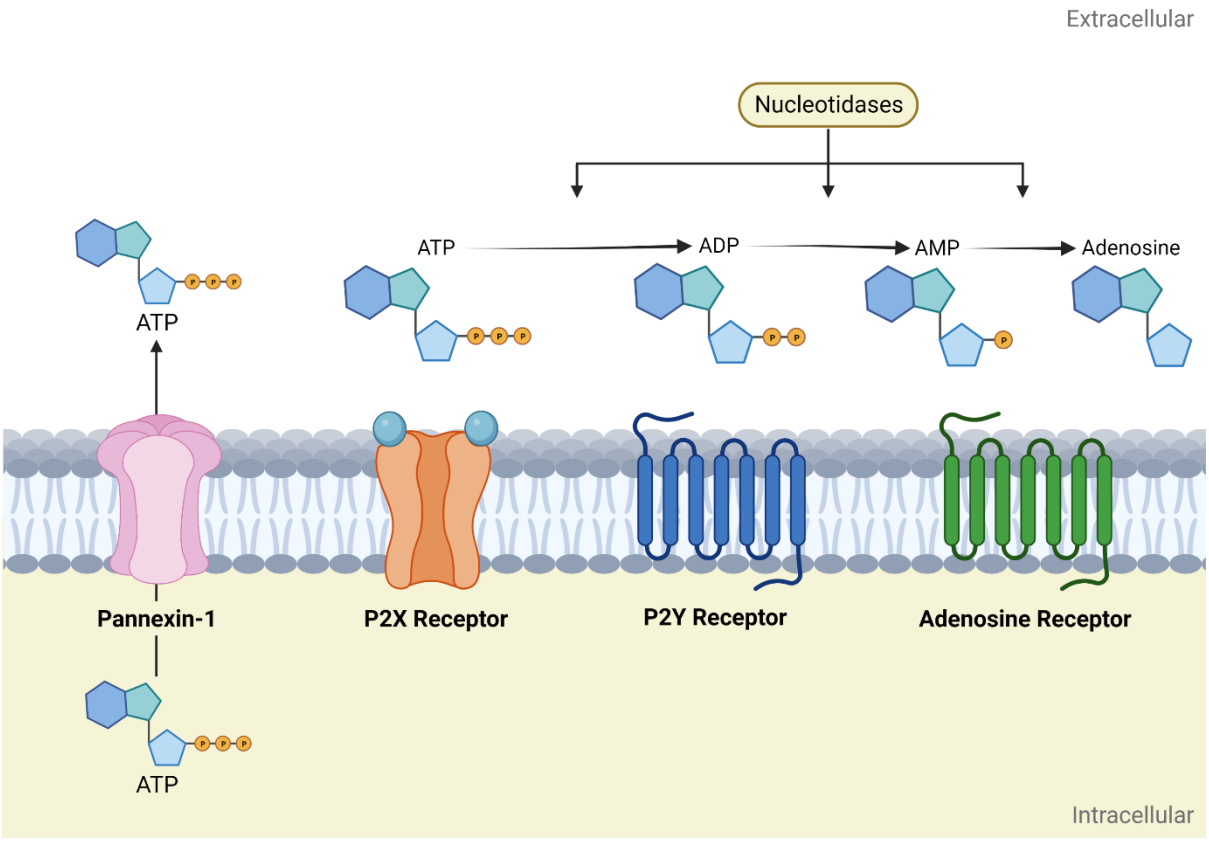

Figure 1.1 – Diagram showing the membrane proteins involved in interactions with ATP. Adapted from Velasquez *et al* (Velasquez and Eugenin, 2014).

In addition to purinergic receptors, several enzymes, termed ectonucleotidases, contribute to purinergic signalling by regulating concentrations of nucleoside phosphate compounds (Zimmermann et al., 2012). These cell-surface enzymes are responsible for the hydrolysis of nucleoside tri-, di-, and mono-phosphates into nucleoside diphosphates, nucleoside monophosphates, and nucleosides respectively (Zimmermann et al., 2012). With regards to adenosine triphosphate (ATP), adenosine diphosphate (ADP), AMP, and adenosine, the availability of ligands for P2 and adenosine receptors is either increased or decreased by hydrolysis of these compounds by ectonucleotidases (Zimmermann et al., 2012). However, these enzymes are also capable of hydrolysing other nucleoside-based ligands, such as uridine triphosphate (UTP), guanidine diphosphate (GDP), and cytidine triphosphate (CTP), amongst others (Zimmermann et al., 2012). There are four main classes of ectonucleotidases; these are: ectonucleoside triphosphate diphosphohydrolases (E-NTPDases), ecto-5'-nucleotidase (eN), ectonucleotide pyrophosphatase/phosphodiesterases (E-NPPs), and alkaline phosphatases (APs) (**Table 1.1**).

Table 1.1 – Summary of ectonucleotidases involved in hydrolysis of nucleoside phosphates.
Adapted from Zimmermann *et al*, 2012.

Family Name	Protein Name	Other names	Ligands
Ectonucleoside Triphosphate Diphosphohydrolases	**NTPDase1**	CD39, ATPDase, ecto-apyrase	NTP, NDP
	NTPDase2	CD39L1, ecto-ATPase	NTP (NDP)
	NTPDase3	CCD39L3, HB6	NTP, NDP
	NTPDase4	UDPase, hlALP70	NTP, NDP, ADP, some ATP
	NTPDase5	CD39L4, PCPH, ER UDPase	UDP, GDP, CDP, ADP, some ATP
	NTPDase6	CD39L2	GDP, IDP, UDP, CDP
	NTPDase7	LALP1	NTP (NDP)
	NTPDase8	hATPDase	NMP
Ecto-5'-nucleotidase	**eN**	CD73	NMP
Ectonucleotide Pyrophosphatase / Phosphodiesterases	**NPP1**	PC-1, NPPγ, PDNP1	NTP, NDP, dinucleoside polyphosphates, NAD^+
	NPP2	Autotaxin, PD-1α, NPPα	NTP, NDP, dinucleoside polyphosphates, NAD^+, ADP-ribose, UDP-glucose
	NPP3	CD203c, NPPβ	NTP, NDP, dinucleoside polyphosphates, NAD^+, lysophosphatidylcholine, sphingosylphosphorylcholine
	NPP4	-	
	NPP5	-	
	NPP6	Choline-specific glycerophosphodiester phosphodiesterase	
	NPP7	Alkaline sphingomyelinase	
Alkaline Phosphatases	**TNAP**	Tissue nonspecific AP	NTP, NDP, NMP, monoesters of phosphoric acid
	PLAP	Placental AP	
	GCAP	Germ cell ATP	
	IAP	Intestinal AP	

1.2 P2X receptors

The P2X family of purinergic receptors are trimeric ion channels which can be either heteromeric (made up of different subunits) or homomeric (made up of three identical subunits) (Kaczmarek-Hájek et al., 2012). All seven individual P2X subunits (termed P2X1 through P2X7) share similar characteristics, in that they have intracellular N and C termini with a large extracellular domain, although the length of the C terminus varies greatly between receptor subtypes. In human P2X4, the smallest of the P2X receptor subtypes, the C terminal 'tail' is only 88 amino acids in length, whereas for the largest P2X receptor, human P2X7, this tail extends to 240 amino acids (Illes et al., 2021). Most P2X receptors are able to exist as homomeric receptors, with the exception of P2X6 which only forms heteromeric structures, preferentially with either P2X4 or P2X2 subunits to form a P2X4/6 or P2X2/6 receptor respectively (Kaczmarek-Hájek et al., 2012).

The binding site of the preferred endogenous ligand, ATP, is highly conserved between the P2X family, existing at the interface between two subunits as confirmed by x-ray crystallography and, more recently, the cryogenic electron microscopy (cryo-EM) structure of rat P2X7 which offers visualisation of the lengthy C terminus not seen before (see **Figure 1.2**) (Hattori and Gouaux, 2012, McCarthy et al., 2019).

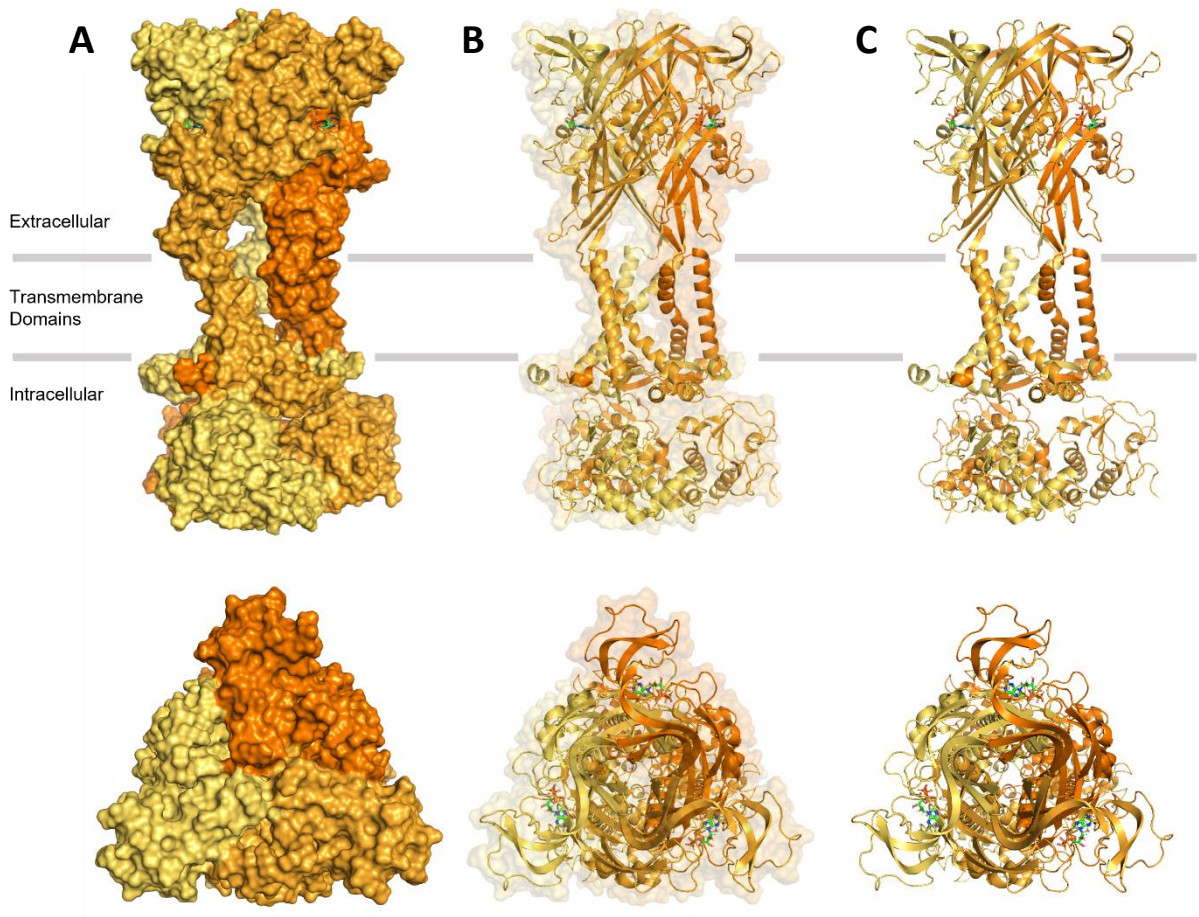

Figure 1.2 – Cryo-EM structures of rat P2X7 in the ATP-bound open state. ATP is shown in green at the interface between subunits, with individual rP2X7 subunits coloured in various shades of orange to highlight the trimeric structure. Grey lines represent the lipid bilayer of the cell membrane; positions are approximate to highlight extracellular, transmembrane, and intracellular domains. **A:** Surface representation of the complete rat P2X7 receptor (above) and from the top of the receptor (below) **B:** Ribbon structure overlayed on top of the surface representation of the complete rat P2X7 receptor (above) and from the top of the receptor (below). **C:** Ribbon structure of the complete rat P2X7 receptor (above) and from the top of the receptor (below). Images generated using PyMol (PDB: 6U9W), generated by McCarthy et al, 2019.

Despite this conserved orthosteric ligand site, the pharmacology of each receptor varies greatly. Some receptors, such as P2X1, P2X3, and P2X4 require concentrations of ATP in the hundred nanomolar to low micromolar range, whereas P2X7 often requires concentrations of ATP in the hundred micromolar range to activate (Gever et al., 2006, Syed and Kennedy, 2012). Moreover, each receptor subtype has varying desensitisation kinetics: they can be grouped into those that desensitise quickly (P2X1 and P2X3) and those that desensitise more slowly (P2X2, P2X4, P2X5, and P2X7) (Koshimizu et al., 1999, Jarvis and Khakh, 2009). Desensitisation kinetics for P2X6 are poorly understood due to poor expression, but it is believed to be slowly desensitising (Illes et al., 2021). One of the most unique

characteristics surrounding purinergic ion channels is that some have the ability to form a large, non-specific pore in the cell membrane (Kaczmarek-Hájek et al., 2012). The most well-known receptor for this unique characteristic is P2X7, although there has been evidence that P2X2 and P2X4 are also capable of taking up membrane impermeant dyes via a large pore mechanism (Khakh et al., 1999a). As a result of this, assays utilising measurement of fluorescent dye uptake such as YO-PRO-1 and TO-PRO-3 are often used to assess activity of P2X receptors (Wei et al., 2016, Barczyk et al., 2021). Due to the fact P2X receptors are ion channels, assays measuring changes in intracellular ion concentrations, such as FURA-2AM, and changes in membrane currents, such as patch-clamp electrophysiology, are often used experimentally (He et al., 2003, Bibic et al., 2019, Jiang and Roger, 2020).

1.2.1 P2X1

P2X1 was the first P2X receptor to be cloned (Valera et al., 1994, Abbracchio and Burnstock, 1994), and is one of the smaller P2X receptor structures, with a protein length of 399 amino acids (Illes et al., 2021). It is quickly desensitising, with the rat P2X1 receptor displaying an average time constant of desensitisation of approximately 60 ms (Parker, 1998). P2X1 is also quick to activate (within a few milliseconds), but once desensitised can take in excess of 10 minutes to recover reproducible responses (North, 2002). The P2X1 receptor is permeable to cations, with a preference for Ca^{2+} and little discrimination between Na^{+} and K^{+} (Evans et al., 1996). It remains relatively impermeable to larger cations Tris and *N*-methyl-D-glucamine (NMDG) (Evans et al., 1996), suggesting that the receptor is not capable of the uptake of larger compounds, such as the dyes YO-PRO-1 iodide and ethidium bromide.

P2X1 was first cloned from the rat vas deferens in 1994 (Valera et al., 1994), and since has been found in a number of systems within the body. Predominantly, P2X1 is present in smooth muscle of tissues such as the bladder, small intestine, and vasculature (Longhurst et al., 1996, Vulchanova et al., 1996, Chan et al., 1998, Bo et al., 2003b) but also has a significant presence on platelets (Hourani, 1996, MacKenzie et al., 1996, Savi et al., 1997, Vial et al., 1997, Scase et al., 1998) and promyelocytes (Buell et al., 1996b), but not on fully differentiated leukocytes (Clifford et al., 1998). In addition to this, expression of P2X1 receptors have also been detected in the central and peripheral nervous systems, particularly in myenteric neurons, cerebellum, and the dorsal horn (Zhou and Galligan, 1996, Loesch and Burnstock, 1998, Zhong et al., 1998).

Given the prevalence of this receptor in the cardiovascular system, it is not wholly unexpected that there may be a role for this receptor in certain diseases such as thrombosis and cardiovascular disorders. Transgenic mice overexpressing the human P2X1 receptor had worse outcomes compared to wild-type mice in thromboembolic models, and aggregation of platelets to low concentrations of collagen (<4 µg/mL) was increased in transgenic mice compared to their wild-type counterparts (Oury et al., 2003). Conversely, mortality rates in P2X1 KO (knockout) mice were improved in models of thromboembolism compared to wild-type mice and thrombi formed were smaller in the KO mice (Hechler et al., 2003) Mouse models of colitis showed that P2X1 KO mice suffered from increased intestinal blood loss due to reduced platelet aggregation (Wéra et al., 2020). Interestingly, however, these KO mice also showed a prothrombotic phenotype in response to laser-induced thrombus formation in non-intestinal arteries despite reduced platelet aggregation, suggesting that the thrombotic profile may vary between inflamed and non-inflamed regions (Wéra et al., 2020). These data suggest that P2X1 activation is largely related to a prothrombotic phenotype, and therefore

antagonism or downregulation of the receptor could improve outcomes in thromboembolic disease. Indeed, the P2X1 antagonist NF449 reduced aggregation of platelets induced by collagen (Hechler et al., 2005), establishing a therapeutic basis for modulators of P2X1 receptors in prothrombotic conditions. However, it would be wise to consider the conflicting impact of P2X1 antagonists in inflammatory conditions as outcomes may be worsened due to adverse bleeding and increased thrombosis formation (Wéra et al., 2020).

With regards to the cardiovascular system, the P2X1 receptor has been implicated in vasoconstriction in the renal vasculature (van der Giet et al., 1999), with P2X1 KO mice displaying reduced vasoconstriction compared to wild type (Inscho et al., 2003) and P2X1 being implicated as a key mediator in the autoregulation of blood flow in the kidneys (Inscho et al., 2004, Osmond and Inscho, 2010). RT-PCR of pial tissue from rats showed the presence of RNA transcripts for P2X1, amongst other purinergic receptors, suggesting expression of this receptor in the cerebral vasculature also (Lewis et al., 2000). Deletion of CD39 (an ectonucleotidase responsible for conversion of ATP to ADP and then AMP, see **Figure 1.2**) resulted in increased expression of P2X1 receptors in mice, and in addition, treatment with the P2X1 receptor antagonist NF279 resulted in decreases in pulmonary arterial pressure, particularly in hypoxic states (Visovatti et al., 2016). Further to this, P2X1 KO mice have also shown increases in blood pressure (Bennetts et al., 2022), in line with the role of P2X1 activation in vasoconstriction. Due to the array of other treatments available for hypertension, and the implications on thrombotic profiles, P2X1 antagonists have not received much attention with regards to their potential role in hypertension.

Another key area of research surrounding the P2X1 receptor is in fertility, particularly with respect to males; the first P2X1 receptors were cloned from the vas deferens of rats. Fertility in male P2X1 KO mice was drastically reduced despite normal reproductive behaviour (Mulryan et al., 2000). Sperm function was not affected, rather there was a reduction in the sperm present in the ejaculate thought to be directly related to the degree of contraction of the vas deferens. P2X1 receptors are similarly present in other types of smooth muscle, such as testicular smooth muscle (Banks et al., 2006). Female KO mice were still able to produce viable pregnancies with wild-type and partial KO mice (Mulryan et al., 2000). The distribution of P2X1 receptors in the male reproductive tract is not limited to rodents; ATP has been shown to act as a co-transmitter alongside noradrenaline to contract the human vas deferens and is thought to act via the P2X1 receptor (Banks et al., 2006). Antagonism or downregulation of the P2X1 receptor could offer a novel form of non-hormonal contraception with perhaps limited side effects, given that male KO mice displayed normal sexual behaviour and ability (Mulryan et al., 2000) and sperm from P2X1 and α1A double KO mice appeared normal and motile on

examination (White et al., 2013). Likewise, potentiation of P2X1 could offer a novel infertility treatment. Despite the emerging role of P2X1 in male fertility , the role of this receptor in the female reproductive tract is less well understood, although it has been suggested that P2X1, alongside other purinergic receptors, such as P2X2/3, P2Y2, and P2Y4, may mediate uterine contractions in pregnant humans (Burnstock, 2014).

1.2.2 P2X2

Unlike P2X1 , P2X2 is a slowly desensitising ion channel (Koshimizu et al., 1999), with little decay in the response to a sustained application of ATP (Lynch et al., 1999). In rats, splice variants of P2X2 affect this desensitisation rate considerably, with P2X2b (a splice variant lacking residues 370-438 in the C terminus) displaying far quicker desensitisation rates than the complete P2X2 receptor, P2X2a (Brändle et al., 1997). However, this effect is not seen in the human versions of P2X2 , highlighting the importance of species differences despite largely conserved sequences between the two species (Lynch et al., 1999). In terms of size, the P2X2 protein is the second largest at 471 amino acids in length, with a C terminal length of 113 amino acids (Illes et al., 2021). P2X2 is permeable to cations, but has a reduced permeability for Ca^{2+} compared to P2X1 (Evans et al., 1996). Rat P2X2 has also been shown to be permeable to larger cations such as $NMDG^{+}$ and YO-PRO-1^{+} following sustained application of ATP (Virginio et al., 1999). This property has been shown to vary between transiently transfected and stably transfected cell lines, with approximately 40 % of transiently transfected cells able to display uptake of larger cations and only 20 % of stably transfected cells (Virginio et al., 1999, North, 2002).

First cloned from rat pheochromocytoma cells (PC12) (Brake et al., 1994), P2X2 has been shown to be expressed in a number of tissues, particularly in the nervous system (Nörenberg and Illes, 2000). Here, immunocytochemistry has shown presence of P2X2 receptors in the rat anterior pituitary, olfactory bulb, substantia nigra, and locus coeruleus, amongst other regions (Vulchanova et al., 1996). Staining has also demonstrated expression in both the rat and guinea pig cerebellum (Kanjhan et al., 1996). Polymerase chain reaction in-situ hybridisation (PCR-ISH), a technique which involves amplifying nucleic acid concentrations before detecting distribution within tissues, demonstrated expression of the P2X2 receptor beyond the central and peripheral nervous systems in the rat retina, along with expression on neurons that innervate the rat eye (Greenwood et al., 1997). In the ear, ATP is thought to play a protective role, and this is thought to be mediated by P2X2 receptors that have shown to be present in multiple components of the ear, including spiral ganglion neurons, hair cells, and the endolymphatic compartment (Housley et al., 1999).

In the guinea pig cochlea, ATP has been detected in both the perilymph and endolymph, with levels increasing in response to noise exposure (Muñoz et al., 1995, Muñoz et al., 2001, Lee et al., 2001). This is thought to reduce endocochlear potential via activation of P2X receptors, likely P2X2, resulting in mobilisation of K^{+} ions (Housley et al., 2002). Further to this, noise exposure has been shown to increase not only the levels of ATP but the expression of P2X2 receptors in spiral ganglion neurons and outer hair cell stereocilia in the rat cochlea (Wang et al., 2003). This effect is reduced in older animals,

suggesting that this adaptive response may decline over time (Telang et al., 2010). These data suggest that the P2X2 receptor is involved in protecting the ear against loud noise exposure and could highlight an area of interest for future therapeutics. Indeed, several inherited mutations in P2X2 have been identified in patients with premature hearing loss (Yan et al., 2013, Faletra et al., 2014, Moteki et al., 2015). The first, where valine 60 (V60) is instead a leucine, appeared in two Asian families that had fully penetrant hearing loss (Yan et al., 2013). This mutation alters the characteristics of the P2X2 receptor, leading to reduced inward currents and reduced uptake of the dye FM1-43 in response to ATP when expressed *in vitro* in HEK-293 cells (Yan et al., 2013). In agreement with this, P2X2 KO mice also displayed premature hearing loss compared to wild type counterparts, and hearing loss in response to noise exposure was also exaggerated in these KO mice (Yan et al., 2013). A second inherited mutation, glycine 353 to arginine, was located in a European family (Faletra et al., 2014). This mutation led to a similar phenotype, with premature hearing loss occurring from approximately the age of 20 onwards (Faletra et al., 2014). Soon after, a third mutation was discovered to have an impact on hearing in patients with MELAS (mitochondrial myopathy, encephalopathy, lactic acidosis, and stroke-like episodes) (Moteki et al., 2015). This mutation (asparagine 201 to tyrosine) to the P2X2 receptor was found to cause sensorineural hearing loss, whereas MELAS patients without this mutation to the P2X2 receptor were able to hear normally (Moteki et al., 2015). Further to hearing loss, assessment of P2X2 KO mice has shown that balance was significantly altered compared to wild type mice, and that this was due to vestibular function rather than impairments to vision (Takimoto et al., 2018). Taken together, these data suggest that modulation of P2X2 receptors, particularly by enhancing their function, could offer novel treatments for conditions such as age-related hearing loss and Meniere's disease.

The potential for P2X2 modulation in neuronal systems is not fully understood, given the complexities and nuanced regulation in these systems. One particular study investigated the potential anti-depressive effects of ATP in mouse models (Cao et al., 2013). In a model of chronic social defeat, whereby mice are subjected to repeated interactions with an aggressor mouse and then their movements in the presence and absence of an alternate aggressor mouse are analysed, ATP levels were found to be decreased in susceptible mice (i.e., those that were susceptible in this model of chronic stress); this was also the case in mice subjected to a forced swim test (Cao et al., 2013). Administration of ATP was able to reverse the effects of depressive models in mice faster than treatment with the known antidepressant imipramine, suggesting a rapid anti-depressive effect for ATP (Cao et al., 2013). Moreover, levels of ATP in the medial prefrontal cortex have been shown to be directly related to depressive behaviour in mice (Lin et al., 2022). However, a recent study into the impact of P2X2 receptors on depressive behaviour in mice has shown that P2X2 can contribute to

increased sensitivity to depressive behaviours in mouse models, whereas KO of P2X2 receptors promoted a more resilient phenotype, in contrast to what was described by Lin *et al* using small interfering RNA (siRNA) to knockdown P2X2 expression (Kuang et al., 2022, Lin et al., 2022). Chronic stress models increased expression of P2X2 in the medial prefrontal cortex, with conditional KO mice showing decreased susceptibility to stress models (Kuang et al., 2022). Whilst P2X2 appears to be directly linked to depressive behaviours, it is not clear whether activation of P2X2 results in a largely anti-depressive or pro-depressive effect. Further investigation would be necessary, but it is clear that there is an emerging role for the P2X2 receptor in depressive disorders. In addition , P2X2 and P2X3 receptors are known to be involved in taste perception (Bo et al., 1999). Although these effects appear to be largely mediated by heteromeric P2X2/3 receptors rather than homomeric P2X2, P2X2 KO mice have displayed impaired taste sensitivity compared to their wild type counterparts (Vandenbeuch et al., 2015, Finger et al., 2005).

1.2.3 P2X3

The P2X3 receptor displays similar properties to that of the P2X1 receptor in that it responds quickly to agonists and is rapidly desensitising (Lewis et al., 1995). It is of similar size to P2X1 at 397 amino acids in length, with a slightly longer C terminus length of 56 amino acids compared to 41 for the P2X1 receptor (Illes et al., 2021). Although largely believed to be incapable of forming a pore due to its quickly desensitising nature, permeability to the larger cations $NMDG^+$ and spermidine have been measured on HEK-293 cells expressing the human P2X3 receptor (Harkat et al., 2017).

First identified from the rat dorsal root ganglion (Chen et al., 1995), the P2X3 receptor has shown to be present in the neuronal systems of other species, such as in embryonic zebrafish trigeminal neurons (Boué-Grabot et al., 2000) and multiple regions of the rat brain (Séguéla et al., 1996). In addition, P2X3 receptor expression has been detected on nociceptive rat sensory neurons but not in non-nociceptive neurons containing muscle-stretch receptors (Cook et al., 1997). Further to this, weak expression of P2X3 has also been detected in rat hepatic mesentery arteries (Phillips et al., 1998), with expression detected in the human heart and spinal cord by RT-PCR (Garcia-Guzman et al., 1997b) and also by RT-PCR in the rat retina (Brändle et al., 1998).

Perhaps the most well-known role for purinergic therapeutics relates to P2X3 and its role in chronic cough, with the first-in-class drug gefapixant, a P2X2/3 and P2X3 antagonist, being approved for use in Japan for chronic cough (Markham, 2022). Regulatory approval has not yet been given in the US by the FDA, as requests have been made for additional data regarding efficacy of the drug, but Merck is expected to resubmit early in 2023 (Armstrong, 2022). Meanwhile, other P2X3 receptor antagonists are also undergoing late phase clinical trials, such as BLU-5937 in development by Bellus Health (Dicpinigaitis et al., 2020). The phase 2 SOOTHE trial (ClinicalTrials.gov identifier NCT04678206) completed in late 2021 and is awaiting publication of results, and phase 3 trials for BLU-5937 are expected to begin in 2022 (BellusHealth, 2022, ClinicalTrials.gov, 2021). One of the key issues with P2X3 antagonists is selectivity: as the P2X2/3 receptor is majorly implicated in taste perception (Finger et al., 2005), any antagonist that affects both P2X3 and P2X2/3 may cause taste disturbances that are not tolerated. This was one such issue with gefapixant, where adverse side effects related to taste resulted in between 7 and 20 % of patients discontinuing treatment in one trial, increasing with stronger dosing (Niimi et al., 2022). In phase 3 clinical trials, taste disturbances were reported in up to 21.1 % of patients receiving gefapixant (dysgeusia, COUGH-2 trial) (McGarvey et al., 2022). This highlights an area for development of selective homomeric P2X3 antagonists to minimise taste disturbances, and this is where BLU-5937 shows promise. In guinea pig studies, the antitussive effects of BLU-5937 were prevalent at doses significantly less (50-fold) lower than the dose that would block

heteromeric P2X2/3 receptors (Garceau and Chauret, 2019a). In addition, BLU-5937 did not alter taste perception in a model of taste perception in rats, but N-00588, a P2X2/3 and P2X3 antagonist, did (Garceau and Chauret, 2019a). It will be interesting to see whether this continues in human studies, although BLU-5937 has been shown to be a more potent inhibitor of αβ-MeATP-mediated responses at human homomeric P2X3 channels over heteromeric P2X2/3 expressed in HEK-293 cells (Garceau and Chauret, 2019a). Another P2X3 antagonist, eliapixant (BAY 1817080), has undergone numerous clinical trials (Davenport et al., 2021). Eliapixant has shown improved selectivity for P2X3 compared to gefapixant (Davenport et al., 2021, Morice et al., 2021b) and has shown few incidences of taste disturbances in clinical trials (Friedrich et al., 2022, Klein et al., 2022). Interestingly, eliapixant has also shown potential in other conditions associated with neuronal hypersensitivity such as endometriosis and overactive bladder syndromes (Davenport et al., 2021). Results showed that eliapixant was able to reduce inflammatory pain in rats using the complete Freund's adjuvant (CFA) induced model of inflammatory pain, and furthermore was also able to attenuate responses to inflammatory mediators in the uterus (Davenport et al., 2021). Since these trials were conducted, support for eliapixant has been withdrawn by Bayer (Evotec, 2022). Nonetheless, these data, in combination with the increase in patent applications for P2X3 antagonists in the past 5 – 10 years, show that there is potential for the P2X3 receptor in varying types of pain and chronic cough and could offer a novel non-opioid target for such conditions (Marucci et al., 2019).

1.2.4 P2X4

The P2X4 receptor was first cloned in 1995 by Bo *et al* from rat brain and P2X4 mRNA was detected in the spinal cord, lung, vas deferens, bladder, testis, thymus, and adrenal glands using Northern blot analysis (Bo et al., 1995). P2X4 displays slow desensitisation, similar to P2X2, and requires recovery times of over 10 minutes to restore full activity (Bo et al., 1995). Along with P2X1, it is one of the most permeable to calcium of the P2X receptors (Virginio et al., 1998a) and is capable of organic dye uptake similar to P2X2 and P2X7 receptors (Khakh et al., 1999a, Kaczmarek-Hájek et al., 2012, Bernier et al., 2012, Stokes et al., 2017).

Soon after initial cloning of P2X4 receptors from rat brain, mRNA encoding the P2X4 receptor was also found in peripheral neurons and epithelial cells of salivary glands (Buell et al., 1996a), and in rat lung, liver, and colon, but not in skeletal muscle (Wang et al., 1996). Subsequent studies have found P2X4 expression in skeletal muscle, along with heart, small intestine, and large intestine via Northern blot analysis (Dhulipala et al., 1998). PCR detected expression of P2X4 in the foetal human heart alongside other purinergic receptors, including P2X1 and P2X3 (Bogdanov et al., 1998).

The role of P2X4 in neuronal systems has been explored, with a focus on the roles of the receptor in neuropathic pain and alcohol misuse disorders in particular. Blockade of P2X4 receptors have been shown to minimise allodynic responses in mice (that is, pain in response to stimuli that do not usually cause pain) following nerve injury (Tsuda et al., 2003). This is thought to be due to release of Brain-Derived Neurotrophic Factor (BDNF) by spinal microglia, which is diminished in P2X4 KO mice (Coull et al., 2005, Ulmann et al., 2008). Additionally, P2X4 KO mice did not display hypersensitivity following sciatic nerve ligature, whereas wild type mice did (Ulmann et al., 2008). Acute and chronic responses to pain have also been assessed in P2X4 KO mice; there was little difference between the two groups in models of acute pain from heat, mechanical, and chemical sources (Tsuda et al., 2009). In chronic pain models, however, there was a marked difference between male wild type and P2X4 KO mice. In inflammatory models, swelling and subsequent weight increase of affected paws was reduced in KO mice compared to wild type, and paw withdrawal thresholds were higher (Tsuda et al., 2009). In neuropathic pain models, the difference was even greater, with KO mice having significantly greater paw withdrawal thresholds compared to their wild type counterparts (Tsuda et al., 2009). More recently, P2X4 has been implicated in nerve regeneration following sciatic nerve injury, whereby inhibition of the P2X4 receptor soon after injury improved nerve regeneration in mice (Molnár et al., 2022). Activation of P2X4 receptors has been associated with degeneration of dopaminergic neurons in Parkinson's disease models in rats, with downregulation of the P2X4 receptor providing beneficial effects related to an increase in autophagy (Zhang et al., 2021). One study found that treatment with

the P2X4 antagonist, 5-BDBD, was able to reduce the impact of chronic pain and depressive models on rats, showing reductions in hyperalgesia, depressive-like behaviours, and NLRP-3-mediated caspase-1 activation (Li et al., 2020). The increase in adverse behaviours is thought to be directly related to the increase in expression of P2X4 receptors in the hippocampus in response to negative stimuli (Li et al., 2020). These data suggest that blockade of P2X4 could be a useful therapeutic notion, particularly with regards to chronic pain where treatment options are limited. In addition to treatment, expression of P2X4 could offer a novel biomarker for certain neurodegenerative conditions such as ALS where no such marker currently exists (Bertin et al., 2022).

Several studies have implicated P2X4 in alcohol misuse disorders (Yardley et al., 2012, Wyatt et al., 2014). Treatment with ivermectin, an antiparasitic agent and potentiator of P2X4 receptors, resulted in a significant decrease in alcohol consumption in a 24-hour period compared to control (Yardley et al., 2012). Subsequent studies have also shown reduced ethanol intake in both male and female rats across both 4-hour and 24-hour time periods, but sucrose intake remained unaffected (Franklin et al., 2015). KO mouse models showed that treatment with ivermectin was still effective in reducing alcohol intake despite the lack of P2X4 receptor, however, this effect was approximately 50 % less than what was observed in the wild type mice (Wyatt et al., 2014). In addition to modulation of the P2X4 receptor affecting intake of alcohol in rodent models, data has suggested that inhibition of the P2X4 receptor can reduce inflammation of the liver in alcoholic steatohepatitis (Xia et al., 2022). This highlights that although potentiation of the receptor may be useful in reducing alcohol intake, it could potentially have detrimental effects with regards to the liver in those that have liver disease as a result of alcohol consumption.

The role of P2X4 in the cardiovascular system has also been explored. Mice that overexpressed the P2X4 receptor exhibited greater cardiac contractility and output compared to wild type mice, despite similar blood pressure, heart rates, and heart weights between both sets (Hu et al., 2001). This suggests that the P2X4 receptor has a key role in mediating cardiac performance, although it is noted that the P2X6 receptor is also present in cardiac tissue (Hu et al., 2001). It is possible for these two receptor subtypes to form heteromers (Illes et al., 2021), and therefore these effects may not be due to P2X4 alone, but it is likely to be implicated. In fact, P2X4 receptor KO mice have shown poorer outcomes in models of heart failure compared to wild type mice (Yang et al., 2014). In models of ischemic heart failure, cardiac function was reduced in P2X4 KO mice: fractional shortening was less, indicating that the heart is less able to eject blood, and this was apparent shortly after the infarct caused by left anterior descending coronary artery ligation (Yang et al., 2014). Recently, an abstract suggested that activation of P2X4 can cause reductions in heart rate that improve cardiac function in models of heart failure associated with pulmonary arterial hypertension (Ribeiro et al., 2022).

1.2.5 P2X5

The P2X5 receptor was first cloned in 1996 from coeliac ganglia, at the same time as the P2X6 receptor (Collo et al., 1996). It is expressed poorly compared to the other cloned P2X receptors evaluated, with distribution only detected in the ventral horn, sensory ganglia, and the mesencephalic nucleus of the trigeminal nerve in the brain (Collo et al., 1996). It demonstrates slow desensitisation following rapid activation by ATP, with human P2X5 receptors producing much larger currents than the rat receptor (Bo et al., 2003a). Interestingly, the P2X5 receptor shows unique permeability to Cl^- ions and is permeable to both NMDG and YO-PRO-1 iodide (Bo et al., 2003a). The P2X5 receptor is not thought to have an important physiological role in humans, given that most humans express a variant containing a single nucleotide polymorphism (SNP) which results in a non-functional P2X5 receptor that is retained in the cytoplasm (Kotnis et al., 2010). This is not the case for other species, where the full-length receptor is more commonly expressed and hence why the receptor has been able to be investigated in more detail for those species (Kotnis et al., 2010). It is believed that approximately 10 % of all humans possess the full-length P2X5 receptor, with the full-length receptor being found in populations of black Americans (Kotnis et al., 2010, King, 2022). Evidence has shown that the full-length human receptor can be inhibited by nimodipine and amlodipine (Schiller et al., 2022), the latter used extensively to treat hypertension in the United Kingdom; the fact that the full-length receptor is known to be prevalent only in black Americans suggests that ethnicity could have an impact on treatment choice for certain patient groups, although more research would be necessary to determine the possible adverse effects from inhibiting P2X5 receptor function in these populations. An excellent in-depth review by Brian King explores the knowledge to date regarding the P2X5 receptor and addresses issues with regards to the lack of interest this particular subtype has received (King, 2022).

1.2.6 P2X6

Cloned at the same time as the P2X5 receptor, the P2X6 receptor is more widely distributed (Collo et al., 1996), found in multiple neuronal tissues, including the brain, spinal cord, and sensory ganglia, and also in the epithelium of bronchi (Collo et al., 1996). Expression of P2X6 receptors tends to be poor, with only two groups successfully managing to express the rat P2X2 receptor in HEK-293 cells and even then, only a small proportion of cells responded to ATP (Illes et al., 2021). The P2X6 receptor is unable to form homomeric receptors, and instead forms heteromeric receptors with P2X1, P2X2, P2X4 and P2X5 subunits (Torres et al., 1999). Patch clamp electrophysiology from the original cloning of both P2X5 and P2X6 subunits shows the rat P2X6 receptor to be slowly desensitising (Collo et al., 1996). Mutating leucine 251 to lysine, analogous to the K246 residue that has been shown to be important to desensitisation kinetics in the P2X2 receptor (Buell et al., 1996a), slowed desensitisation even further (Collo et al., 1996). In terms of distribution, the P2X6 receptor appears to be present in the skeletal muscle of several different species, and often overlaps with P2X2 and P2X4 receptors in expression in neuronal tissues, likely due to the heteromeric nature of this receptor (Kaczmarek-Hájek et al., 2012). Expression has also been detected in endothelial tissues, again along with expression of the P2X4 receptor (Kaczmarek-Hájek et al., 2012).

1.2.7 P2X7

The P2X7 receptor, originally termed the P2Z receptor (Gordon, 1986), was first described on microglial cells in 1996 (Ferrari et al., 1996) and cloned from rat brain soon after (Surprenant et al., 1996). It is unique amongst the P2X receptors - it is the largest of all the purinergic receptors at 595 amino acids long and with a long C terminal tail 240 amino acids in length (Illes et al., 2021). The P2X7 receptor does not desensitise (North, 2002) – the recent information gained from the full-length cryo-EM structure of rat P2X7 highlights a palmitoylation site that prevents desensitisation by anchoring the receptor to the cell membrane (McCarthy et al., 2019). The ATP binding site is highly conserved between all P2X receptor subtypes, making it difficult to explain why the P2X7 receptor requires a much higher concentration of ATP to activate compared to other P2X receptors, although solvent accessibility at the rP2X7 receptor may be reduced – this in turn would affect the timescale of ATP entry to the pocket (McCarthy et al., 2019). Other explanations for the low sensitivity to ATP at this receptor include reduced agonist affinity compared to other P2X receptor subtypes, or reduced efficacy of the ligand itself, meaning it is less able to induce a conformational change in the P2X7 receptor (Pasqualetto et al., 2018). Another prominent feature of the P2X7 receptor is its ability to form a large, non-specific pore (Di Virgilio et al., 2018). Multiple membrane impermeant dyes have been shown to permeate P2X7-expressing cells, such as YO-PRO-1, ethidium bromide, and even larger dyes such as TO-PRO-3 and MTS-Rhodamine (Browne et al., 2013, Barczyk et al., 2021). The pore formation of P2X7 receptors has been shown to be independent of other cellular components, such as Pannexin-1, and so is believed to be a property intrinsic to the ion channel itself (Karasawa et al., 2017).

The P2X7 receptor is largely expressed in haemopoetic cells, including granulocytes, lymphocytes, monocytes, macrophages, and dendritic cells (Collo et al., 1997, Coutinho-Silva et al., 1999, Rassendren et al., 1997b, Ferrari et al., 1997a). In addition, expression is also widespread throughout the nervous system, with particular emphasis on microglia and astrocytes (Collo et al., 1997, Ferrari et al., 1997b, Ballerini et al., 1996). P2X7 expression has also been detected in osteoclasts and osteoblasts (Hoebertz et al., 2000, Gartland et al., 2001, Jørgensen et al., 2002), with evidence suggesting a role for P2X7 may exist in bone formation and maintenance (Ke et al., 2003). Ultimately, the P2X7 receptor has key roles in modulation of inflammation, including activation of the NLRP3 inflammasome (Franceschini et al., 2015), caspases (Ferrari et al., 1999), and cytokine release (Le Feuvre et al., 2002), with direct impacts on cell death and apoptosis (von Albertini et al., 1998, Adinolfi et al., 2018).

Due to the role of the P2X7 receptor in apoptosis and cell death, there has been increasing interest as to whether this could be relevant to cancer (Lara et al., 2020). Exploitation of pro-apoptotic features of P2X7 could be beneficial in inducing cell death in cancers, particularly as ATP levels in the tumour microenvironment have been shown to reach levels sufficient to activate the P2X7 receptor (Pellegatti et al., 2008). P2X7 expression has been detected in numerous cancers, including prostate, breast, and blood cancers (Lara et al., 2020). P2X7 overexpression has been associated with melanoma (Lara et al., 2020), despite the receptor being involved largely in cell death. Splice variants of P2X7 have been implicated here: the full-length P2X7 receptor is thought to be directly linked to the pro-apoptotic characteristics of P2X7 (Cheewatrakoolpong et al., 2005, Adinolfi et al., 2010), whereas truncated splice variants have been associated with cell growth rather than death (Adinolfi et al., 2010). Evidence has shown that transfection with the P2X7b splice variant increases proliferation of osteosarcoma cells to a greater extent that transfection with the full length P2X7a splice variant (Giuliani et al., 2014). Overall, effects of the P2X7 receptor can be conflicting in cancer, with varying effects depending on splice variants in addition to cancer types and cell lines assessed: this has been reviewed in detail by Savio *et al* (Savio et al., 2018).

One such instance where potentiation of P2X7 has been shown to be beneficial in cancer is with regards to the small molecule, HEI3090. This compound has been suggested to potentiate P2X7 receptors, and in combination with an anti-PD-1 antibody has been shown to improve outcomes in mice with lung cancer (Douguet et al., 2021). This has been associated with increased IL-18 production, leading to increased levels of IFN-γ produced by natural killer and $CD4^+$ T-cells (Douguet et al., 2021). Conversely, inhibition of P2X7 may prove beneficial. Injection of oxidised ATP, an inhibitor of P2X7, resulted in reduced colonic tumour volume in mice (Adinolfi et al., 2012). In addition, treatment with AZ10606120 (a specific P2X7 antagonist (Allsopp et al., 2017)) resulted in decreased tumour volume in melanoma models (Adinolfi et al., 2012). AZ10606120 has also been shown to reduce human pancreatic ductal adenocarcinoma cell proliferation (Giannuzzo et al., 2015). Given the complexity of the role of P2X7 in cancer, it would be interesting to explore in more detail the contribution of splice variants to the anti- or pro-neoplastic properties. A variant of P2X7 unable to form the macropore, termed non-functioning P2X7 or nfP2X7, has been shown to be expressed on a variety of cancer cell tissues (Gilbert et al., 2019). This variant, despite being unable to form the large, non-specific pore characteristic of P2X7, still displays ion channel functionality (Gilbert et al., 2019). Antibodies have been designed to target nfP2X7, but not overexpressed wild type P2X7, in the prostate cancer cell line PC3 (Gilbert et al., 2019), although it is not clear whether this variant is a splice variant or an alternate conformation to the wild type P2X7 receptor. More work is needed to determine this key difference, as nfP2X7 has been found to be expressed in cancer cells but not healthy cells and could pose a novel

target for cancer therapies (Nesselhut et al., 2013). A recent clinical trial found that ointment containing sheep anti-nfP2X7 antibodies was well tolerated in patients with basal cell carcinoma, with 65% of patients displaying a reduction in lesion size after 28 days; however, some patients had no change or an increase in the size of their lesions, suggesting that it may not be sufficient to control growth in all cases (Gilbert et al., 2017). Although P2X7 does not form heteromeric channels, it may be able to form channels made up of different splice variants of P2X7, such as combinations of P2X7a and P2X7b (Adinolfi et al., 2010): this concept would be interesting to explore further with regards to possible implications in cancer.

Activation of P2X7 receptors on immune cells has been shown to induce intracellular pathogen killing, particularly with regards to mycobacterium (Lammas et al., 1997). Using Bacillus Calmette-Guerin (BCG), an attenuated form of the *Mycobacterium bovis* (bovine tuberculosis) commonly used as a vaccine against tuberculosis infections, extracellular ATP has been demonstrated to induce intracellular killing by macrophages, thought to be due to P2X7 based on pharmacological analysis (Lammas et al., 1997). This was later confirmed using macrophages from P2X7 KO mice (Fairbairn et al., 2001). P2X7 has also been implicated in *Pseudomonas aeruginosa* infections, whereby inhibition of P2X7 by oxidised ATP blocked cell death in macrophages (Zaborina et al., 1999). Potentiation of intracellular pathogen killing mediated by P2X7 could offer a novel therapeutic for these otherwise hard to target infections (Stokes et al., 2020). Other infections where P2X7 has been implicated include *Candida albicans* (Koshlukova et al., 2000), *Porphyromonas gingivalis* (Yilmaz et al., 2008), *Leishmania amazonesis* (Chaves et al., 2009), *Toxoplasma gondii* (Corrêa et al., 2010), and *Chlamydia psittaci* (Coutinho-Silva et al., 2001, Darville et al., 2007). Single nucleotide polymorphisms in the P2X7 gene have been associated with reduced intracellular mycobacterium killing, suggesting that different populations may be more susceptible to such conditions (Saunders et al., 2003).

Inflammation is associated with more than just infection: in the nervous system, inflammation has been linked to depressive disorders (Bennett, 2007, Wetsman, 2017, Bhattacharya, 2018). Recently, P2X7 antagonist JNJ-54175446, a potent, selective P2X7 antagonist capable of crossing the blood brain barrier, has been undergoing clinical trials for depressive disorders (ClinicalTrials.gov identifier NCT04116606) after previously completing a safety and tolerability trial (ClinicalTrials.gov identifier NCT02475148). The P2X7 receptor has also been implicated in bipolar disorder, with models of mania involving D-amphetamine showing that blockade of P2X7 with A438079 reduced responsiveness to D-amphetamine, with P2X7 KO mice mimicking this effect (Gubert et al., 2016). This study has been replicated in humans with similar results (Recourt et al., 2020). In these studies, the focus is blockade of P2X7 leading to reduced neuroinflammation and improved psychiatric outcomes.

In pain conditions, administration of oxidized ATP has been shown to reduce inflammatory pain in mice models of arthritis by increasing paw pressure threshold times compared to those that had not been treated, thought to be via blockade of P2X7 receptors (Dell'Antonio et al., 2002). In P2X7 KO mice, both inflammatory and neuropathic pain, caused by application of FCA and partial nerve ligation respectively, were reduced, characterised by increased paw retention times in hot plate models and equal weight distribution across both inflamed and non-inflamed paws (Chessell et al., 2005). The antagonist A-740003 displayed antinociceptive properties to multiple models of pain, including models of both neuropathic (sciatic nerve constriction/vincristine treatment) and inflammatory (FCA application) pain (Honore et al., 2006). The potential for P2X7 in pain conditions has been reviewed recently in detail by Ren and Illes (Ren and Illes, 2022).

A less well explored role for P2X7 is in the modulation of skeletal tissue, particularly through expression in both osteoclasts and osteoblasts (Ke et al., 2003). Polymorphisms in the P2X7 receptor have been shown to affect lumbar spine bone mineral density in post-menopausal women, with the arginine 307 to glycine SNP being associated with lower baseline bone mineral density (Gartland et al., 2012). Conversely, a gain of function SNP (alanine 348 to threonine) was associated with increased lumbar spine bone mineral density (Wesselius et al., 2013), further establishing the role for P2X7 in maintenance of bone. In-vivo studies have shown that P2X7 receptor KO mice have an increased risk of osteoporosis following ovariectomy (a process used to mimic oestrogen loss observed during menopause) thought to be directly related to the retention of osteoclasts in the presence of reduced oestrogen and P2X7 (Wang et al., 2018). Potentiating P2X7 receptors in those particularly at risk of osteoporosis, such as menopausal patients, may provide a novel therapeutic avenue.

1.3 Pharmacology of P2X Receptors

1.3.1 Pharmacology of P2X1

Agonists

Original pharmacology of the rat P2X1 receptor yielded the following rank order of potency: 2-MeSATP≥ATP>αβ-MeATP, with EC_{50} values of approximately 1 µM for 2-MeSATP and ATP and 2 µM for αβ-MeATP (Valera et al., 1994). ADP also yielded responses when expressed in HEK-293 cells, with an EC_{50} value of approximately 30 µM (Valera et al., 1994), although responses were not measured at human P2X1 receptors expressed in *Xenopus* oocytes (Mahaut-Smith et al., 2000) and this is not believed to be a true agonist of P2X1 receptors (Syed and Kennedy, 2012). Further studies on the rat vas deferens elicited responses to αβ-MeATP with an EC_{50} of 3.6 µM, in line with that measured by

Valera *et al*, and also responses to βγ-MeATP, although this was less potent with an EC_{50} value of 17.1 μM (Trezise et al., 1995).

Antagonists

Suramin was shown to inhibit currents elicited by αβ-MeATP, but not noradrenaline or carbachol, in the rat vas deferens; most likely via P2X1 receptors (Dunn and Blakeley, 1988). Analogues of suramin have also been found to be potent P2X1 antagonists. The first, 'compound 3' or NF023, was found to reduce the vasopressor effects of αβ-MeATP in rats by approximately 8-fold (Urbanek et al., 1990). This compound was further explored at rat P2X1 receptors expressed in *Xenopus* oocytes, whereby it was able to inhibit responses to 1 μM ATP (Soto et al., 1999). The effects of NF023 were also tested at human P2X1 receptors, yielding IC_{50} values of 0.24 μM and 0.21 μM for rat and human receptors respectively (Soto et al., 1999). Later, the suramin analogue NF279 was characterised as a selective and potent antagonist for the rat P2X1 receptor, acting in a competitive manner with an IC_{50} value of 19 nM to 1 μM ATP following a 10 second pre-incubation (Rettinger et al., 2000). Another suramin derived antagonist, NF449, has been shown to have activity at both rat and human P2X1 receptors (Braun et al., 2001, Hülsmann et al., 2003). At recombinant rat receptors, NF449 has been shown to have an IC_{50} of 0.28 nM against 1 μM ATP measured using patch-clamp electrophysiology (Rettinger et al., 2005). At the human receptor, the IC_{50} for NF449 was 53.7 pM and 407 pM at 1 μM and 100 μM respectively; results were measured using patch-clamp electrophysiology on *Xenopus* oocytes expressing the human P2X1 receptor (Hülsmann et al., 2003).

Both PPADS and iso-PPADS were able to inhibit rat P2X1 receptors, with IC_{50} values determined against 3 μM ATP of 98.5 nM and 42.5 nM respectively (Jacobson et al., 1998). MRS2159, a derivative of PPADS, has been shown to selectively inhibit rat P2X1 with an IC_{50} value of approximately 9 nM (Kennedy, 2007, Syed and Kennedy, 2012). Another PPADS derivative, MRS2220, was shown to inhibit rat P2X1 expressed on *Xenopus* oocytes, with an IC_{50} of 10.2 μM determined using patch-clamp electrophysiology (Jacobson et al., 1998).

TNP-ATP, along with TNP-ADP, TNP-AMP, and TNP-GTP, was able to inhibit patch-clamp responses at the human P2X1 receptor expressed in HEK-293 cells (Virginio et al., 1998b). TNP-ATP inhibition gave an IC_{50} of approximately 6 nM; IC_{50} values were not determined for the other TNP-substituted analogues in this study (Virginio et al., 1998b).

RO-0437626 is another antagonist of the P2X1 receptor, with an IC_{50} of 3 μM at human P2X1 expressed in CHO-K1 cells using the FLIPR calcium assay (Jaime-Figueroa et al., 2005). This was tested using 0.1 μM αβ-MeATP, which is believed to be considerably less than the EC_{50} value of the human P2X1 receptor (0.2 μM) (Melnik et al., 2006). A newer analogue, PSB-2001, also known as compound 1, is a

selective and potent antagonist of human P2X1 receptors with an IC_{50} of approximately 19 nM (Tian et al., 2020). A salicylanilide derivative, it offers one of the first non-acidic antagonists of the P2X1 receptor (Tian et al., 2020). Another compound, compound 14, was also found to have good selectivity for the P2X1 receptor, with an IC_{50} of 23.1 nM and >10 fold selectivity for P2X1 over P2X4 and P2X7, and >500 fold selectivity over P2X2 and P2X3 (Tian et al., 2020).

A recent finding shows that the aqueous extract of *Urtica dioica* (stinging nettle) leaves can reduce male fertility in mice by 53 %. Although not clear whether this extract acts directly on P2X1, there was limited reduction in the contractility of prostate smooth muscle in the presence of noradrenaline and acetylcholine compared to the P2X1 agonists ATP and αβ-MeATP. Further investigations would be necessary, but this could suggest the presence of a natural product compound capable of inhibiting the P2X1 receptor (Eise et al., 2022).

Positive Allosteric Modulators

Few compounds have been discovered to potentiate P2X1 responses. The PPADS derivative, MRS2219, was found to potentiate ion channel responses to 3 µM ATP in *Xenopus* oocytes expressing rat P2X1, with an EC_{50} of 5.9 µM (Jacobson et al., 1998). Another, gintonin (a natural product found in *Panax ginseng*), was found to potentiate responses to 1 µM ATP at human P2X1 receptors expressed in *Xenopus* oocytes (Choi et al., 2013), although the mechanism by which this acts is unknown (Stokes et al., 2020).

Effects of Metals, Cations, and pH

Divalent cations often have modulatory effects on P2X receptors, although this is not the case at the P2X1 receptor (Evans et al., 1996). Increasing the extracellular calcium concentration up to 10 mM was found to have no effect on the amplitude of current responses (Evans et al., 1996). The human P2X1 receptor is inhibited by increasingly acidic pH; conversely, it is potentiated by alkaline pH, although to a lesser extent than the inhibition seen at pH 6.3 (Stoop et al., 1997). Zinc (Zn^{2+}) and cadmium (Cd^{2+}) at concentrations of 100 µM were found to have no effect on the response to ATP measured at P2X1 receptors using patch-clamp electrophysiology, although the species here is not clear (Nakazawa and Ohno, 1997).

1.3.2 Pharmacology of P2X2

Agonists

The human P2X2 receptor is activated by the endogenous ligand ATP, and also BzATP and 2-MeSATP (Lynch et al., 1999). Unlike P2X1, it is not sensitive to either αβ-MeATP or βγ-MeATP (Lynch et al.,

1999). The most potent agonist of human P2X2 (P2X2a) is BzATP, with an EC_{50} value of approximately 417 nM, followed by 2-MeSATP (813 nM), ATP (1.02 µM) and ATPγS (1.35 µM) (Lynch et al., 1999). Interestingly, despite the inactivity of ADP, ADPβS had an EC_{50} of 30.9 µM at the full length human P2X2 receptor, although this did not produce a sigmoidal concentration response curve on the figure shown (Lynch et al., 1999). These data were all measured using a fluorometric calcium assay (Fluo-3) in 1321N1 human astrocytoma cells (Lynch et al., 1999).

Antagonists

Antagonists of P2X2 are limited, particularly with regards to the human receptor. At the time of writing, there are no commercially available selective antagonists of P2X2 receptors of any species. Non-selective antagonists, such as suramin and PPADS, have displayed activity at P2X2 receptors (Bianchi et al., 1999). At the rat receptor, PPADS is more potent than suramin, with IC_{50} values of 3.8 µM and 33.1 µM respectively (Bianchi et al., 1999). The human receptor shows a similar sensitivity to both antagonists as the rat receptor, although suramin is a poor antagonist of human P2X2 when expressed in 1321N1 astrocytoma cells compared to *Xenopus* oocytes (IC_{50} >50 µM in 1321N1 cells compared to 6 µM in oocytes) (Lynch et al., 1999). PPADS had a similar IC_{50} to what was observed in the rat receptor of 5.46 µM (Lynch et al., 1999). Another non-specific antagonist, TNP-ATP, has been shown to have antagonistic properties at the rat P2X2 receptor, with an IC_{50} value of approximately 2 µM (Virginio et al., 1998b). Evidence has also shown that TNP-ATP can block P2X2 receptors in human submucous neurons (Liñán-Rico et al., 2015).

Progress has been made with regards to the rat receptor in particular, with NF279, an antagonist of the P2X1 receptor, being shown to competitively inhibit rat P2X2 receptors with an IC_{50} of approximately 750 nM following pre-incubation before application of ATP (Rettinger et al., 2000). More recently, PSB-10211 and other derivatives of the commercially available anthraquinone dye Reactive Blue 4 have been shown to selectively inhibit the rat P2X2 receptor (Baqi et al., 2011). Interestingly, reactive blue 4 itself (compound 57, PSB-1011) was found to be the most potent inhibitor of the rat P2X2 receptor, acting in a competitive manner with an IC_{50} value of 79 nM (Baqi et al., 2011). The effect of this compound on human P2X2 receptors was not studied.

Some natural products have been shown to inhibit P2X2 receptors, with bile acids shown to inhibit rat P2X2 receptors (Sivcev et al., 2020, Schmidt et al., 2019). The taurine-conjugated bile acid taurolithocholic acid (TCLA) and taurohyodeoxycholic acid (THDCA) both inhibited rP2X2, with an IC_{50} value of 10.7 µM for THDCA; interestingly, TCLA but not THDCA potentiated the human receptor (Schmidt et al., 2019). Additional studies have also confirmed that lithocholic acid (LCA) inhibits the rat P2X2 receptor with an IC_{50} value of 4.6 µM (Sivcev et al., 2020). Ambroxal, another natural product

derived from *Justicia adhatoda* (Malabar nut), has recently been shown to inhibit human P2X2 receptors expressed in 1321N1 astrocytoma cells (Schneider et al., 2021). In an intracellular calcium assay, ambroxal was found to inhibit human P2X2 receptors with an IC_{50} value of 5.69 µM, with no activity at the other P2X receptors tested, suggesting selectivity for the P2X2 receptor over other receptor subtypes (Schneider et al., 2021).

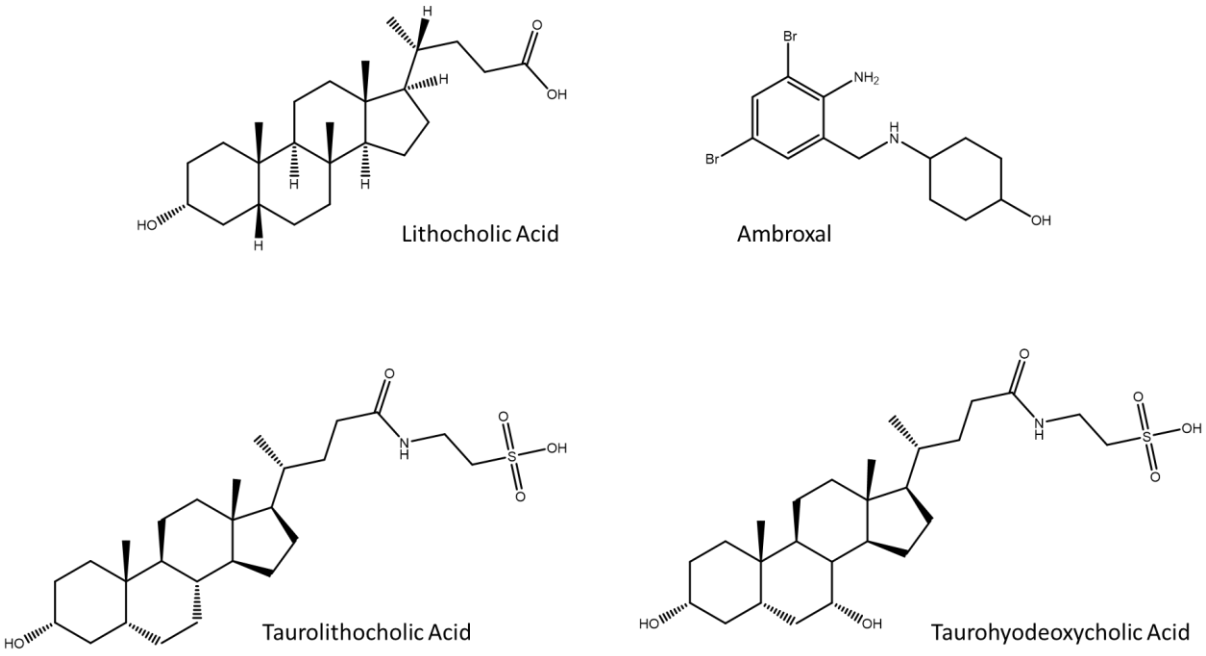

Figure 1.3 – Structures of modulators of P2X2 receptors. Lithocholic acid has been shown to inhibit rat P2X2, as have taurolithocholic acid and taurohyodeoxycholic acid. Taurolithocholic acid potentiates the human P2X2 receptor. Ambroxal has been shown to inhibit the human P2X2 receptor. References are as follows: lithocholic acid (Sivcev et al., 2020), ambroxal (Schneider et al., 2021), taurolithocholic acid and taurohyodeoxycholic acid (Schmidt et al., 2019). Structures were produced using ChemDraw Prime (PerkinElmer).

Positive Allosteric Modulators

Little is known about positive modulators of the human P2X2 receptor, but several neurosteroids have been shown to potentiate the rat P2X2 receptor. The first, dehydroepiandrosterone (DHEA), has been shown to potentiate responses to submaximal ATP concentrations in neurons, likely due to the P2X2 receptor (De Roo et al., 2003). Following on from this, progesterone has been found to potentiate homomeric P2X2, but not P2X2/3 heteromeric receptors, unlike DHEA that has been shown to potentiate both (De Roo et al., 2010). Progesterone was able to shift the ATP concentration response curve to the left in rat P2X2 receptors, reducing the EC_{50} value from 32.12 µM for ATP alone to 21.03 µM in the presence of 20 µM progesterone (De Roo et al., 2010). Derivatives of testosterone have also

been shown to modulate P2X2-mediated responses; testosterone butyrate was found to decrease the EC_{50} to ATP from 3.2 µM to 1.9 µM (Sivcev et al., 2019). One particular analogue, testosterone perfluorobutyrate, was found to potentiate response by approximately 200 % at the rat P2X2 receptor but only 140 % at the rat P2X4 receptor, suggesting some differences in conservation of the binding site between these receptor subtypes (Sivcev et al., 2019). Some of the anthraquinone derivates explored by Baqi *et al* also showed potentiating activity at the rat P2X2 receptor, with 100 nM PSB-10211 increasing the maximum response to ATP but only slightly reducing the EC_{50} from 22.2 µM to 20.6 µM (Baqi et al., 2011).

Effects of Metals, Cations, and pH

Unlike the other P2X receptors, the P2X2 receptor is positively modulated by acidic pH (King et al., 1997). The rat receptor, when expressed in *Xenopus* oocytes, was significantly more sensitive to ATP at a pH of 6.5 compared to 7.4, with EC_{50} values to ATP of 1.2 µM and 4.6 µM respectively (King et al., 1997). This effect was mirrored by other P2X2 receptor agonists (King et al., 1997). Extracellular calcium has been shown to have inhibitory effects on the rat P2X2 receptor, with inhibition increasing in a dose dependent manner but activity restored by increasing the ATP concentration (Evans et al., 1996). Other divalent cations, such as Mg^{2+}, Ba^{2+}, and Mn^{2+}, have also been shown to decrease currents elicited by P2X2 receptors, although it is not clear what species was assessed here (Ding and Sachs, 2000).

The effects of copper are opposite at rat and human P2X2 receptors; at rat P2X2, 20 µM Cu^{2+} was shown to substantially potentiate responses to 2 µM ATP, whereas at human P2X2, the same concentration of copper inhibited responses to 5 µM ATP (Punthambaker and Hume, 2014). Likewise, 20 µM zinc, cadmium, and cobalt all inhibited human P2X2 currents with a faster onset of action than copper (Punthambaker and Hume, 2014). Nickel was also able to inhibit currents at human P2X2, although to a lesser extent than the other metals tested (Punthambaker and Hume, 2014). Zinc has been shown to differentially modulate human P2X2b receptors depending on the concentration of ATP applied; at low ATP concentrations (2.5 µM), zinc inhibited responses, but at high concentrations of ATP (500 µM), zinc potentiated currents (Tittle and Hume, 2008). At rat P2X2 receptors, concentrations of zinc >100 µM inhibited responses whereas lower concentrations potentiated, as described previously (Tittle and Hume, 2008). Modulation of zinc at human P2X2 is thought to be partly dependent on a cluster of histidines (H204, H209, and H330) in the central vestibule of the receptor (Punthambaker et al., 2012). Whilst these residues are not thought to make up the zinc

binding site in human P2X2, they are thought to enable access to other residues that may be involved in zinc binding; most likely E75 but perhaps also S76 and S77 (Punthambaker et al., 2012).

1.3.3 Pharmacology of P2X3

Agonists

The human P2X3 receptor is most sensitive to BzATP, with an EC_{50} value of approximately 40 nM using the Fluo-4 intracellular calcium indicator (Neelands et al., 2003). The activity of 2-MeSATP and the endogenous ligand ATP are similar; the rat receptor shows slight preference for 2-MeSATP with an EC_{50} of 12.7 µM compared to 20 µM for ATP using patch-clamp electrophysiology (Séguéla et al., 1996). The human receptor shows similar affinity, with an EC_{50} of 180 nM for 2-MeSATP and 400 µM for ATP determined using a calcium assay (Neelands et al., 2003). Less potent, but still active at the human P2X3 receptor, are ATPγS, with an EC_{50} of 550 nM, and αβ-MeATP, with an EC_{50} of 780 nM, with ADP being inactive at the receptor (Neelands et al., 2003). Interestingly, β,γ-MeATP shows activity at the rat P2X3 receptor, but this is stereoselective: only the *D* isomer is active (Rae et al., 1998). Overall, the order of activity at human P2X3 appears to be BzATP>2-MeSATP≥ATP>ATPγS>αβ-MeATP.

Antagonists

Several antagonists for the P2X3 receptor exist, although there is often crossover between homomeric P2X3 receptors and heteromeric P2X2/3 receptors. As discussed previously, gefapixant (AF-219, MK-7264) has undergone clinical trials for its role in chronic cough, gaining approval in Japan under the brand name Lyfnua® (Merck, 2022). One issue with gefapixant is that it inhibits both homomeric and heteromeric P2X3 receptors, resulting in taste disturbance related side effects (Smith et al., 2020, Abdulqawi et al., 2015). Eliapixant, another P2X3 antagonist, was shown to be more selective than gefapixant for homomeric P2X3 receptors compared to P2X2/3, however, support for this drug has since been withdrawn (Evotec, 2022, Klein et al., 2022). A more selective antagonist is in development by Bellus Health: BLU-5937, shows increased selectivity to homomeric P2X3 compared to heteromeric P2X2/3, resulting in fewer undesirable side effects (Garceau and Chauret, 2019b). Ro-85 is another selective P2X3 antagonist, showing increased potency at the homomeric receptor compared to the heteromeric P2X2/3 receptor (Brotherton-Pleiss et al., 2010).

Antagonists that inhibit both P2X3 and P2X2/3 include A-317491, which has been shown to inhibit both rat and human heteromeric and homomeric P2X3 receptors with micromolar affinity (Jarvis et al., 2002) and also to reduce nociception in *in vivo* models (McGaraughty et al., 2003). Interestingly, only the *S* enantiomer appears to be active (Jarvis et al., 2002). Others include AF-353 (Ro-4) (Gever et al., 2010), Ro-3 (Ford et al., 2006), and NF110 (Hausmann et al., 2006). The peptide spinorphin has

suggested selectivity for P2X3, but no data is available on heteromeric P2X2/3 receptors (Jung et al., 2007). The P2 receptor antagonists PPADS, suramin, and TNP-ATP also show antagonist activity at P2X3, as does the anthraquinone dye reactive blue 2 (Séguéla et al., 1996).

Positive Allosteric Modulators

Known positive allosteric modulators of the P2X3 receptor are extremely limited; DHEA has been shown to positively modulate P2X2/3 receptors, although this is likely to be influenced mainly by the P2X2 subunit as DHEA also modulates homomeric P2X2 receptors (De Roo et al., 2010). Cibacron blue has been reported to potentiate human P2X3 receptors, increasing the efficacy and potency (i.e., a decrease in the EC_{50} and an increase in the maximum response) of P2X3-mediated calcium influx (Alexander et al., 1999). Other dyes have also been shown to potentiate P2X3, including reactive red 2, reactive blue 5, and basilen blue (Alexander et al., 1999). ATP-mediated currents in rat P2X3 have been shown to be potentiated by ethanol, although the change in the EC_{50} value was small (2.35 µM in the absence of ethanol compared to 0.97 µM in the presence of ethanol) (Davies et al., 2005). There did not appear to be any increase in the maximum response in the presence of ethanol compared to the response to ATP alone (Davies et al., 2005).

Effects of Metals, Cations, and pH

In one study, rat P2X3 does not appear to be potentiated by either zinc or cadmium (Nakazawa and Ohno, 1997). Pre-treatment with zinc at concentrations of 1, 10, and 100 µM for 10 seconds did not appear to change the current measured compared to that of 1 µM ATP alone, with cadmium appearing to inhibit responses slightly at 100 µM (Nakazawa and Ohno, 1997). However, another study has shown that responses to 10 µM ATP were able to be potentiated by 10 µM zinc (Séguéla et al., 1996). A further study has shown that rat P2X3 is again potentiated by zinc, with currents invoked by 0.3 µM ATP increasing in response to treatment with 100 µM zinc (Wildman et al., 1999). Longer incubation times were found to improve potentiation and highlighted a secondary inhibition at higher concentrations of zinc (greater than approximately 30 µM) which was not apparent until $[Zn^{2+}]$ of approximately 300 µM (Wildman et al., 1999). Acidic pH has an inhibitory action on rat P2X3, with the EC_{50} to ATP reducing from 1.83 µM at pH 7.35 to 28.3 µM at pH 5.5 (Wildman et al., 1999). The effect of other divalent cations such as Ca^{2+} and Mg^{2+} are less clear; one study showed that co-application of 30 µM ATP with 10 mM Ca^{2+} resulted in a smaller current than was measured with co-application of ATP and 1 mM Ca^{2+} (Cook et al., 1998). Prolonged treatment with calcium resulted in faster recovery from desensitisation, with a two-minute calcium treatment giving a larger current at 10 mM compared to 1 mM (Cook et al., 1998). A more recent study has shown that Mg^{2+} increases the affinity for ATP at the P2X3 receptor and explores a binding pocket for divalent cations on the receptor (Li et al., 2019).

1.3.4 Pharmacology of P2X4

Agonists

The P2X4 receptor is most sensitive to ATP, with an EC_{50} of approximately 1.4 μM at the human receptor (Jones et al., 2000). Interestingly, αβ-MeATP is a partial agonist only at the human and mouse receptors with an EC_{50} value of approximately 19 μM and 7 μM respectively; at the rat receptor, this compound instead acts as an antagonist, reducing current in response to ATP in a concentration dependent manner (Jones et al., 2000). BzATP is also a partial agonist at rat and human P2X4 receptors (Bowler et al., 2003, Stokes et al., 2011) with an EC_{50} of approximately 9.4 μM at the latter (Stokes et al., 2011). The agonists 2-MeSATP and CTP are also both active at the rat and human receptors, but βγ-MeATP is not (Stokes et al., 2017).

Antagonists

Several selective antagonists for P2X4 are commercially available: PSB-12062 (Hernandez-Olmos et al., 2012), 5-BDBD (Balázs et al., 2013), and BX430 (Ase et al., 2015). Another phenoxazine derivative, PSB-12054, was shown to be increasingly potent at human P2X4 receptors but was less active at rat and mouse P2X4 and also inhibited human P2X1 receptors (Hernandez-Olmos et al., 2012). PSB-12062 is of similar potency to the non-specific P2X receptor antagonist, TNP-ATP, with an IC_{50} of 1.38 μM for PSB-12062 and 1.46 μM for TNP-ATP at the human receptor (Hernandez-Olmos et al., 2012). The antagonists 5-BDBD and BX430 are more potent, with IC_{50} values of 1.2 μM and 550 nM respectively (Balázs et al., 2013, Ase et al., 2015). A novel antagonist, NP-1815-PX, was found to inhibit human, rat, and mouse P2X4 receptors with an IC_{50} of approximately 260 nM at the human receptor (Matsumura et al., 2016). In addition to this, NP-1815-PX was able to reduce neuropathic pain in mouse models when administered via a parenteral route (Matsumura et al., 2016). As mentioned previously, P2X4 receptors have also been shown to be inhibited by ethanol. Ethanol at a concentration of 50 mM has been shown to shift the concentration response curve to ATP to the right, reducing the EC_{50} from approximately 9.1 μM to 16 μM at the rat receptor expressed in oocytes (Xiong et al., 2000). PPADS is active at human and rat P2X4 receptors, but not mouse P2X4 receptors, and suramin is not an effective antagonist of mouse, rat, or human P2X4 (Jones et al., 2000). The naturally occurring bile acid, taurodeoxycholic acid, is able to inhibit human P2X4 receptors expressed in oocytes by stabilising the receptor's closed state (Ilyaskin et al., 2019). A neurosteroid, pregnanolone, was found to inhibit currents mediated by the rat P2X4 receptor; pregnanolone sulphate, however, did not inhibit the P2X4 receptor (Codocedo et al., 2009).

Positive Allosteric Modulators

Perhaps the best-known positive modulator of P2X receptors, and one that was used to distinguish P2X4 from other receptor subtypes, is ivermectin (Khakh et al., 1999b). In one study, ivermectin has been shown to potentiate native rat P2X4 receptors by increasing the maximum response to ATP but not by decreasing the EC_{50} (Bowler et al., 2003), but another showed that ivermectin could both increase the maximum response and decrease the EC_{50} to ATP at P2X4 receptors expressed in oocytes (Khakh et al., 1999b); the species of P2X4 is not clear from this study, but is likely to be rat P2X4 given the date of publishing. Human P2X4 is also able to be potentiated by ivermectin, although the mechanism of potentiation is complex: this study suggests that there are two modes of ivermectin modulation, one where ivermectin (at lower concentrations) is able to increase the maximum response, and one where ivermectin (at higher concentrations) is able to increase the affinity for ATP (Priel and Silberberg, 2004). Ultimately, ivermectin is believed to both increase the maximum response and the affinity for ATP (Stokes et al., 2020). Several analogues of ivermectin have also been shown to potentiate rat P2X4 responses (Asatryan et al., 2014).

Several natural products can potentiate P2X4: the ginsenosides CK and Rd have been shown to potentiate human P2X4 (Dhuna et al., 2019) as has the bile acid lithocholic acid (Sivcev et al., 2020). Ginsenoside CK was able to increase the maximum response and the slightly increase the affinity to ATP of human P2X4 receptors expressed in HEK-293 cells using a dye uptake assay (YO-PRO-1); responses measured using the calcium assay FURA-2AM (expressed in both HEK-293 and 1321N1 astrocytoma cells) and patch-clamp electrophysiology (expressed in HEK-293 cells) were also increased (Dhuna et al., 2019). Lithocholic acid, similar structurally to ginsenoside CK in that they both have the same steroidal scaffold (see **Figure 1.4**), was able to potentiate P2X4-mediated currents, decreasing the EC_{50} value from 2.7 µM in the absence of lithocholic acid to 1.1 µM in the presence of 10 µM lithocholic acid (Sivcev et al., 2020).

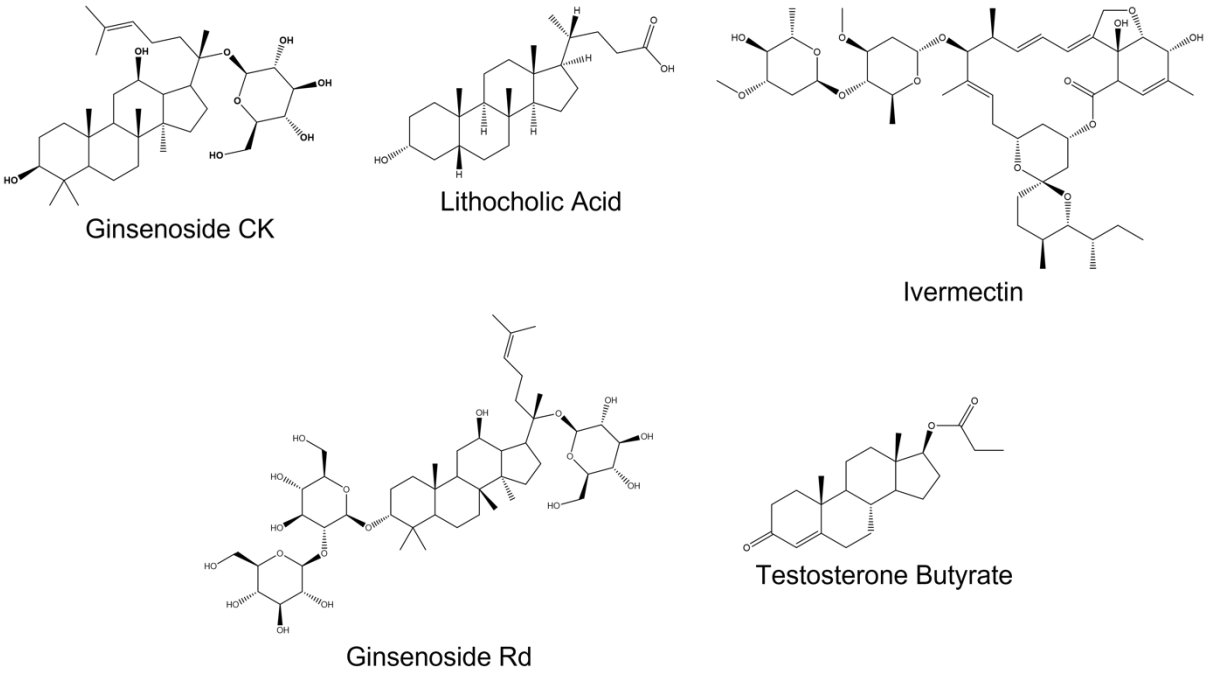

Figure 1.4 – Structures of several modulators of P2X4 receptors. Ginsenoside CK, ginsenoside Rd (Dhuna et al., 2019), lithocholic acid (Sivcev et al., 2020), ivermectin (Khakh et al., 1999b), testosterone butyrate (Sivcev et al., 2019). Structures were produced using ChemDraw Prime (PerkinElmer).

Again, similar in structure to both ginsenoside CK and lithocholic acid, several steroids have been shown to modulate the P2X4 receptor. Some neurosteroids, namely alfaxalone, allopregnanolone, and tetrahydrodeoxycorticosterone (THDOC), have been shown to positively modulate the rat P2X4 receptor expressed in either HEK-293 cells or oocytes (Codocedo et al., 2009). Several analogues of testosterone, in particular testosterone butyrate, testosterone valerate, and testosterone isovalerate, have been shown to increase responses produced by the rat P2X4 receptor to 1 μM ATP (Sivcev et al., 2019). Testosterone butyrate at a concentration of 30 μM was able to decrease the EC_{50} to ATP from approximately 2.4 μM to 0.7 μM, and in addition to this, reduced how quickly the receptor desensitised (Sivcev et al., 2019). Interestingly, testosterone valerate is thought to compete for a similar binding pocket to ivermectin despite their structural differences, due to a dose-dependent reduction in potentiation by 3 μM ivermectin in the presence of increasing concentrations of testosterone valerate (Sivcev et al., 2019). Cibacron blue, a derivative of reactive blue 2, is able to potentiate rat P2X4 currents induced by ATP when pre-applied at low concentrations (< ~50 μM) (Miller et al., 1998).

Effects of Metals, Cations, and pH

P2X4 is strongly inhibited by acidic pH, similar to most other P2X receptors (Stoop et al., 1997). At the rat receptor (expressed in HEK-293 and Chinese hamster ovary (CHO) cells, results in this study are from both cell types combined), currents were almost abolished at pH 6.3 (Stoop et al., 1997). Although increasing the pH to 8.3 potentiated responses slightly, the degree of potentiation was smaller than the degree of inhibition by pH 6.3 (Stoop et al., 1997). Similar effects were observed at the human P2X4 receptor (Clarke et al., 2000). Zinc, at concentrations of approximately 10 µM and less, potentiates responses to 5 µM ATP at the human P2X4 receptor (Garcia-Guzman et al., 1997a). Above this concentration, zinc appears to produce considerable inhibitory effects (Garcia-Guzman et al., 1997a). At the rat receptor, this dual potentiatory/inhibitory action of zinc was also observed (Nakazawa and Ohno, 1997). Another divalent cation, cadmium, showed a similar pattern (Coddou et al., 2005), although the degree of potentiation at concentrations of approximately 10 µM was much less than that observed with zinc at a similar concentration (Nakazawa and Ohno, 1997). Copper, however, inhibits the rat P2X4 receptor (Acuna-Castillo et al., 2000). Recently, molecular dynamics simulations have implicated magnesium, but not potassium, in stabilising the open state of the P2X4 receptor (Immadisetty et al., 2021, Immadisetty et al., 2022).

1.3.5 Pharmacology of P2X7

Agonists

The P2X7 receptor is the most insensitive to ATP of all the P2X receptors, requiring concentrations in the hundred micromolar range to be activated (Syed and Kennedy, 2012, Surprenant et al., 1996). Furthermore, the endogenous ligand ATP acts only as a partial agonist of P2X7 receptors (Gargett et al., 1997). BzATP, a synthetic derivative of ATP, is a full agonist at the human and rat P2X7 receptors with an EC_{50} of approximately 50 µM and 3 µM respectively measured using patch-clamp electrophysiology (Rassendren et al., 1997b). The rat P2X7 receptor is also sensitive to 2-MeSATP and ATPγS, but not to αβ-MeATP or βγ-MeATP (Surprenant et al., 1996). The sensitivity of the P2X7 receptor to agonists is largely dependent on the extracellular buffer used, with the presence of divalent cations decreasing the sensitivity of the receptor to agonists (Surprenant et al., 1996).

Antagonists

There are a considerable number of selective P2X7 antagonists available, including commercially; some have undergone clinical trials for inflammatory conditions such as arthritis (Stock et al., 2012), and more recently JNJ-54175446 is undergoing trials for the treatment of depression (ClinicalTrials.gov Identifier NCT04116606). JNJ-54175446 has activity at multiple species, including, human, rat, and mouse, with an IC_{50} value of approximately 1.5 nM at the human receptor (Letavic et al., 2017). A-740003 is selective for P2X7, but less potent than JNJ-54175446 (IC_{50} 40 nM at human P2X7 (Honore et al., 2006)).

Other antagonists include A-438079 (IC_{50} 251 nM at the human P2X7 receptor (Nelson et al., 2006)) and A-839977 (IC_{50} 21 nM at human P2X7 (Honore et al., 2009)), and A-804598 (IC_{50} 11 nM at human P2X7 (Donnelly-Roberts et al., 2009b); non-competitive antagonists include AZ10606120 (IC_{50} approximately 10 nM at human P2X7 (see Compound 17), expressed on human monocytic THP-1 cells (Ford et al., 2003)) KN-62 (IC_{50} of 12.7 nM at human P2X7, expressed in human lymphocytes (Gargett and Wiley, 1997)) and AZ11645373 (IC_{50} approximately 1 – 10 nM at human P2X7 (Stokes et al., 2006a). The P2X7 receptor is also strongly inhibited by dyes, including brilliant blue G which is capable of inhibiting the rat and human receptor with IC_{50} values of 10 nM and 200 nM respectively (Jiang et al., 2000).

The non-selective antagonists, PPADS and suramin, have some inhibitory activity at the human P2X7 receptor. PPADS has been shown to inhibit currents stimulated by BzATP with an IC_{50} of approximately 1 – 4 µM (Chessell et al., 1998, Honore et al., 2006), whereas suramin has reduced efficacy with an IC_{50} of approximately 70 µM (Chessell et al., 1998). Oxidised ATP has been shown to inhibit the mouse

P2X7 receptor, but requires long incubation times to be effective and is non-reversible (Murgia et al., 1993). TNP-ATP, another non-specific P2 receptor antagonist, inhibits P2X7 with an EC_{50} of approximately 3.55 µM at the chicken receptor (Kasuya et al., 2017). The crystal structure of this receptor with TNP-ATP bound reveals binding within the ATP binding pocket (Kasuya et al., 2017). Interestingly, the endogenous steroid 17β-estradiol has been shown to modulate P2X7 receptors (Cario-Toumaniantz et al., 1998). When expressed in CV-1 monkey kidney cells, currents induced by BzATP at the human P2X7 receptor were reduced by the presence of 17β-estradiol at concentrations between 1 µM and 10 µM, with almost complete inhibition of BzATP induced currents at 10 µM, yielding an IC_{50} value of approximately 3 µM (Cario-Toumaniantz et al., 1998).

Positive Allosteric Modulators

Given that activation of P2X7 receptors require such a high level of ATP to be activated, positive modulation of this receptor can reduce this threshold and lead to activation of the receptor at lower concentrations of ATP. Older studies show that tenidap, polymyxin B, and clemastine are all capable of potentiating the P2X7 receptor (Sanz et al., 1998, Ferrari et al., 2004, Nörenberg et al., 2011). Tenidap, at a concentration of 50 µM, has been shown to increase lucifer yellow uptake in the presence of 3 mM ATP when tested on J774 mouse macrophages (Sanz et al., 1998). In addition, LDH release by these macrophages was also enhanced by the presence of tenidap (Sanz et al., 1998). Pre-treatment of HEK-293 cells expressing the P2X7 receptor (the species is not clear) with 10 µg/mL polymyxin-B for 3 minutes increased responses to 1 mM ATP measured using the FURA-2AM assay (a measure of intracellular calcium) (Ferrari et al., 2004). Ethidium bromide uptake was also increased, suggesting that both the ion influx and pore formation properties of P2X7 can be potentiated by this compound (Ferrari et al., 2004). Clemastine, a first-generation antihistamine, increases inward currents and intracellular calcium responses in response to 300 µM ATP in HEK-293 cells transfected with the human P2X7 receptor (Nörenberg et al., 2011). YO-PRO-1 uptake, a key measurement of the pore-forming aspect of P2X7 receptor function, was also increased in the presence of 30 µM clemastine at ATP concentrations of both 300 µM (approximately EC_{50}) and 1 mM (approximately maximal) (Nörenberg et al., 2011).

Several natural products have been shown to potentiate the P2X7 receptor. A series of ginsenosides, triterpenoid glycosides found in *Panax ginseng*, were found to potentiate human P2X7 responses (Helliwell et al., 2015). Dye uptake in response to 100 µM ATP was enhanced by ginsenoside CK, and this was not seen in the presence of P2X7 antagonist AZ10606120 or A438079, suggesting that potentiation was indeed P2X7 dependent (Helliwell et al., 2015). In addition to dye uptake, both calcium responses and inward currents measured using patch-clamp electrophysiology were

enhanced by ginsenosides (Helliwell et al., 2015). Furthermore, the aglycone compound PPD (a precursor to ginsenoside CK) did not enhance dye uptake responses, suggesting that the sugar moiety is key to the compound's potentiatory nature (Helliwell et al., 2015). Further studies from the Stokes laboratory have proposed a binding pocket located in the central vestibule of the human P2X7 receptor (Bidula et al., 2019b) and a structure-activity relationship for determining the activity of ginsenosides (and structurally similar glycosides) at the human P2X7 receptor (Piyasirananda et al., 2021). Residues in the central vestibule region proposed to make polar contacts with ginsenoside CK include D318, N100, and S60. Mutating residues D318, L320, and S60 abolished potentiation by ginsenosides CK and Rd in the YO-PRO-1 and FURA-2AM assays, with reduced potentiation of inward currents by ginsenoside CK at the D318A, D318L, and S60A mutants (Bidula et al., 2019b). With regards to the structure-activity relationship, it was determined that a glucose sugar moiety must be present at either C3 or C20, with *S*-stereochemistry at the C20 position (Piyasirananda et al., 2021). In addition, C6 must be unsubstituted (Piyasirananda et al., 2021) (see **Figure 1.5**).

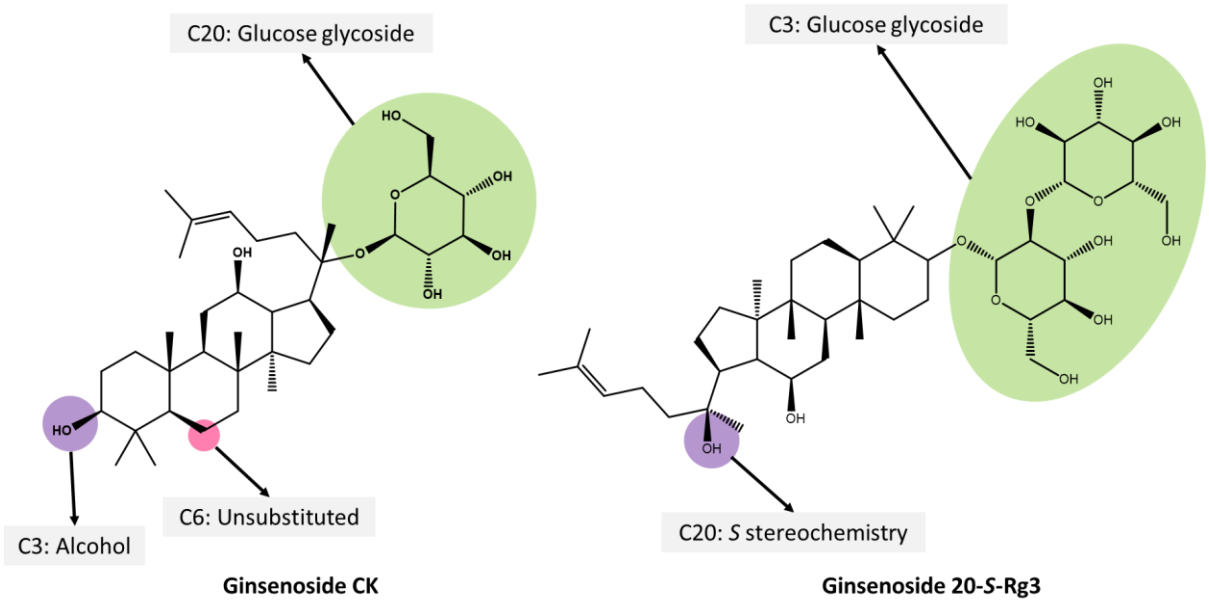

Figure 1.5 - Proposed structure activity relationship for ginsenosides at hP2X7. Glucose moieties are highlighted in green, whereas hydroxyl groups are highlighted in purple. C6 (shown in pink) should remain unsubstituted. Adapted from Piyasirananda *et al*, 2021 (Piyasirananda et al., 2021).

Other natural products that have shown activity at the P2X7 receptor include garcinolic acid and agelastine, both of which have been shown to potentiate both intracellular calcium measurements and YO-PRO-1 dye uptake (Fischer et al., 2014). Ivermectin, a known potentiator of P2X4, has also

been suggested to potentiate human, but not mouse, P2X7 (Nörenberg et al., 2012). In this study, ivermectin was able to increase the maximum current in response to ATP, but did not alter the EC_{50} value (Nörenberg et al., 2012). Furthermore, ivermectin at a concentration of 50 µM was able to potentiate calcium responses measured using Fluo-4 (Nörenberg et al., 2012). There was minimal potentiation observed with 3 µM ivermectin (Nörenberg et al., 2012). Potentiation observed with 50 µM ivermectin in combination with 1 mM ATP was abolished with the addition of the P2X7 antagonist A438079, suggesting that the potentiation is P2X7-dependent; conflicting with this, YO-PRO-1 responses, often used to interpret P2X7 receptor activity, were not potentiated by ivermectin at a concentration of 30 µM (Nörenberg et al., 2012). This conflicting evidence between assays was confirmed by Fischer *et al*, who showed that calcium responses mediated by 1 mM ATP measured using the Fluo-4 assay were potentiated by 12.5 µM ivermectin, but YO-PRO-1 uptake was not (Fischer et al., 2014). In both cases, ivermectin was pre-applied to cells before the addition of ATP (Nörenberg et al., 2012, Fischer et al., 2014).

Recently, small molecule HEI3090 has been suggested to potentiate P2X7, and as a result improve outcomes in models of non-small cell lung cancer (Douguet et al., 2021). At the mouse receptor, HEI3090 has been shown to increase both calcium responses and uptake of the dye TO-PRO-3 when co-applied with 333 µM ATP, although full concentration response curves have not been produced (Douguet et al., 2021). Co-treatment of HEI3090 with an anti-PD-1 antibody resulted in improved outcomes in lung cancer models in mice compared to the anti-PD-1 antibody alone, highlighting a therapeutic role for potentiation of P2X7 in cancer (Douguet et al., 2021). Another small molecule, GW791343, potentiates the rat P2X7 receptor but not the human P2X7 receptor (Michel et al., 2008). Instead, at hP2X7 GW791343 acts as a non-competitive antagonist with an IC_{50} of between 63 – 126 nM (Michel et al., 2008). Potentiation of the rat receptor was observed in the presence of both ATP and BzATP, inducing a leftward shift in the concentration response curve and subsequent reduction in the EC_{50} value but no increase in the maximum response was observed (Michel et al., 2008).

Effects of Metals, Cations, and pH

The P2X7 receptor is strongly inhibited by divalent cations; the presence of magnesium in extracellular buffer greatly reduces the EC_{50} value to agonists at the human P2X7 receptor, with an IC_{50} value of approximately 600 µM (Rassendren et al., 1997b). Although permeable to calcium, responses mediated by the P2X7 receptor are also diminished in the presence of 2 mM $CaCl_2$ compared to responses in 0.3 mM $CaCl_2$ (Rassendren et al., 1997b). In addition, the receptor is also inhibited by acidic pH independently of which agonist (ATP or BzATP) is used (Flittiger et al., 2010).

At the rat P2X7 receptor, both zinc and copper exhibit inhibitory effects (Moore and MacKenzie, 2008). Interestingly, this effect is not observed at the mouse receptor: instead, 300 μM zinc appears to potentiate responses to ATP (Moore and MacKenzie, 2008). Whilst there appears to be some degree of leftward shift with BzATP in the presence of 300 μM zinc at the mouse receptor, the maximum response is reduced, although 100 μM zinc appears to potentiate BzATP responses at the mouse receptor (Moore and MacKenzie, 2008). Unlike zinc, copper consistently inhibits both rat and mouse P2X7 responses to either ATP or BzATP (Moore and MacKenzie, 2008). Inhibitory effects of divalent metal cations have also been determined at the human P2X7 receptor, with nickel, zinc, and copper ions dose-dependently reducing YO-PRO-1 uptake in HEK-293 cells transfected with the human P2X7 receptor (Fujiwara et al., 2017). There are several proposed mechanisms by which divalent cations inhibit the P2X7 receptor: one is that the active form of ATP is ATP^{4-} (Cockcroft and Gomperts, 1979), and that divalent cations reduce the amount of free, active ATP by binding to ATP^{4-}, hence reducing the amount of available ligand for the receptor (Jiang, 2009). Another is that divalent cations act as an allosteric modulator, reducing the affinity of ATP binding to the receptor (Virginio et al., 1997). More recently, sites thought to be involved in modulation of the receptor by Mg^{2+} and Zn^{2+} have been identified in the crystal structure of an invertebrate P2X channel, with the M2 site directly overlapping the ATP binding pocket (Kasuya et al., 2017). The identification of two separate pockets suggests that there may be multiple mechanisms involved; one by which allosteric modulation of the receptor by divalent cations is possible, and another where free ATP and ATP bound to divalent cations (e.g. $MgATP^{2-}$) compete for the orthosteric ligand site (Kasuya et al., 2017).

1.4 Natural Products

The natural world offers a continual source of inspiration for novel medicines; indeed, many therapies used worldwide for a number of conditions originate from natural products. One of the most well-known examples is aspirin, derived from salicin (Desborough and Keeling, 2017). Famously, Edward Stone, an English clergyman, treated his fever by chewing on the bark of the willow tree in the mid-18th century (Stone, 1763). Other famous examples of drugs originating from the natural world include penicillin, a gram-positive antibiotic produced by the fungus *Penicillum notatum*, morphine, a strong painkiller derived from the opium poppy *Papaver somniferum*, and digoxin, a cardiac glycoside derived *Digitalis lanata* (IARC, 2016). Many cancer therapies also owe their origins to the natural world: paclitaxel was originally isolated from the Pacific yew (*Taxus brevifolia*), although demand exceeded supply and now the drug is made via a semi-synthetic route using the more widely abundant European yew (*Taxus baccata*) (Gennari et al., 1997, Goodman et al., 2001). Other therapies include vincristine and vinblastine, both derived from the Madagascan periwinkle (*Catharanthus roseus*), and bleomycin, a bacterial anticancer agent from *Streptoalloteichus hindustanus* (Dias et al., 2012, Demain and Vaishnav, 2011). Camptothecin is derived from the Chinese happy tree (*Camptotheca spp.*), a plant used in traditional Chinese medicine for a variety of ailments (Li and Zhang, 2014) although more recently camptothecin (and related topoisomerase inhibitors) are used to treat a variety of cancers, including colorectal, uterine, and lung cancer (Demain and Vaishnav, 2011). **Table 1.2** summarises a number of natural product therapeutics and their origins.

Table 1.2 — Examples of natural product drugs used clinically. References: 1. A Historical Overview of Natural Products in Drug Discovery (Dias et al., 2012). 2. Total Synthesis of Vinblastine, Related Natural Products, and Key Analogues and Development of Inspired Methodology Suitable for the Systematic Study of Their Structure–Function Properties (Sears and Boger, 2015). 3. Natural products for cancer chemotherapy (Demain and Vaishnav, 2011). 4. Camptothecin and taxol: from discovery to clinic (Wall and Wani, 1996). 5. Colchicine: an ancient drug with novel applications (Dasgeb et al., 2018). 6. Bioconversion of mevastatin to pravastatin by various microorganisms and its applications – A review (Syed and Ponnusamy, 2018). 7. Some Drugs and Herbal Products (IARC, 2016)

Drug Name	Origin	Indication
Aspirin[1]	Plant (*Salix alba*)	Pain Thrombosis
Bleomycin[3]	Bacterium (*Streptoalloteichus hindustanus*)	Cancer
Camptothecin[3, 4]	Plant (*Camptotheca acuminata*)	Cancer
Colchicine[5]	Plant (*Colchicum autumnale*)	Gout
Digoxin[7]	Plant (*Digitalis lanata*)	Heart Failure
Lovastatin[6]	Fungi (*Monascus ruber/Aspergillus terreus*)	High Cholesterol
Mevastatin[6]	Fungi (*Penicillium citrinum/Penicillium brevicompactum*)	High Cholesterol
Morphine[1]	Plant (*Papaver somniferum*)	Pain Cough
Paclitaxel[1, 4]	Plant (*Taxus brevifolia*)	Cancer
Penicillin[1]	Fungus (*Penicillim notatum*)	Bacterial Infection
Pilocarpine[1]	Plant (*Pilocarpus jaborandi*)	Glaucoma Sjögren's syndrome
Quinine[1]	Plant (*Cinchona succirubra*)	Malaria
Vinblastine[2]	Plant (*Catharanthus roseus*)	Cancer
Vincristine[2]	Plant (*Catharanthus roseus*)	Cancer

1.4.1 Ginsenosides

Another plant used extensively in traditional Chinese medicine is ginseng (*Panax ginseng*), used for thousands of years in its native Asia (Mancuso and Santangelo, 2017). With its diverse range of applications, it's no wonder that ginseng is seen as a 'cure-all' plant – the genus *Panax* itself is derived from the Greek 'panacea' (Wee et al., 2011). Several varieties of ginseng belong to the genus *Panax (Hou et al., 2021); Panax ginseng,* or Asian ginseng, is native to the mountainous regions of far east Russia, northeastern China, and North Korea (USDA et al., 2023a, Hou et al., 2021), with other species including *Panax notoginseng*, which is native to southern China and Vietnam (USDA et al., 2023b, Hou et al., 2021), and *Panax japonicus*, which is native to Japan (Baeg and So, 2013), used across Asia in traditional medicine. A further variety, *Panax quinquefolius*, is native to North America (Baeg and So, 2013). Other herbal products are marketed as 'ginseng', such as Siberian ginseng (*Eleutherococcus senticosus*), although these are not from the genus *Panax* and do not contain the same bioactive compounds as true ginseng plants (Mancuso and Santangelo, 2017). Traditionally, ginseng is consumed in several ways. In Korea, two main preparation techniques exist: red ginseng is prepared by steaming fresh ginseng root and then subsequent drying, whereas white ginseng is the dried root (Koh et al., 2015). Red ginseng is often subject to further processing, after which it can then be consumed as a supplement in either tablet or capsule form, although other methods of preparation such as powders, extracts, drinks, and sweets are also available (Baeg and So, 2013).

The bioactive compounds found in ginseng are termed ginsenosides; these are triterpene glycosides mostly derived from either protopanaxadiol (PPD) or protopanaxatriol (PPT) depending on the location of hydroxyl groups within the compounds (**Figure 1.6**) (Mancuso and Santangelo, 2017). Their native role as saponin-type molecules is in plant defence (Osbourn, 1996, Leung and Wong, 2010). Ginsenosides have been explored for their antifungal properties, with particular activity against *Alternaria panax* (Alternaria blight) (Nicol et al., 2002) and *Candida albicans* (Sung and Lee, 2008). In addition, their bitter taste makes them unpleasant for consumption, conveying antifeedant properties (Leung and Wong, 2010). Furthermore, ginsenosides may act to mimic ecdysteroids, hormones involved in insect moulting and metamorphosis, disrupting the life cycle of predatory insects (Leung and Wong, 2010).

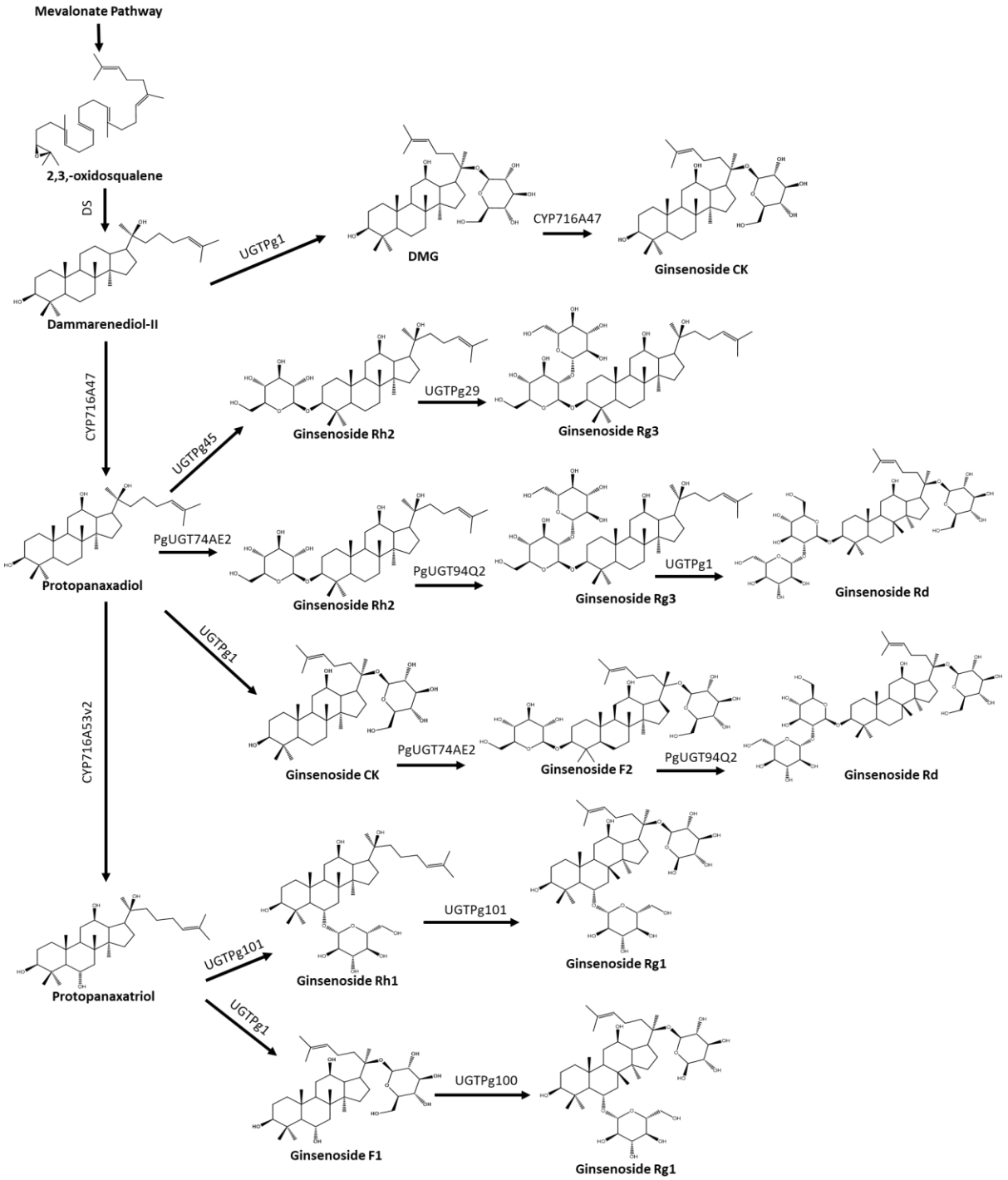

Figure 1.6 – Biosynthesis pathway of ginsenosides. Enzymes involved in the pathway are shown above or next to arrows. Enzyme abbreviations are as follows: dammarenediol synthase (DS), UDP-glycosyl transferase (UGTP), cytochrome P450 (CYP). Adapted from Yang *et al,* 2018 (Yang et al., 2018).

In *Panax ginseng*, ginsenosides are found throughout the plant, including in the leaves, roots, and stem, where they contribute to plant defence mechanisms (Chen et al., 2018). Distribution in *Panax ginseng* tends to be greater in the roots and rhizome of the plant compared to the leaves and stem,

with the most abundant ginsenosides in the rhizome being Rb1, Rg1, malonylginsenoside Rb1 (mRb1), Re, Rf, Rb2, mRb2, Rc, and mRc (Hou et al., 2021). Interestingly, ginsenosides Rb1 and mRb1 were not found in the leaves or stem of the plant, despite being two of the most abundant in the root systems - instead, the leaves contained varying concentrations of ginsenosides Re, Rg1, Rd, mRd, Rb2, mRb2, and Rc, whereas the stem contained ginsenosides Re, Rg1, and mRd at generally lower concentrations than those found in other plant tissues (Hou et al., 2021). In addition to variation between plant tissues, processing can affect resulting ginsenoside concentrations. Ginseng root samples collected from four regions in South Korea were analysed for their ginsenoside content as either fresh, air-dried, or steamed and air-dried samples (Koh et al., 2015). In fresh ginseng, the most concentrated ginsenosides present were found to be ginsenosides Rg1, Re, Rb1, and Rb2, whereas ginsenosides Rg1 and Rb1 were most prevalent in processed samples (Koh et al., 2015). Interestingly, despite processing largely leading to a decline in the total amount of ginsenoside compounds present, some ginsenoside concentrations increased following processing (Koh et al., 2015). One such ginsenoside is Rb1, which was found to increase in concentration in all samples following steaming and air-drying (Koh et al., 2015). Ginsenoside Rg2 was found at low levels in fresh samples, and processing by either air-drying or steaming followed by air-drying resulted in an almost complete elimination of this ginsenoside. In samples from two of the four regions analysed (regions B and C), air-drying was found to dramatically increase the concentration of ginsenoside Rg3, whereas samples from regions A and D saw a decrease in the concentration of this ginsenoside (Koh et al., 2015). These differences in results highlight key variation in plants grown in different regions within the same country; indeed, these differences may be even greater between *Panax ginseng* plants grown in different countries.

Although many ginsenosides exist within the plant itself, metabolism of these compounds can result in further pharmacologically active compounds: some ginsenosides, such as Rg3 and F1, are the products of deglycosylation of other ginsenosides (namely Rd and Rg1 respectively in this case) (Dong et al., 2017), but perhaps the most notably pharmacologically active is compound K (also known as ginsenoside CK) (Mancuso and Santangelo, 2017). Ginsenoside CK does not ordinarily exist in the plant; instead, it is produced *in vivo* following oral administration and subsequent metabolism of other ginsenosides by beta-glycosidases (Yan et al., 2014). The effects of ginsenoside CK have been investigated in a number of conditions, particularly cancer (Sharma and Lee, 2020). In HGC-27 human gastric carcinoma cells, ginsenoside CK has been shown to reduce proliferation whereas ginsenoside Rb1 was unable to produce the same effect (Wan et al., 2022). The underlying mechanisms for this were shown to be related to a decrease in the levels of the anti-apoptotic protein Bcl-2 and an increase in the levels of pro-apoptotic proteins Bcl-2-associated X protein (Bax) and caspase-3 (Wan et al., 2022). A similar phenomenon has been observed in two human colorectal cancer cell lines (HCT-116

and SW-480), whereby proliferation was reduced by increasing concentrations of ginsenoside CK, but not ginsenoside Rb1, in both cell lines, at concentrations >30 μM (Wang et al., 2012). Furthermore, the proportion of cells treated with either 30 μM or 50 μM CK that were apoptotic was greater than the control and those treated with 50 μM Rb1 (Wang et al., 2012). These effects are not limited to alimentary canal cancers; treatment of HeLa human cervical cancer cells with ginsenoside CK resulted in arresting of the cell cycle in the G_0/G_1 phase, accompanied by an increase in the production of reactive oxygen species and reduced proliferation and metastasis (Yin et al., 2021). An increase in reactive oxygen species was also measured in human breast cancer cell lines treated with ginsenoside CK (Zhang et al., 2022). Furthermore, ginsenoside CK was able to reduce the growth rate of both high and low glutamine-dependent cell lines, including the high glutamine-dependent triple negative breast cancer cell line MDA-MB-231, and increased expression of cleaved pro-apoptotic proteins including caspase-3, caspase-9, and PARP (Zhang et al., 2022). These effects have also been measured *in vivo*, with the combination of ginsenoside CK and γ-ray radiation reducing tumour volume in mouse models of human lung cancer compared to either treatment alone, although each treatment alone was also able to reduce the tumour volume compared to the control (Chae et al., 2009).

Outside of cancer, ginsenosides have also been shown to have potential in a number of other conditions (Xiang et al., 2008). One of the key properties of traditional ginseng use is its anti-inflammatory potential. Ginsenoside Rb1, one of the most abundant ginsenosides found in the root of the plant, has been shown to inhibit TNF-α production in lipopolysaccharide (LPS)-stimulated mouse macrophages (a model of inflammation caused by bacterial challenge (Meng and Lowell, 1997)) (Cho et al., 2001). In addition, ginsenoside Rb1, along with the metabolite ginsenoside CK, has been shown to inhibit nuclear transcription factor κβ (NF-κβ, referred to as pp65 in this paper) activation in LPS-primed mouse macrophages and decrease production of pro-inflammatory cytokines, namely interleukin (IL)-1β, TNF-α, IL-6, and IL-10, in a 2,4,6-trinitrobenzene sulfonic acid (TNBS)-induced model of colitis in mice (Joh et al., 2011). Other ginsenosides, such as Rb2 and Rd, have also been shown to inhibit production of TNF-α, with ginsenoside Re directly inhibiting the interaction between LPS and toll-like receptor 4 (TLR4) on macrophages (Kim et al., 2017, Lee et al., 2012). These anti-inflammatory effects are interesting, given that ginsenosides act as positive modulators of P2X7 (Helliwell et al., 2015) and activation of this receptor on macrophages leads to the production of pro-inflammatory mediators (Savio et al., 2018). Nonetheless, the complex mechanisms by which ginsenosides interact with the immune system in both the inflammation and resolution phases is an interesting area of natural product research. Related to their role in inflammation, ginsenosides have been shown to improve outcomes in atopic dermatitis. Atopic dermatitis is characterised by pruritic and erythematous lesions due to increased inflammation in the skin; indeed, ginseng has historically

been used for its anti-inflammatory effects in such conditions (Lorz et al., 2020). One study found that treatment with a tablet form of Korean red ginseng reduced trans-epidermal water loss and eczema area and severity scores in participants, with a significant reduction in pruritis associated with atopic dermatitis (Kim et al., 2018). Reductions in topical product use was not significantly reduced in the treatment group compared to use prior to commencing the study (Kim et al., 2018). It is important to note, however, that this study was conducted for eight weeks on a small group (41 participants) – it would be interesting to assess the long-term impacts of ginseng supplementation. In addition, mice treated with oxazolone (a chemical used to simulate contact dermatitis) had reduced ear thickening following oxazole exposure when treated with ginsenosides Rg3, Rf, and Rh2, suggesting a reduction in inflammation-induced oedema (Bae et al., 2006).

Ginsenosides have been implicated in numerous other conditions, including the reproductive system, whereby ginsenoside Re has been found to increase sperm motility due to induction of nitric oxide (NO) synthase in both fertile and infertile (caused by asthenospermia) samples in a concentration dependent manner (Zhang et al., 2006). Through modulation of NO synthase, ginsenoside Rg3 has been shown to inhibit phenylephrine induced vasoconstriction of rat aortic rings, whilst ginsenosides Rb1, Rc, Re, and Rg1 did not have the same effect (Kim et al., 2003). In fatigue syndromes, ginsenosides have been shown to activate the phosphoinositide 3-kinase (PI3K)/protein kinase B (Akt) pathway, leading to a reduction in reactive oxygen species production and an improvement in fatigue symptoms in rat models of post-operative fatigue syndrome (POFS) (Zhuang et al., 2014). Moreover, ginsenoside Rg3 was found to increase exhaustive exercise time in mice by decreasing the accumulation of metabolites such as blood lactic acid and serum urea nitrogen, increasing glycogen levels in liver and muscle tissues, and protecting against oxidative stress by increasing expression of superoxide dismutase (SOD), glutathione peroxidase (GPx), and catalase (CAT) (Li and Chan, 2018). Individual ginsenosides and their effects can be explored further in this review by Xiang *et al* (Xiang et al., 2008)), whilst the therapeutic potential for ginseng and ginsenosides is summarised by Ratan *et al* (Ratan et al., 2021).

1.5 Aims and Objectives

P2X receptors offer novel drug targets for a wide variety of conditions given their diverse activity and widespread distribution throughout the body. Although commercially available, selective antagonists are available for the majority of P2X receptors (with the main exception of the P2X2 receptor), positive allosteric modulators for these receptors are less well understood. Positive allosteric modulation of P2X receptors has therapeutic potential: for P2X7, positive modulation of these receptors could enhance the immune response against intracellular pathogens such as *Chlamydiae* and *Porphyromonas gingivalis* and parasites such as *Toxoplasma gondii*, whereby P2X7-dependent increases in reactive oxygen species and acidification of intracellular organelles enhances elimination (Stokes et al., 2020). In P2X4 receptors, positive allosteric modulation, particularly by ivermectin, has been implicated in the treatment of alcohol misuse disorders (Khoja et al., 2018b). The potential of positive allosteric modulators at other P2X receptors is only beginning to be uncovered: positive modulation of P2X2 receptors could offer a novel treatment for vertigo and other balance disorders such as Ménière's disease (Takimoto et al., 2018), whilst positive allosteric modulation of P2X1 receptors could offer a novel, non-hormonal treatment for male infertility (Mulryan et al., 2000). Recently, several ginsenosides, the bioactive compounds found in *Panax ginseng*, have been shown to dramatically potentiate P2X7 receptors (Helliwell et al., 2015). They have also been shown to have activity at P2X4 receptors (Dhuna et al., 2019), although their activity at the other P2X receptors is unknown. Investigations into the binding of ginsenoside CK to the human P2X7 receptor have highlighted a potential binding pocket within the central vestibule region of the extracellular domain (Bidula et al., 2019b). Given that the ginsenosides have activity at both P2X7 and P2X4 receptors, it may be that potentiation is conserved throughout the P2X receptor family. To investigate this further, a rapid screening assay (FLIPR Membrane Potential Blue) will be used to screen a range of ginsenosides and related compounds at a variety of P2X receptors for activity. Although established assays for measuring ion channel function exist, such as calcium influx assays (FURA-2AM, Fluo-4) and dye uptake assays (YO-PRO-1 iodide, ethidium bromide), the varying properties of P2X receptors makes it difficult to use one assay across all receptor subtypes. For example, the P2X7 receptor can form a large, non-specific pore, and therefore dye uptake assays can be used to interpret receptor activity here, however, the P2X1 and P2X3 receptors are quickly desensitising, and dye uptake assays are not appropriate for these receptors. Although patch-clamp electrophysiology is often considered the 'gold-standard' when measuring ion channel activity (Di Virgilio et al., 2019), it is a difficult and time consuming technique. The FLIPR Membrane Potential Blue kit measures the change in voltage across the cell membrane, like patch-clamp electrophysiology, but instead uses a fluorescence plate reader and provides a rapid method to screen multiple compounds for activity. Furthermore, it provides an

option that can be used across the P2X receptor family: as it measures total ion movement across the cell membrane, it is not affected by calcium permeability, and is not dependent on the ability of the receptor to form a large pore. In addition, the binding pocket will be explored further in both the P2X4 and P2X2 receptors using mutagenesis studies, and the effects of mutating the binding pocket on receptor activity and potentiation by ginsenosides will be analysed. Finally, extended mutagenesis of the P2X7 central vestibule region will aim to enhance understanding of ginsenoside binding and modulation of the receptor by these compounds.

The specific aims of this thesis were:

- To validate the use of the FLIPR Membrane Potential Blue kit as a tool for investigating modulation of P2X receptors, including those that quickly desensitise.
- To screen a range of ginsenosides at P2X receptors to determine activity at each of them.
- To use site directed mutagenesis to investigate the central vestibule region in P2X4 and P2X2, including resulting receptor activity and modulation by ginsenosides.
- To use site directed mutagenesis to further investigate the proposed P2X7 binding pocket, including cysteine mutagenesis to investigate accessibility of the central vestibule.

By investigating these points, the FLIPR Membrane Potential Blue kit will enable assessment of multiple P2X receptors, irrespective of their desensitisation properties, without having to utilise difficult techniques such as patch-clamp electrophysiology. Ginsenoside activity will be explored further across the P2X receptor family, helping to identify whether modulation by ginsenosides is receptor specific or a conserved effect. Knowledge of the proposed binding pocket will be enhanced, allowing for future development of novel, specific modulators of P2X receptors.

Chapter 2 – Materials and Methods

Materials

2.1 Agonists

- Adenosine 5’-triphosphate (ATP) (Sigma Aldrich)
- 2'(3')-O-(4-Benzoylbenzoyl)adenosine-5'-triphosphate (BzATP) (Sigma Aldrich)
- Adenosine 5’-diphosphate (ADP) (Sigma Aldrich)
- Cytidine 5’-triphosphate (CTP) (Sigma Aldrich)
- α,β-Methyleneadenosine 5’-triphosphate (αβ-MeATP) (Tocris Bioscience)
- Uridine 5’-triphosphate (UTP) (Sigma Aldrich)
- Uridine 5’-diphosphate (UDP) (Sigma Aldrich)

2.2 Antagonists

- General P2X
  - Suramin (Tocris Bioscience)
  - Pyridoxal phosphate-6-azo(benzene-2,4-disulfonic acid) (PPADS) (Tocris Bioscience)
- P2X7
  - AZ10606120 (Tocris Bioscience)
  - AZ11645373 (Sigma Aldrich)
  - A839977 (Tocris Bioscience)
  - JNJ54175446 (Tocris Bioscience)
- P2X4
  - 5-BDBD (Tocris Bioscience)
  - PSB12062 (Sigma Aldrich)
  - BX430 (Tocris Bioscience)
- P2X2
  - Reactive Blue 4 (Sigma Aldrich)

2.3 Reagents

- Dimethyl sulfoxide (DMSO) (Sigma Aldrich)
- Ethanol (Sigma Aldrich)

2.4 Ginsenosides and Related Structures

All from Chemfaces (Wuhan, Hubei, China) with the exception of ginsenoside CK which is either from Chemfaces or Biosynth (Carbosynth, MG33283).

- CK
- F2
- F1
- Rb1
- PPD
- PPT
- Rd
- 20-*S*-Rg3
- 20-*R*-Rg3
- 20-*S*-Rh2
- 20-*R*-Rh2

2.5 Glycosides

Either from Chemfaces (Wuhan, Hubei, China) or Chengdu Must Bio-Technology Co. Ltd. (Chengdu, Sichuan, China).

- Daucosterol
- Glycyrrhizic acid
- Stevioside
- Mogroside V
- Esculentoside
- Stevenleaf
- Gypenoside XLIX
- Gypenoside XVII
- Oleanic Acid

2.6 Steroids

- Allopregnanolone (Sigma Aldrich)
- Pregnenolone sulphate (Sigma Aldrich)

- 17β-estradiol (Sigma Aldrich)
- Progesterone (Sigma Aldrich)
- Alfaxalone (NCI Chemical Repository)
- Dehydroepiandrosterone (DHEA) (NCI Chemical Repository)
- Tetrahydrocortisol (NCI Chemical Repository)
- Testosterone (Sigma Aldrich)
    - AB1 – Andrew Beekman modified testosterone glucoside, produced by Dr. Andrew Beekman, University of East Anglia.
- Cholesterol (Sigma Aldrich)
- Pregnanolone (Sigma Aldrich)

2.7 Other Modulators and Dyes

All purchased from Sigma Aldrich (Merck).

- Ivermectin
- Amaranth
- Allura Red AC
- Brilliant Black

2.8 Assay reagents

- Calcium Assays
    - FURA-2AM
        - (+)-Sulfinpyrazone (Sigma-Aldrich)
        - FURA-2 AM (HelloBio)
        - HBSS (Sigma Aldrich)
- Dye Uptake Assays
    - YO-PRO-1
        - YO-PRO-1 iodide (Oxazole Yellow, HelloBio)
    - Ethidium Bromide
        - Ethidium Bromide (Sigma Aldrich)
    - TO-PRO-3
        - TO-PRO-3 iodide (Fisher Life Sciences)
- Membrane Potential Assays
    - Membrane Potential Blue
        - FLIPR Membrane Potential Assay Kit (Blue), Molecular Devices
    - Membrane Potential Red

- FLIPR Membrane Potential Assay Kit (Red), Molecular Devices

- MTS Reagents
  - Sulforhodamine methanethiosulfonate (referred to as MTS-rhodamine) (Cambridge Biosciences)
  - N-Biotinylaminoethyl methanethiosulfonate (referred to as MTSEA-biotin) (Cambridge Biosciences)

2.9 Buffer components

All available from either Sigma-Aldrich (Merck) or Fisher Scientific.

- NaCl
- HEPES
- D-Glucose
- KCl
- $MgCl_2$
- $CaCl_2$
- milli-Q water
- NaOH
- HCl

2.10 Cells

HEK-293 cells were from the University of Sheffield, UK.

Methods

2.10 Cell Culture

Experiments were conducted on human embryonic kidney (HEK-293) cells maintained in Dulbecco's Modified Eagle's Medium/F-12 media (DMEM/F-12, Gibco) supplemented with 10% foetal bovine serum (FBS, either Gibco (ThermoFisher Scientific) or PAN Biotech), 100 U/mL penicillin and 100 µg/mL streptomycin (Life Technologies, Fisher Scientific). Cells were kept at 37°C in a humidified 5% CO_2 incubator. Cells transfected with wild-type or mutant human P2X4 or P2X7 were maintained in medium outlined as above supplemented with 400 µg/mL G418 (Sigma). Cells transfected with wild-type or mutant human P2X2a were maintained in medium outlined as above supplemented with 400 µg/mL G418 and 1 mM $MgCl_2$.

Cells were kept in either 25 cm^2 or 75 cm^2 cell culture flasks and passaged twice weekly at approximately 90% confluency. Cell culture medium was removed, and cells were trypsinised with between 1-4 mL of either 0.05% Trypsin-EDTA in PBS (ThermoFisher Scientific) or 0.25 % Trypsin-EDTA, phenol red solution (ThermoFisher Scientific). Cells were incubated with trypsin for 5 minutes to allow detachment from the flask before being inactivated with 1-2 times the volume of media and transferred to sterile 15mL centrifuge tubes. Cell suspensions were then centrifuged at 300*g* for 5 minutes to form a visible pellet. The supernatant was discarded, and the remaining pellet resuspended in 1 mL of fresh DMEM/F-12 media for counting or re-seeding of cell culture flasks.

2.11 Transfection

HEK-293 cells were plated into 6-well plates (CytoOne, Starlab) at 15-120 µL of cell suspension per 2 mL of supplemented DMEM/F-12 medium 1-3 days prior to transfection. Immediately prior to transfection, if there were floating cells visible, media was replaced with 900 µL of fresh DMEM/F-12. If not, 1 mL of medium was removed to leave the cells in approximately 1 mL of medium. Transfection reagents were prepared in sterile microcentrifuge tubes containing 1 µg of plasmid DNA and 3 µL of Lipofectamine® 2000 (Invitrogen, ThermoFisher Scientific) in Opti-MEM™ reduced serum medium (ThermoFisher Scientific) per well of cells to be transfected. To prepare transfection reagents, a master mix of Opti-MEM™ was prepared. For each well to be transfected, 100 µL of Opti-MEM™ containing 3 µL of Lipofectamine® 2000 was prepared. Plasmid DNA was prepared in separate sterile microcentrifuge tubes at a concentration of 1 µg of DNA per 100 µL of Opti-MEM™. These were allowed to equilibrate for five minutes before 100 µL of the Lipofectamine® 2000 solution was added to each 100 µL of DNA solution. The total 200 µL of each DNA-lipid complex was allowed to equilibrate

for 15-20 minutes before being carefully added to each well of cells to be transfected in a dropwise spiral pattern to minimise disturbance to the cells. After 24 hours post-transfection, cells were inspected under a light microscope to determine cell viability before being trypsinised and counted for use in experiments.

2.12 Generation of Stable Cell Lines

HEK-293 cells transfected with human P2X7, P2X4 or P2X2 plasmid DNA were selected in supplemented DMEM/F-12 medium containing 800 µg/mL G418 (Life Technologies, Fisher Scientific) for approximately two weeks until non-transfected (native HEK-293) cells had died, leaving HEK-293 cells expressing the desired P2X receptor DNA and/or the neomycin resistance genes *APH (3') – I* and *APH (3') – II*. Single-cell cloning was performed via serial dilution according to the Corning serial dilution protocol and as outlined below (protocol available at https://www.corning.com/catalog/cls/documents/protocols/Single_cell_cloning_protocol.pdf, accessed 19/01/22). Single cells were identified 2-3 days post-plating and monitored for growth before being transferred to 12- (Falcon, Scientific Laboratory Supplies (SLS)) or 24- well (Jet Biofil) plates for further expansion. These G418 resistant populations were further selected by testing the degree of their response to agonists via a fluorescence assay (Membrane Potential Blue, Molecular Devices) or by expression via antibody staining and flow cytometry. Successful cell populations were identified as those that gave dose-dependent responses to ATP in the fluorescence assay or those that had a distinct shift in fluorescence in flow cytometry. Successful clones were then transferred to T25 cell culture flasks for expansion and maintained as outlined above.

2.13 Site directed mutagenesis

Primer Design

Primers were designed according to the QuikChange II Site Directed Mutagenesis Kit (200521, Agilent, US) protocol (available at https://www.agilent.com/cs/library/usermanuals/Public/200523.pdf, accessed 19/01/22) to be between 25 and 45 bases in length with a melting temperature greater than 78°C (calculated using the T_m equation specified within the protocol outlined above, also available as a calculator courtesy of David Kim at https://depts.washington.edu/bakerpg/primertemp/ (accessed 19/01/22)). Mutations were designed to make as little changes as possible to the original base sequence whilst resulting in the desired amino acid, with the mutations designed to be central within the primer sequence with approximately 10-15 bases either side. Primers had a GC content ≥ 40% and finished at either end on one or more G or C bases.

PCR

PCR was performed according to the following conditions: 95°C for one minute, followed by 18 cycles consisting of: 95°C for 50 seconds, 60°C for 50 seconds, and 68°C for 6 minutes, and finally one step of 68°C for 7 minutes. PCR was performed using PFU Ultra High-Fidelity DNA polymerase (QuikChange II Site Directed Mutagenesis Kit, Agilent) and products digested with Dpn1 for 1 hour at 37°C.

Transforming Bacteria

NEB® 5-alpha F'Iq Competent *E. coli* High Efficiency cells (C2992, New England Biolabs, UK) or JM109 Competent *E. coli* cells (L2001/L2005, Promega, UK) were transformed using 5µL of digested PCR product according to the QuikChange II Site Directed Mutagenesis Kit (200521, Agilent, US) protocol using LB broth (Fisher) in place of NZY$^+$ broth. Bacteria to be transformed were thawed on ice before being aliquoted into pre-chilled microcentrifuge tubes (50 µL per tube). Then, 5 µL of Dpn1 treated DNA was added to each tube and incubated on ice for 30 minutes. Following this, bacterial cells were heat shocked for 45 seconds at 42°C and put back on ice for two minutes. Transformed bacterial lines were grown in SOC media (Sigma-Aldrich) for 45 minutes at 37°C with shaking and then plated onto LB-agar (Sigma) plates containing the appropriate antibiotic at a concentration of either 100 µg/L for ampicillin or 50 µg/mL for kanamycin at 37°C overnight.

Expanding Colonies

Agar plates were inspected for colonies the day after plating. Discrete colonies were picked and transferred to 50 mL centrifuge tubes containing LB broth and the appropriate antibiotic at a concentration of 50-100 µg/mL. Colonies were then cultured overnight in LB-broth containing the appropriate antibiotic in a shaking incubator set to 37°C, 190-225 rpm.

Preparation of Plasmids

Plasmids were harvested from bacterial suspensions using the QIAprep Spin Miniprep Kit (27104, QIAGEN, Germany). Wash steps were performed using the centrifugation method as outlined in the QIAprep Kit protocol (available at https://www.qiagen.com/us/resources/download.aspx?id=56b0162c-23b0-473c-9229-12e8b5c8d590&lang=en, accessed 19/01/22). Resulting plasmid concentrations were determined using a NanoDrop Microvolume Spectrophotometer (ThermoFisher Scientific). The average of 1-3 readings was taken using the nucleic acid feature on the NanoDrop software (ND-1000) as the plasmid concentration in ng/mL. Plasmid sequences and mutations were then confirmed by sequencing performed by Mix2Seq (Eurofins Genomics).

2.14 Fluorescence assays

Cell Plating

To prepare plates for cell plating, 96-well plates (10212811, ThermoFisher Scientific) were coated with 50 µg/mL Poly-D-Lysine (PDL, P6407, Sigma-Aldrich) and left for at least one hour before being washed with sterile water and allowed to dry. Cells were plated in 100 µL of supplemented DMEM/F-12 (without antibiotic or $MgCl_2$ supplementation) the day prior to experimentation into PDL-coated 96-well plates at concentrations between $2x10^4$-$3x10^4$ cells per well. Plated cells were kept in a humidified 5% CO_2 incubator at 37°C until needed for experimentation, usually the following day.

Buffers

- Standard extracellular buffer (Etotal): 145 mM NaCl, 2 mM KCl, 2 mM $CaCl_2$, 1 mM $MgCl_2$, 13 mM glucose, 10 mM HEPES, pH 7.3-7.4, osmolarity 300–310.
- Low divalent cation buffer (ELDV): 145 mM NaCl, 2 mM KCl, 0.2 mM $CaCl_2$, 13 mM glucose, 10 mM HEPES, pH 7.3-7.4, osmolarity 300–310.
- No magnesium buffer (ECalcium): 145 mM NaCl, 2 mM KCl, 2 mM $CaCl_2$, 13 mM glucose, 10 mM HEPES, pH 7.3-7.4, osmolarity 300–310.

Dye Uptake Assays

YO-PRO-1 Iodide Measurements

The compound YO-PRO-1 iodide (Oxazole Yellow, Quinolinium, 4-((3-methyl-2(3H)-benzoxazolylidene)methyl)-1-(3-(trimethylammonio)propyl)-, diiodide) is a membrane impermeant dye known to fluoresce on intercalation with DNA (Ex: 490 nm, Em: 520 nm). It is used as a measure of activity of P2X receptors as it is thought to move through the P2X7 pore upon activation of the receptor (Karasawa et al., 2017). Cell medium was removed from the 96-well plate and replaced with 90 or 180 µL per well of low divalent cation buffer (ELDV) containing YO-PRO-1 iodide at a concentration of 2 µM. Cells in YO-PRO-1 iodide buffer were then warmed at 37°C for 5-10 minutes prior to experimentation. Compounds to be tested were made up at 10x final concentration in ELDV and injected onto cells 30-40 seconds into read time at a rate of between 2-4. YO-PRO-1 iodide fluorescence was measured using a Flexstation 3 Multimode Plate Reader (Molecular Devices) at 37°C and data analysed using SoftMax Pro v5.4 software (Molecular Devices). Fluorescence emission was

measured at 520 nm for 300 seconds (6 reads per well, PMT medium, interval 3.5 seconds) with an excitation wavelength of 490 nm. Data are plotted as the area under the curve (AUC) from 50-300 seconds, zero baseline 1 point and normalised to control response where appropriate.

TO-PRO-3 Iodide Measurements

Like YO-PRO-1 iodide, TO-PRO-3 iodide is a membrane impermeant dye known to fluoresce on intercalation with DNA (Douguet et al., 2021). Cell medium was removed from the 96-well plate and replaced with 180 µL per well of low divalent cation buffer (ELDV) containing TO-PRO-3 iodide at a concentration of 2 µM. Cells in TO-PRO-3 iodide buffer were warmed at 37°C for 5-10 minutes immediately prior to experimentation. Compounds to be tested were made up at 10x final concentration in ELDV and injected onto cells 40 seconds into read time at a rate of 2. TO-PRO-3 iodide fluorescence was measured using a Flexstation 3 Multimode Plate Reader (Molecular Devices) at 37°C and data analysed using SoftMax Pro v5.4 software (Molecular Devices). Fluorescence emission was measured at 665 nm for 300 seconds (6 reads per well, PMT medium, interval 3 seconds) with an excitation wavelength of 650 nm. Data are plotted as the AUC from 50-300 seconds, zero baseline 1 point and normalised to control response where appropriate.

Membrane Potential

The Membrane Potential Blue Kit (Molecular Devices) or Membrane Potential Red Kit (Molecular Devices) was reconstituted according to the manufacturer's instructions using either low divalent cation buffer (ELDV) or standard extracellular buffer (Etotal). This was then used diluted 1 in 2 with the respective buffer immediately prior to use unless otherwise stated. Cell medium was removed from the 96-well plate and replaced with 100 µL of membrane potential blue/red (MPB/MPR) buffer. Cells were incubated in this buffer for 30-45 minutes at 37°C in a humidified incubator with 5% CO_2. Cells in MPB/MPR buffer were then transferred to a FlexStation 3 plate reader (Molecular Devices) and warmed at 37°C for 5-10 minutes prior to experimentation. Fluorescence measurements were measured using a Flexstation 3 Multimode Plate Reader (Molecular Devices) and data analysed using SoftMax Pro v5.4 software (Molecular Devices). Fluorescence emission was measured at 565 nm for 120-200 seconds with an excitation wavelength of 525 nm (3 reads per well, PMT medium, interval 2 seconds). Agonists and screened compounds were made up at either 5x or 10x final concentrations in either ELDV or Etotal buffer and applied to cells after 20 seconds of read time at a rate of 2-4.

Dual Injection Screening

For dual injection screening experiments conducted in membrane potential blue, fluorescence emission was measured at 565 nm for a total of 180 seconds with an excitation wavelength of 525 nm (3 reads per well, PMT medium, interval 2 seconds). The compound to be screened was injected at 20 seconds, followed by a 60 second interval before the injection of the agonist ATP at 80 seconds (allowing for 60 seconds of pre-treatment with the compound before the application of ATP). Data were plotted as follows, before being normalised as a percentage of the resulting control response to produce final figures:

$$\boldsymbol{Membrane\ Potential\ Fluorescence}\ (AUC, 80 - 180s) =$$

$$(AUC\ 0 - 180s, zero\ baseline\ for\ 3\ points) - (AUC\ 0 - 80s, zero\ baseline\ for\ 3\ points)$$

This is outlined as a diagram in **Figure 2.1** below:

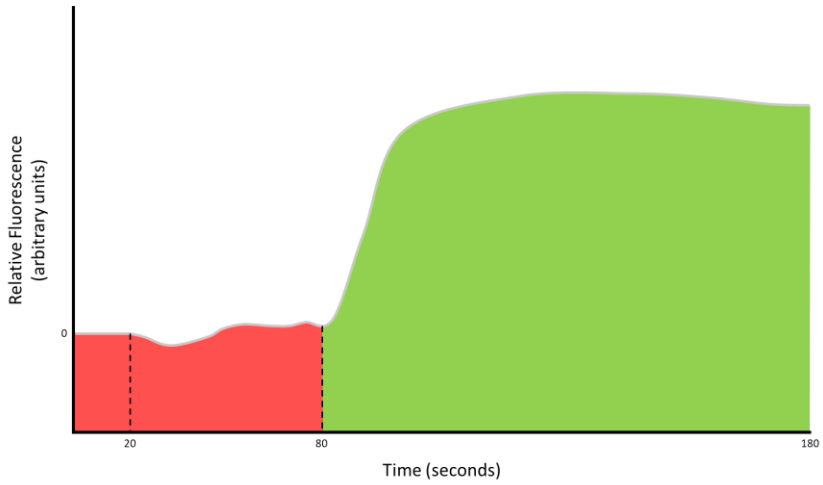

Figure 2.1 – Schematic diagram of how data for dual injection screening were plotted. Data were acquired between 0 and 180 seconds, with compounds applied at 20 seconds and ATP applied at 80 seconds. The area under the curve (AUC) between 0-80 seconds (zero baseline 3 points, shown in red) was subtracted from the total AUC for 0-180 seconds (zero baseline 3 points) to give the AUC value highlighted in green which was then plotted. The average of this value was taken for each experiment and normalised to the control response (DMSO) for final figures. Not to scale.

The AUC was plotted rather than max-min/min as this represents the full receptor response rather than being dependent on the initial peak response. Responses in quickly desensitising receptors differed to those observed for slowly desensitising receptors – quickly desensitising receptors gave an initial peak response followed by a decline in the response over time, whereas slowly or non-desensitising receptors gave a sustained response that plateaued (see representative data in **Figure 2.2)**. Therefore, the AUC was determined to give the best representation of the data. Furthermore, the method outlined in **Figure 2.1** allows for the ATP-mediated response, therefore the P2-receptor

dependent response, to be measured independently of any effects that the tested compound may have on fluorescence measurements itself. It also allows for the effects of the compound alone without applied ATP to be assessed.

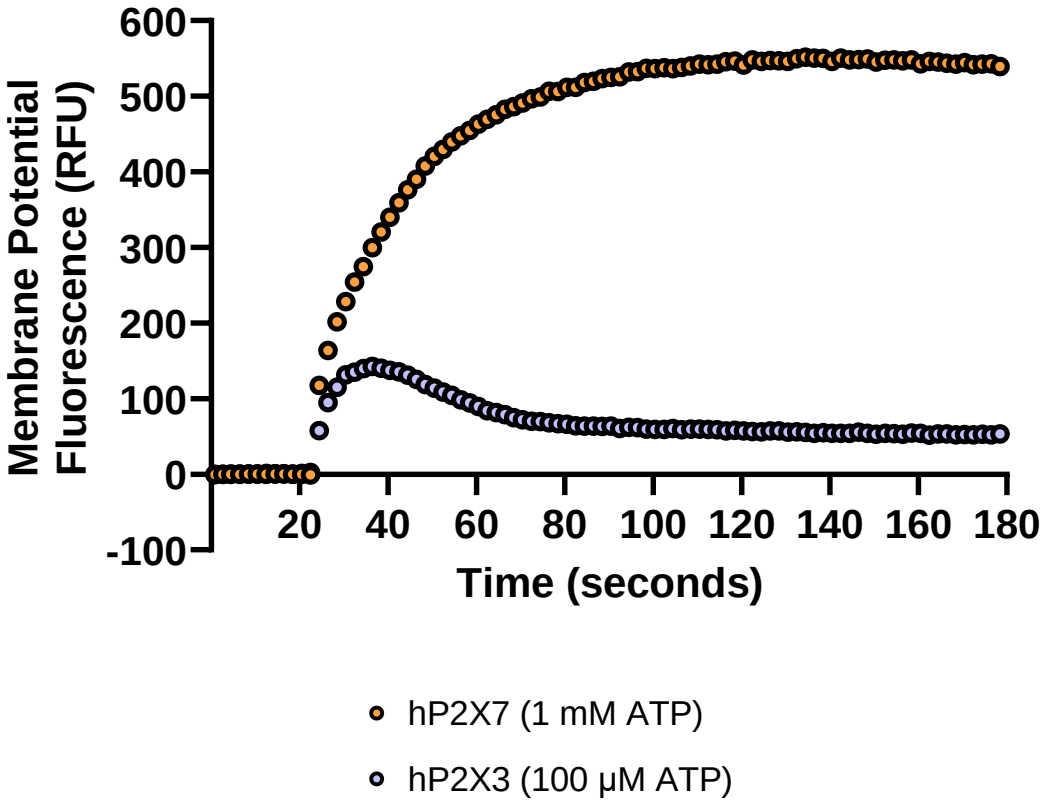

Figure 2.2 – Representative raw trace data showing the response to ATP in HEK-293 cells stably expressing either the human P2X7 or P2X3 receptor. The response to 1 mM ATP for HEK-hP2X7 is shown in orange, whereas the response to 100 µM ATP for HEK-hP2X3 is shown in light purple. In both cases, fluorescence readings were made over 180 seconds with ATP applied at 30 seconds. Data are plotted as average fluorescence values from three independent experiments.

FURA-2AM

Cells were loaded with 100µL of loading buffer per well (Hank's Buffered Saline Solution (HBSS, Gibco), ELDV, or Etotal containing 250µM sulfinpyrazone and 2µM Fura-2-acetoxymethyl (AM) calcium indicator dye (Hello Bio, UK)) and incubated for 45 minutes at 37°C with 5% CO_2. This allows the membrane-permeant FURA-2 AM ester to move into cells, after which it is cleaved by cellular esterases to reveal the active FURA-2 Ca^{2+} indicator dye (Martínez et al., 2017). After loading, the loading buffer was removed and replaced with 180µL per well of standard extracellular buffer (Etotal). Compounds to be tested were made up at 10x final concentration and were injected 40 seconds into read time at a rate of 2-4. Intracellular Ca^{2+} measurements were made using a Flexstation 3 Multimode Plate Reader (Molecular Devices) and data analysed using SoftMax Pro v5.4 software (Molecular Devices). Fluorescence emission was measured at either 510 or 520 nm for 300 seconds (3 reads per well, PMT medium, interval 3 seconds) with dual excitation wavelengths of 340nm and 380nm to give a ratio between Ca^{2+}-bound and Ca^{2+}-unbound FURA-2 respectively. Data are plotted as the AUC from 0-300 seconds, zero baseline 3 points (interpolate raw data checked) and normalised to control response where appropriate.

Dual Assay Readings

For some experiments, the FURA-2 calcium assay was performed simultaneously with a dye uptake assay (either TO-PRO-3 iodide or ethidium bromide uptake) to allow real-time direct comparisons between the two assays. In these cases, cells were loaded with either HBSS or ELDV containing 100 µM sulfinpyrazone and 2 µM FURA-2 AM for 45 minutes before being changed to a running buffer containing the dye to be measured.

FURA-2AM and TO-PRO-3 Iodide

For the FURA-2AM/TO-PRO-3 experiments, loading buffer was replaced with 180 µL per well of running buffer (ELDV containing 2 µM TO-PRO-3 iodide and 100 µM sulfinpyrazone). Both TO-PRO-3 fluorescence and intracellular calcium measurements were made using a Flexstation 3 Multimode Plate Reader (Molecular Devices). Fluorescence emission was measured at 510 nm (FURA-2) and 661 nm (TO-PRO-3) with excitation wavelengths of 340 nm, 380 nm (FURA-2), and 642 nm (TO-PRO-3). Compounds to be tested were made up at 10x final concentration in ELDV and injected onto cells 40 seconds into read time at a rate of 3. Fluorescence was measured using a Flexstation 3 Multimode Plate Reader (Molecular Devices) at 37°C and data analysed using SoftMax Pro v5.4 software (Molecular Devices).

FURA-2AM and Ethidium Bromide

For the FURA-2/EtBr experiments, loading buffer was replaced with 180 µL per well of running buffer (ELDV containing 1:1000 EtBr and 100 µM sulfinpyrazone). Both EtBr fluorescence and intracellular calcium measurements were made using a Flexstation 3 Multimode Plate Reader (Molecular Devices). Fluorescence emission was measured at 510 nm (FURA-2) and 600 nm (EtBr) with excitation wavelengths of 300 nm (EtBr), 340 nm, and 380 nm (FURA-2). Cells were warmed at 37°C for 5-10 minutes immediately prior to experimentation. Compounds to be tested were made up at 10x final concentration in ELDV and injected onto cells 40 seconds into read time at a rate of 3. Fluorescence was measured using a Flexstation 3 Multimode Plate Reader (Molecular Devices) at 37°C and data analysed using SoftMax Pro v5.4 software (Molecular Devices). Data are plotted as the AUC from 50-300 seconds, zero baseline 1 point and normalised to control response where appropriate.

2.15 Flow Cytometry

Expression

To quantify cell surface expression of hP2X4, cells were pelleted prior to resuspension in primary rabbit anti-P2X4 antibody at a dilution of 1:100 in PBS/0.5% BSA buffer (Bovine Serum Albumin (BSA), Fisher Scientific). Cells were incubated for 60 minutes on ice in the absence of light before a wash step using PBS/0.5% BSA buffer at 300 *g* for five minutes. Following this, cells were resuspended in goat anti-rabbit Alexa 488 at a dilution of 1:200 in PBS/0.5% BSA and incubated on ice in the absence of light for 30-60 minutes. Cells were again washed using PBS/0.5% BSA buffer at 300 *g* for five minutes before being resuspended in 300 µL 0.5% BSA/PBS buffer. Fluorescence was measured on a CytoFLEX flow cytometer (Beckman Coulter). Data were analysed using CytExpert Software (Beckman Coulter).

2.16 MTS-Reagent Experiments

Investigation of MTS-reagents on Cysteine Mutants – Fluorescence Assays

Cells were loaded with 100 µL per well of ELDV containing 2 µM FURA-2AM and 250 µM sulfinpyrazone per well for 43 minutes. Following this, 100 µL of ELDV buffer containing MTS-rhodamine at 2x final concentration (i.e., 6 µM for a final concentration of 3 µM when added to the running buffer) was added and incubated, together with the loading buffer, for the remaining two minutes before removal. This was then replaced with running buffer (180 µL per well of ELDV containing 250 µM sulfinpyrazone). Cells were then read according to the usual FURA-2AM protocol.

Investigation of MTS-reagents on Cysteine Mutants – Flow Cytometry

MTS-Rhodamine Labelling

Cells expressing the F322C mutant hP2X7 receptor were aliquoted into brown microcentrifuge tubes ($1x10^5$ cells per tube). Following this, 500 µL of ELDV containing 3 µM of freshly thawed MTS-rhodamine was added and cells incubated at room temperature for 5 minutes. After, cells were spun down using a microcentrifuge at 500 *g* for 3 minutes and resuspended in ELDV to remove excess MTS-rhodamine. Fluorescence was measured using a CytoFlex flow cytometer (Beckmann Coulter) using the PE-A channel with the following acquisition settings: FSC: 88, SSC: 121, FITC: 143, PE: 132, PC5.5: 25, PC7: 20, APC: 20, APC-A750: 20.

TO-PRO-3 Uptake Following MTSEA-Biotin Treatment

To assess the effect of MTS-reagents on potentiation by ginsenoside CK, cells were first incubated in 450 µL ELDV containing 1 µM TO-PRO-3 (this concentration was chosen as less than that used for Flexstation based experiments to reduce the chance of saturation) and either no MTS reagent or 100 µM MTSEA-biotin at 37°C for five minutes. After five minutes, 50 µL of ELDV containing ATP ± 10 µM CK, or ELDV buffer control, was added at 10x final concentration to allow for the dilution factor. Cells were incubated for a further five minutes at 37°C before being read on the flow cytometer using the APC-A channel with the following acquisition settings: FSC: 88, SSC: 121, FITC: 143, PE: 132, PC5.5: 25, PC7: 20, APC: 20, APC-A750: 20.

Imaging of Cells using MTS-Rhodamine

Cells were resuspended at $1x10^5$ cells per mL in ELDV. MTS-rhodamine was then added to 1 mL of cell suspension to give a final concentration of 3 µM and incubated at room temperature for two minutes. After this, cells were spun down using a microcentrifuge at 500*g* for 3 minutes and resuspended in 500 µL Etotal to maintain the receptor in the closed state (divalent cations present in Etotal would likely inhibit the activity of any ATP released as a result of cell disturbance). Cells were then washed a second time (spun down, resuspended in 500 µL Etotal, then spun down again) before finally being resuspended in 150 µL of Etotal and 10 µL pipetted onto glass slides for imaging. Images were captured using a Nikon Eclipse TE2000 Inverted Microscope with a TRITC filter and NIS-Elements software following 4 second exposure.

2.17 Molecular Docking

Molecular docking was performed by Dr Sam Walpole, UEA, using Glide (Schrödinger) and analysed by the doctoral candidate. Homology models are based on the crystal structure of zebrafish-P2X4 (PDB: 4DW1), unless otherwise specified, as this work was carried out before the cryo-EM structure of full-length rat P2X7 was published.

2.18 Data Analysis

Data were analysed using GraphPad Prism software, version 9.2. Data are plotted as mean ± standard error of the mean (SEM) and fitted with four-parameter non-linear regression curves unless otherwise stated. The four parameters used to fit the line are: maximum, minimum, EC_{50} (or IC_{50}), and the slope factor (Hill Coefficient). The equation for this is as follows:

$$Y = Bottom + (Top - Bottom)/(1 + 10\text{^}((LogEC50 - X) * HillSlope)).$$

Tables show average EC_{50} values ± standard deviation. Statistical tests used are stated in figure legends, with significance defined as *P<0.05, **P<0.01, ***P<0.001, and ****P<0.0001.

Chapter 3 – Screening Ginsenosides at P2X Receptors Using the Membrane Potential Assay

3.1 Introduction

Since purinergic receptors were first described in 1976 (Burnstock, 1976), there has been increasing interest in their roles in the body and subsequently as drug targets (Burnstock, 2018). Numerous clinical trials have been conducted on antagonists of P2X receptors; the first were antagonists of P2X7, thought to have a role in mediating inflammatory responses in arthritis (Stock et al., 2012). More recently, antagonists of the P2X2/3 receptor have been drawing increased attention for their potential role in chronic cough conditions (Morice et al., 2021a). Opioids act as cough suppressants, although they pose a global issue, with dependence and overdose key risks (Shipton et al., 2018, Reynolds et al., 2004), and so there is increasing desire to find alternate therapies. The P2X2/3 antagonist Gefapixant has shown promising results in clinical trials as a first-in-class drug, however, side effects of blocking these receptors can include substantial taste disturbances affecting compliance of patients (McGarvey et al., 2020, Birring et al., 2021a, Abdulqawi et al., 2015). A similar antagonist with increased selectivity for the homomeric P2X3 receptor over the heteromeric P2X2/3 receptor and therefore less taste disturbances, named BLU-5937, has also begun the clinical trial process and offers another alternative to opioids in the treatment of chronic cough (Birring et al., 2021b, Garceau and Chauret, 2019b). Most therapeutic investigations have been based around blocking the P2X receptors to minimise unwanted effects, however, there may also be a role in potentiating these receptors for therapeutic benefit (Stokes et al., 2020).

One group of modulators of P2X7 and P2X4 receptors are the ginsenosides (**Figure 3.1**).

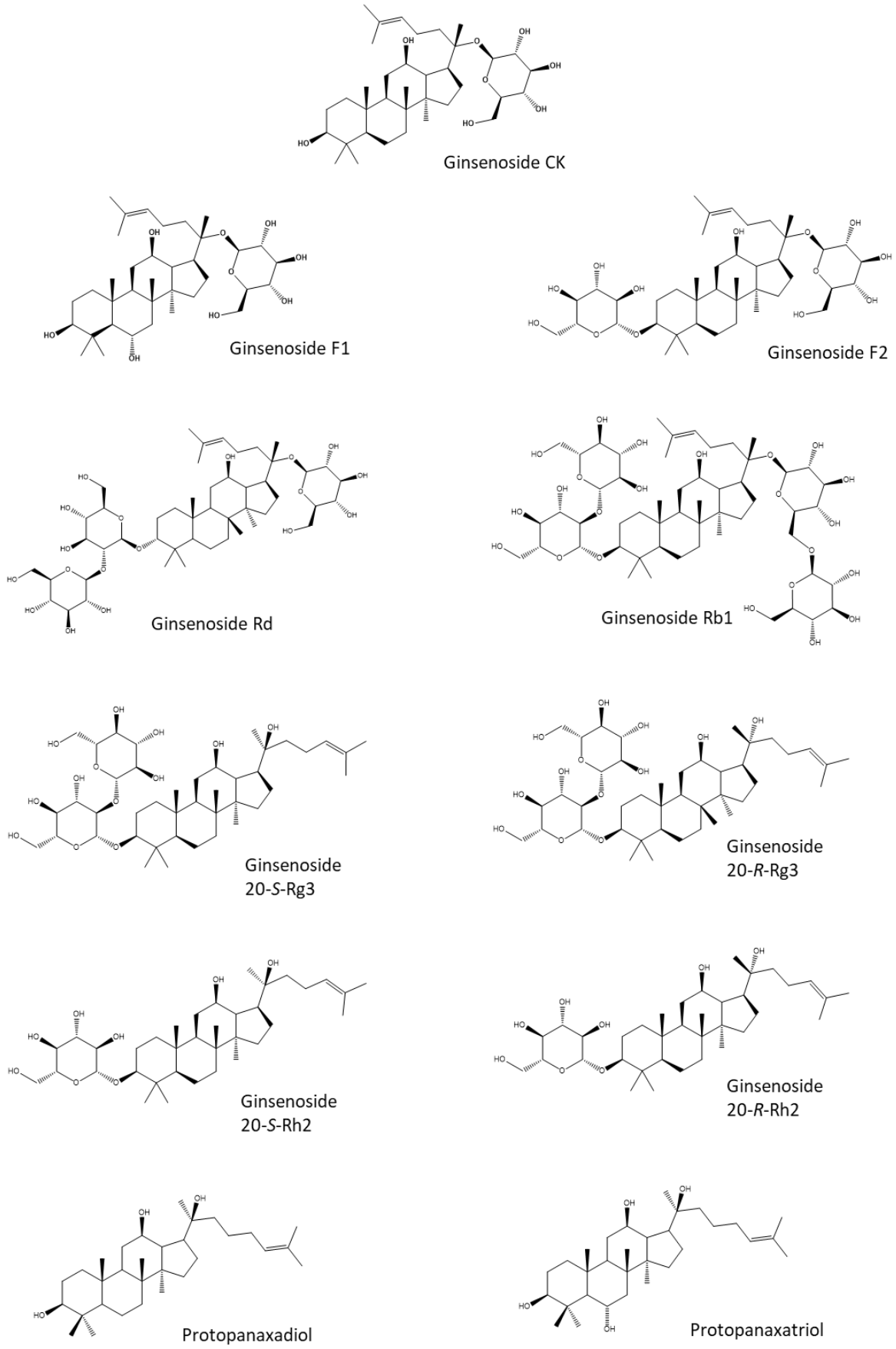

Figure 3.1 – Structures of several ginsenosides and two precursor aglycones, protopanaxadiol and protopanaxatriol. Structures were produced using ChemDraw Prime (PerkinElmer).

These natural products are triterpene glycosides (and their metabolites) found in the *Panax ginseng* plant, traditionally used in Chinese medicine for thousands of years (Xiang et al., 2008). In 2015, select ginsenosides were found to potentiate responses to ATP at human P2X7 in both dye uptake and intracellular calcium assays (Helliwell et al., 2015). The knowledge surrounding their mechanism of binding was later explored in more detail, leading to the location of a predicted binding pocket in the central vestibule region of the human P2X7 receptor (Bidula et al., 2019b). Related compounds in the glycoside family have also been shown to be able to potentiate human P2X7 in dye uptake assays, with key differences highlighted in the activity of stereoisomers and a structure-activity relationship has been proposed (Piyasirananda et al., 2021). In addition to their activity at P2X7, some ginsenosides (particularly ginsenosides CK and Rd) have been shown to have activity at the human P2X4 receptor in both dye uptake and intracellular calcium assays (Dhuna et al., 2019); however, the effects of these modulators at other P2X receptors, and indeed the knowledge of whether this potentiation effect is conserved between P2X receptor subtypes, remains unclear.

It is evident there are key therapeutic benefits to modulating P2X receptors, as summarised by Stokes *et al* (Stokes et al., 2020). With regards to the P2X2 receptor, there may be a role for positive modulation of this receptor in otoprotection – indeed, P2X2 receptors are activated following exposure to loud noises and a subsequent increase in the endolymph ATP concentration (Thorne et al., 2004). This otoprotective property could be enhanced by a positive modulator, decreasing the threshold at which these receptors are activated, which may be particularly useful in older individuals where P2X2 expression is reduced (Telang et al., 2010). P2X4 KO mice have been shown to have increased ethanol intake compared to their wild type counterparts (Khoja et al., 2018a), and positive modulation of the P2X4 receptor has been shown to reverse inhibition of the P2X4 receptor caused by ethanol and alter alcohol preference in rodent models mice (Yardley et al., 2012, Asatryan et al., 2014, Franklin et al., 2014). Positive modulation of the P2X7 receptor could have a role in bone protection, given that it is involved in osteoblast development (Sun et al., 2013) and differentiation of stem cells into osteoprogenitor cells, contributing to osteogenesis (Gartland et al., 2001, Ke et al., 2003, Panupinthu et al., 2008). There is also potential for positive modulation of this receptor in cancer, with small molecule positive allosteric modulator HEI3090 shown to improve outcomes in mouse models of non-small cell lung cancer when combined with αPD-1 treatment (Douguet et al., 2021).

To investigate the benefit of positive modulators of these receptors further, it is first necessary to have an efficient and reliable method of characterising and testing for new modulators of these receptors. Whilst P2X7 has been well characterised for the ability to form a large, non-specific pore (Kaczmarek-Hájek et al., 2012), most other P2X receptors do not have this ability. The P2X2 and P2X4 receptors

have been shown to successfully demonstrate YO-PRO-1 iodide uptake in response to agonists (Marques-da-Silva et al., 2011, Dhuna et al., 2019), however, the P2X1 and P2X3 receptor subtypes are quickly desensitising and therefore their ability to form a large, non-specific pore is uncertain (Peverini et al., 2018). As a result, calcium influx assays are often used to assess P2X receptor responses. Although useful, as calcium influx is a feature of all P2X receptors (Kaczmarek-Hájek et al., 2012), it is important to remember that this assay measures the influx of one ion alone and does not give a full picture of the total movement of ions in and out of a cell. In addition, other receptors outside of ion channels, such as the P2Y G-protein coupled receptors (GPCRs), can induce intracellular calcium release which is separate to the influx of ions from an extracellular source (Burnstock, 2007). Patch-clamp electrophysiology is often considered the gold standard when measuring responses of ion channels, but this technique can be difficult to master and time consuming when conducting screening assays. The FLIPR Membrane Potential Kit offers a relatively novel method of measuring changes in the membrane potential in response to activation of ion channels; techniques similar to this have been used to measure mitochondrial membrane potential (Sakamuru et al., 2016). The main component of the FLIPR membrane potential assay intercalates in the cell membrane, with the majority of this on the outer layer of the lipid bilayer (Molecular Devices, 2023). As ions move into the cell and depolarisation occurs, the dye moves to the inner layer of the lipid bilayer and increases the fluorescence signal. Conversely, as ions move out of the cell, the dye moves to the outer layer of the lipid bilayer and the signal decreases. In addition to this, the kits contain an extracellular quencher dye, available in either red or blue colouring, which reduces background fluorescence (Molecular Devices, 2023).

So far, there has been little published data on the use of the FLIPR Membrane Potential Kit on P2X ion channels – at the time of writing, there are only two papers: one uses the FLIPR Membrane Potential Kit to measure responses in HEK-293 cells expressing the human P2X1 receptor to various ligands (Ruepp et al., 2015), whereas the other conducts the assay for a prolonged period of time to assess long-term ion movement in J774 mouse macrophages endogenously expressing the P2X7 receptor (Bidula et al., 2019a). The aims of this chapter are to validate the use of the Membrane Potential Blue assay as a tool for investigating responses of P2X receptors to agonists and antagonists, in addition to screening multiple ginsenosides and related compounds at human P2X1, P2X2, P2X3, P2X4, and P2X7 receptors expressed in HEK-293 cells to determine activity.

3.2 Determination of the ATP Concentration Response Relationship of Human P2X Receptors Using the Membrane Potential Blue Assay

To be able to screen ginsenosides across P2X receptors, it was first important to establish an assay that is effective in measuring responses at multiple P2X receptors. The membrane potential blue assay measures the change in voltage across the cell membrane, meaning that it can measure total ion influx and efflux. Unlike patch clamp electrophysiology, the current is not clamped to a specific value. To establish this assay, concentration responses to ATP were conducted on HEK-293 cells stably expressing one of the following human P2X receptors: P2X1; P2X2; P2X3; P2X4; P2X7; or native HEK-293 cells (**Figure 3.2**). This allowed determination of EC_{50} values for each of the receptors analysed. **Table 3.1** outlines the EC_{50} values determined for each receptor in each experiment and an average value for these three experiments. An EC_{50} value was not determined for native HEK-293 cells as the four-parameter non-linear regression curve did not produce a sigmoidal shape and therefore the EC_{50} value would not be reliable.

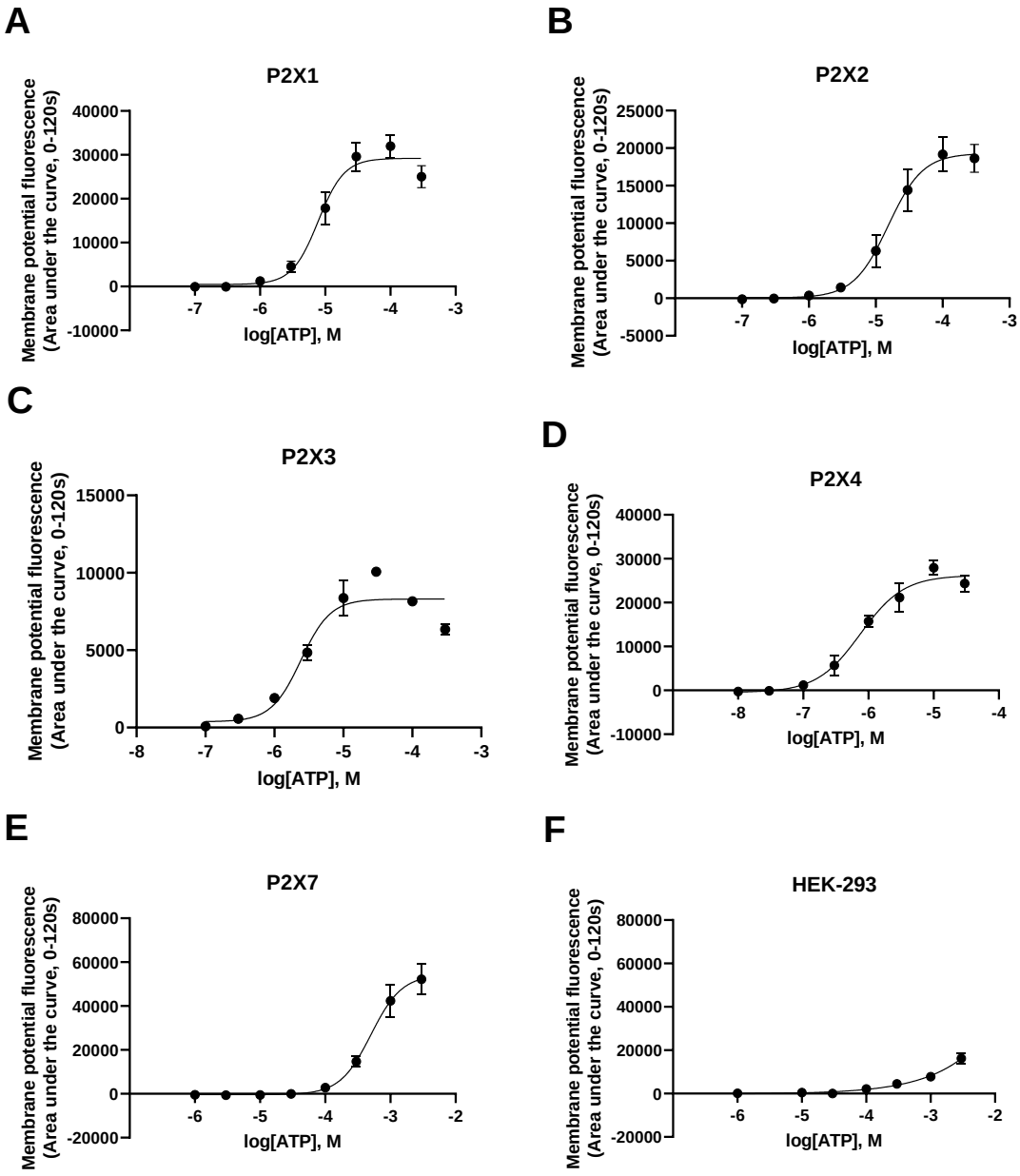

Figure 3.2 – Membrane potential responses to ATP measured in HEK-293 cells stably expressing human P2X receptors or native HEK-293 cells. Concentration response curves to ATP are shown for **A**: hP2X1 **B**: hP2X2 **C:** hP2X3 **D**: hP2X4 **E**: hP2X7 and **F**: Native HEK-293 cells**.** Experiments were conducted in standard extracellular buffer (Etotal). Graphs in panels **A-E** are plotted as mean area under the curve (AUC) values from three independent experiments ± SEM and are fitted with a four-parameter non-linear regression curve. Average EC_{50} values for panels **A-E** are calculated using individual EC_{50} values from three independent experiments (see **Table 3.1**). The graph in panel **F** is plotted as mean AUC values from one experiment ± SEM and is fitted with a four-parameter non-linear regression curve.

Table 3.1 – EC_{50} values for ATP at P2X receptors measured using the membrane potential blue assay. Experiments were conducted in standard extracellular buffer (Etotal) on HEK-293 cells stably expressing each of the hP2X receptors. Average EC_{50} values ± SD were calculated using individual EC_{50} values from three independent experiments where graphs are plotted as mean area under the curve (AUC) values ± SEM and fitted with a four-parameter non-linear regression curve.

Receptor	Average EC_{50} (µM ± SD)
hP2X1	8.21 ± 2.43
hP2X2a	17.56 ± 3.97
hP2X3	2.54 ± 0.54
hP2X4	0.80 ± 0.26
hP2X7	638.53 ± 354.90

Raw traces of responses to ATP at each of the receptors tested are shown in **Figure 3.3**, where the general trend of a rapid increase in response followed by a plateau, or slight decline in response in the case of the quickly desensitising P2X1 and P2X3 receptors, can be observed.

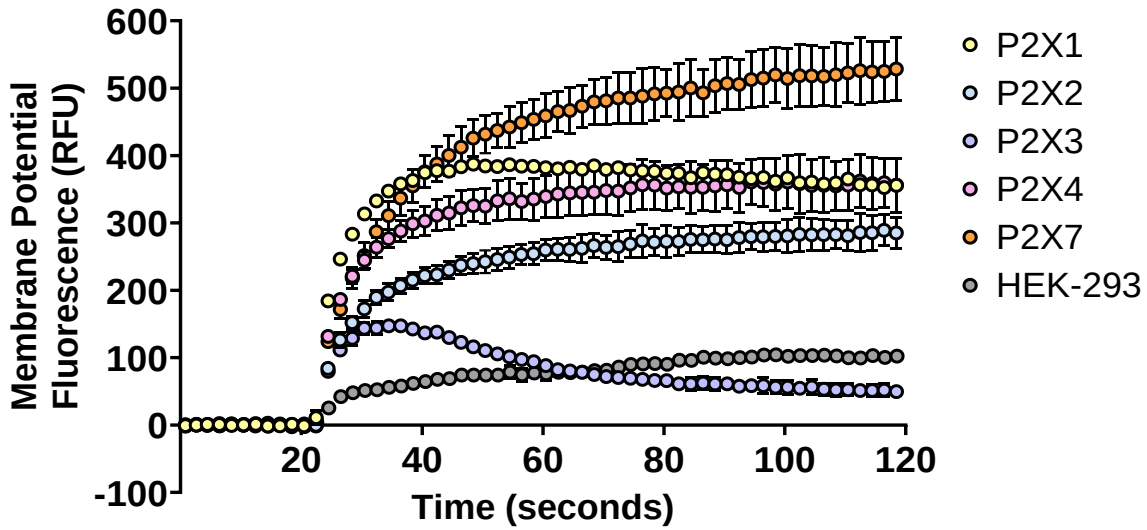

Figure 3.3 – Representative responses to ATP in HEK-293 cells stably expressing P2X receptors or native HEK-293 cells measured using the membrane potential blue assay. Responses were to the following concentrations of ATP: P2X1 100 µM; P2X2 100 µM; P2X3 100 µM; P2X4 10 µM; P2X7 1 mM; native HEK-293 1 mM. Responses were measured for a total of 120 seconds following ATP application at 20 seconds. Data are plotted as fluorescence ± SEM from one independent experiment. Time is plotted as the average time of read from two wells for each of the conditions measured.

As expected, P2X7 was the least sensitive receptor with an EC_{50} value to ATP of 638.5 ± 354 μM. These experiments were conducted in standard extracellular buffer (see **Chapter 2** for details) and so the presence of divalent cations would mean that the EC_{50} value is higher than that seen in low divalent cation extracellular buffer. The quickly desensitising receptors P2X1 and P2X3 had EC_{50} values of 8.210 ± 2.43 μM and 2.538 ± 0.537 μM respectively, whilst the slowly desensitising P2X2 and P2X4 receptors had EC_{50} values to ATP of 17.56 ± 3.97 μM and 0.8015 ± 0.264 μM respectively (summarised in **Table 3.1**). It is important to note that responses to ATP were measured in native HEK-293 cells, likely because of endogenously expressed P2Y channels that upon activation with ATP can lead to calcium-induced calcium-release from intracellular stores, which would in turn cause a change in the membrane potential across the cell membrane that could be measured using the membrane potential blue assay.

3.3 Pharmacological Characterisation of Human P2X2 Receptors Using the Membrane Potential Blue and FURA-2AM Assays

Data surrounding the pharmacology of P2X2 is poor in the literature, particularly regarding the human receptor. The membrane potential blue assay was used to determine the responses of HEK-hP2X2a cells to multiple agonists to enhance knowledge of the pharmacology of the human receptor. A range of agonists were screened including ATP, BzATP, ADP, CTP, and UTP (**Figure 3.4**). ATP and BzATP are known agonists of P2X receptors, whereas ADP, CTP, and UTP are active at P2Y receptors and not typically at P2X receptors (von Kügelgen, 2019, Syed and Kennedy, 2012). Using the membrane potential blue assay, EC_{50} values were determined for ATP and BzATP, giving mean ± SD values of 16.13 ± 5.78 µM and 24.67 ± 5.83 µM respectively. The responses to the other purinergic agonists ADP, CTP and UTP did not yield full concentration response curves, although slight responses can be seen at higher concentrations (≥100 µM, **Figure 3.4**). This is likely due to endogenous P2Y channels expressed on HEK-293 cells which are activated by these agonists, leading to intracellular calcium release.

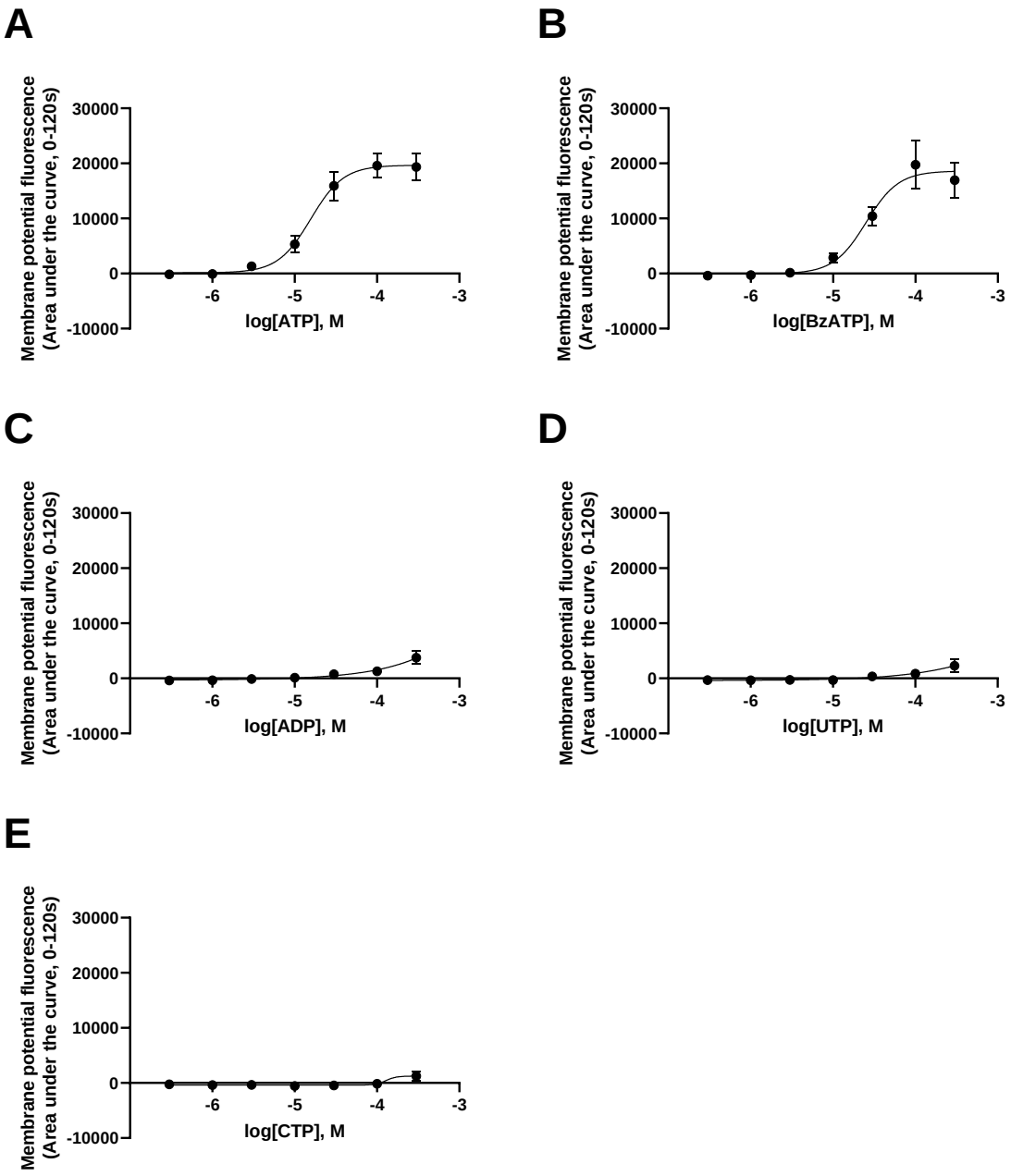

Figure 3.4 – Membrane potential responses to agonists measured in HEK-293 cells stably expressing the human P2X2a receptor. Concentration responses are to the following agonists: **A**: ATP **B**: BzATP **C**: ADP **D**: UTP **E**: CTP. Average EC_{50} values (± SD) for each agonist tested are as follows: **A**: ATP 16.13 µM (± 5.67 µM); **B**: BzATP 24.67 µM (± 5.83 µM); **C**: *ND.* **D**: *ND.* **E**: *ND*. Experiments were conducted in standard extracellular buffer (Etotal). Graphs are plotted as mean area under the curve (AUC) values from four independent experiments ± SEM and are fitted with a four-parameter non-linear regression curve. Average EC_{50} values are calculated using individual EC_{50} - values from four independent experiments.

Currently, there is no commercially available specific antagonist of the human P2X2 receptor. The compound PSB-1011, the sodium salt of Reactive Blue 4 (Rb4), has been shown to have inhibitory effects at the rat P2X2 receptor (Baqi et al., 2011), whilst the compounds PPADS and suramin have been shown to be non-specific inhibitors of various P2 receptors (Burnstock, 2004). These three antagonists were tested using both the membrane potential blue and intracellular calcium assays to determine activity at HEK-293 cells stably expressing the human P2X2a receptor (**Figure 3.5**). Antagonists were screened at concentrations between 1 µM to 1 mM against a fixed concentration of ATP, 10 µM. IC_{50} values for both assays are summarised in **Table 3.2**.

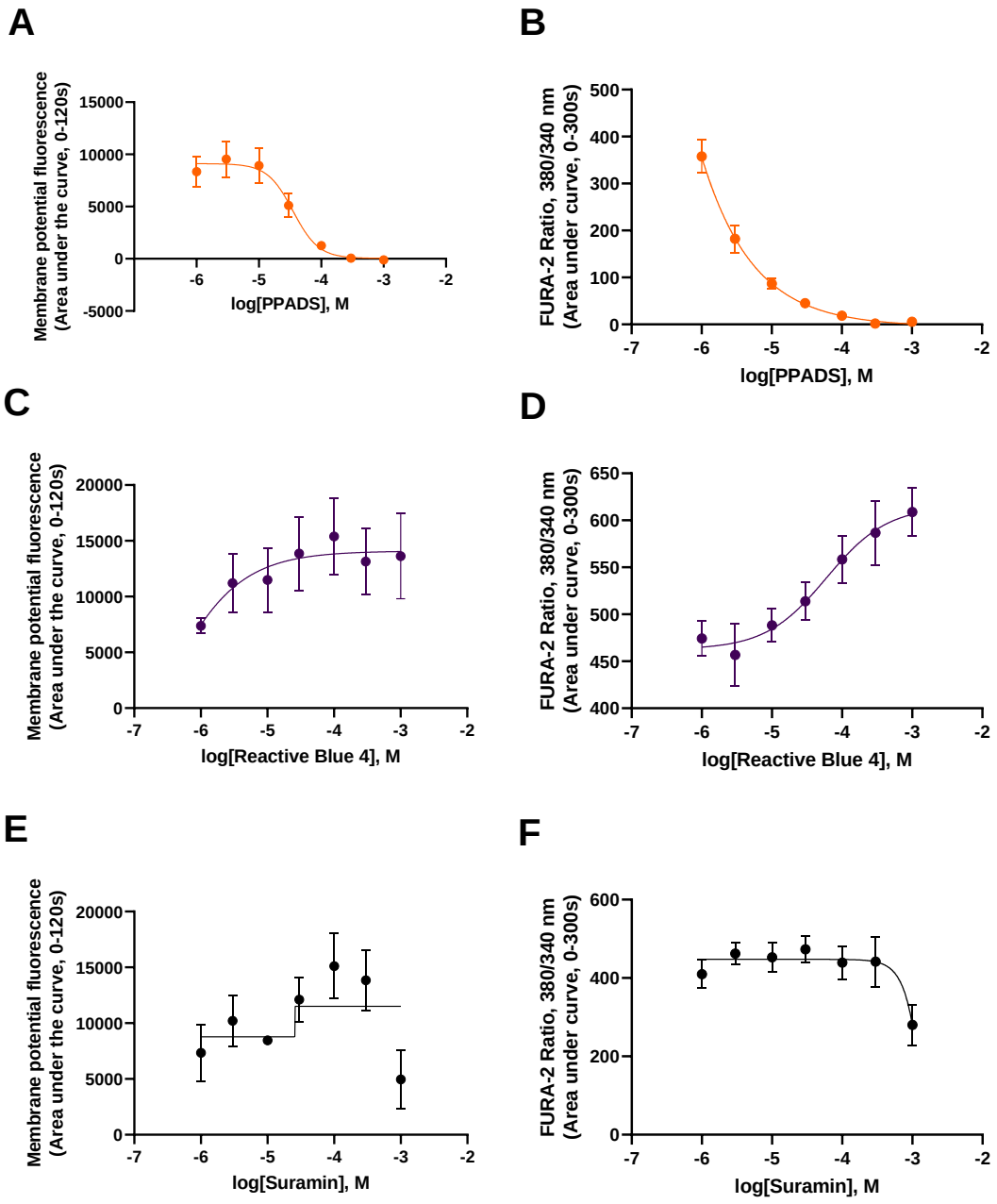

Figure 3.5 – Membrane potential responses to antagonists measured in HEK-293 cells stably expressing the human P2X2a receptor. Antagonists were screened at concentrations between 1 µM and 1mM against ATP at a fixed concentration of 10 µM. Concentration inhibition curves are shown for ATP in the presence of **A, B**: PPADS, **C, D**: Reactive Blue 4 (Rb4), and **E, F**: Suramin. Average IC50 values (± SEM) for each agonist tested are as follows: **A**: PPADS, 35.84 µM (± 3.67 µM); **B**: PPADS, ND; **C**: Reactive Blue 4, 9.446 µM (± 9.44 µM); D: Reactive Blue 4, 40.99 µM (± 7.99 µM); **E**: ND; **F**: ND. Experiments were conducted in standard extracellular buffer (Etotal) using the membrane potential blue *assay (panels **A, C, E**)* or the *FURA-2AM* assay *(panels **B, D, F**)*. Graphs are plotted as mean area under the curve (AUC) values from three independent experiments ± SEM for all concentrations of antagonist except for 1 mM (which was from two independent experiments) and are fitted with a four-parameter non-linear regression curve. Average EC50 values are calculated using individual EC50 values from two or three independent experiments (see **Table 3.2**).

Table 3.2 – IC_{50} values for PPADS and Reactive Blue 4 at human P2X2 receptors in the membrane potential blue and FURA-2AM assays. Experiments were conducted in standard extracellular buffer (Etotal) on HEK-293 cells stably expressing the human P2X2 receptor. Antagonists were screened at concentrations between 1 µM and 1mM against ATP at a fixed concentration of 10 µM. Average IC_{50} values calculated using individual IC_{50} values from three independent experiments where graphs are plotted as mean area under the curve (AUC) values ± SEM and fitted with a four-parameter non-linear regression curve. **Note that Reactive Blue 4 appears to be acting as a potentiator rather than an inhibitor at human P2X2 (see **Figure 3.5**) so the IC_{50} value can be interpreted as the EC_{50} value.*

	Average IC_{50} (± SEM)	
Antagonist	**Membrane Potential Blue**	**FURA-2AM**
PPADS	35.84 µM ± 6.35	*ND*
Reactive Blue 4*	9.446 µM ± 13.4	40.99 µM ± 11.3

PPADS was able to inhibit ATP-induced responses in HEK-hP2X2a in the membrane potential blue assay with micromolar potency but appeared to be more potent in the intracellular calcium assay (**Figure 3.5**). Concentration inhibition curves for PPADS measured using the intracellular calcium assay were not of a sigmoidal shape due to the lack of concentrations < 1 µM, and so IC_{50} values were not determined for this assay.

Although PSB-1011 (sodium salt of Rb4, see **Figure 3.6**) has been shown to inhibit rat P2X2, there is no evidence of its activity at the human receptor (Baqi et al., 2011). Surprisingly, Rb4 appeared to potentiate responses to 10 µM ATP (**Figure 3.5**) at the human P2X2a receptor which is different to what was observed at the rat P2X2 receptor with compound PSB-1011 (Baqi et al., 2011). The EC_{50} value for Rb4 at human P2X2a in the membrane potential blue assay was 9.446 µM, whereas in the FURA-2AM assay it was less potent, giving an EC_{50} value of 40.99 µM (summarised in **Table 3.2**). Values for suramin were not determined as the results did not converge to form a sigmoidal concentration inhibition curve, but inhibition can be observed at the highest concentration of 1 mM in both the membrane potential blue and the FURA-2AM assays (**Figure 3.5**).

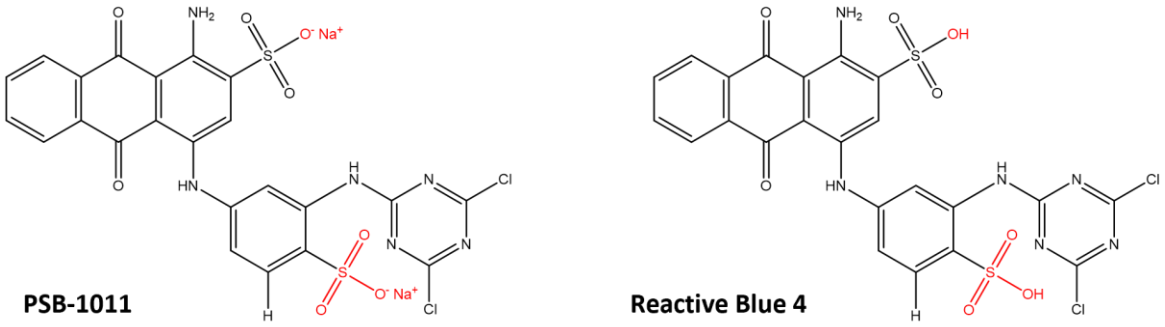

Figure 3.6 – Structures of PSB-1011 and Reactive Blue 4. Key differences are highlighted in red. Notice that PSB-1011 is the sodium salt of Reactive Blue 4, but Baqi *et al* confirmed that these were the same active compound.

The antagonist PPADS was also tested in low divalent cation buffer and at lower concentrations to determine potency of the antagonist (**Figure 3.7**). Here, it can be seen that the potency of PPADS is decreased in low divalent cation extracellular buffer (panel **B**) compared to standard extracellular buffer (panel **A**), likely due to less inhibition by divalent cations working synergistically with PPADS. Although an EC_{50} value for PPADS in standard extracellular buffer could not be determined due to the lack of lower concentrations tested, the average EC_{50} (± SD) for PPADS in low divalent cation extracellular buffer was 25.30 µM ± 0.0425. In comparison, the EC_{50} value in standard extracellular buffer is likely to lie in the nanomolar range for the FURA-2AM assay, although additional data showing responses < 1 µM would be necessary to confirm this.

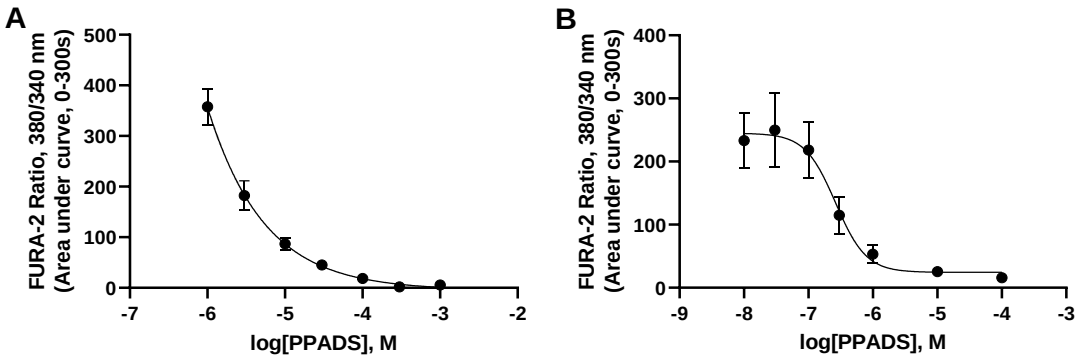

Figure 3.7 – Comparison of extracellular buffer on intracellular calcium responses to the antagonist PPADS measured using the FURA-2AM assay in HEK-293 cells stably expressing the human P2X2a receptor. PPADS was screened at concentrations between 1 µM and 1 mM in panel **A**, and 10 nM and 100 µM in panel **B**. Both were screened using 10 µM ATP. **A**: Concentration inhibition curve to PPADS in standard extracellular buffer, as seen in Figure 3.4. **B**: Concentration inhibition curve to PPADS in low divalent cation extracellular buffer. Graphs are plotted as mean area under the curve (AUC) values from three-four independent experiments ± SEM for all concentrations of antagonist except for 1 mM (which was from two independent experiments) and are fitted with a four-parameter non-linear regression curve.

Figure 3.8 shows the results of one experiment where a concentration response to ATP was conducted in the presence of either Rb4 or PPADS, or ATP alone. In agreement with what was observed in **Figure 3.5**, 300 µM Rb4 potentiates the ATP response, causing a leftward shift in the concentration response curve and a subsequent decrease in the EC_{50} from 17.78 µM to 6.40 µM (**Figure 3.8**). It does not increase the maximum response measured. In contrast, 100 µM PPADS caused a rightward shift to the concentration response curve, increasing the EC_{50} value from 17.78 µM to 56.70 µM. The stock powder of Reactive Blue 4 contains 35 % active dye; therefore, the concentration was increased to 300 µM (3-fold) to result in actual concentrations of Reactive Blue 4 that match closely the concentrations of PPADS screened (within 5 %).

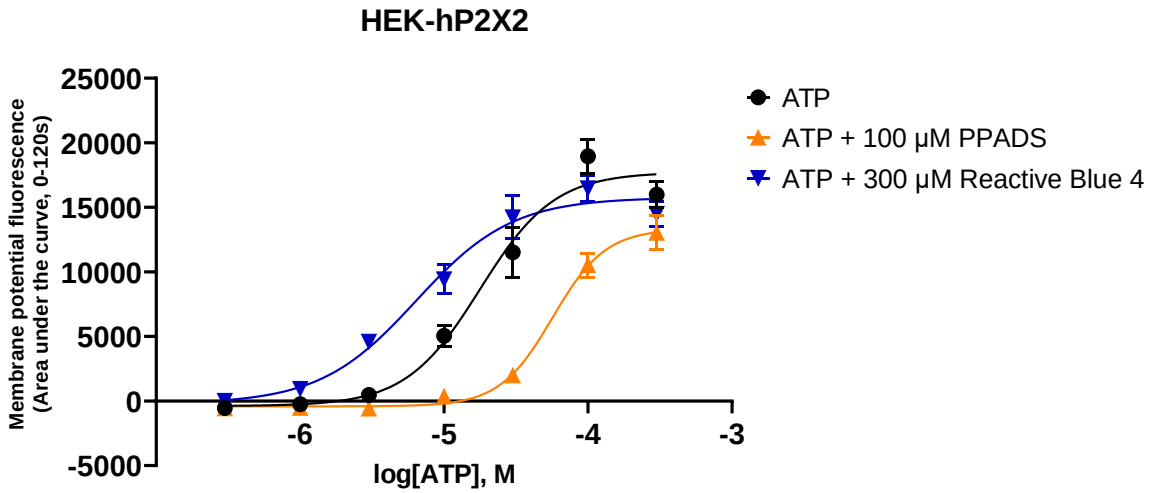

Figure 3.8 – Concentration response to ATP in the presence and absence of either 100 µM PPADS or 300 µM Reactive Blue 4 conducted on HEK-hP2X2 cells using the membrane potential blue assay. A leftward shift can be observed in the presence of Rb4, whereas a rightward shift can be observed in the presence of the non-selective P2 antagonist, PPADS. EC_{50} values are as follows: ATP 17.78 µM; ATP + PPADS 56.70 µM; ATP + Rb4 6.40 µM. Note that the stock powder for Rb4 contains only 35 % active compound; therefore, the concentration of Rb4 was increased 3-fold to make the actual concentrations similar to those tested for PPADS. This experiment was conducted in standard extracellular buffer (Etotal) on HEK-293 cells stably expressing the human P2X2 receptor. Data are plotted as mean fluorescence values (AUC) ± SEM from one independent experiment and fitted with a four-parameter non-linear regression curve.

3.4 Screening of Ginsenosides at Human P2X Receptors Using the Membrane Potential Blue and YO-PRO-1 Assays

Following investigation of response to agonists and antagonists in the membrane potential blue assay at various P2X receptors, the assay was then used to determine the activity of various ginsenosides at human P2X7 to compare observed data with that in the literature. Ginsenoside CK is a known potentiator of human P2X7 (Helliwell et al., 2015), and more recently several other ginsenosides have shown activity at human P2X7, including ginsenosides 20-*S*-Rg3, 20-*S*-Rh2, and F2 (Piyasirananda et al., 2021). To test the activity of ginsenosides at the human P2X7 receptor compounds were screened at concentrations of 10 µM in either the membrane potential blue or YO-PRO-1 assay. ATP (200 µM) was applied after a 60 second pre-incubation period with the ginsenoside or DMSO control in the membrane potential blue assay, whereas compounds were co-applied with ATP in the YO-PRO-1 assay. **Figure 3.9** shows representative responses to 200 µM ATP in the presence of either ginsenoside CK or DMSO control in both the membrane potential blue and YO-PRO-1 assays. In both cases, it can be seen that the responses in the presence of ginsenoside CK is greater than that of the DMSO control.

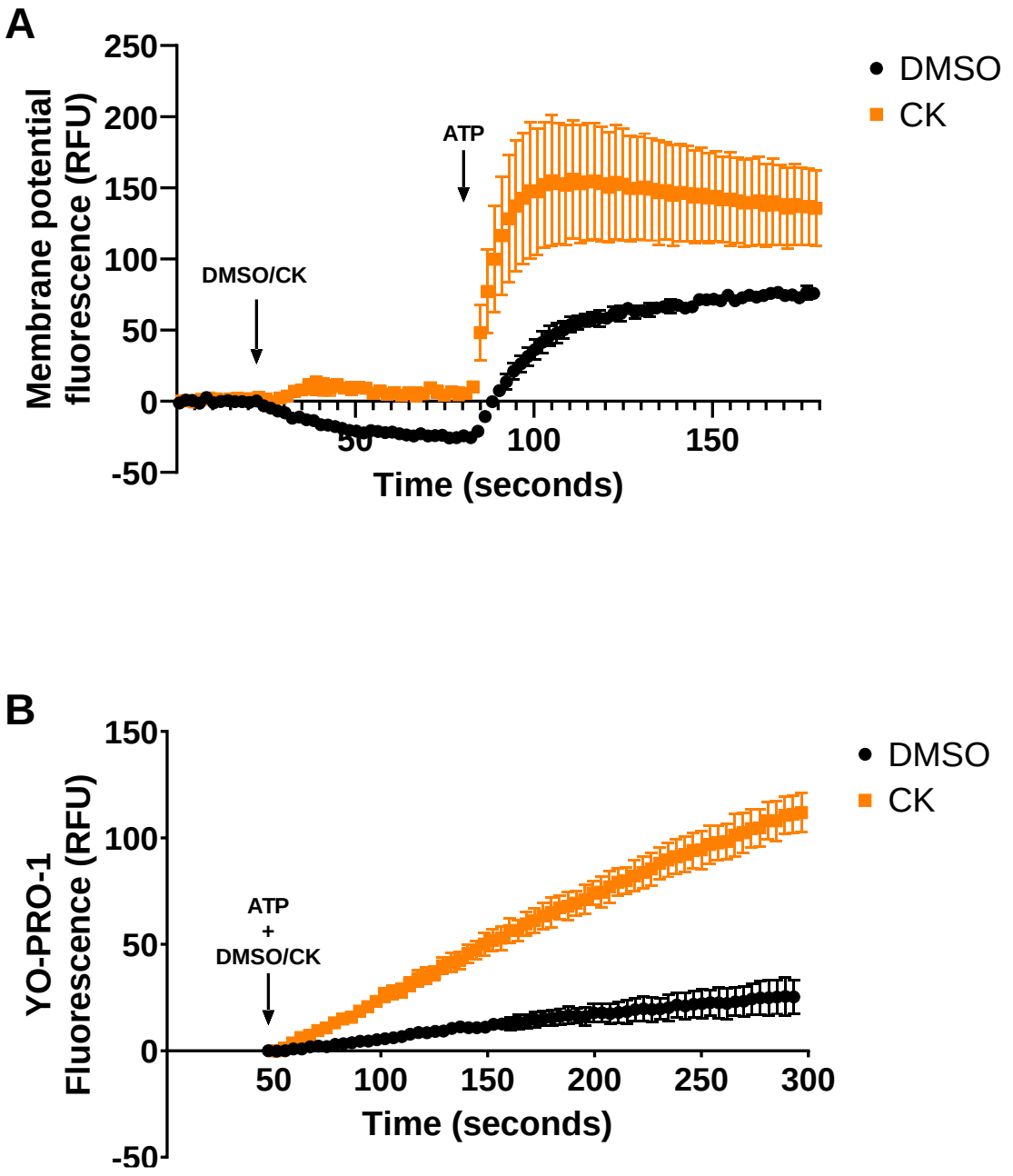

Figure 3.9 – Representative raw fluorescence data measured in stably expressing HEK-hP2X7 cells following stimulation with 200 µM ATP in the presence or absence of either DMSO or ginsenoside CK. **A**: Fluorescence measured using the membrane potential blue assay for a total of 180 seconds with DMSO or ginsenoside CK application at 20 seconds followed by ATP application at 80 seconds. **B**: Fluorescence measured using the YO-PRO-1 assay between 50 and 300 seconds with concurrent application of ATP and either DMSO or ginsenoside CK at 50 seconds. Data are plotted as fluorescence ± SEM from one independent experiment. Time is plotted as the average time of read from three wells for each of the conditions measured.

Figure 3.10 A shows the effects of nine different ginsenosides, alongside two ginsenoside aglycone compounds (protopanaxadiol and protopanaxatriol), on HEK-293 cells stably expressing the human P2X7 receptor in the membrane potential blue assay. Experiments were conducted in standard extracellular buffer (Etotal), and data is normalised to the average area under the curve observed for the control response and plotted as a percentage of the control response ± SEM. The rank order of activity is as follows: 20-*S*-Rg3>CK>F2>20-*S*-Rh2>Rd, with the other compounds tested showing minimal to no potentiation of the response to 200 µM ATP. This agrees with previously published data on ginsenosides, as ginsenosides that have activity in the membrane potential blue assay were also noted to have activity in the YO-PRO-1 assay (Piyasirananda et al., 2021). The biggest potentiation was measured in the presence of 20-*S*-Rg3, with a response that was 281.5 % of the control, closely followed by CK that gave a response that was 253.4 % of control. The responses observed in the presence of ginsenosides F2, 20-*S*-Rh2 and Rd were 225, 206.4 , and 148.7 % of control respectively.

To compare how this rank order and degree of potentiation differed to other assays, select ginsenosides were screened on HEK-hP2X7 using the YO-PRO-1 assay (**Figure 3.10 B**). In these experiments, the compound to be screened was applied to cells at the same time as the ATP, so there was no pre-treatment time. Furthermore, these experiments were conducted in low divalent cation buffer (ELDV). Out of the ginsenosides that were screened, the rank order of activity remained the same, giving a rank order of: CK; F2; Rd; followed by compounds that gave minimal to no potentiation of responses (F1, PPD, and PPT). Compared to the membrane potential blue assay, the fold potentiation of responses compared to the control was much greater. The most active ginsenoside tested in the YO-PRO-1 assay was CK, giving a response that was 527.5 % of control. Ginsenosides F2 and Rd gave responses that were 513.4 and 330.8 % of control respectively.

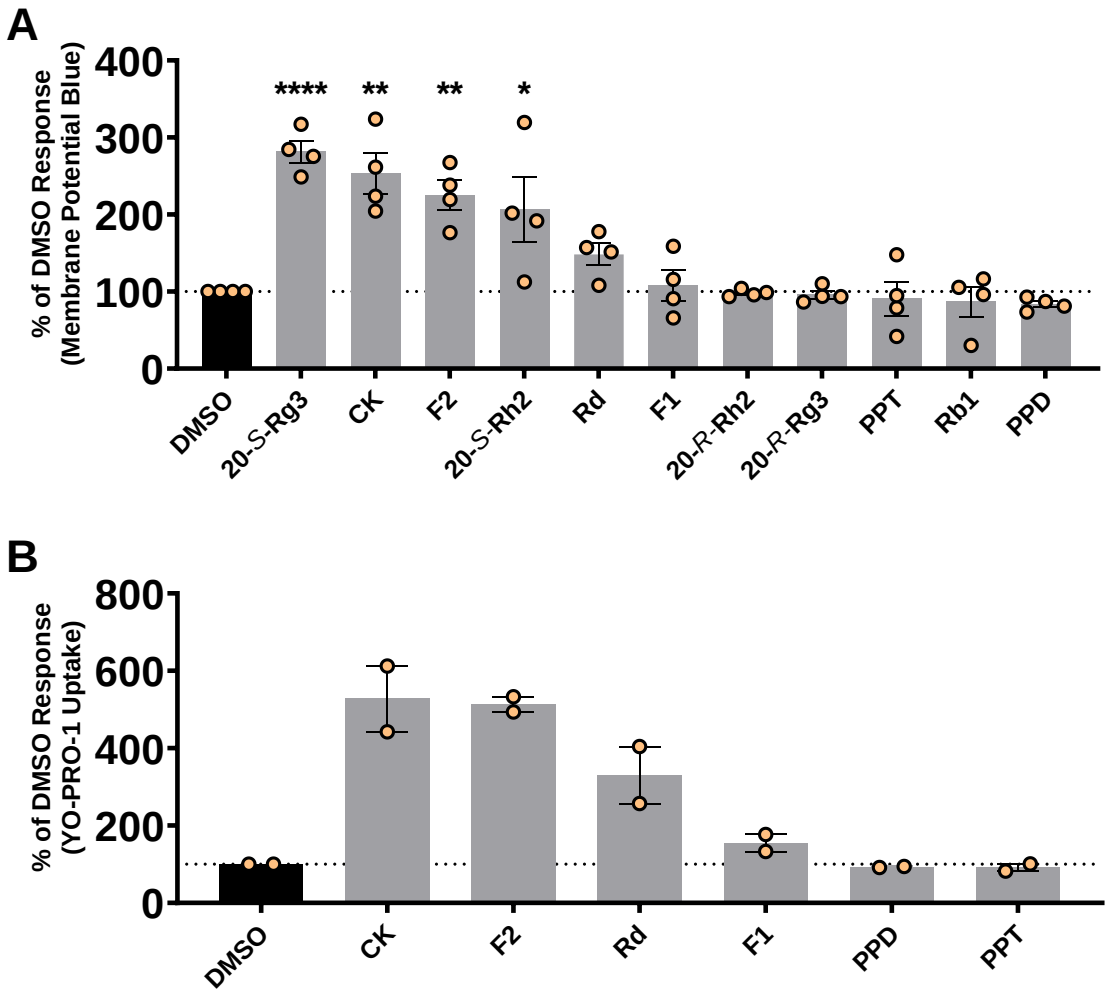

Figure 3.10 – Ginsenoside screens conducted on HEK-293 cells stably expressing the human P2X7 receptor in the membrane potential blue assay and YO-PRO-1 assay. Compounds were screened at 10 µM and ATP was applied at 200 µM. **A**: Modulatory effects of ginsenosides at HEK-hP2X7 in the membrane potential blue assay. In rank order, the five most effective ginsenosides (% of control) are: 20-*S*-Rg3 (281.5 %)>CK (253.4 %)>F2 (225.4 %)>20-*S*-Rh2 (206.4 %)> Rd (148.7 %). **B**: Modulatory effects of ginsenosides at HEK-hP2X7 in the YO-PRO-1 assay. The rank order of ginsenosides (% of control) closely matches that which is observed in the membrane potential blue assay: CK (527.5 %)> F2 (513.4 %)> Rd (330.8 %). For panel **A**, HEK-hP2X7 cells were pre-treated with the appropriate compound at 10 µM for 60 seconds before the application of 200 µM ATP. For panel **B**, compounds were co-injected at a concentration of 10 µM alongside 200 µM ATP. The experiments in panel **A** were conducted in standard extracellular buffer (Etotal). The experiments in panel **B** were conducted in low divalent cation buffer (ELDV). For experiments in panel **A**, data are averaged and normalised to the mean DMSO response between 80-180 seconds for four independent experiments and plotted as percentage of control (DMSO) ± SEM as outlined in **Chapter 2**. For panel **B**, data are averaged and normalised to the mean DMSO response between 50-300 seconds for two independent experiments and plotted as percentage of control (DMSO) ± SEM as outlined in **Chapter 2**. *P<0.05, **P<0.01, ****P<0.0001 determined by one-way ANOVA with Dunnett's multiple comparisons test on raw data.

Now that it has been shown that responses can be measured at multiple P2X receptors using the membrane potential assay, it is possible to screen ginsenosides using this assay at receptors other than P2X7. Next, ginsenosides were screened against human P2X4 for activity (**Figure 3.11**). Previously published data showed that ginsenosides CK and Rd are potentiators of the human P2X4 receptor, although with less activity compared to at the human P2X7 receptor (Dhuna et al., 2019). To test whether activity was also observed in the membrane potential blue assay, compounds were screened at concentrations of 10 µM. ATP (300 nM) was applied after a 60 second pre-incubation period with the ginsenoside in standard extracellular buffer (Etotal).

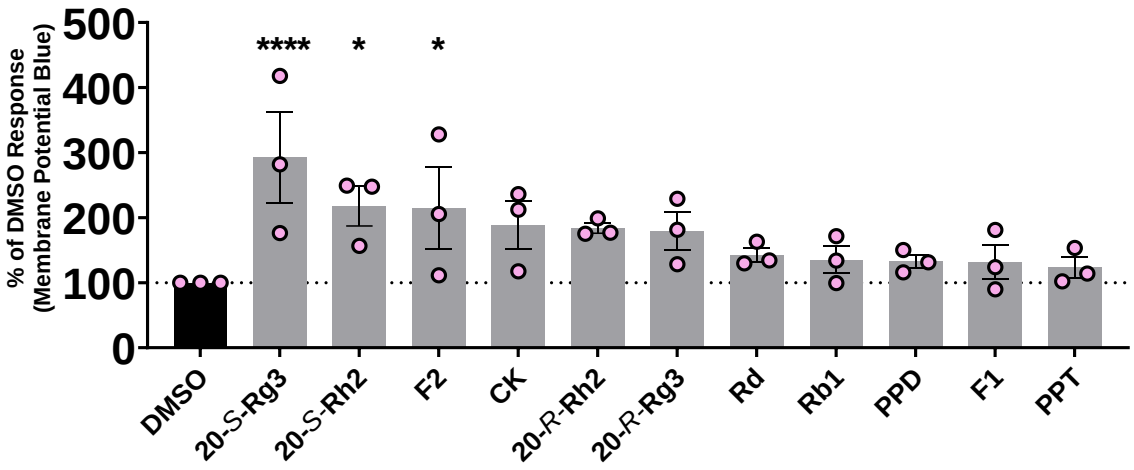

Figure 3.11 – Ginsenoside screens conducted on HEK-293 cells stably expressing the human P2X4 receptor in the membrane potential blue assay. Compounds were screened at 10 µM and ATP was applied at 300 nM. In rank order, the five most effective ginsenosides are: 20-*S*-Rg3 (292.0 % of control); 20-*S*-Rh2 (217.8 % of control); F2 (215.0 % of control); CK (188.6 % of control); 20-*R*-Rh2 (183.6 % of control). In each experiment, HEK-hP2X4 cells were pre-treated with the appropriate compound at 10 µM for 60 seconds before the application of 300 nM ATP. Experiments were conducted in standard extracellular buffer (Etotal). Data are averaged and normalised to the mean DMSO response between 80-180 seconds for three independent experiments and plotted as percentage of control (DMSO) ± SEM as outlined in **Chapter 2**. *P<0.05, ****P<0.0001 determined by one-way ANOVA with Dunnett's multiple comparisons test on raw data.

Figure 3.11 shows the activity of the same eleven compounds on HEK-293 cells stably expressing the human P2X4 receptor. The rank order of activity is as follows: 20-*S*-Rg3; 20-*S*-Rh2; F2; CK; 20-*R*-Rh2; 20-*R*-Rg3; Rd; Rb1; PPD; F1; PPT. As documented previously, CK exhibits good potentiation of the ATP response (188.6 % of control), however, three ginsenosides show more potentiation compared to CK. These are: 20-*S*-Rg3, giving a response that is 292.0 % of control; 20-*S*-Rh2, giving a response that is

217.8 % of control; and F2, giving a response that is 215.0 % of control. Interestingly, ginsenoside Rd was less effective in the membrane potential assay compared to previously published data in other assays, giving a response that was 142.3 % of control. Previously, ginsenoside Rd has been shown to increase YO-PRO-1 uptake in HEK-hP2X4 cells by approximately 160 % (at a concentration of 10 µM alongside 5 µM ATP) and has been shown to increase the FURA-2 response by approximately 150 % (at a concentration of 10 µM alongside 1 µM ATP) (Dhuna et al., 2019).

Figure 3.12 shows representative responses to 300 nM ATP in the presence of ginsenoside CK, ginsenoside 20-*S*-Rg3, or DMSO control in the membrane potential blue assay. In both cases, it can be seen that responses in the presence of ginsenosides are greater than that of the DMSO control, with the addition of ginsenoside 20-*S*-Rg3 giving the largest response compared to the DMSO control.

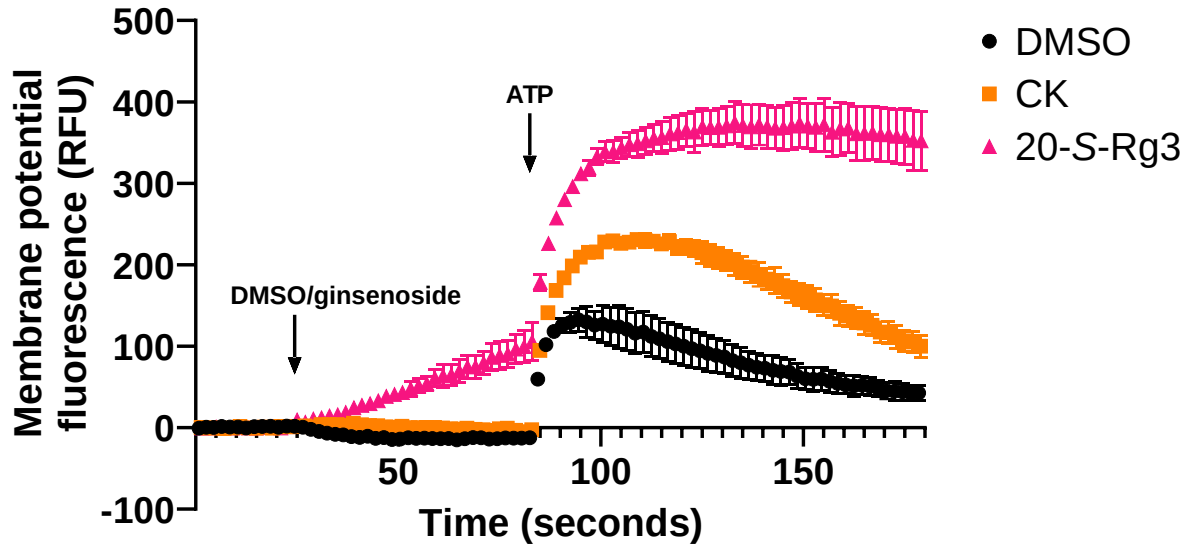

Figure 3.12 – Representative raw fluorescence data measured in stably expressing HEK-hP2X4 cells following stimulation with 300 nM ATP in the presence or absence of DMSO, ginsenoside CK, or ginsenoside 20-S-Rg3. Fluorescence measured using the membrane potential blue assay for a total of 180 seconds with DMSO or ginsenoside application at 20 seconds followed by ATP application at 80 seconds. Data are plotted as fluorescence ± SEM from one independent experiment. Time is plotted as the average time of read from three wells for each of the conditions measured.

Although data has been previously published on the effect of ginsenosides on P2X7 and P2X4 receptors, there have been no investigations into the effects of these compounds on human P2X2 receptors. Ginsenosides were screened at HEK-293 cells stably expressing the human P2X2a receptor using the membrane potential blue assay (**Figure 3.13**). Compounds were pre-applied for 60 seconds at a concentration of 10 µM followed by ATP (10 µM) and experiments were conducted in standard extracellular buffer (Etotal).

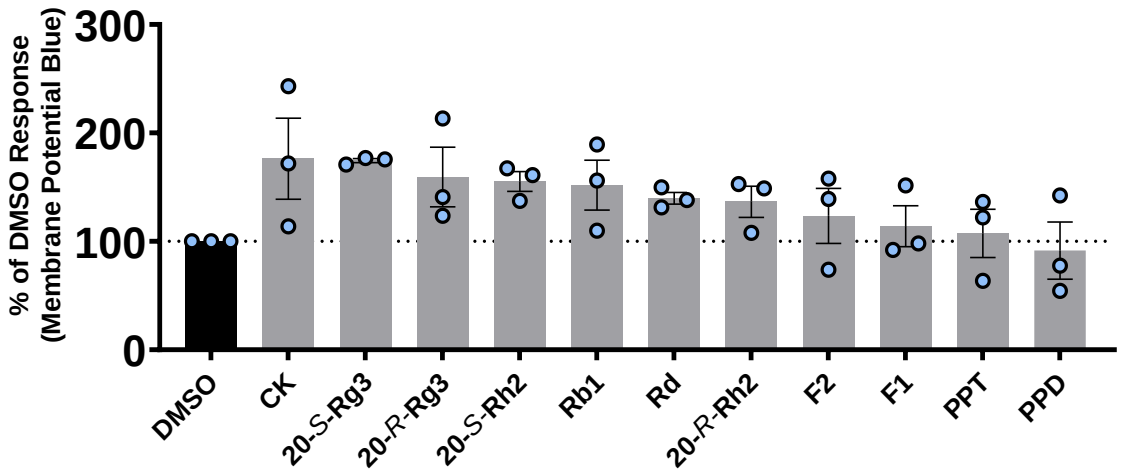

Figure 3.13 – Ginsenoside screens conducted on HEK-293 cells stably expressing the human P2X2a receptor in the membrane potential blue assay. Compounds were screened at 10 µM and ATP was applied at 10 µM. In rank order, the five most effective ginsenosides are: CK (176.3 % of control); 20-*S*-Rg3 (174.5 % of control); 20-*R*-Rg3 (159.3 % of control); 20-*S*-Rh2 (155.2 % of control); Rb1 (151.8 % of control). In each experiment, HEK-hP2X2 cells were pre-treated with the appropriate compound at a concentration of 10 µM for 60 seconds before the application of 10 µM ATP. Experiments were conducted in standard extracellular buffer (Etotal). Data are averaged and normalised to the mean DMSO response between 80-180 seconds for three independent experiments and plotted as percentage of control (DMSO) ± SEM as outlined in **Chapter 2**. One-way ANOVA with Dunnett's multiple comparisons test on raw data did not yield significance.

Interestingly, some ginsenosides were able to potentiate responses to 10 µM ATP in HEK-hP2X2a cells, although to a lesser extent than at P2X7 and P2X4 receptors. The rank order of activity is as follows: CK; 20-*S*-Rg3; 20-*R*-Rg3; 20-*S*-Rh2; Rb1; Rd; 20-*R*-Rh2; F2; followed by F1, PPT, and PPD that had minimal effects on the response (**Figure 3.13**). Unlike P2X7 and P2X4, this is the first time an *R*-enantiomer ginsenoside has been in the top three potentiators. The biggest potentiation was seen with CK (176.3 % of control response), followed by 20-*S*-Rg3 (174.5 % of control response, and then 20-*R*-Rg3, 20-*S*-Rh2, and Rb1, which all gave similar responses of 159.3, 155.2 and 151.8 % of control response respectively. This shows that ginsenosides appear to be able to potentiate human P2X2a responses to 10 µM ATP, but to a lesser extent than at P2X7 and P2X4 receptors where potentiation >2 fold has been observed.

Figure 3.14 shows representative responses to 10 µM ATP in the presence of ginsenoside CK, ginsenoside 20-*S*-Rg3, or DMSO control in the membrane potential blue assay. In both cases, it can be seen that responses in the presence of ginsenosides are greater than that of the DMSO control.

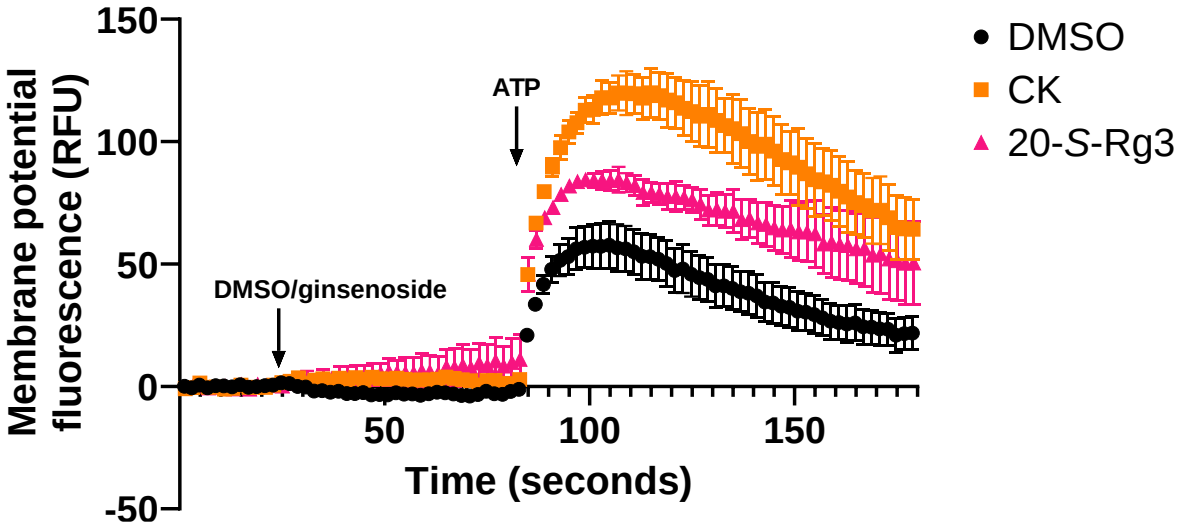

Figure 3.14 – Representative raw fluorescence data measured in stably expressing HEK-hP2X2a cells following stimulation with 10 µM ATP in the presence or absence of DMSO, ginsenoside CK, or ginsenoside 20-S-Rg3. Fluorescence measured using the membrane potential blue assay for a total of 180 seconds with DMSO or ginsenoside application at 20 seconds followed by ATP application at 80 seconds. Data are plotted as fluorescence ± SEM from one independent experiment. Time is plotted as the average time of read from three wells for each of the conditions measured.

Given that P2X1 receptors are quickly desensitising purinergic receptors (Kaczmarek-Hájek et al., 2012), it is difficult to measure their activity using a fluorescence plate reader. The membrane potential assay appears to allow reliable measurement of responses to ATP (see **Figure 3.2**) meaning that it may be suitable to screen compounds against fast desensitising receptors. Therefore, this assay was also used to screen ginsenosides at HEK-293 cells stably expressing the human P2X1 receptor.

Figure 3.15 shows responses to eleven ginsenosides and related compounds at a concentration of 10 µM against a fixed concentration of ATP (10 µM). Compounds were applied 60 seconds before the application of ATP and experiments were conducted in standard extracellular buffer (Etotal). A small degree of potentiation is seen with some ginsenosides, with a rank order as follows: 20-*S*-Rh2; CK; 20-*S*-Rg3, followed by compounds with little to no activity at HEK-hP2X1. The extent of potentiation is much less than that observed in HEK-hP2X7 and HEK-hP2X4, and even less than that observed at HEK-hP2X2, with responses of 140.5, 129.2, and 124.2 % of control for 20-*S*-Rh2, CK, and 20-*S*-Rg3

respectively. This suggests that even though some potentiation can be observed at human P2X1, the ginsenosides are less active at this quickly desensitising receptor subtype.

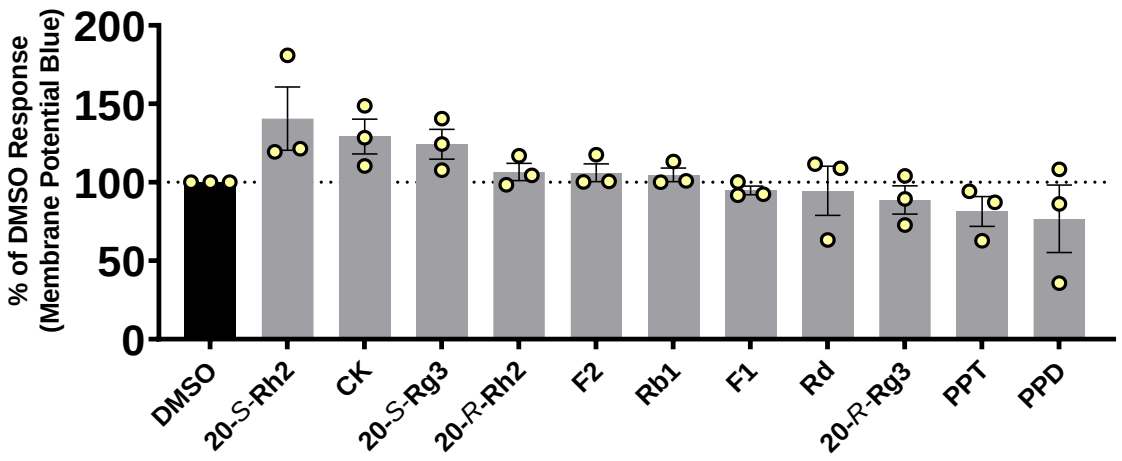

Figure 3.15 – Ginsenoside screens conducted on HEK-293 cells stably expressing the human P2X1 receptor in the membrane potential blue assay. Compounds were screened at 10 µM and ATP was applied at 10 µM. In rank order, the five most effective ginsenosides are: 20-*S*-Rh2 (140.5 % of control); CK (129.2 % of control); 20-*S*-Rg3 (124.2 % of control); 20-*R*-Rh2 (106.6 % of control); F2 (106.1 % of control). In each experiment, HEK-hP2X1 cells were pre-treated with the appropriate compound at a concentration of 10 µM for 60 seconds before the application of 10 µM ATP. Experiments were conducted in standard extracellular buffer (Etotal). Data are averaged and normalised to the mean DMSO response between 80-180 seconds for three independent experiments and plotted as percentage of control (DMSO) ± SEM as outlined in **Chapter 2**. One-way ANOVA with Dunnett's multiple comparisons test on raw data did not yield significance.

Figure 3.16 shows representative responses to 10 µM ATP in the presence of ginsenoside CK, ginsenoside 20-*S*-Rh2, or DMSO control in the membrane potential blue assay. In both cases, it can be seen that responses in the presence of ginsenosides are greater than that of the DMSO control, although to a lesser extent than that observed at the more slowly desensitising P2X receptors.

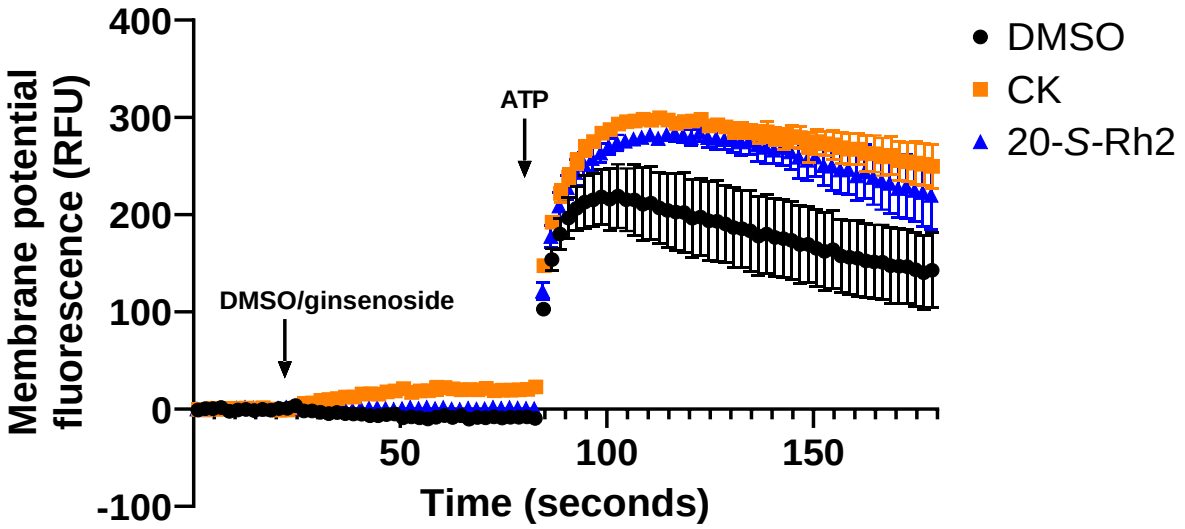

Figure 3.16 – Representative raw fluorescence data measured in stably expressing HEK-hP2X1 cells following stimulation with 10 µM ATP in the presence or absence of DMSO, ginsenoside CK, or ginsenoside 20-S-Rh2. Fluorescence measured using the membrane potential blue assay for a total of 180 seconds with DMSO or ginsenoside application at 20 seconds followed by ATP application at 80 seconds. Data are plotted as fluorescence ± SEM from one independent experiment. Time is plotted as the average time of read from three wells for each of the conditions measured.

Similar to P2X1, P2X3 is also a quickly desensitising receptor (Kaczmarek-Hájek et al., 2012), and therefore usually difficult to measure responses using fluorescence assays. The membrane potential blue assay was used to screen ginsenosides and related compounds at HEK-293 cells stably expressing the human P2X3 receptor (**Figure 3.17**). Compounds were applied at a concentration of 10 µM 60 seconds before the application of 10 µM ATP. Experiments were conducted in standard extracellular buffer (Etotal). In parallel to P2X1, potentiation observed at the P2X3 receptor was much less than that previously observed at the more slowly desensitising receptors. The rank order of effective ginsenosides was 20-*S*-Rh2, F2, F1, and PPD, followed by the remaining compounds screened that had minimal to no effect on the ATP response. The biggest potentiation was seen with 20-*S*-Rh2, with a response that was 133.2 % of the control response, followed by 125.2 % for F2, 124.0 % for F1, and 118.6 % for the aglycone PPD. Again, this suggests that potentiation of this quickly desensitising receptor is possible, but the effects are smaller than that observed at other P2X receptors. Furthermore, ginsenoside CK has been shown to be one of the most effective potentiators at all P2X receptor subtypes screened so far, including the quickly desensitising P2X1 receptor, although that is not the case at the human P2X3 receptor where it shows no difference compared to the control response.

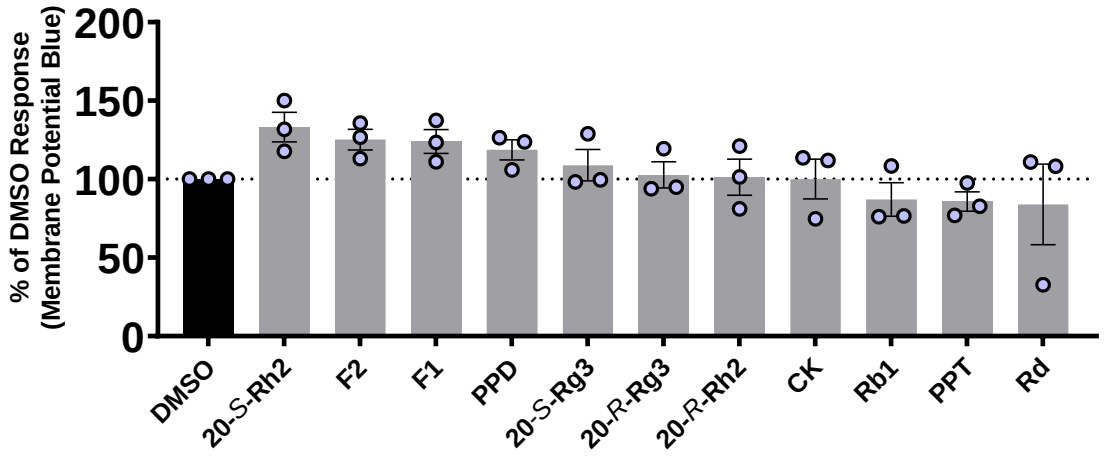

Figure 3.17 – Ginsenoside screens conducted on HEK-293 cells stably expressing the human P2X3 receptor in the membrane potential blue assay. Compounds were screened at 10 µM and ATP was applied at 10 µM. In rank order, the five most effective ginsenosides are: 20-*S*-Rh2 (133.2 % of control); F2 (125.2 % of control); F1 (124.0 % of control); PPD (118.7 % of control); 20-*S*-Rg3 (108.9 % of control). In each experiment, HEK-hP2X3 cells were pre-treated with the appropriate compound at a concentration of 10 µM for 60 seconds before the application of 10 µM ATP. Experiments were conducted in standard extracellular buffer (Etotal). Data are averaged and normalised to the mean DMSO response between 80-180 seconds for three independent experiments and plotted as percentage of control (DMSO) ± SEM as outlined in **Chapter 2**. One-way ANOVA with Dunnett's multiple comparisons test on raw data did not yield significance.

Figure 3.18 shows representative responses to 10 µM ATP in the presence of ginsenoside CK, ginsenoside 20-*S*-Rh2, or DMSO control in the membrane potential blue assay. It can be seen that the response in the presence of ginsenoside 20-*S*-Rh2 is greater than that of the DMSO control, however, the response in the presence of ginsenoside CK is similar to the control response.

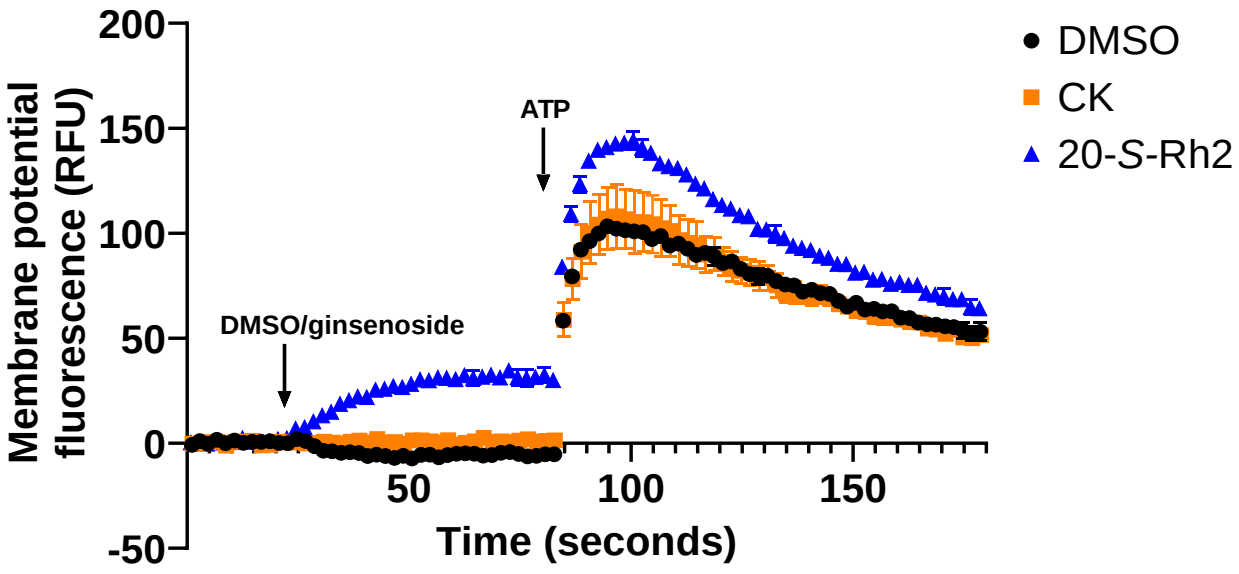

Figure 3.18 – Representative raw fluorescence data measured in stably expressing HEK-hP2X3 cells following stimulation with 10 µM ATP in the presence or absence of DMSO, ginsenoside CK, or ginsenoside 20-S-Rh2. Fluorescence measured using the membrane potential blue assay for a total of 180 seconds with DMSO or ginsenoside application at 20 seconds followed by ATP application at 80 seconds. Data are plotted as fluorescence ± SEM from one independent experiment. Time is plotted as the average time of read from three wells for each of the conditions measured.

3.5 Screening of Steroids and Glycosides at Human P2X Receptors Using the Membrane Potential Blue and YO-PRO-1 Assays

Several potentiators of P2X2 have been documented in the literature; most notably, steroids and their derivative compounds (Stokes et al., 2020). Progesterone and dehydroepiandrosterone (DHEA) have been shown to potentiate responses in HEK-293 cells expressing the rat P2X2 receptor (De Roo et al., 2010), however, it is not clear what the effects of these compounds is on the human P2X2 receptor. To test this, progesterone and DHEA were screened against G418-selected HEK-293 cells expressing the human P2X2a receptor and native non-transfected HEK-293 cells. In addition to progesterone and DHEA, several other steroids were also screened including one modified testosterone analogue, AB1 (synthesized by Dr Andrew Beekman, UEA), which is a testosterone scaffold with a glucose moiety at position 17 instead of a hydroxyl group (**Figure 3.19**).

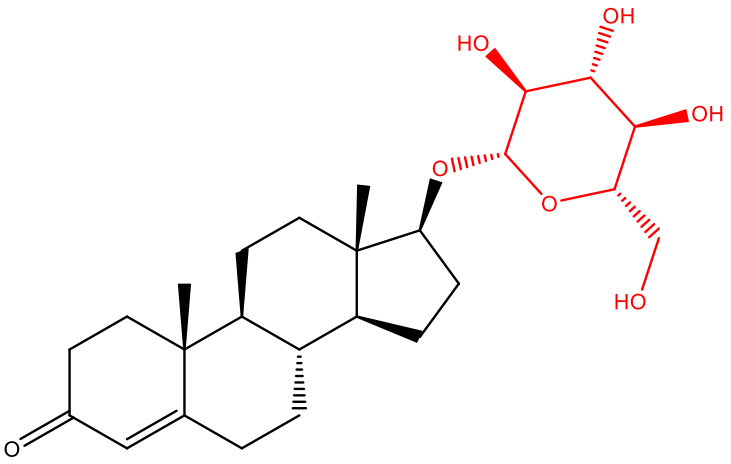

Figure 3.19 – Structure of testosterone derivative AB1. Note the glucose moiety highlighted in red, which is an -OH group in unmodified testosterone.

Figure 3.20 outlines the effects of steroids screened at a concentration of 10 µM on responses to 20 µM ATP in selected HEK-hP2X2a and native HEK-293 cells using the membrane potential blue assay. Compounds were reconstituted in either DMSO (lighter grey bars) or ethanol (darker grey bars) and so two control responses in the presence of either DMSO or ethanol alone were included in the experiment. At hP2X2a (**Figure 3.20 A**), progesterone can potentiate the response to ATP by approximately 2.3-fold, with DHEA potentiating the ATP response by approximately 2.7-fold compared to their respective controls. In addition, testosterone was also able to potentiate the response to 20 µM ATP, giving a response that was approximately 2.4-fold greater than the control response (ethanol alone). The addition of a glucose moiety to testosterone at position 17 (AB1)

resulted in a reduction in potentiation, giving a response that was 1.8-fold greater than the control response. Allopregnanolone and tetrahydrocortisol were also able to potentiate responses to 20 μM ATP, giving responses that were 1.7- and 1.3-fold of the control response respectively. The steroids pregnanolone, alfaxalone, 17β-estradiol and pregnenolone sulphate had minimal effects on the ATP response, and cholesterol appeared to slightly inhibit the response to 20 μM ATP, giving a response that was approximately 82 % of the control response to ethanol alone. This suggests that the activity previously measured on rat P2X2 receptors can be replicated at the human P2X2a receptor, with both progesterone and DHEA both potentiating the response to ATP. Interestingly, DHEA appears to have a bigger fold potentiation when compared to the control response; it is important to note that this is the result of one experiment on G418-selected HEK-hP2X2 cells, and therefore the experiment was conducted on a mixed population of cells that would have varying levels of expression of the human P2X2 receptor.

To determine whether these effects were due to the P2X2 receptor alone, native HEK-293 cells were also screened with several steroid compounds with ATP at a concentration of 20 μM (**Figure 3.20 B**). Interestingly, progesterone and DHEA also potentiated the ATP response in the native HEK-293 cells, although the maximum response seen with progesterone was approximately 2.2-fold less than that seen in the G418-selected HEK-hP2X2 cells. Testosterone, which potentiated responses in G418-selected HEK-hP2X2 cells, also potentiated responses in native HEK-293 cells, although again the maximum response seen was less than in the former. Other compounds that showed potentiation in the G418-selected HEK-hP2X2 cells, such as AB1, allopregnanolone, and tetrahydrocortisol showed minimal effects on the ATP-induced response measured in native HEK-293 cells. When taken together, the data shown in these experiments makes it difficult to determine whether the effects of steroids on the hP2X2a receptor are due to the receptor alone or whether other endogenously expressed receptors could be influencing the measured responses. It is also important to note that this assay has not been used in this capacity before, and therefore results are likely to differ to previously published results using other assays such as patch-clamp electrophysiology.

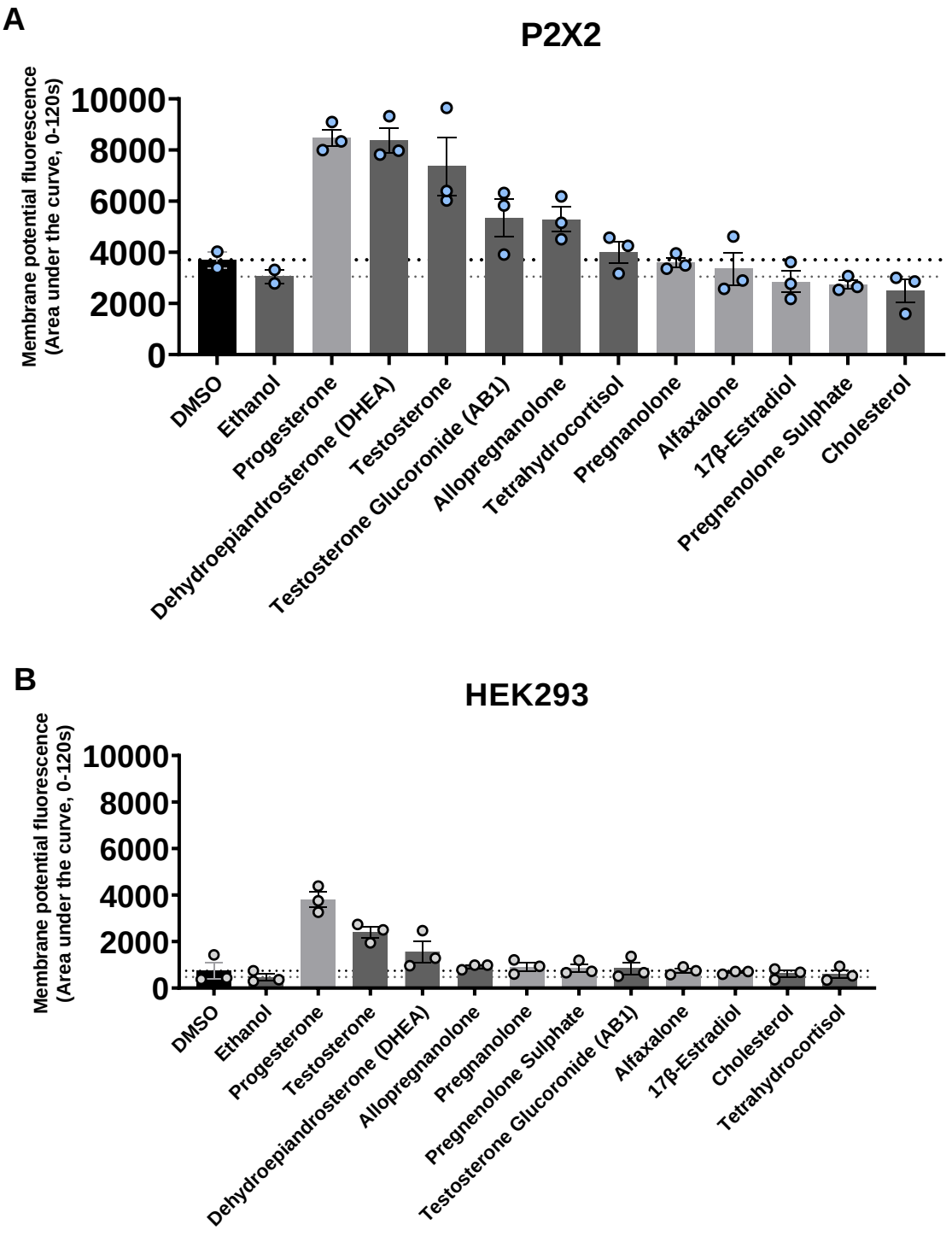

Figure 3.20 – Steroid screens conducted on G418-selected HEK-293 cells expressing the human P2X2a receptor or native HEK-293 cells. Compounds were co-injected at a concentration of 10 µM alongside 20 µM ATP. Steroids were reconstituted in either DMSO (lighter grey bars) or ethanol (darker grey bars). **A**: Modulatory effects of steroids at G418-selected HEK-hP2X2. **B**: Modulatory effects of steroids at native HEK-293 cells. Data are plotted as AUC between 0-120 seconds ± SEM. For both P2X2 and HEK-293, data are the result of one experiment.

In addition to activity at rat P2X2, steroids have also been shown to modulate responses to ATP at the P2X7 receptor. The steroid 17β-estradiol has been shown to inhibit the human P2X7 receptor, whilst progesterone did not have the same effect (Cario-Toumaniantz et al., 1998). To test this effect in the membrane potential assay, steroids, and related testosterone glucoside compound AB1, were screened at a concentration of 10 μM against ATP (200 μM) (**Figure 3.21 A**). Unlike what was shown previously, progesterone appears to potentiate the response to 200 μM ATP, giving a response that is approximately 1.5-fold greater than the control response. DHEA also potentiated responses to ATP in HEK-hP2X7 by approximately 1.3-fold. Most other steroids screened appeared to have minimal effects on the response to ATP, although pregnanolone, testosterone, 17β-estradiol, and tetrahydrocortisol all appeared to inhibit responses to an extent. Pregnanolone gave a response approximately 89 % of the control, followed by testosterone at 86 %, 17β-estradiol at 82 % and finally tetrahydrocortisol at 77 % of the control response.

To confirm if these results were also observed in dye uptake assays, steroids were also screened against stably expressing HEK-hP2X7 in the YO-PRO-1 assay (**Figure 3.21 B**). Interestingly, progesterone that had been shown to potentiate membrane potential responses at HEK-hP2X7 in the previous panel displayed inhibitory activity in the YO-PRO-1 assay, giving a response that was approximately 37 % of the control response. Indeed, the only steroidal compound screened that resulted in potentiation of the response was the modified testosterone analogue AB1, which gave a response that was 1.1-fold that of the control. Testosterone inhibited the response to 200 μM ATP the most, giving a response that was only 16 % of the control response, suggesting that the modification at position 17 was detrimental to the inhibitory activity of the parent analogue. In agreement with previously published work, 17β-estradiol reduced responses to 200 μM ATP, giving a response that was approximately 21 % of the control response. All other steroid compounds tested appeared to inhibit the dye uptake response, with progesterone, 17β-estradiol, and testosterone all displaying responses that were < 50 % of the control response. These data highlight key differences between assays.

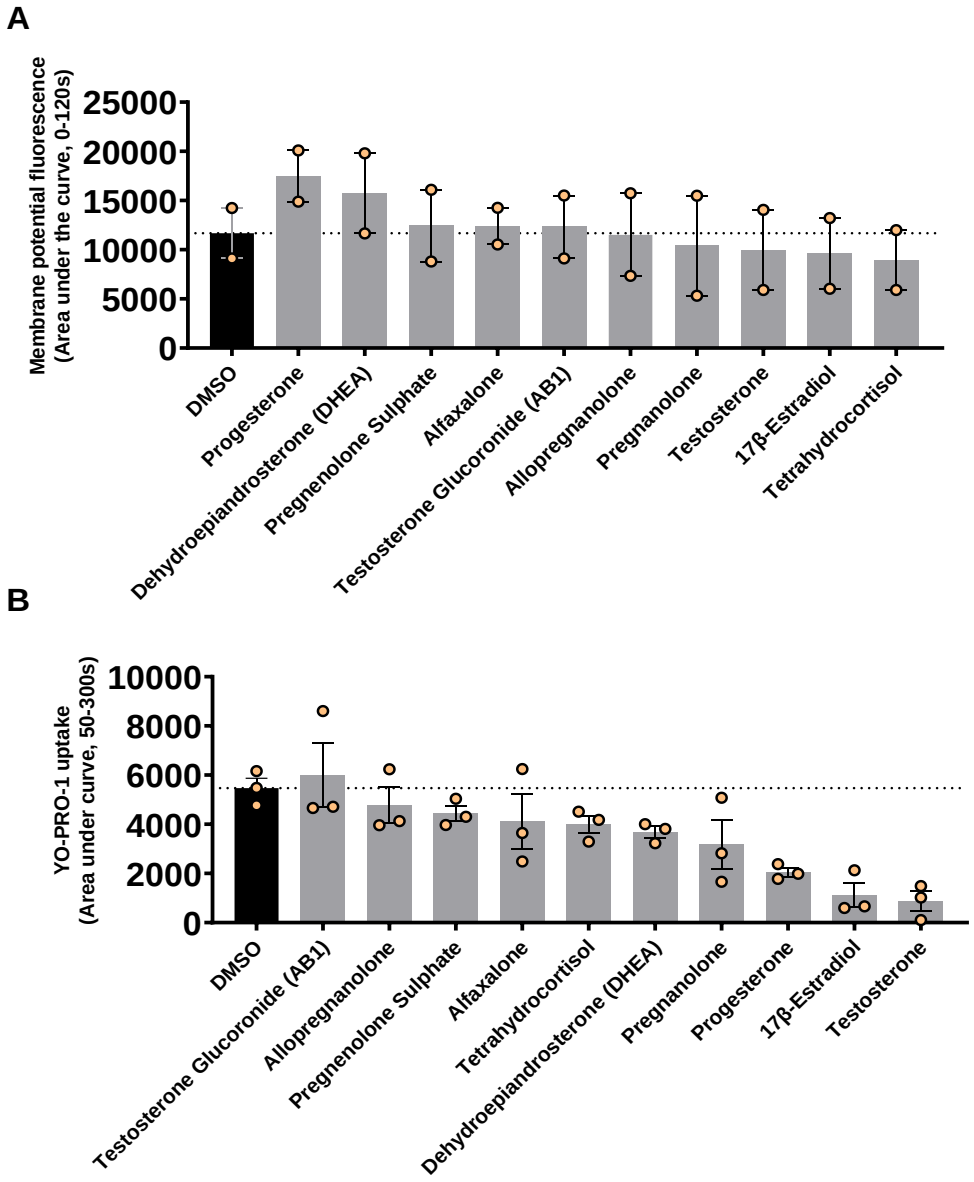

Figure 3.21 – Steroid screens conducted on HEK-293 cells stably expressing the human P2X7 receptor in the membrane potential blue assay and the YO-PRO-1 assay. Compounds were co-injected at 10 µM in DMSO with 200 µM ATP. **A**: Modulatory effects of steroid compounds at HEK-hP2X7 in the membrane potential blue assay. The steroids progesterone and dehydroepiandrosterone (DHEA) showed minor potentiation of the response to 200 µM ATP (giving responses of 17383.7 and 15727.6 respectively, compared to 11678.3 for the DMSO control). This equates to a 1.5-fold increase in the presence of 10 µM progesterone and a 1.3-fold increase in the presence of 10 µM DHEA compared to the DMSO control. **B**: Modulatory effects of steroid compounds at HEK-hP2X7 in the YO-PRO-1 assay. In contrast to the membrane potential blue assay, numerous steroid compounds appear to be inhibitory at P2X7 in this assay. Testosterone and 17β-estradiol gave responses of 870.6 and 1130.6 respectively compared to 5371.8 for the DMSO control. This equates to a 6.1-fold reduction in the presence of 10 µM testosterone and a 4.7-fold reduction in the presence of 10 µM 17β-estradiol compared to the DMSO control. For panel **A**, data are from two independent experiments conducted in standard extracellular buffer (Etotal) and plotted as AUC ± SEM. For panel **B**, data are from one experiment conducted in low divalent cation buffer (ELDV) and plotted as AUC ± SEM.

In addition to screening steroid and ginsenoside compounds, several glycosides were also screened at HEK-293 cells stably expressing either the human P2X2, human P2X4, or human P2X7 receptor using the membrane potential blue assay. Like the ginsenosides, these glycosides are natural products, most with similar steroidal-type scaffolds making up the bulk of the chemical structure. Previously, these glycosides have been shown to have varying levels of activity at the human P2X7 receptor in the YO-PRO-1 assay, but they have not been assessed for their effects in the membrane potential assay. Their effects on the human monocytic cell line, THP-1, have been briefly assessed using the FURA-2AM assay, however, this has not been done on recombinant cell lines. **Figure 3.22** shows the effects of nine glycoside compounds on stably expressing HEK-hP2X7, HEK-hP2X4, and HEK-hP2X2a. Compounds were screened at 10 μM against ATP concentrations of 200 μM (P2X7), 300 nM (P2X4) and 10 μM (P2X2) in standard extracellular buffer (Etotal).

Figure 3.22 A shows responses to various glycosides in HEK-hP2X7 cells. One glycoside appears to have positive allosteric modulator at the receptor; stevenleaf, which produces a response that is 152.7 % of the control. Daucosterol also appears to have a mild effect on the response to ATP, giving a response that is 112.6 % of control. The other glycosides screened appear to have little to no effect on the response to 200 μM ATP, with responses within 10 % of control, apart from stevioside that has slight inhibitory effects, with a response that is 80.9 % of the control response. At HEK-hP2X4, the glycoside compounds appear to have more pronounced effects (**Figure 3.22 B**). Oleanic acid gives rise to the biggest potentiation, giving a response that is 173.1 % of control, followed by stevenleaf (166.7 %), gypenoside XLIX (158.4 %), glycyrrhizic acid (154.2 %), and stevioside (150.9 %). Mogroside V, daucosterol, and gypenoside XVII appear to potentiate responses, whereas esculentoside does not, giving a response that is 108.9 % of control. **Figure 3.22 C** outlines the effects of these glycosides on the human P2X2a receptor. Like P2X7 and P2X4, stevenleaf also appears to potentiate at P2X2 (182.9 % of control), meaning that this is non-selective effect. Glycyrrhizic acid, oleanic acid, stevioside, gypenoside XVII, daucosterol, and gypenoside XLIX all have responses that are >140 % of control, whereas mogroside V and esculentoside have responses that are 117.8 and 115.4 % of control respectively.

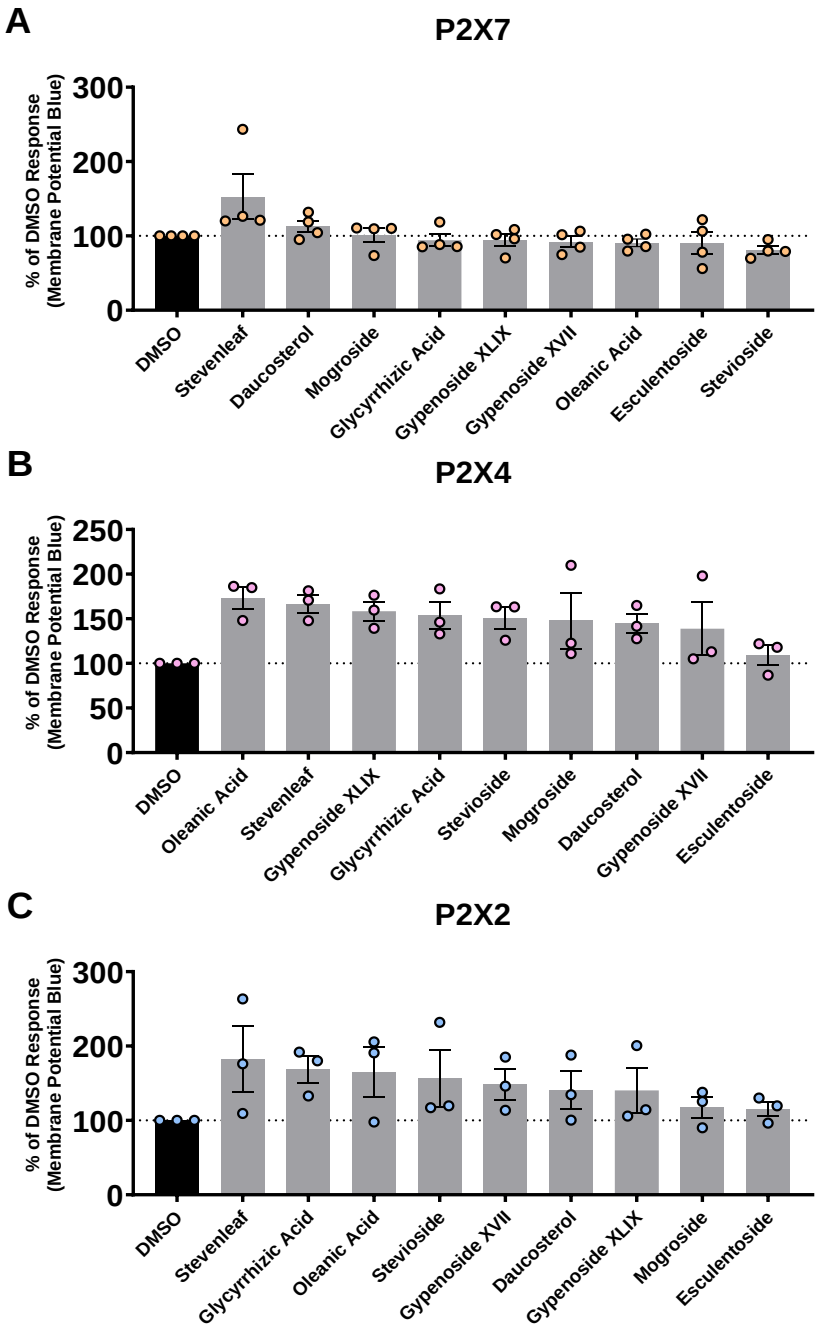

Figure 3.22 – Glycoside screens conducted on HEK-HEK-293 cells stably expressing the human P2X7 receptor, the human P2X4 receptor, and the human P2X2 receptor in the membrane potential blue assay. Compounds were screened at 10 µM and ATP was applied at the following concentrations: **A**: 200 µM; **B**: 300 nM; **C**: 10 µM. Cells were pre-treated with the appropriate compound at a concentration of 10 µM for 60 seconds before the application of ATP. **A**: Modulatory effects of glycosides at HEK-hP2X7. **B**: Modulatory effects of glycosides at HEK-hP2X4. **C**: Modulatory effects of glycosides at HEK-hP2X2. Data are the result of either four (panel **A**) or three (panels **B** and **C**) independent experiments conducted in standard extracellular buffer (Etotal). Data are averaged and normalised to the mean DMSO response between 80-180 seconds for each experiment and plotted as percentage of control (DMSO) ± SEM as outlined in **Chapter 2**. One-way ANOVA with Dunnett's multiple comparisons test on raw data did not yield significance.

3.6 Chapter 3 Discussion

To establish whether responses to ATP at P2X receptors could be measured successfully using the FLIPR Membrane Potential Kit (Blue), the effects of ATP at HEK-293 cells expressing various P2X receptors was measured, and concentration response curves generated from the results (**Figure 3.2**). Dose-dependent responses to ATP could be measured at all receptors tested, showing that it is possible to use this assay to measure responses at P2X receptors. Indeed, the effects of this assay have only been assessed at P2X receptors twice in the literature; the first was by Ruepp *et al*, 2015, where the FLIPR membrane potential kit (it is not clear whether this was the blue or red version) was used to measure the effects of various agonists and antagonists at human P2X1 receptors expressed in HEK-293 cells (Ruepp et al., 2015), and the second looked at the sustained responses to ATP and ginsenoside CK in J774 mouse macrophages, known to endogenously express the P2X7 receptor (Bidula et al., 2019a). In the study by Ruepp *et al* (Ruepp et al., 2015), the EC_{50} for sodium ATP (NaATP) was determined to be 5.49 µM, which is similar to the value measured for human P2X1 in **Figure 3.2** (8.21 µM ± 1.40, see also **Table 3.1**). The EC_{50} values determined both in **Figure 3.2** and in the study by Ruepp *et al* using the FLIPR membrane potential kits are higher than that seen in other assays and/or cell lines; when expressed in *Xenopus* oocytes, the EC_{50} value for ATP at human P2X1 was determined to be 0.87 µM using patch-clamp electrophysiology (Roberts and Evans, 2004), almost 10-fold less than that determined using the membrane potential assay. The buffer used was a variant of standard extracellular buffer, so this effect was not due to the absence of divalent cations which are known to modulate P2X receptor responses (although their effects on P2X1 responses are less) (Jarvis and Khakh, 2009, Gever et al., 2006, Evans et al., 1996). A similar phenomenon has been observed for P2X2, with the EC_{50} value for ATP at human P2X2 expressed in *Xenopus* oocytes determined to be 1.35 µM using patch-clamp electrophysiology (Lynch et al., 1999), whereas it was determined to be around 13-fold higher in **Figure 3.2** (17.56 µM ± 2.29). The determined EC_{50} value for ATP at human P2X3 was 2.54 µM ± 0.31, which was somewhat less potent than that seen in the literature. Using patch-clamp electrophysiology, one study determined the EC_{50} for ATP at human P2X3 expressed in HEK-293 cells to be 1.6 µM ± 0.1 (Pratt et al., 2005), which is similar to the value determined here using the membrane potential blue assay and the same plasmid. The human P2X4 receptor gave an EC_{50} value for ATP in the membrane potential blue assay of 0.80 µM ± 0.15, which was more potent than that published in the literature for other assays. EC_{50} values for human P2X4 in HEK-293 cells have been reported to be between approximately 1.4-2.1 µM using patch-clamp electrophysiology (Jones et al., 2000, Balázs et al., 2013) , which are slightly higher than that determined here but still within a similar range. The EC_{50} value obtained for human P2X7 was considerably higher than that for the other P2X receptors, as expected. In the membrane potential blue assay, the ATP EC_{50} was determined to be

638.5 µM ± 204.3 (see **Figure 3.2, Table 3.1**). It is important to note that many studies on P2X7 receptors use low divalent cation buffer as P2X7 responses are greatly affected by the presence of divalent cations such as Mg^{2+} and Ca^{2+} (Gever et al., 2006), however, in the interest of consistency between the P2X receptors tested in the membrane potential blue assay, standard extracellular buffer (Etotal) was used instead and therefore the EC_{50} value determined here may be greater than that observed in the literature using other assays. One study found, using patch-clamp electrophysiology, that the EC_{50} value for ATP at human P2X7 was as high as 1.8 mM ± 0.2 in normal divalent buffer (Stokes et al., 2006b), whilst two studies conducted in low divalent buffer using the YO-PRO-1 dye have determined EC_{50} values for ATP between 85 µM – 219 µM (Surprenant et al., 1996, Piyasirananda et al., 2021). In an intracellular calcium assay (Fluo-4), the EC_{50} value for ATP at human P2X7 was determined to be approximately 74.1 µM in Dulbecco's Phosphate Buffered Saline buffer (DPBS); the same study also calculated EC_{50} values for agonists in the YO-PRO-1 assay at human P2X7 receptors and determined this to be approximately 11.5 µM for ATP in DPBS without Mg^{2+} or Ca^{2+} ions (Donnelly-Roberts et al., 2009a). Although values can vary greatly between cell type and assays used, it is widely accepted that the EC_{50} value for P2X7 lies in the hundred micromolar range (Kaczmarek-Hájek et al., 2012, Jarvis and Khakh, 2009, Gever et al., 2006). Native HEK-293 cells were also able to produce a response to ATP in the membrane potential assay; this is likely due to the presence of native P2Y receptors, G-protein coupled receptors (GPCRs) that lead to the release of intracellular calcium from intracellular stores (Burnstock, 2007). In addition, calcium-dependent chloride channels would also lead to efflux of chloride ions (Cl^-) which would amplify the change in membrane potential caused by an increase in intracellular calcium (Hartzell et al., 2004). RT-PCR experiments conducted on HEK-293 cells has shown evidence for expression of voltage-gated channels, such as the voltage-gated sodium channel NaV 1.7 (He and Soderlund, 2010), which could in turn affect the membrane potential - all leading to a measurable response in the native HEK-293 cells. However, responses reached a maximum of approximately 15000 RFU at a concentration of 3 mM ATP (in P2X7-expressing cells, the response observed at this concentration was approximately 52000 RFU) and the resulting data did not produce a sigmoidal dose-response curve which differed to what was observed for HEK-293 cells stably expressing the P2X receptors. In the membrane potential assay, it appears that determined EC_{50} values for ATP are largely greater than that observed in other assays (such as patch-clamp electrophysiology and YO-PRO-1) apart from P2X4 which yields a lower EC_{50} for ATP in this assay compared to the literature. It is important to note that the FLIPR Membrane Potential Kits (both red and blue) include a quencher dye to minimise background fluorescence; with some coloured dyes known to modulate responses in P2X receptors (Syed and Kennedy, 2012), it is possible that these could be affecting the sensitivity of the receptors to ATP.

The literature surrounding the pharmacology of the human P2X2a receptor is poor; the pioneering study by Lynch *et al*, 1999, is still the most comprehensive investigation of agonists at human P2X2, including both the full receptor (P2X2a) and the truncated splice variant P2X2b (Lynch et al., 1999). The human P2X2a receptor is activated by the endogenous ligand ATP, but also by BzATP, ATPγS, and 2-MeS-ATP (Lynch et al., 1999). The agonist αβ-MeATP has been shown to be inactive at the receptor, as have the agonists ADP, UTP, and ADPβS (Lynch et al., 1999). The rank order of potency for agonists at human P2X2a has been described as follows: BzATP>2-MeS-ATP>ATP>ATPγS, with EC_{50} values of 416.9 nM, 812.8 nM, 1.02 µM, and 1.35 µM respectively when expressed in 1321N1 cells and assessed using the Fluo-3 AM calcium assay (Lynch et al., 1999). Using the membrane potential blue assay, the agonists ATP and BzATP can produce dose-dependent responses and generate EC_{50} values of 16.13 µM ± 2.89 and 24.67 µM ± 2.91 respectively (see **Figure 3.4**). This differs slightly to the data observed by Lynch *et al*, 1999 (Lynch et al., 1999), where BzATP was a more potent agonist when compared to ATP (EC_{50} values 416.9 nM and 1.02 µM respectively), although HEK-293 cells were used in the membrane potential assay whereas human 1321N1 astrocytoma cells were used by Lynch *et al*, 1999 (Lynch et al., 1999), which could lead to differences in observed results. Again, the EC_{50} values determined in the membrane potential assay are greater than that seen using other assays, and this appears to be a feature of the membrane potential assay. In agreement with previously published data, ADP and UTP did not generate concentration response curves at the human P2X2 receptor; in addition, the agonist CTP has also been shown to be inactive at the human P2X2 receptor (see **Figure 3.4**). Although the rank order may differ slightly to that observed in the literature for other assays, the membrane potential assay is able to measure responses to multiple agonists at the human P2X2 receptor.

In addition to limited published data on agonists, antagonists of the P2X2 receptor remain elusive. To date, there are no selective antagonists commercially available for the P2X2 receptor, making it difficult to assess receptor-mediated effects. The anthraquinone-derived compound PSB-10211 (**Figure 3.23**) has shown good activity at the rat P2X2 receptor (Baqi et al., 2011), although it is unknown whether this effect is consistent at the human receptor. The IC_{50} value for PSB-10211 when screened against responses to 10 µM ATP in *Xenopus* oocytes expressing the rat P2X2 receptor is in the nanomolar range (86 nM), showing good efficacy at this receptor (Baqi et al., 2011). Another compound, PSB-1011 (see **Figure 3.6** and **Figure 3.23**), also showed good inhibitory activity at the rat P2X2 receptor with an IC_{50} value of 79 nM, although it also showed activity at the P2X1 and P2X3 receptor subtypes with IC_{50} values of 422 nM and 494 nM respectively (Baqi et al., 2011). Furthermore, it shows selectivity over heteromeric P2X2 receptors, where it is 13.2-fold less effective at rat P2X2/3 than at homomeric rat P2X2 (Baqi et al., 2011). Other antagonists of P2X2 include PPADS and suramin,

which are known to be non-selective at P2 receptors with activity at several P2X and P2Y receptors, although P2X7 receptors require very high concentrations of either antagonist to show an effect and they are inactive at P2X4 receptors (Syed and Kennedy, 2012).

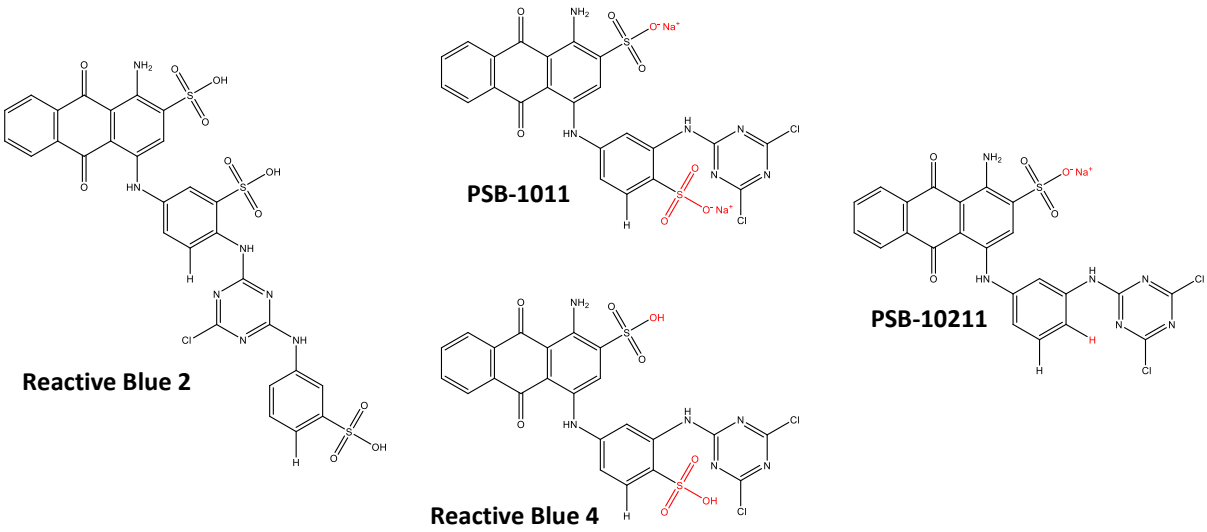

Figure 3.23 – Structures of Reactive Blue 2, Reactive Blue 4, and modulators of P2X2 mentioned in Baqi et al, 2011. Structural differences between PSB-1011, Reactive Blue 4, and PSB-10211 are highlighted in red. Note the similarities between PSB-1011 and Reactive Blue 4 (PSB-1011 appears to be the sodium salt of Reactive Blue 4).

Figure 3.5 A shows that the non-selective P2 receptor antagonist PPADs can abolish responses to 10 µM ATP in the membrane potential blue assay. This effect was confirmed using the FURA-2AM assay (panel **B**), although it appears to be more potent in this assay than in the membrane potential blue with IC_{50} values of 789.7 pM ± 789.6 and 35.8 µM ± 3.67 respectively. In patch-clamp electrophysiology experiments, the IC_{50} value for PPADS in *Xenopus* oocytes expressing the P2X2 receptor (it is unclear whether this is rat or human) was 1.6 µM (King et al., 1997); another study determined the IC_{50} of PPADS at rat P2X2 to be 3.8 µM (Bianchi et al., 1999). Literature values appear to lie somewhere in the middle of the two values determined in **Figure 3.5** (see also **Table 3.2**). Suramin was only seen to reduce the response to 10 µM ATP at the highest concentration tested (1 mM). In the literature, the IC_{50} value for suramin has been determined to be in the ten-micromolar range (unknown species P2X2: 10.4 µM (King et al., 1997), rat P2X2: 33.1 µM (Bianchi et al., 1999). The commercially available, structurally similar compound Reactive Blue 4 (Rb4) was tested at human P2X2a using the membrane potential blue assay to determine whether the inhibitory effects of PSB-1011 were consistent between species. Although PSB-1011 is the sodium salt of Rb4, it is likely that the active component of both compounds is the same when in solution. Indeed, Baqi *et al* even highlight in their study that PSB-1011

(compound 57) is the commercially available Rb4 (Baqi et al., 2011). The dye content of commercially available Rb4 is 35 %, and so the concentrations plotted are approximately 2.9-fold greater than the actual active Rb4 component in **Figure 3.5 C** and **D**. Interestingly, Rb4 did not inhibit responses to 10 µM ATP in HEK-hP2X2 cells; instead, it appeared to potentiate the response (**Figure 3.5**). EC_{50} values for Rb4 were determined to be 9.446 µM ± 9.44 and 40.99 µM ± 7.99 in the membrane potential blue and FURA-2AM assays respectively. The curve generated for the membrane potential blue results does not resemble a sigmoidal shape; the slope appears to decline at around the 3 µM concentration, so the true EC_{50} value is likely to lie somewhere between 1 – 5 µM. It would be useful to screen at lower concentrations to obtain an accurate picture of the extent of potentiation by Rb4, however, concentrations were kept equal between assays and antagonists to allow fair comparison between them. **Figure 3.8** shows an alternate view of potentiation by Rb4; the ATP concentration response is left-shifted, resulting in increased sensitivity to ATP in the presence of Rb4 and a decreased EC_{50} (from 17.78 µM to 6.40 µM, a reduction of 2.8-fold). In addition, PPADS can also be seen to decrease the sensitivity to ATP by right-shifting the concentration response curve and increasing the EC_{50} from 17.78 µM to 56.70 µM (a 3.2-fold increase). These data suggest that Rb4 is indeed potentiating the responses to ATP at human P2X2, in contrast to what was shown with the sodium salt PSB-1011 by Baqi *et al* (Baqi et al., 2011). Although PSB-1011 and Rb4 are different salts, in solution the ionic form (and the likely active component of the compounds) is likely to be the same, which suggests a different mode of action between the species. This would need to be confirmed with compound PSB-1011 to be certain of its effects at the human P2X2a receptor.

In addition to agonists and antagonists, it has been shown that the membrane potential assay can also be used to screen modulators of P2X receptors, with **Figure 3.10 A** showing that numerous ginsenosides can increase the response to 200 µM ATP. These ginsenosides have previously been screened at HEK-hP2X7 cells using the YO-PRO-1 assay (Piyasirananda et al., 2021), however, their effects in the membrane potential assay are unknown. Here, ginsenoside CK, a known modulator of P2X7, can increase responses to ATP by approximately 2.5-fold; this is similar to the increase in maximum response observed by Piyasirananda *et al* (Piyasirananda et al., 2021). Interestingly, ginsenoside 20-*S*-Rg3 shows the biggest increase at 200 µM ATP, with a fold increase of approximately 2.8-fold. Although the rank order differs to that observed by Piyasirananda *et al* (Piyasirananda et al., 2021), 20-*S*-Rg3 was also an effective modulator of the P2X7 receptor in the YO-PRO-1 assay. The fold-increase in the response in the presence of F2 was almost exactly that seen at maximal ATP concentrations by Piyasirananda *et al* (Piyasirananda et al., 2021) (2.23-fold in the YO-PRO-1 assay and 2.25-fold in the membrane potential assay), whereas the increase in the presence of 20-*S*-Rh2 and Rd was less in the membrane potential assay compared to the YO-PRO-1 assay (2.06-fold and 1.49-fold

in membrane potential, 2.6-fold and 2.77-fold in YO-PRO-1 respectively). The YO-PRO-1 data obtained in **Figure 3.10 B** differs slightly in rank order to that seen by Piyasirananda *et al* (Piyasirananda et al., 2021), but it agrees with the membrane potential blue assay, suggesting that the membrane potential blue assay is able to reliably screen for positive modulators of P2X7.

Although selected ginsenosides are known to potentiate P2X4 receptors, a screen of this magnitude has never been published (Dhuna et al., 2019). In **Figure 3.11**, it can be seen that in addition to ginsenosides CK, Rd, Rb1 and Rh2 (which are known to potentiate responses to varying extents (Dhuna et al., 2019)), other ginsenosides including 20-*S*-Rg3, F2, and the *R*-enantiomers of Rh2 and Rg3 (20-*R*-Rh2 and 20-*R*-Rg3) are also able to potentiate the responses to 300 nM ATP. Interestingly, Rd has been shown previously to be almost equipotent to CK at the P2X4 receptor in both the YO-PRO-1 assay and FURA-2AM assay; here, it is less potent, with CK potentiating the response by approximately 1.9-fold and Rd potentiating by approximately 1.4-fold. Ginsenoside F2, a structurally similar ginsenoside to CK (Piyasirananda et al., 2021), is also able to potentiate P2X4 responses to a similar extent as CK, much like the effects observed at human P2X7 (see **Figure 3.10**). Interestingly, the *R*-enantiomers of Rh2 and Rg3 also have activity at P2X4; previously, they have been shown to be inactive at human P2X7 in the YO-PRO-1 assay (Piyasirananda et al., 2021). Some potentiation can be observed with the application of ginsenoside 20-*S*-Rg3 alone, however, this could be due to residual ATP produced by the cells following experimental challenge given that P2X4 receptors are activated by lower concentrations of ATP than the other receptors tested (see **Figure 3.12**).

A similar picture can be seen for the human P2X2a receptor: again, select ginsenosides appear to potentiate responses at this receptor, with a different rank order (**Figure 3.13**), although statistical analysis did not find these results to be significant. At human P2X2, ginsenoside CK is the most effective potentiator of the response to 10 μM ATP, increasing the response by approximately 1.8-fold. This is less than that seen at P2X7 and P2X4, where responses were increased by 2.5-fold and 1.9-fold respectively for ginsenoside CK. Again, another *R*-enantiomer has shown activity at P2X2 that does not show activity at the P2X7 receptor (ginsenoside 20-*R*-Rg3) with a fold increase of approximately 1.6 compared to control. The ginsenoside Rb1, which does not show activity at human P2X7 or P2X4 receptors in the membrane potential blue assay, is able to potentiate the response to 10 μM ATP somewhat, increasing the response to ATP by approximately 1.5-fold. These data suggest that whilst the binding pocket between the receptors is likely similar as potentiation can be seen at both P2X7 and P2X4 by various ginsenosides, key structural differences may affect the binding of ginsenosides and lead to varying levels of efficacy between the P2X receptors, meaning that apparent potentiation seen at the P2X2 receptor was not statistically significant. Screening data from the quickly desensitising P2X1 and P2X3 receptors shows that minor potentiation can be observed at these

receptors by 20-*S*-Rh2 (see **Figure 3.15** and **Figure 3.17**), although the mean fold increase for this ginsenoside is 1.4-fold and 1.3-fold for P2X1 and P2X3 receptors respectively, which is far less than that seen at the other P2X receptors screened. As the binding pocket for ginsenosides in P2X7 is thought to be located in the central vestibule (Bidula et al., 2019b), it is likely that the receptor needs to be open in order for the ginsenosides to bind and exert their action on the receptor. It could be that the P2X1 and P2X3 receptors are not open long enough to allow binding of the ginsenosides, and therefore the potentiation observed is minimal and not statistically significant. Furthermore, the concentration of ATP used to screen the ginsenosides at P2X1 and P2X3 was perhaps higher than optimal – all other receptors have been screened at a roughly EC_{20}-EC_{30} concentrations, whereas P2X1 and P2X3 were both screened at 10 µM which is approximately EC_{50} for hP2X1 and maximal for hP2X3; as a result, the effects may be less pronounced at these receptors than for a lower concentration.

In terms of other natural product modulators of P2X receptors, selected steroids have been shown to potentiate responses in rat P2X2 namely progesterone and DHEA (De Roo et al., 2003, De Roo et al., 2010). The steroid 17β-estradiol has also been shown to inhibit responses to ATP at P2X7 (Cario-Toumaniantz et al., 1998). Given that the ginsenosides have a steroidal-like central scaffold, it could be that the activity of these is linked to that of steroids. To begin with, a range of steroids were screened at human P2X2a to confirm if potentiation by progesterone and DHEA is conserved between species (**Figure 3.20 A**). As there are no specific antagonists of human P2X2, native HEK-293 cells were also screened as a control (**Figure 3.20 B**). Although progesterone and DHEA are able to potentiate responses to 20 µM ATP in the HEK-hP2X2a cell line, they also potentiate ATP-induced responses in the native HEK-293 cell line. This makes it difficult to determine to what degree the potentiation at hP2X2a actually is, as it seems they are having an effect on the membrane potential response in the absence of P2X2 receptors. This could be due to effects on other native receptors expressed in HEK-293 cells, or due to an interaction with the assay itself; a receptor-specific antagonist and/or more repeats would be needed to increase confidence in the effects of progesterone and DHEA on human P2X2 receptors. Interestingly, other steroids have also been shown to potentiate P2X2, including testosterone and the modified testosterone glucoside analogue AB1, although the latter is less effective (2.4-fold and 1.8-fold respectively). Although effects can be seen in both the native and P2X2-transfected cell lines, it is important to note that the maximum response seen with progesterone in the native HEK-293 cells reaches approximately 3800 RFU, whereas in the HEK-hP2X2a cells the maximum with progesterone is approximately 8500 RFU, suggesting increased potentiation in the transfected cells over the native HEK-293 cells and therefore some contribution to the potentiation seen with progesterone. This theory would also apply to the steroids testosterone and DHEA. Progesterone and DHEA also potentiate human P2X7 (**Figure 3.21**) in the membrane potential blue

assay, however, both were inhibitory in the YO-PRO-1 assay, highlighting key differences between the two. It is important to note that the membrane potential assay measures ion influx and efflux (or the change in membrane potential as a result), whereas the YO-PRO-1 assay measures dye uptake which is interpreted as a measure of receptor activity. There are large differences in the actions that each assay measures, and so it is likely that the responses measured in each would differ also. In agreement with data published in the literature for alternate assays, 17β-estradiol inhibited responses to 200 μM ATP in both the YO-PRO-1 and membrane potential blue assays, although the effect was more pronounced in the YO-PRO-1 assay. Here, testosterone was the biggest inhibitor of the response to ATP at HEK-hP2X7 in the YO-PRO-1 assay, but the modified testosterone glucoside compound AB1 (see **Figure 3.19**) did not inhibit the response (**Figure 3.21 B**). The sugar moiety is key to the activity of the ginsenosides (Piyasirananda et al., 2021), and this data shows that the introduction of a sugar moiety can reverse the inhibitory effects of testosterone, perhaps changing the binding mode and introducing positive modulator activity instead.

Numerous glycosides, natural products similar to the ginsenosides, have been shown to potentiate YO-PRO-1 responses to ATP in HEK-hP2X7 cells (Piyasirananda et al., 2021), but their effects in the membrane potential assay and at other P2X receptors is unknown. At human P2X7, it can be seen that the effects of glycosides are limited in the membrane potential assay compared to that observed in the YO-PRO-1 assay in Piyasirananda *et al* (Piyasirananda et al., 2021), with only stevenleaf demonstrating potentiation (**Figure 3.22 A**). Even still, the potentiation by stevenleaf is minimal and not statistically significant, giving a response that is 1.5-fold greater than the control. In the YO-PRO-1 assay, gypenosides XVII and XLIX increased the maximum response by approximately 2-fold (Piyasirananda et al., 2021), whereas in the membrane potential assay there was little difference to the control response, highlighting crucial differences in potentiation between the two assays. Modulatory effects at the P2X4 receptor are more pronounced (**Figure 3.22 B**), with all glycosides screened increasing the response to 300 nM ATP somewhat. A similar effect was seen at hP2X2a (**Figure 3.22 C**), although with a different rank order of efficacy. These differences in both rank order and between previously published data conducted using different assays highlight the importance of using multiple assays to confirm activity at a receptor, as it is possible that one aspect of P2X channel opening can be modulated over another, particularly for P2X7 where the non-specific pore is a relatively unique feature. In addition, it would be useful to decipher a structure-activity relationship at each of the P2X receptors in order to develop novel modulators specific for one over another, as the activity of certain ginsenosides overlaps between the receptors tested. Computational docking and homology models will be studied in the next chapter, where a greater

understanding of what residues are thought to be involved in binding to enable modulation by ginsenosides is explored.

Chapter 4 – Investigating Mutants of hP2X2a and hP2X4 Receptors

4.1 Introduction

Several ginsenosides have been shown to potentiate the P2X7 receptor (Helliwell et al., 2015), with investigations into a potential binding site suggesting a novel pocket located in the central vestibule region of the extracellular domain (Bidula et al., 2019b) (see **Figure 4.1** below).

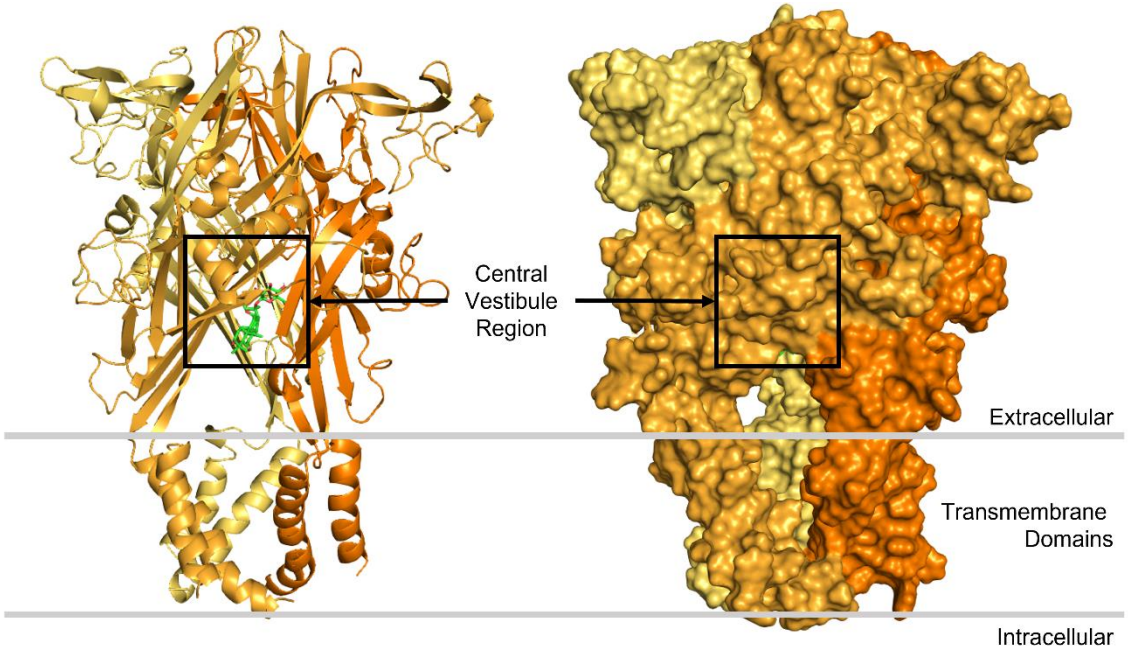

Figure 4.1 – Diagram showing the location of human P2X7 relative to the cell membrane, highlighting the central vestibule region. Homology model of human P2X7 (shown in yellow/orange, both left and right) with ginsenoside CK (shown in green) docked to the central vestibule region. Location of the receptor relative to the cell membrane (grey lines) is approximate. The homology model of human P2X7 is based on the crystal structure of zebrafish-P2X4 (PDB: 4DW1) with the human sequence for P2X7 overlayed. The C-terminal tail is truncated as with the crystal structure of zebrafish-P2X4. The zebrafish-P2X4 crystal structure was used as modelling and computational docking was performed prior to the cryo-EM structure of rat P2X7 being available. Computational docking was performed by Dr Sam Walpole, UEA, using Glide (Schrödinger).

More recently, ginsenosides have also been shown to have activity at the human P2X4 (hP2X4) receptor (Dhuna et al., 2019). In the previous chapter, ginsenosides were screened at multiple P2X receptors for activity, showing that in the presence of a single concentration of ATP all P2X receptors were potentiated by at least one of the ginsenosides but to varying extents and significance, suggesting that there are key differences in the binding and therefore activity of the ginsenosides

between the P2X family (see **Chapter 3**). It is not unreasonable to hypothesise that this central vestibule region could be somewhat conserved; when looking at phylogenetic analyses, the human P2X4 and P2X7 (hP2X7) receptors are closely related, with human P2X2a (hP2X2a) less closely related but more so to hP2X4 than hP2X7 (Kaczmarek-Hájek et al., 2012). The hP2X2a, hP2X4, and hP2X7 receptor subtypes have all been described as slowly desensitising (Marques-da-Silva et al., 2011, Kaczmarek-Hájek et al., 2012), able to allow uptake of large dyes such as YO-PRO-1 iodide (Kaczmarek-Hájek et al., 2012, Marques-da-Silva et al., 2011), and sequence alignments show conservation of several residues between receptor subtypes (Bidula et al., 2019b).

Site directed mutagenesis is a key tool used to investigate binding of modulators or ligands to a receptor; it involves mutating single or multiple residues to other residues, in this case alanine, and assessing the impact this has on receptor activity. In this chapter, mutations to both hP2X2a and human hP2X4 were made at positions analogous to key residues involved in binding at hP2X7 (Bidula et al., 2019b) or those that have been shown to be important in computational docking models of ginsenoside CK at either receptor. Although these mutations are small, they can drastically change how modulators affect receptor activity. Even between species, small differences in P2X receptor sequences can lead to opposite effects: for example, key species differences exist between rat and human P2X2a with regards to modulation by zinc (Zn^{2+}), with human P2X2a strongly inhibited by [Zn^{2+}] up to 100 µM and rat P2X2a potentiated by equivalent concentrations (Punthambaker et al., 2012). This is in part due to one histidine at position 213 in rat P2X2a, which is an arginine in human P2X2a (Punthambaker et al., 2012, Tittle and Hume, 2008), showing how vital single differences in residues can be to modulation characteristics.

Although activity of ginsenosides has been confirmed at multiple P2X receptors, these key differences in activity highlight the possibility of nuanced binding modes between P2X receptor subtypes. While some investigations into the binding pocket of ginsenoside CK at P2X7 have been conducted (Bidula et al., 2019b), little is known about whether this binding pocket is conserved between the P2X receptors or whether this region is highly variable. This chapter will explore in further detail the binding of ginsenosides to the central vestibule region of two P2X receptors, human P2X2a and human P2X4. Given that hP2X4 receptors have been shown to be significantly potentiated by numerous ginsenosides in the previous chapter, and hP2X2a receptors to a much lesser extent, these both present as interesting candidates to compare to and expand on the current knowledge surrounding human P2X7. The aims of this chapter are to explore in detail the proposed binding of ginsenoside CK to the P2X2 and P2X4 receptors, and to then use site directed mutagenesis to examine the effects of mutating key residues on potentiation of the receptor in the Membrane Potential Blue and FURA-2AM assays.

4.2 Analysis of Ginsenoside CK Docking to the Central Vestibule Region of Human P2X Receptors

To first determine which residues should be investigated using site directed mutagenesis, computational docking of ginsenoside CK to homology models of hP2X2a and hP2X4 was performed by Dr Sam Walpole, UEA, and analysed below. **Figure 4.2** outlines the predicted binding of CK to the central vestibule region of both hP2X2a and hP2X4.

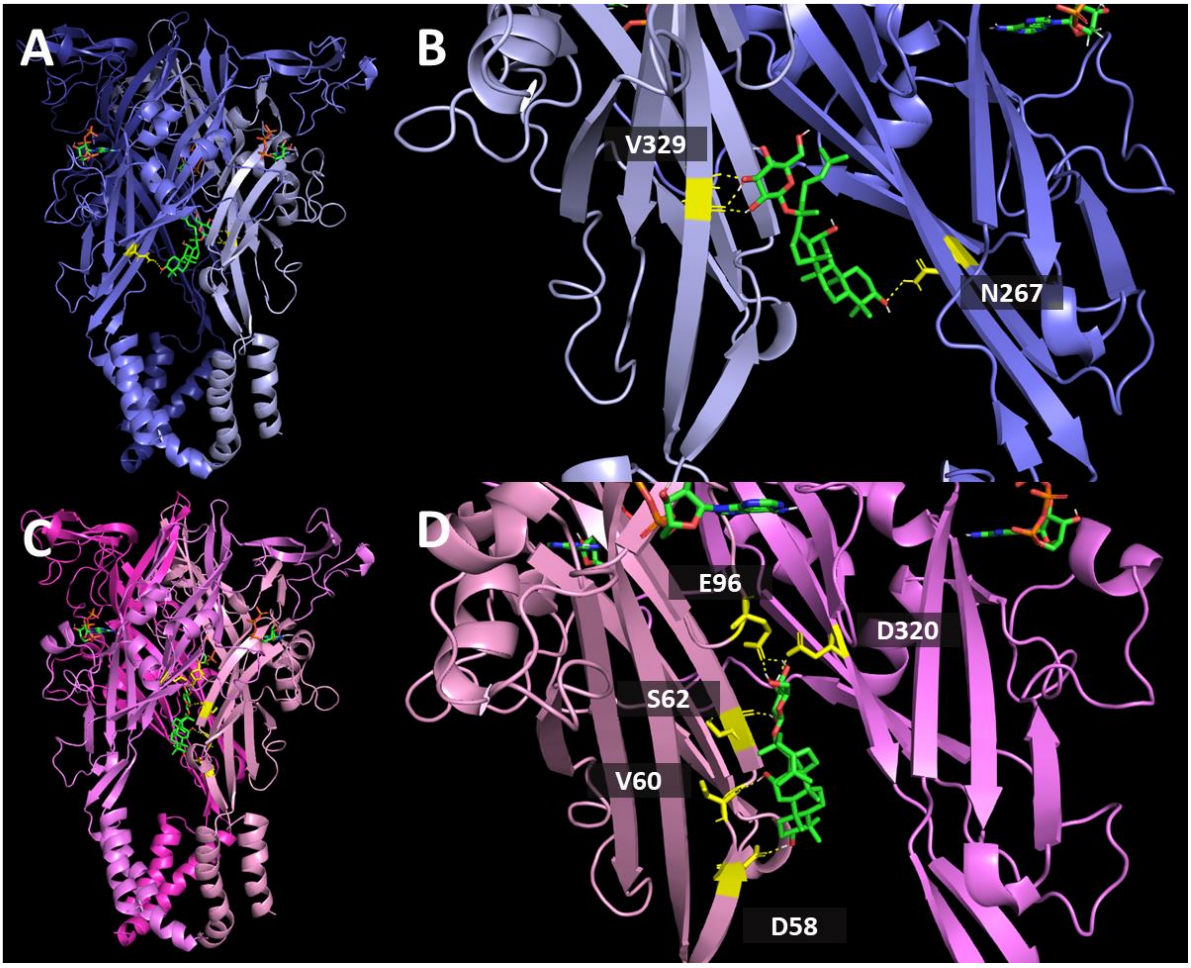

Figure 4.2 – Homology models of human P2X2 and human P2X4 in the ATP-bound open state with ginsenoside CK docked. Homology models of **A**: hP2X2a (blue) and **C**: hP2X4 (pink) showing CK (green) docked to the central vestibule region with ATP (green, above CK) present. Close up images of the central vestibule region with ginsenoside CK docked are shown for **B**: hP2X2a and **D**: hP2X4. Residues with polar contacts are highlighted in yellow and shown with sticks. Polar contacts are shown by yellow dashed lines. Note that the orientation of panels **B** and **D** is different to panels **A** and **C** respectively. Homology models are based on the crystal structure of zebrafish-P2X4 (PDB: 4DW1) with the human sequence for either P2X2a or P2X4 overlayed. Docking was performed by Dr Sam Walpole using Glide (Schrödinger).

In panel **A** (hP2X2a), CK can be seen to bind with the sugar moiety towards the top of the pocket, and the steroidal scaffold hangs down into the central vestibule space. Residues with polar interactions with CK are V329 and N267, which are thought to make polar interactions with the sugar moiety and C3 hydroxyl group respectively. In panel **B**, this interaction can be seen more clearly, with the main chain of residue V329 making interactions with the C2 and C3 hydroxyl groups of the glucose sugar moiety, and the C3 hydroxyl group of CK making an interaction with the side chain of N267. ATP can also be viewed to the top-right of the central vestibule region, bound to the ATP-binding site that lies between subunits. At hP2X4 (**4.2 C**), ginsenoside CK fits tighter to the edge of the central vestibule region, making more polar contacts with the receptor. This can be seen in panel **D**, where five different residues are involved in interactions with ginsenoside CK. Residues that make polar interactions with CK are E96, D320, S62, V60, and D58. Residues E96, D320 and S62 all make polar interactions with the sugar moiety, with the side chain of E96 interacting with C5 and C6 of the glucose sugar moiety, the side chain of D320 interacting with C3, and the main chain of S62 interacting with C2. Residue D58 interacts with the C3 hydroxyl group of ginsenoside CK, similar to the interaction made between ginsenoside CK and residue N267 in hP2X2a, whereas the main chain of V60 interacts with the hydroxyl group on C12.

Next, a sequence alignment was performed to compare key regions of the hP2X7 amino acid sequence involved in the binding of ginsenoside CK with that of hP2X2a and h2X4 receptors (**Figure 4.3**).

```
Q99572 P2RX7_HUMAN  52  QRKEPVI-SSVHTKV  95   PLQ-GNSFFVMTNFL
Q9UBL9 P2RX2_HUMAN  68  QESETGPESSIITKV  101  PPEGGSVFSIITRVE
Q99571 P2RX4_HUMAN  55  QETDSVV-SSVTTKV  92   PAQEENSLFVMTNVI

Q99572 P2RX7_HUMAN  249 GGIMGIEIYWDCNLD  313  FGIRFDILVFGTGGK
Q9UBL9 P2RX2_HUMAN  258 GGVIGVIINWDCDLD  321  YGIRIDVIVHGQAGK
Q99571 P2RX4_HUMAN  250 GGIMGIQVNWDCNLD  315  YGIRFDIIVFGKAGK
```

Figure 4.3 – Amino acid sequence alignment for human P2X7, human P2X2, and human P2X4. Residues thought to make polar interactions with ginsenoside CK in computational docking analysis shown in **Figure 4.2** are coloured according to receptor (P2X2: blue, P2X4: pink), whereas residues that have analogous residues in other receptors are highlighted in **bold**.

According to computational docking data in **Figure 4.2**, Ginsenoside CK is predicted to make the most polar interactions with hP2X4 (five), with only two predicted polar interactions with hP2X2a. Sequence alignments in **Figure 4.3** show that there is some conservation in the amino acid sequence between the P2X receptors studied, although P2X2 differs the most from both P2X4 and P2X7. Only two residues are analogous across all three receptors; these are D318 in hP2X7 (D326 in hP2X2a and D320 in hP2X4) and V321 in P2X7 (V329 in hP2X2a and V323 in hP2X4). This region in particular is highly conserved between these three P2X receptors, with the key sequences for hP2X7, hP2X2a, and hP2X4 respectively being DILV, DVIV, and DIIV. Although there are some notable differences between sequences for each of the P2X receptors, this region appears to be key to the binding of ginsenoside CK, particularly with regards to interactions with the sugar moiety, in all three receptors examined.

Table 4.1 summarises the proposed interactions between ginsenoside CK and both the P2X2 and P2X4 receptors, in addition to the three polar interactions proposed between ginsenoside CK and the P2X7 receptor by Bidula *et al* (Bidula et al., 2019b). Side chain interactions are proposed to be between ginsenoside CK and the unique side chain of each amino acid, whereas main chain interactions are proposed to be between ginsenoside CK and the main backbone of the amino acid chain, and therefore these are unlikely to be dependent on the residue itself.

Table 4.1 – Summary of proposed polar interactions between ginsenoside CK and human P2X2, P2X4, and P2X7 receptors. Analysis of P2X2 and P2X4 is based on computational docking shown in **Figure 4.2**. [1]Adapted from data presented by Bidula *et al*.

Receptor	Interacting Residue	Main or Side Chain Interaction
P2X2	**N267**	Side chain
	V329	Main chain
P2X4	**D58**	Side chain
	V60	Main chain
	S62	Main chain
	E96	Side chain
	D320	Side chain
P2X7[1]	**S60**	Side chain
	N100	Side chain
	D318	Side chain

4.3 Investigating Mutants of the Human P2X2a Receptor Using the Membrane Potential Blue and FURA-2AM Assays

To further assess potentiation by ginsenosides at the hP2X2a receptor and validate the results of **Chapter 3**, full concentration response curves to ATP in the presence and absence of ginsenosides found to have some activity in screening experiments (see **Chapter 3**) were conducted. In addition, site directed mutagenesis was utilised to assess the effects of mutating key residues on the response of the receptor to ATP and potentiation by ginsenosides. Mutations were generated at key positions thought to be involved in ginsenoside binding or that were noteworthy when investigating the binding pocket in the hP2X7 receptor (Bidula et al., 2019b). For hP2X2a, these were: D326A; I328A; S77A; S76A; N267A, V329A, with residues V329 and N267 thought to be directly involved in binding with ginsenoside CK (see **Figure 4.2**) and the other residues analogous to those found to be important to ginsenoside binding and activity in hP2X7 (Bidula et al., 2019b). Concentration responses to ATP at concentrations between 300 nM and 300 µM were conducted on HEK-293 cells transiently transfected with each of the hP2X2a mutants, either alone or in the presence of 10 µM ginsenoside CK or ginsenoside Rb1 (**Figure 4.4** and **Figure 4.5**).

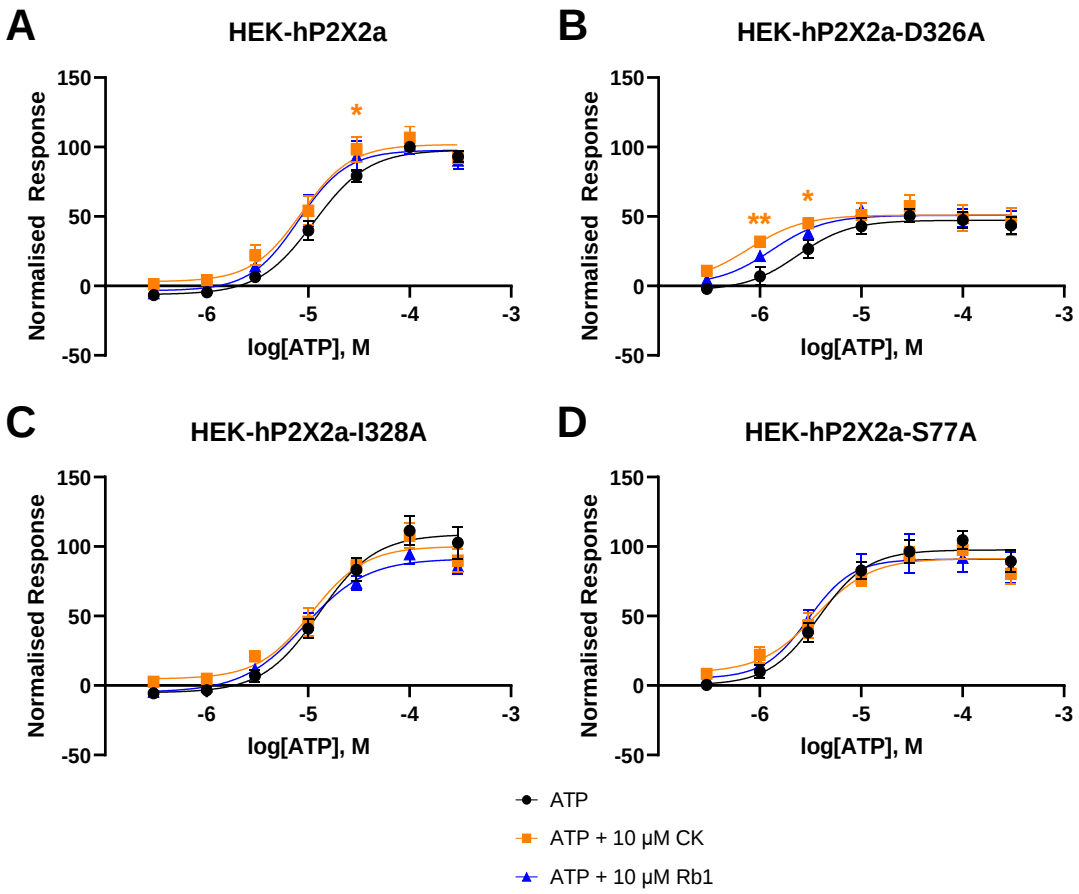

Figure 4.4 – Responses to ATP in the presence and absence of either ginsenoside CK or Rb1 in HEK-293 cells transiently transfected with wild type or mutant hP2X2a measured using the membrane potential blue assay. The control ATP response is shown in black, whereas ATP with 10 µM CK is shown in orange and ATP with 10 µM Rb1 is shown in blue for **A**: wild type hP2X2a (n=6-9) **B**: D326A mutant hP2X2a (n=4-6) **C**: I328A mutant hP2X2a (n=5-6) **D**: S77A mutant hP2X2a (n=4-5). Experiments were conducted in standard divalent cation buffer (Etotal). Graphs are plotted as normalised area under the curve (AUC) values, where the response to 100 µM ATP in wild type HEK-hP2X2a cells is taken as the maximum (100 %) value, from the specified number of independent experiments ± SEM and fitted with a four-parameter non-linear regression curve. Average EC_{50} values ± SD are calculated using individual EC_{50} values from the specified number of independent experiments (see **Table 4.2**). *P<0.05, **P<0.01 determined by two-way ANOVA with Dunnett's multiple comparisons test on normalised data to account for transfection differences.

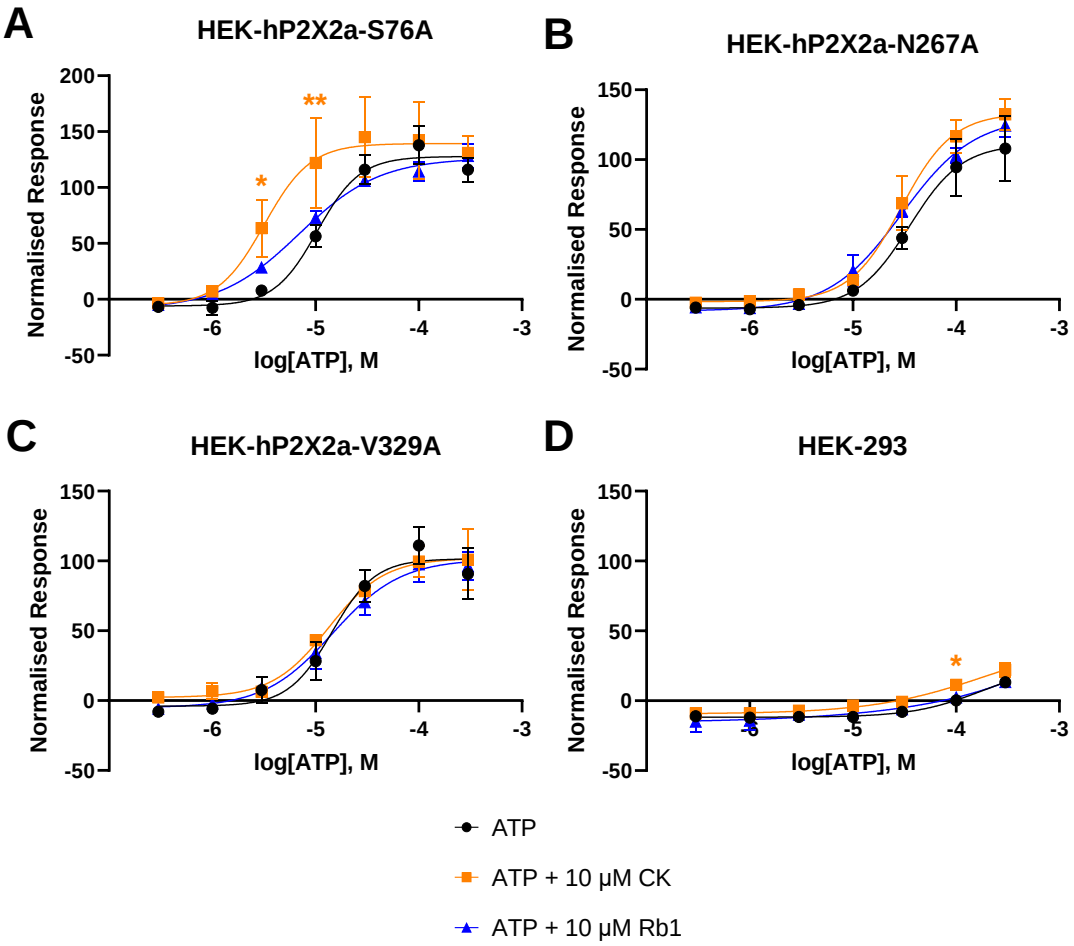

Figure 4.5 – Responses to ATP in the presence and absence of either ginsenoside CK or Rb1 in HEK-293 cells transiently transfected with mutant hP2X2a measured using the membrane potential blue assay. The control ATP response is shown in black, whereas ATP with 10 µM CK is shown in orange and ATP with 10 µM Rb1 is shown in blue for **A**: S76A mutant hP2X2a (n=2-4) **B**: N267A mutant hP2X2a (n=2-4) **C**: V329A mutant hP2X2a (n=2-3) **D**: Native HEK-293 cells (n=5-8). Experiments were conducted in standard divalent cation buffer (Etotal). Graphs are plotted as normalised area under the curve (AUC) values, where the response to 100 µM ATP in wild type HEK-hP2X2a cells is taken as the maximum (100 %) value (see **Figure 4.4**), from the specified number of independent experiments ± SEM and fitted with a four-parameter non-linear regression curve. Average EC_{50} values ± SD are calculated using individual EC_{50} values from the specified number of independent experiments (see **Table 4.2**). *P<0.05, **P<0.01 determined by two-way ANOVA with Dunnett's multiple comparisons test on normalised data to account for transfection differences.

First, the sensitivity to ATP was considered for each of the mutants generated. The EC_{50} for ATP measured for wild type HEK-hP2X2a was similar to that previously obtained, giving a value of 12.62 µM (**Figure 4.4**). Mutant HEK-hP2X2a-D326A was considerably more sensitive to ATP, with an EC_{50} approximately 5.5-fold less than the wild type receptor, although the maximum response value was

less, reaching only approximately 50 % of the maximum response observed at the wild type receptor (**Figure 4.4**). Mutant HEK-hP2X2a-I328A displayed similar pharmacology to HEK-hP2X2a, whereas the HEK-hP2X2a-S77A mutant was more sensitive to ATP than the wild type receptor (**Figure 4.4**). Interestingly, mutant HEK-hP2X2a-S76A had a similar sensitivity to ATP to the wild type receptor, however, the maximum response to ATP was considerably higher than the wild type hP2X2a receptor (approximately 138 %) (**Figure 4.5**). Mutant HEK-hP2X2a-N267A was the only one of the mutants tested to be less sensitive to ATP than the wild type. Mutant HEK-hP2X2a-V329A again had similar sensitivity to ATP compared to the wild type hP2X2a receptor, with a similar maximum response to the wild type receptor at approximately 111 % that measured at HEK-hP2X2a (**Figure 4.5**). Native HEK-293 cells did not produce a sigmoidal dose-response curve to ATP, with the maximum response measured to ATP approximately 13 % that of the wild type receptor (**Figure 4.5**). EC_{50} values are summarised in **Table 4.2**.

Table 4.2 – Average EC_{50} values to ATP in the presence and absence of ginsenosides in HEK-293 cells transiently transfected with wild type or mutant human P2X2a measured using the membrane potential blue assay. Experiments were conducted in standard divalent cation buffer (Etotal). Average EC_{50} values ± SD are calculated using individual EC_{50} values from the specified number of independent experiments (see **Figure 4.4** and **Figure 4.5**) where graphs are plotted as normalised area under the curve (AUC) values ± SEM and fitted with a four-parameter non-linear regression curve. *P < 0.05 from one-way ANOVA with Dunnett's multiple comparisons test.

Mutant	Compound	Average EC_{50} (μM ± SD)	pEC_{50}	Difference in pEC_{50} ($-pEC_{50}$ ATP + ginsenoside – $-pEC_{50}$ ATP)
Wild-type P2X2	**ATP**	12.62 ± 5.40	-4.899	
	ATP + CK	8.93 ± 4.24	-5.049	0.150
	ATP + Rb1	8.52 ± 3.27	-5.070	0.171
HEK-P2X2-D326A	**ATP**	2.36 ± 1.23	-5.626	
	ATP + CK	1.72 ± 0.86	-5.764	0.138
	ATP + Rb1	1.72 ± 0.49	-5.763	0.137
HEK-P2X2-I328A	**ATP**	13.33 ± 3.90	-4.875	
	ATP + CK	11.74 ± 6.94	-4.930	0.055
	ATP + Rb1	10.02 ± 3.76	-4.999	0.124
HEK-P2X2-S77A	**ATP**	4.14 ± 1.75	-5.384	
	ATP + CK	3.68 ± 2.11	-5.434	0.050
	ATP + Rb1	3.17 ± 0.79	-5.136	0.116
HEK-P2X2-S76A	**ATP**	10.97 ± 3.05	-4.96	
	ATP + CK	4.22 ± 1.75 *	-5.375	0.415
	ATP + Rb1	7.31 ± 3.02	-5.136	0.176
HEK-P2X2-N267A	**ATP**	33.30 ± 7.14	-4.478	
	ATP + CK	31.23 ± 9.96	-4.505	0.028
	ATP + Rb1	29.21 ± 0.62	-4.535	0.057
HEK-P2X2-V329A	**ATP**	14.74 ± 7.74	-4.831	
	ATP + CK	14.39 ± 6.83	-4.842	0.011
	ATP + Rb1	14.93 ± 4.05	-4.826	-0.005

Next, the effects of ginsenosides CK and Rb1 on these mutants were assessed. In wild type HEK-hP2X2a cells, a slight leftward shift in the concentration response curve can be observed with both CK and Rb1. Despite a lack of statistical significance in screening data in **Chapter 3**, ginsenoside CK showed significant potentiation of the response to 30 µM ATP here. Neither ginsenoside CK nor Rb1 increased the maximum response compared to ATP alone (107 % and 102 % respectively) (**Figure 4.4**). Despite the increased sensitivity to ATP, similar effects were observed at HEK-hP2X2a-D326A. The addition of 10 µM CK resulted in a decrease in the $EC_{50,}$ with ginsenoside Rb1 causing a similar degree of leftward shift. Again, there was little increase in the maximum response value observed (**Figure 4.4**). Potentiation by either ginsenoside CK or Rb1 was not observed at the mutant HEK-hP2X2a-I328A receptor to the same extent as the wild type hP2X2a receptor. In **Figure 4.4**, it appears that there is no shift in the presence of either of these ginsenosides, although there is a slight decrease in the EC_{50} value (**Table 4.2**). Like the I328A mutant, HEK-hP2X2a-S77A shows little to no shift with either ginsenoside CK or Rb1 in **Figure 4.4**.

Mutant HEK-hP2X2a-S76A appears considerably more sensitive to the ginsenoside CK compared to the wild type hP2X2a receptor, with a large shift in the concentration response curve visible in **Figure 4.5**. Indeed, the EC_{50} value is reduced in the presence of both CK and Rb1 (**Table 4.2**). Mutant HEK-hP2X2a-N267A, less sensitive to ATP than the wild type receptor, is modulated by ginsenosides CK and Rb1 but to a lesser extent than the wild type. Finally, mutant HEK-hP2X2a-V329A, despite having similar EC_{50} values to the wild type receptor and the proposed interaction being with the main chain of the residue rather than the side chain, does not appear to be modulated by CK or Rb1. In **Figure 4.5**, little to no shift is observed in the presence of either ginsenoside. Ginsenosides CK and Rb1 did not display any noteworthy changes to the native HEK-293 cell response (**Figure 4.5**). For all mutants tested, including wild type HEK-hP2X2a and native HEK-293 cells, there was little change to the maximum response measured in the presence of either ginsenoside using the membrane potential blue assay (**Figure 4.4** and **Figure 4.5**).

To verify the effects observed with the ginsenosides on wild type and mutant hP2X2a in the membrane potential blue assay, the intracellular calcium assay FURA-2AM was used. To begin with, the responses to ATP in transient HEK-hP2X2a and native HEK-293 cells were compared. **Figure 4.6** shows the average intracellular calcium measurements across time in transiently transfected HEK-hP2X2a and native HEK-293 cells to 100 µM ATP.

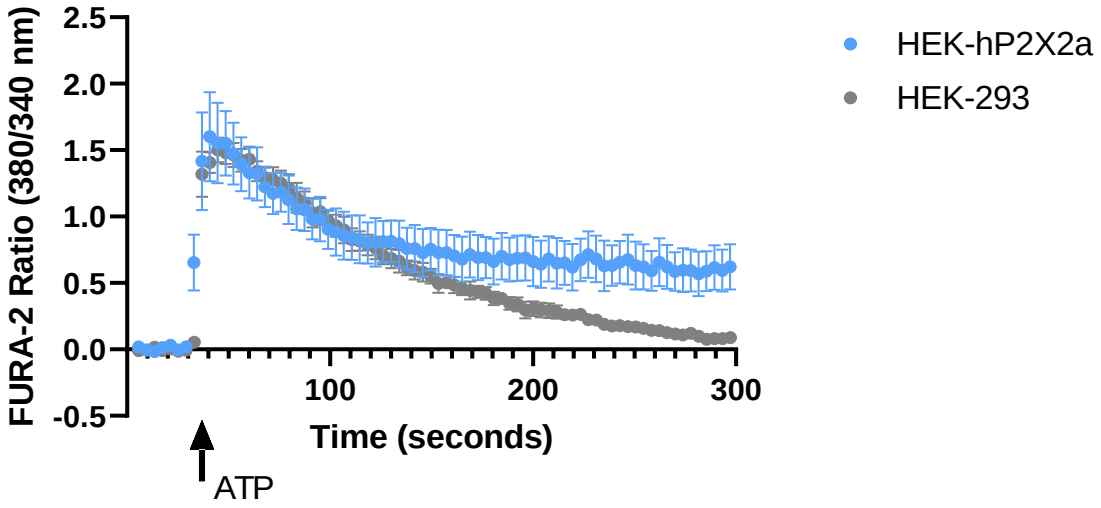

Figure 4.6 – Average intracellular calcium measurements in transiently transfected HEK-hP2X2a or native HEK-293 cells following stimulation with 100 µM ATP. Fluorescence was measured for a total of 300 seconds with ATP application at 30 seconds. Data are plotted as mean fluorescence (FURA-2 ratio) ± SEM from four independent experiments and transfections. Time is plotted as the average time of read from four independent experiments for each of HEK-hP2X2a and HEK-293.

Here, the peak responses are comparable, with maximum FURA-2 ratio values of 1.6 for HEK-hP2X2a and 1.5 for native HEK-293 at approximately 10-15 seconds post-ATP application. In native HEK-293 cells, this response declines over time, returning to almost baseline fluorescence by 300 seconds, however, in transient HEK-hP2X2a cells, there is a sustained calcium response (**Figure 4.6**). Although fluorescence declines at a similar rate to the native HEK-293 cells between approximately 40 seconds and 120 seconds, the response declines more slowly from 120 seconds to 300 seconds and does not return to baseline. Instead, the response remains sustained at approximately 40 % that of the peak response. Responses to ATP in the HEK-hP2X2a cells were lower than expected – as this is a transient cell line, this could be due to poor transfection efficiency and as a result a lower level of expression of the hP2X2a receptor than anticipated.

Figure 4.7 shows concentration responses to ATP in HEK-293 cells transiently transfected with wild type or mutant hP2X2a and native HEK-293 cells in the presence or absence of ginsenosides CK or 20-*S*-Rg3.

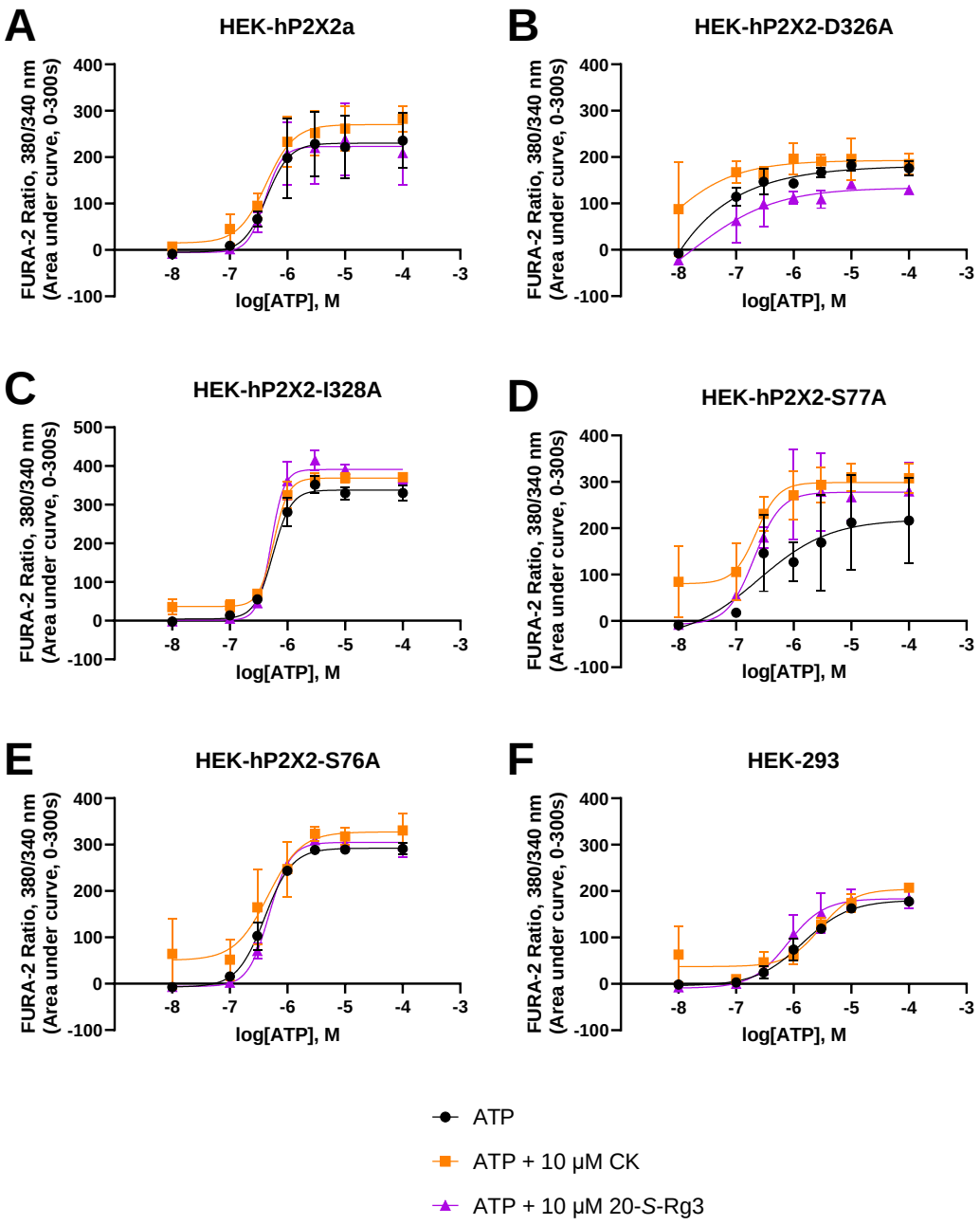

Figure 4.7 – Intracellular calcium measurements in HEK-293 cells transiently transfected with wild type or mutant hP2X2a measured using the FURA-2AM assay. Concentration responses were conducted in the presence of [ATP] between 10 nM and 100 µM. The control ATP response is shown in black, whereas ATP with 10 µM ginsenoside CK is shown in orange and ATP with 10 µM ginsenoside 20-*S*-Rg3 is shown in purple for **A**: wild type hP2X2a (n=3) **B**: D326A mutant hP2X2a (n=2) **C**: I328A mutant hP2X2a (n=2-3) **D**: S77A mutant hP2X2a (n=2) **E**: S76A mutant hP2X2a (n=2) and **F**: native HEK-293 cells (n=3). Cells were loaded in HBSS buffer containing 2 µM FURA-2AM and 250 µM sulfinpyrazone and experiments conducted in low divalent cation buffer (ELDV) containing 250 µM sulfinpyrazone. Graphs are plotted as mean area under the curve (AUC) values between 0-300 seconds from up to three independent experiments ± SEM and fitted with a four-parameter non-linear regression curve. Average EC_{50} values ± SD are calculated using individual EC_{50} values from the specified number of independent experiments (see **Table 4.3**). Two-way ANOVA with Dunnett's multiple comparisons test on raw data did not yield significance.

The wild type hP2X2a receptor showed increased sensitivity to ATP in this assay compared to that observed in the membrane potential blue assay (see **Table 4.3**). Similar to what was observed in the membrane potential assay, the HEK-hP2X2a-D326A mutant is more sensitive to ATP than its wild type counterpart. The maximum measured response is comparable to that observed at wild type HEK-hP2X2a, with the maximum response to ATP of 221 and 181 for HEK-hP2X2a and HEK-hP2X2a-D326A respectively (**Figure 4.7**). Mutant HEK-hP2X2a-I328A is of similar sensitivity to ATP as the wild type receptor, although the maximum response to ATP observed is higher at approximately 351 (**Figure 4.7**). Mutant HEK-hP2X2a-S77A was more sensitive to ATP than the wild type receptor in the membrane potential blue assay (see **Table 4.2**) and the same can be seen in the FURA-2AM assay. The maximum measured response is akin to that seen at wild type HEK-hP2X2a with a value of approximately 209. Mutant HEK-hP2X2a-S76A has similar sensitivity to ATP as the wild type hP2X2a receptor in both the membrane potential and intracellular calcium assays. The maximum response to ATP was also similar at approximately 278 (**Figure 4.7**).

Table 4.3 – Average EC_{50} values to ATP in the presence and absence of ginsenosides in HEK-293 cells transiently transfected with wild type or mutant human P2X2a measured using the FURA-2AM assay. Cells were loaded in HBSS buffer containing 2 µM FURA-2AM and 250 µM sulfinpyrazone and experiments were conducted in standard extracellular buffer (Etotal) containing 250 µM sulfinpyrazone. Average EC_{50} values ± SD are calculated using individual EC_{50} values from the specified number of independent experiments (see **Figure 4.7**) where graphs are plotted as mean area under the curve (AUC) values ± SEM and fitted with a four-parameter non-linear regression curve. One-way ANOVA with Dunnett's multiple comparisons test did not yield significance.

Mutant	Compound	Average EC_{50} (nM ± SD)	pEC_{50}	Difference in pEC_{50} ($-pEC_{50}$ ATP + ginsenoside – $-pEC_{50}$ ATP)
HEK-hP2X2a	**ATP**	455.9 ± 170	-6.341	
	ATP + CK	542.2 ± 174	-6.266	-0.075
	ATP + 20-*S*-Rg3	391.5 ± 49.2	-6.407	0.066
HEK-hP2X2a-D326A	**ATP**	82.87	-7.082	
	ATP + CK	*ND*	*ND*	*ND*
	ATP + 20-*S*-Rg3	219.5 ± 198	-6.659	-0.423
HEK-hP2X2a-I328A	**ATP**	535.1 ± 133	-6.272	
	ATP + CK	600.7 ± 235	-6.221	-0.051
	ATP + 20-*S*-Rg3	464.7 ± 151	-6.333	0.061
HEK-hP2X2a-S77A	**ATP**	193.2 ± 36.6	-6.714	
	ATP + CK	560.5 ± 520	-6.251	-0.463
	ATP + 20-*S*-Rg3	242.4	-6.615	-0.099
HEK-hP2X2a-S76A	**ATP**	405.3 ± 64.3	-6.392	
	ATP + CK	445.8 ± 217	-6.351	-0.041
	ATP + 20-*S*-Rg3	480.8 ± 2.19	-6.318	-0.074

Ginsenoside 20-*S*-Rg3 was shown to be the second most effective potentiator of responses in HEK-hP2X2a cells when screened using the membrane potential assay in Chapter 3, so this effect was explored in more detail using the FURA-2AM assay (**Figure 4.7**). In the membrane potential assay, a small shift in the concentration response curve could be seen in the presence of CK at wild type HEK-hP2X2a (**Figure 4.4**); in the FURA-2 assay, this is not the case. There is a slight shift in the presence of 20-*S*-Rg3, whilst the maximum responses measured are similar in both the presence and absence of ginsenosides (**Figure 4.7**). Due to the increased sensitivity of the HEK-hP2X2a-D326A mutant, it is difficult to fully understand the effects of the ginsenosides with regards to shifting the concentration response curve at the ATP concentrations tested (these were kept the same between mutants to allow

direct comparisons to be made). **Figure 4.7** shows a slight leftward shift in the presence of ginsenoside CK, but not with 20-*S*-Rg3. This is not reflected in the EC_{50} values calculated (see **Table 4.3**), although values could not be accurately determined for each experiment conducted due to the data not generated a sigmoidal concentration response curve. Mutant HEK-hP2X2a-I328A has a similar response to the ginsenosides as observed at the wild type receptor; both ginsenosides CK and 20-*S*-Rg3 do not appear to shift the concentration response curve (**Figure 4.7**). When considering this alongside the average EC_{50} values, CK does not increase the sensitivity to ATP but there is some reduction in the EC_{50} in the presence of 20-*S*-Rg3 (**Table 4.3**). Maximum measured response values are higher than that seen at the wild type hP2X2a receptor, with ATP giving a maximum response of approximately 352, ATP + 10 µM CK giving a maximum response of approximately 369, and ATP + 10 µM 20-*S*-Rg3 giving a maximum response of approximately 415 (**Figure 4.7**).

The data for HEK-hP2X2a-S77A is quite variable, although **Figure 4.7** appears to show a left shift in the presence of ginsenoside CK. This does not appear to be the case for 20-*S*-Rg3, although there does appear to be an increase in the maximum response in the presence of both ginsenosides compared to ATP alone. The apparent shift is not reflected in the average EC_{50} values (**Table 4.3**), although accurate EC_{50} values could not be determined for all experimental repeats due to the data not forming a sigmoidal concentration response curve. Mutant HEK-hP2X2a-S76A, in line with the wild type hP2X2a receptor, did not appear to show a left shift in the presence of either ginsenoside CK or 20-*S*-Rg3 (**Figure 4.7**). There was also little increase in the maximum value with either of the ginsenosides tested, with the maximum measured response in the presence of CK and 20-*S*-Rg3 being approximately 314 and 310 respectively, compared to 278 for ATP alone (**Figure 4.7**). The lack of potentiation by either of the ginsenosides is reflected in the average EC_{50} (**Table 4.3**). Native HEK-293 cells did generate a FURA-2 response (**Figure 4.7**), although the maximum measured response to ATP in the presence and absence of ginsenosides was less than that observed at transient HEK-hP2X2a. The maximum response for ATP alone was approximately 165, increasing to approximately 194 and 183 in the presence of CK and 20-*S*-Rg3 respectively (**Figure 4.7**). A slight shift can be seen in native HEK-293 cells with 20-*S*-Rg3, although not in the presence of CK (**Figure 4.7**). This is reflected in the average EC_{50} values (**Table 4.3**), where a decrease in the EC_{50} can be seen with 20-*S*-Rg3 in two out of the three experiments conducted, but overall, the average values are comparable with one another.

4.4 Investigating Mutants of the Human P2X4 Receptor Using the Membrane Potential Blue and FURA-2AM Assays

Ginsenosides are known to potentiate hP2X4 receptors (Dhuna et al., 2019), however, the possibility of the site of action being related to that of hP2X7 has not yet been explored. Site directed mutagenesis was used to make single point mutations to key residues on the hP2X4 receptor. Based on computational docking and molecular modelling, key residues involved in the binding of ginsenoside CK to the receptor include D320, E96, and D58, with the main chain of V60 and S62 also interacting (see **Figure 4.2**). As a result, the following mutants were generated: D320L; E96A; D58A. Concentration responses to ATP at concentrations between 30 nM and 30 µM were conducted on HEK-293 cells transiently transfected with each of these hP2X4 mutants (including wild type hP2X4 and native HEK-293 cells), either alone or in the presence of 10 µM ginsenoside CK, 10 µM ginsenoside Rd, or 10 µM ginsenoside 20-*S*-Rg3 **(Figure 4.8**).

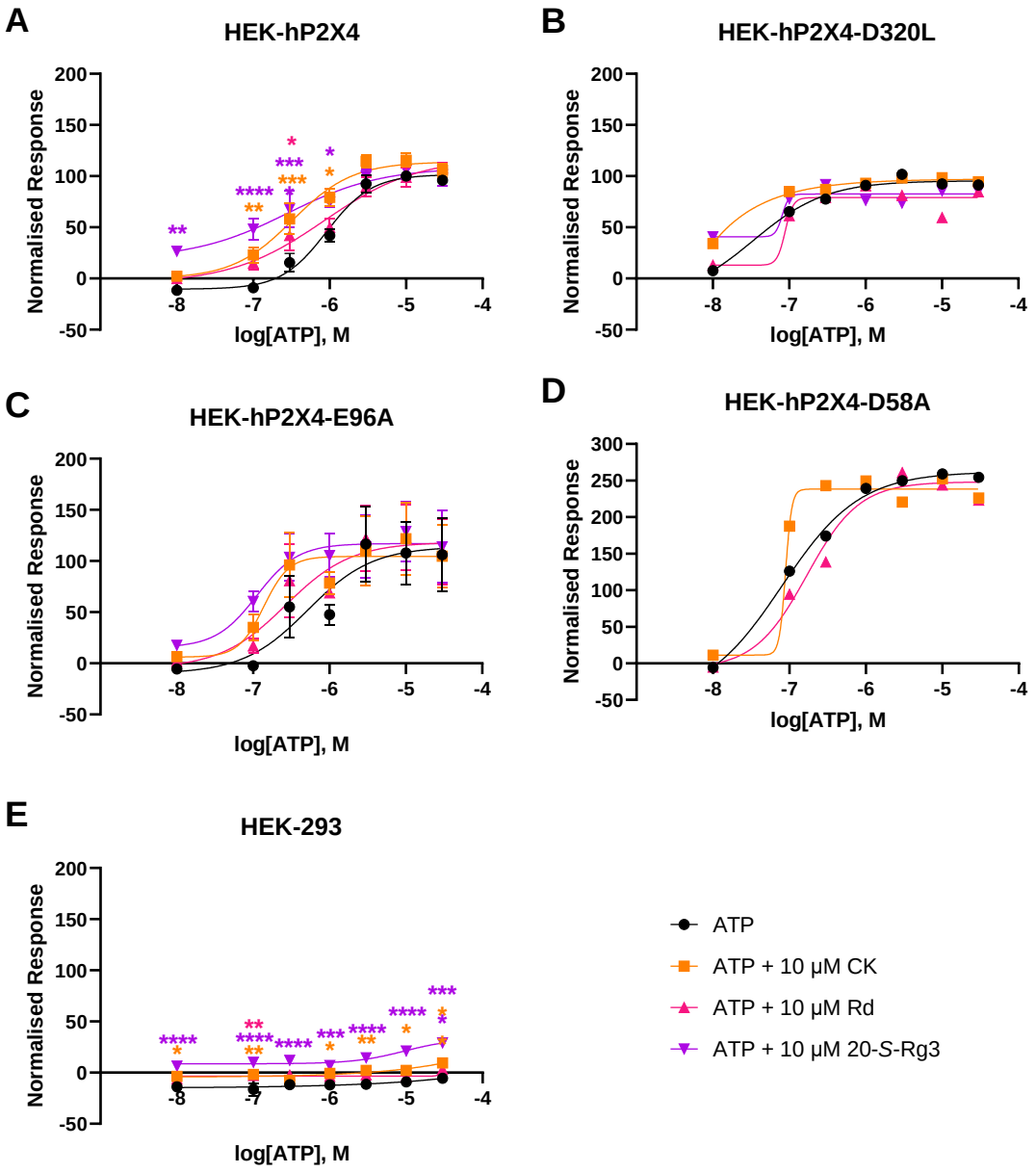

Figure 4.8 - Responses to ATP in the presence and absence of either ginsenoside CK, Rd, or 20-S-Rg3 in HEK-293 cells transiently transfected with wild type or mutant hP2X4 measured using the membrane potential blue assay. The control ATP response is shown in black, whereas ATP with 10 µM CK is shown in orange, ATP with 10 µM Rd is shown in pink, and ATP with 10 µM 20-*S*-Rg3 is shown in purple for **A**: wild type hP2X4 (n=7) **B**: D320L mutant hP2X4 (n=1) **C**: E96A mutant hP2X4 (n=3) **D**: D58A mutant hP2X4 (n=1) and **E**: native HEK-293 cells (n=7). Experiments were conducted in standard divalent cation buffer (Etotal) by an undergraduate student (Saffron King) under the direct supervision of the doctoral candidate (Elizabeth Allum). Graphs are plotted as normalised area under the curve (AUC) values, where the response to 10 µM ATP in wild type HEK-hP2X4 cells is taken as the maximum (100 %) value, from the specified number of independent experiments ± SEM and fitted with a four-parameter non-linear regression curve. Average EC_{50} values ± SD are calculated using individual EC_{50} values from the specified number of independent experiments (see **Table 4.4**). *P<0.05, **P<0.01, ***P<0.001, ****P<0.0001 determined by two-way ANOVA with Dunnett's multiple comparisons test on normalised data to account for transfection differences.

As with the hP2X2a mutants, first the sensitivity to ATP was investigated. For transient HEK-hP2X4, this was comparable to that measured previously on the stable HEK-hP2X4 cell line (~ 800 nM, see **Chapter 3**, **Table 3.1**) using the membrane potential blue assay. Like the analogous alanine mutation in hP2X2a, the D320L mutant was considerably more sensitive to ATP than the wild type P2X4 receptor (EC_{50} values summarised in **Table 4.4**), with a leftward shift of almost an entire log unit (**Figure 4.8**). Mutant HEK-hP2X4-E96A showed similar sensitivity to ATP to the wild type P2X4 receptor, with the maximum normalised response also similar to the wild type receptor at approximately 112 % (**Figure 4.8**). The EC_{50} value for the D58A mutant was lower than that of the wild type P2X4 receptor. The maximum normalised response to ATP was also higher than that seen at HEK-hP2X4 at 259 % (**Figure 4.8**).

At the wild type hP2X4 receptor, ginsenosides CK and 20-*S*-Rg3 can both be seen to potentiate responses, causing a leftward shift in the concentration response curve (a type II PAM effect (Stokes et al., 2020)) and reducing the average EC_{50} (**Figure 4.8** and **Table 4.4**). This effect is less clear for ginsenoside Rd; a similar average EC_{50} value was obtained in the presence of this ginsenoside to that for the ATP control (**Table 4.4**). Ginsenoside CK raised the maximum response slightly to 115 %, whereas ginsenosides Rd and 20-*S*-Rg3 had similar maximums to the response to ATP alone at 108 % and 105 % respectively (**Figure 4.8**). At the mutant HEK-hP2X4-D320L, the shift observed with CK and 20-*S*-Rg3 at the wild type receptor appears to be abolished (**Figure 4.8**), with similar average EC_{50} values observed across all four compound combinations tested (**Table 4.4**). Maximum normalised responses were also similar across the ginsenosides and ATP alone, with the maximum response for ginsenoside CK being approximately 98 %, and 85 % and 86 % for ginsenosides Rd and 20-*S*-Rg3 respectively. The E96A mutant has similar sensitivity to ATP as the wild type receptor, but the effects of the ginsenosides appear more pronounced, particularly with regards to CK and 20-*S*-Rg3 (**Figure 4.8**). Both ginsenosides CK and 20-*S*-Rg3 reduced the average EC_{50} value; this was also the case for ginsenoside Rd, but to a lesser extent (**Table 4.4**). The ginsenosides also slightly increased the maximum normalised response, with ATP + ginsenoside CK having a maximum response of 122 %. Ginsenosides Rd and 20-*S*-Rg3 had maximum response values of 123 % and 129 % respectively, up from 112 % for the maximum response to ATP alone. Mutant HEK-hP2X4-D58A was more sensitive to ATP than the wild type receptor, and it appears that there is a slight shift in the presence of ginsenoside CK but not ginsenoside Rd (**Figure 4.8**). However, this is not reflected in the average EC_{50} values – lower concentrations of ATP would need to be tested to confirm whether there is a shift with ginsenoside CK or not (**Table 4.4**). Ginsenosides CK and Rd did not increase the maximum normalised response compared to ATP alone (**Figure 4.8**). As seen previously with the hP2X2a mutants, there

appears to be little difference in the maximum responses measured in the presence of ginsenosides compared to the ATP control for the wild type and mutants of hP2X4.

Table 4.4 – Average EC_{50} values to ATP in the presence and absence of ginsenosides in HEK-293 cells transiently transfected with wild type or mutant human P2X4 measured using the membrane potential blue assay. Experiments were conducted in standard divalent cation buffer (Etotal). Average EC_{50} values ± SD are calculated using individual EC_{50} values from the specified number of independent experiments (see **Figure 4.8**) where graphs are plotted as normalised area under the curve (AUC) values ± SEM and fitted with a four-parameter non-linear regression curve. One-way ANOVA with Dunnett's multiple comparisons test did not yield significance.

Mutant	Compound	Average EC_{50} (nM ± SD)	pEC_{50}	Difference in pEC_{50} ($-pEC_{50}$ ATP + ginsenoside – $-pEC_{50}$ ATP)
Wild-type P2X4	**ATP**	975.5 ± 333	-6.011	
	ATP + CK	407.2 ± 302	-6.390	0.379
	ATP + Rd	1006 ± 639	-5.997	-0.014
	ATP + 20-*S*-Rg3	563.5 ± 572	-6.249	0.238
HEK-hP2X4-D320L	**ATP**	33.9	-7.469	
	ATP + CK	*ND*	*ND*	*ND*
	ATP + Rd	88.4	-7.054	-0.415
	ATP + 20-*S*-Rg3	86.9	-7.061	-0.408
HEK-hP2X4-E96A	**ATP**	514.9 ± 344	-6.288	
	ATP + CK	138.0 ± 46.2	-6.860	0.572
	ATP + Rd	304.5 ± 189	-6.516	0.228
	ATP + 20-*S*-Rg3	86.42 ± 45.8	-7.063	0.775
HEK-hP2X4-D58A	**ATP**	79.80	-7.098	
	ATP + CK	89.01	-7.051	-0.047
	ATP + Rd	168.70	-6.773	-0.325

The FURA-2AM assay was again used to compare responses to those seen in the membrane potential assay. **Figure 4.9** shows the average intracellular calcium measurements with respect to time in transient HEK-hP2X4 and native HEK-293 cells to 10 µM ATP. Unlike at transient HEK-hP2X2a, HEK-hP2X4 has both an increase in the peak value and throughout the sustained phase compared to native HEK-293 cells. The peak FURA-2 ratio reaches approximately 1.35 for HEK-hP2X4 at a time point of 60 seconds, with the peak for native HEK-293 cells at approximately 60 seconds with value of around 0.45; 3 times less than that observed for P2X4. The native HEK-293 response gradually declines from this peak value, returning to just above baseline by 300 seconds (FURA-2 ratio of 0.15). The HEK-hP2X4 response declines quickly to begin with (between approximately 60 seconds and 120 seconds), but again has a sustained response from 120 seconds onwards approximately half that of the peak response (**Figure 4.9**).

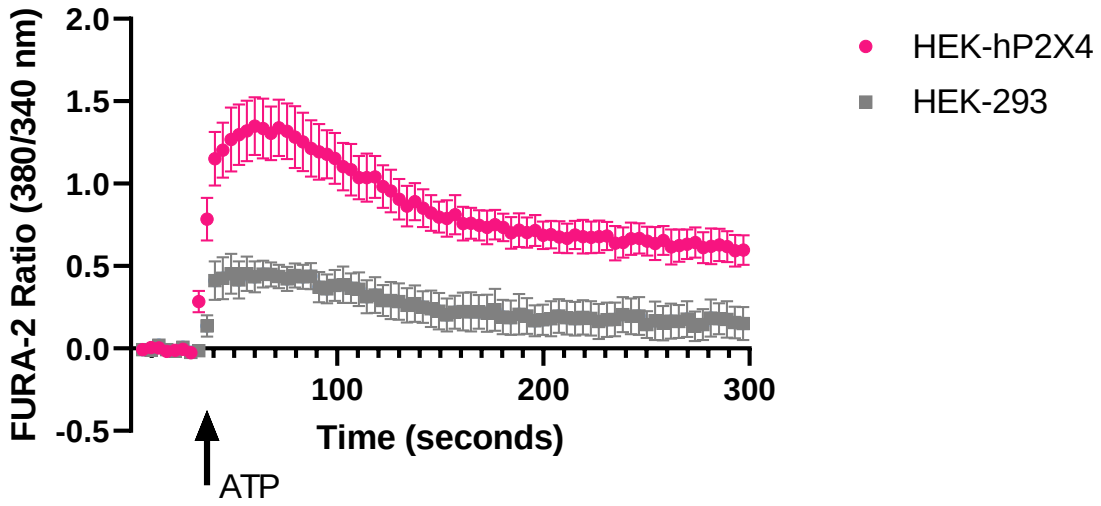

Figure 4.9 – Average intracellular calcium measurements in transiently transfected HEK-hP2X4 or native HEK-293 cells following stimulation with 10 µM ATP. Fluorescence was measured for a total of 300 seconds with ATP application at 30 seconds. Data are plotted as mean fluorescence (FURA-2 ratio) ± SEM from five independent experiments and transfections. Time is plotted as the average time of read from five independent experiments for each of HEK-hP2X4 and HEK-293.

Ginsenosides CK and 20-*S*-Rg3 were screened at HEK-293 cells transiently transfected with either wild type hP2X4, mutant hP2X4, or native HEK-293 cells alongside ATP using the FURA-2AM assay (**Figure 4.10**).

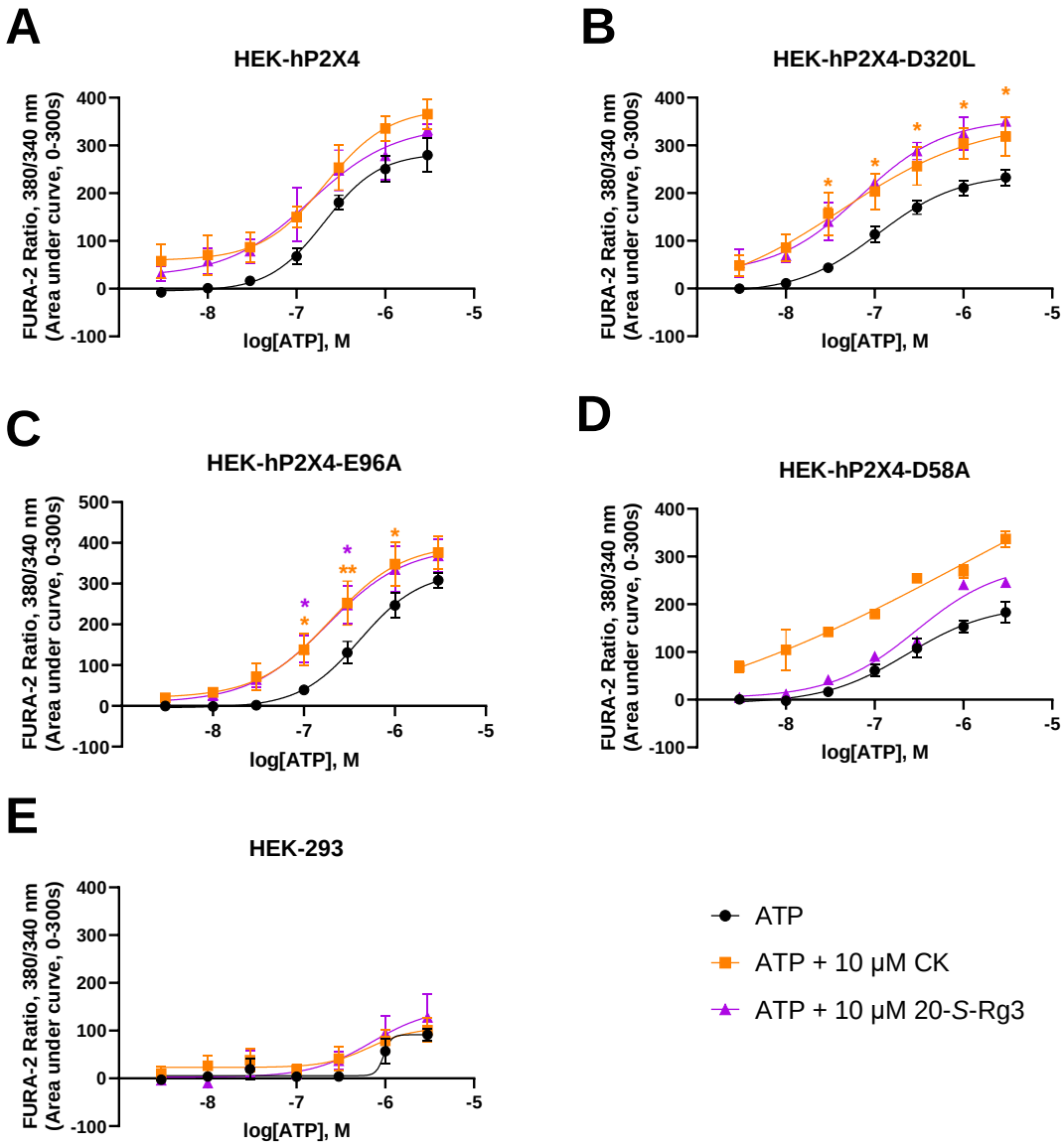

Figure 4.10 – Intracellular calcium measurements in HEK-293 cells transiently transfected with wild type or mutant hP2X4 measured using the FURA-2AM assay. Concentration responses were conducted in the presence of [ATP] between 3 nM and 3 µM. The control ATP response is shown in black, whereas ATP with 10 µM ginsenoside CK is shown in orange and ATP with 10 µM ginsenoside 20-*S*-Rg3 is shown in purple for **A**: wild type hP2X4 (n=3-4) **B**: D320L mutant hP2X4 (n=2-4) **C**: E96A mutant hP2X4 (n=3-4) **D**: D58A mutant hP2X4 (n=1-2) and **E**: native HEK-293 cells (n=3-4). Cells were loaded in HBSS buffer containing 2 µM FURA-2AM and 250 µM sulfinpyrazone and experiments conducted in standard divalent cation buffer (Etotal) containing 250 µM sulfinpyrazone. Graphs are plotted as area under the curve (AUC) values between 0-300 seconds from up to three independent experiments ± SEM and fitted with a four-parameter non-linear regression curve. Average EC_{50} values ± SD are calculated using individual EC_{50} values from the specified number of independent experiments (see **Table 4.5**). *P<0.05, **P<0.01 determined by two-way ANOVA with Dunnett's multiple comparisons test on raw data.

For the wild type hP2X4 receptor, the ATP control response reached a maximum of 280 and had an average EC_{50} approximately 4.7-fold lower than that observed in the membrane potential assay (**Figure 4.10** and **Table 4.5**). The HEK-hP2X4-D320L mutant had a similar EC_{50} value, with the maximum response also comparable to wild type hP2X4 at 233 (**Figure 4.10**). Mutant HEK-hP2X4-E96A was less sensitive to ATP than the wild type receptor, but the maximum response measured to ATP was greater than that observed at the wild type receptor at 308 (**Figure 4.10**). The D58A mutant showed slightly decreased sensitivity to ATP compared to the wild type receptor, similar to what had been observed using the membrane potential blue assay. The maximum FURA-2 response measured at HEK-hP2X4-D58A was also less than that observed at the wild type P2X4 receptor at 183 (**Figure 4.10**). Native HEK-293 cells were able to produce a response in the FURA-2AM assay, although this was less than the response observed for the transfected cells (**Figure 4.10**), with a maximum response of 91. EC_{50} values are summarised in **Table 4.5**.

Table 4.5 – Average EC_{50} values to ATP in the presence and absence of ginsenosides in HEK-293 cells transiently transfected with wild type or mutant human P2X4 measured using the FURA-2AM assay. Cells were loaded in HBSS buffer containing 2 µM FURA-2AM and 250 µM sulfinpyrazone and experiments were conducted in standard extracellular buffer (Etotal) containing 250 µM sulfinpyrazone. Average EC_{50} values ± SD are calculated using individual EC_{50} values from the specified number of independent experiments (see **Figure 4.10**) where graphs are plotted as mean area under the curve (AUC) values ± SEM and fitted with a four-parameter non-linear regression curve. *P<0.05 determined by one-way ANOVA with Dunnett's multiple comparisons test.

Mutant	Compound	Average EC_{50} (nM ± SD)	pEC_{50}	Difference in pEC_{50} (-pEC_{50} ATP + ginsenoside – -pEC_{50} ATP)
Wild-type P2X4	**ATP**	206.15 ± 69.91	-6.686	
	ATP + CK	145.68 ± 21.11	-6.837	0.151
	ATP + 20-*S*-Rg3	88.82 ± 2.59 *****	-7.051	0.365
HEK-hP2X4-D320L	**ATP**	118.75 ± 46.67	-6.925	
	ATP + CK	49.59 ± 46.87	-7.305	0.380
	ATP + 20-*S*-Rg3	69.52 ± 13.05	-7.158	0.233
HEK-hP2X4-E96A	**ATP**	529.85 ± 337.36	-6.276	
	ATP + CK	359.40 ± 417.91	-6.444	0.168
	ATP + 20-*S*-Rg3	204.40 ± 98.19	-6.690	0.414
HEK-hP2X4-D58A	**ATP**	239.95 ± 72.90	-6.620	
	ATP + CK	90.71	-7.042	0.422
	ATP + 20-*S*-Rg3	291.80	-6.535	-0.085

When assessing the effects of the ginsenosides, both ginsenosides CK and 20-*S*-Rg3 were able to shift the concentration response curve and reduce the EC_{50} to ATP in HEK-hP2X4 cells (**Figure 4.10**). The maximum FURA-2 response is also increased in the presence of both ginsenosides to 366 for ATP + CK and 332 for ATP + 20-*S*-Rg3 (**Figure 4.10**). With the D320L mutant, both ginsenosides CK and 20-*S*-Rg3 shift the concentration response curve, producing a mixed type I and II PAM effect (**Figure 4.10**). The FURA-2 ratio is greater in the presence of either ginsenoside CK or 20-*S*-Rg3 at all concentrations, with the maximum response in the presence of ginsenosides CK and 20-*S*-Rg3 being 318 and 350 respectively compared to 233 for ATP alone (**Figure 4.10**). The data for mutant HEK-hP2X4-E96A looks similar to that of the wild type receptor, with both ginsenosides CK and 20-*S*-Rg3 causing a leftward shift in the concentration response curve, although overall the receptor is less sensitive to ATP (**Figure 4.10**). The effects of the ginsenosides at mutant HEK-hP2X4-D58A are more difficult to ascertain as

there are less repeats for this mutant but increases in the FURA-2 response can be observed for each concentration of ATP tested (**Figure 4.10**). Indeed, the maximum responses measured in the D58A mutant in the presence of either ginsenoside CK or 20-*S*-Rg3 were 337 and 245 respectively, compared to 183 for ATP alone (**Figure 4.10**). Ginsenoside CK was able to reduce the EC_{50} value to ATP, whereas ginsenoside 20-*S*-Rg3 did not (**Table 4.5**).

4.5 Expression of Mutants of the Human P2X4 Receptor Using Flow Cytometry

Due to the nature of transient transfections, protein expression can vary between transfections. To determine if increases or decreases in receptor response were intrinsic to receptor function or due to expression of mutants generated, flow cytometry was conducted on HEK-293 cells transiently transfected with either wild type P2X4 or mutant P2X4 (**Figure 4.11**).

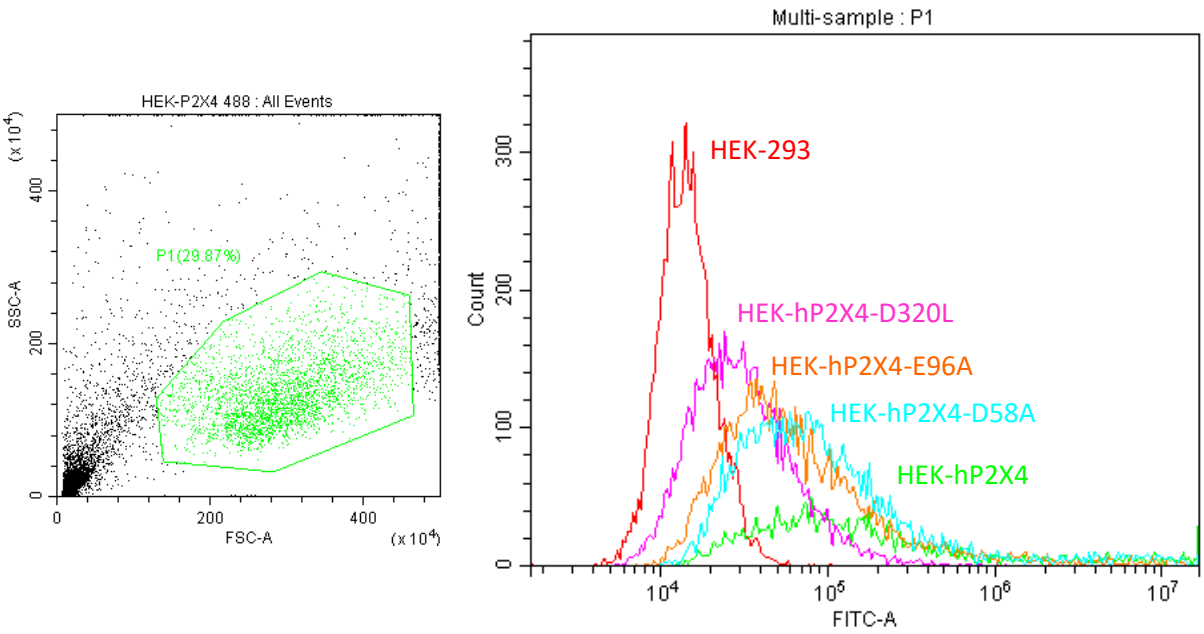

Figure 4.11 – Histogram overlay showing FITC fluorescence measured in HEK-293 cells transiently transfected wild type or mutant hP2X4 and native HEK-293 cells labelled with anti-P2X4-Alexa488. **Left**: Representative dot plot showing gated cells analysed to exclude cellular debris. **Right**: Histogram overlay showing fluorescence measured on gated cells labelled with anti-P2X4-Alexa488. Median and mean FITC fluorescence values are summarised in **Table 4.6**. Data are the result of one independent experiment. Data were acquired using a CytoFlex Flow Cytometer and analysed using CytExpert software (both Beckmann Coulter).

Cells were labelled with an anti-P2X4 antibody (extracellular epitope) and then a secondary Alexa488 antibody was used to generate fluorescent labelling. Cells were gated to exclude debris to allow analysis of live cells, and fluorescence was measured in the FITC channel. Rank order of labelling was as follows, from highest median fluorescence to lowest: HEK-hP2X4>HEK-hP2X4-D58A>HEK-hP2X4-E96A>HEK-hP2X4-D320L>native HEK-293 cells. Fluorescence values are summarised in **Table 4.6**.

Table 4.6 – Summary of mean and median FITC fluorescence values for HEK-293 cells transiently transfected with wild type or mutant hP2X4 or native HEK-293 cells labelled with anti-P2X4-Alexa488. Values represent those obtained for cells stained with both primary anti-P2X4 and secondary Alexa488 antibodies, except for the non-primary antibody-stained HEK-hP2X4 negative control in which only a secondary antibody was used. All data is gated to exclude cell debris. Data were acquired using a CytoFlex Flow Cytometer and analysed using CytExpert software (both Beckmann Coulter).

Mutant	Measurement	Fluorescence Value (AU)
HEK-hP2X4	**Mean Fluorescence**	1164873
	Median Fluorescence	116013
HEK-hP2X4-D320L	**Mean Fluorescence**	54868
	Median Fluorescence	28629
HEK-hP2X4-E96A	**Mean Fluorescence**	289511
	Median Fluorescence	52982
HEK-hP2X4-D58A	**Mean Fluorescence**	488333
	Median Fluorescence	74810
Native HEK-293	**Mean Fluorescence**	18438
	Median Fluorescence	14081
Non-primary antibody-stained HEK-hP2X4 (Negative control)	**Mean Fluorescence**	24783
	Median Fluorescence	18042

Labelling of hP2X2a mutants expressed transiently in HEK-293 cells was also performed, however, the antibody used was found to give a large non-specific signal, indicating that labelling was also occurring on native HEK-293 cells and therefore this could not be reliably used to quantify expression of these mutants (data not shown).

4.6 Chapter 4 Discussion

Computational docking models suggest that ginsenoside CK is able to bind to the central vestibule region of hP2X2 and hP2X4 in a similar manner to hP2X7 (**Figure 4.2**) (Bidula et al., 2019b). Key regions within the central vestibule are proposed to be involved in binding at both hP2X7 and hP2X4, particularly the region surrounding the double-serine motif at position 59-60 in hP2X7 (hP2X4: S62-S63), the QGNS motif at position 97-100 in hP2X7 (hP2X4: QEENS, residues 94-98), and the DILV motif at position 318-321 in hP2X7 (hP2X4: DIIV, residues 320-323) (**Figure 4.3**). This is complemented by the fact that ginsenoside CK is proposed to have numerous polar interactions at both hP2X7 and hP2X4 receptors. This is less clear for the hP2X2a receptor; the number of interactions is less, with little overlap in the key regions thought to be involved in binding between the hP2X7 and hP2X2 receptors (**Figure 4.3**). These differences in both the number and location of interactions could mean that although activity appears possible at all three receptors from screening data (**Chapter 3**), the degree of activity, and indeed the specificity of different ginsenosides for each receptor, is different. Conformation of ginsenoside CK in the binding pocket is likely to differ at each receptor: with the increased similarity between proposed interactions at hP2X7 and hP2X4 compared to hP2X2a, it is probable that activity would be greater at these two receptors: indeed, screening data did not prove significant for the hP2X2a receptor compared to hP2X7 and hP2X4 in **Chapter 3**, although some potentiation could be observed from the full concentration response curves in this chapter.

A small shift in the presence of ginsenoside CK can be observed at the hP2X2a receptor in the membrane potential blue assay, although the degree of shift is less than that which has been described for hP2X7 and hP2X4 in other assays (Dhuna et al., 2019, Helliwell et al., 2015). There are few known potentiators of the hP2X2a receptor to compare the ginsenosides to, but the neurosteroids dehydroepiandrosterone and progesterone both modulate rat hP2X2a receptors expressed in *Xenopus* oocytes (De Roo et al., 2010, De Roo et al., 2003). Progesterone has been shown to induce a leftward shift in the concentration response curve when responses were measured using patch-clamp electrophysiology, although again this shift is small, reducing the EC_{50} from 32 µM to 21 µM (an absolute difference of 0.184 in the pEC_{50} values) (De Roo et al., 2010). Analogues of testosterone have been shown to modulate rat P2X receptors, with some potentiation at rat hP2X2a by testosterone butyrate (Sivcev et al., 2019). Again, the degree of potentiation is small, with the EC_{50} value reducing to 1.9 µM in the presence of this testosterone analogue compared to 3.2 µM for ATP alone (an absolute difference of 0.226 in the pEC_{50} values) (Sivcev et al., 2019). A key point to note is that the maximum current does not appear to be increased by positive allosteric modulators of P2X2,

suggesting that it may only be possible to measure a type II PAM effects at this receptor or in this assay type (patch-clamp electrophysiology) (Sivcev et al., 2019, De Roo et al., 2010). This was similar to what was observed in the membrane potential assay, with no substantial difference in the maximum responses between ATP alone and in the presence of ginsenosides (**Figure 4.4** and **Figure 4.5**). The hP2X4 receptor also displays potentiation by ginsenoside CK in the membrane potential assay, in agreement to has been observed in the FURA-2AM and YO-PRO-1 assays (Dhuna et al., 2019). The shift observed in the membrane potential assay yields an absolute different in the pEC_{50} of 0.379, greater than what has been observed in the YO-PRO-1 assay, where ginsenoside CK caused an absolute shift in the pEC_{50} value of 0.197 (Dhuna et al., 2019). Lithocholic acid, similar in structure to ginsenoside CK but lacking the glucose moiety at carbon 20 and with different stereochemistry for the hydroxyl at carbon 3, has been shown to potentiate rat P2X4, reducing the EC_{50} from 2.7 μM for ATP alone to 1.1 μM for ATP in the presence of 10 μM lithocholic acid (Sivcev et al., 2020). This equates to an absolute difference in the pEC_{50} of 0.390, similar to the change observed with ginsenoside CK at hP2X4 receptors in the membrane potential blue assay (**Figure 4.8**).

The only conserved residue between hP2X2a, hP2X4, and hP2X7 that is thought to be involved with ginsenoside CK binding is an aspartic acid at position 326, 320, and 318 respectively (Bidula et al., 2019b). Mutating this residue to alanine in human P2X7 reduces potentiation by CK, whereas mutating to leucine appears to abolish potentiation completely, although the effects of this mutation in other P2X receptors has not been investigated until now (Bidula et al., 2019b). Mutating D326A in hP2X2 does not abolish potentiation of the ATP response by ginsenoside CK (**Figure 4.4**), although there is a slight reduction in the difference between the pEC_{50} values. Computational docking suggests that this residue does not make interactions with ginsenoside CK at the hP2X2 receptor (**Figure 4.2**) like it is proposed to in hP2X4 (**Figure 4.2**) and hP2X7 (Bidula et al., 2019b). Instead, CK is proposed to interact with V329 lower down in the central vestibule region, and so mutating D326A would not be expected to have a direct impact on the activity of the CK. At the hP2X4 receptor, however, computational docking suggests that D320 in hP2X4 does interact with ginsenoside CK, and so mutating this residue would be expected to interfere with the activity of CK (**Figure 4.2**). Indeed, mutating D320 to leucine reduces potentiation by ginsenoside CK, reducing the shift in the EC_{50} as with the D318L mutant in hP2X7 (Bidula et al., 2019b). Mutating the D320 residue to alanine rather than leucine in rat P2X4 also results in a receptor that is more sensitive to ATP, with a reduction in the EC_{50} value from 3.1 μM to 0.6 μM (Yan et al., 2006). A reduction in the maximum response compared to the wild type was also observed, similar to the D326A in the membrane potential blue assays (Yan et al., 2006). However, in the FURA-2AM assay, potentiation by ginsenoside CK at concentrations of ATP >10 nM appears

increased for the D320L mutant in hP2X4, highlighting differences between the assays. In all receptors, mutating this aspartic acid to a smaller, hydrophobic group results in a receptor more sensitive to ATP, suggesting that the presence of a large, charged residue here is key to enabling ATP to exert the conformational change needed to gate P2X receptors. It would be interesting to investigate whether the alanine mutant in hP2X4 has a similar effect, as the D320L mutant does not display a reduction in the response despite an apparent difference in expression compared to the wild type receptor (**Figure 4.11**). It would also be interesting to investigate the effects of changing the charge from negative to positive on both potentiation of the receptor and sensitivity to agonists.

Two other key mutations found to impact the ability of ginsenosides to potentiate human P2X7 are L320A and S60A (Bidula et al., 2019b). Mutating these residues resulted in a reduction in potentiation of the response to 200 μM ATP in the YO-PRO-1 assay, with both mutant receptors being more sensitive to ATP than the wild type receptor (Bidula et al., 2019b). Neither of these residues are thought to make direct interactions with ginsenoside CK in hP2X7 (Bidula et al., 2019b); the analogous residues I328 and I322 in hP2X2a and hP2X4 respectively are also not thought to be directly involved in ginsenoside CK binding, and nor are the analogous residues S77 in hP2X2a or S63 in hP2X4 (**Figure 4.2**). Mutating I328 to alanine in hP2X2a reduced potentiation by ginsenoside CK but did not increase the sensitivity of the receptor to ATP (**Figure 4.4**) like what has been seen for the L320A mutant in hP2X7 (Bidula et al., 2019b). The effects of mutating I328A were not as clear in the FURA-2AM assay, where potentiation of the wild type hP2X2a receptor could not be seen to begin with. It would be useful to repeat this, perhaps using an alternate loading buffer in line with those used in membrane potential assays. The analogous mutant was not explored in hP2X4, but it would be useful to investigate the effects in this receptor also. Mutating residues analogous to S60 in hP2X7 in hP2X2a (S77A) resulted in a receptor more sensitive to ATP. These data suggest that, in addition to the D318 residue (hP2X7 numbering), the L320 and S60 residues may also be key to receptor gating by ATP; in fact, both these residues lie on the same β-sheets as residues that are thought to be involved in the ATP binding site: S60 is on the same β-sheet as K66, and L320 is on the same β-sheet as K311 (McCarthy et al., 2019). Both of these β-sheets lead directly to the transmembrane domains and may be important in the conformational change that occurs following ATP binding in all P2X receptors.

Residue E96 does not have a directly analogous residue at human P2X7, but it does lie in the same region of the receptor as N100 in P2X7 which is thought to make interactions with ginsenoside CK (Bidula et al., 2019a). Mutant HEK-hP2X4-E96A appears to be more sensitive to ATP than the wild type

receptor, although to a lesser extent than the D320L mutant (**Figure 4.8**). Although not a directly analogous residue, mutating E96A in the P2X4 receptor resulted in a similar effect to the N100A mutant at hP2X7, with a noticeable leftward shift in the does response curve in the presence of all three ginsenosides tested (**Figure 4.8**). In particular, ginsenoside Rd has the largest increase in effect compared to the wild type receptor (**Table 4.4**), suggesting that mutating this residue allows for better binding of ginsenoside Rd to the central vestibule region. Indeed, this residue has more sugar groups than CK (two at carbon 3 and one at carbon 20 compared to only one at carbon 20 for CK), so it would likely be subject to steric hindrance within the central vestibule region, particularly if Rd binds in a different conformation to CK with the two sugars at carbon 3 positioned at the top of the central vestibule region. The positively charged amino acid arginine is present at position 318, in very close proximity to but partially obscured by E96 (**Figure 4.12**).

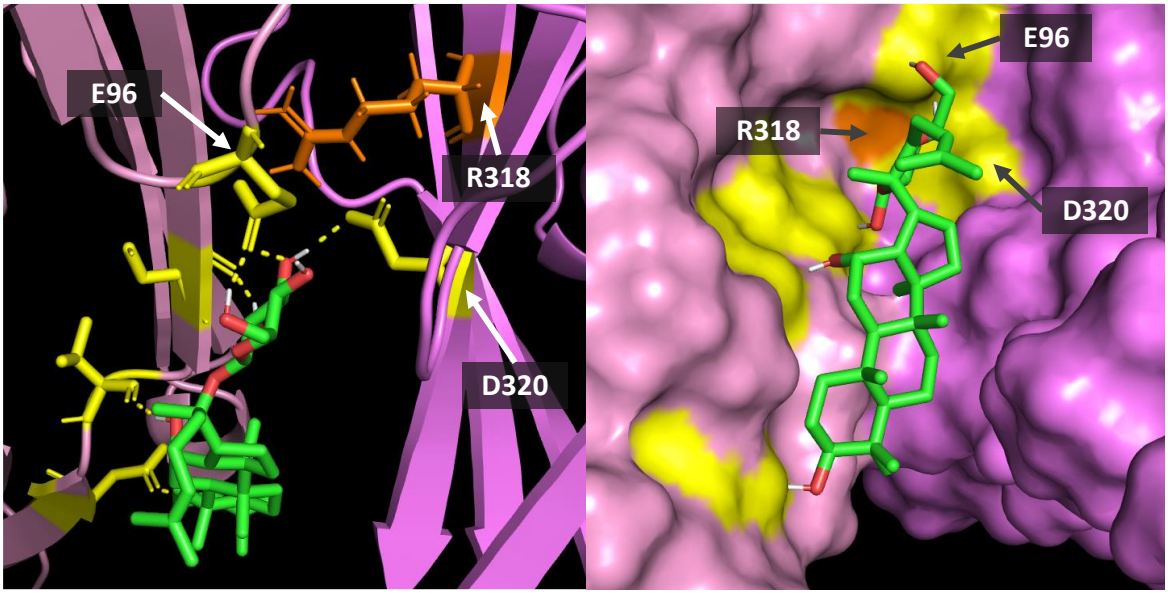

Figure 4.12 – Close up of a homology model of human P2X4 showing CK (green) docked and key residues highlighted. Residues that make polar interactions are highlighted in yellow. The first panel shows the central vestibule viewed from above, whereas the second panel is viewed from below. Note the close proximity E96 (labelled) to R318 (orange, labelled) and D320 (labelled). Homology models are based on the crystal structure of zebrafish-P2X4 (PDB: 4DW1) with the human P2X4 sequence overlayed. Docking was performed by Dr Sam Walpole using Glide (Schrödinger).

Mutating the E96 residue to alanine, therefore removing the bulky glutamic acid, could allow better access to the R318 residue, meaning that the sugar moiety of ginsenoside CK, and the other ginsenosides tested, are better able to form polar interactions. This in turn would likely move ginsenoside CK further up into the pocket, similar to how CK is thought to interact with P2X7 (Bidula et al., 2019a), which could explain the increased potentiatory effects. This effect may be replicated

among the ginsenosides tested (Rd and 20-*S*-Rg3) as their effects are also enhanced at this mutant – computational docking of these ginsenosides to the human P2X4 receptor would be useful, particularly with residue E96 mutated to alanine. No mutations made to P2X4 abolished potentiation by CK completely, with the exception of perhaps D320L where potentiation was reduced in both the membrane potential and FURA-2AM assays. The fact that ginsenoside CK is thought to make so many polar interactions with the hP2X4 receptor could help to stabilise its binding and mean that no one mutation alone is enough to disrupt its function.

The apparent increase in sensitivity to the effects of ginsenoside CK at the S76A mutant in hP2X2a is difficult to explain, given that CK does not appear to make interactions with this region of the receptor. This residue does sit directly opposite V329, which is thought to make three separate polar interactions with the glucose moiety of CK (**Figure 4.13**).

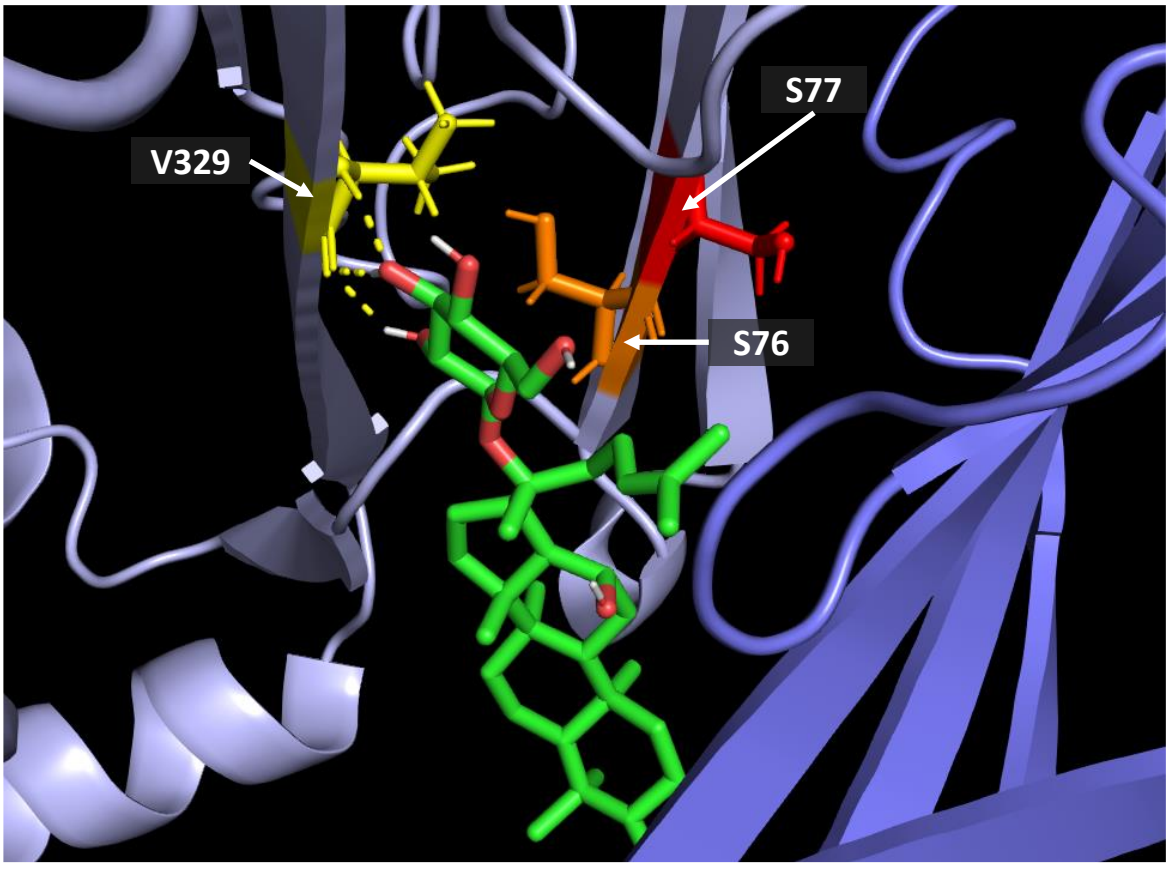

Figure 4.13 – Close up of a homology model of human P2X2 showing CK docked and key residues highlighted. V329 is highlighted in yellow, whereas S76 is highlighted in orange and S77 in red. Note the close proximity of V329 to S76A and how the sugar moiety of ginsenoside CK sits between these two residues.

By mutating S76 to alanine, this would free up space around the V329 residue, reducing steric hindrance and making it easier for CK to interact with the main chain of this residue. It would also

abolish any possible polar interactions between the S76 residue and the sugar moiety which could be pulling ginsenoside CK into a less favourable conformation.

Across all mutants tested using the membrane potential blue assay, there did not appear to be a clear distinction between the maximum responses measured for ATP alone compared to in the presence of ginsenosides, with potentiation generally emerging as a type II effect (**Figure 4.14**).

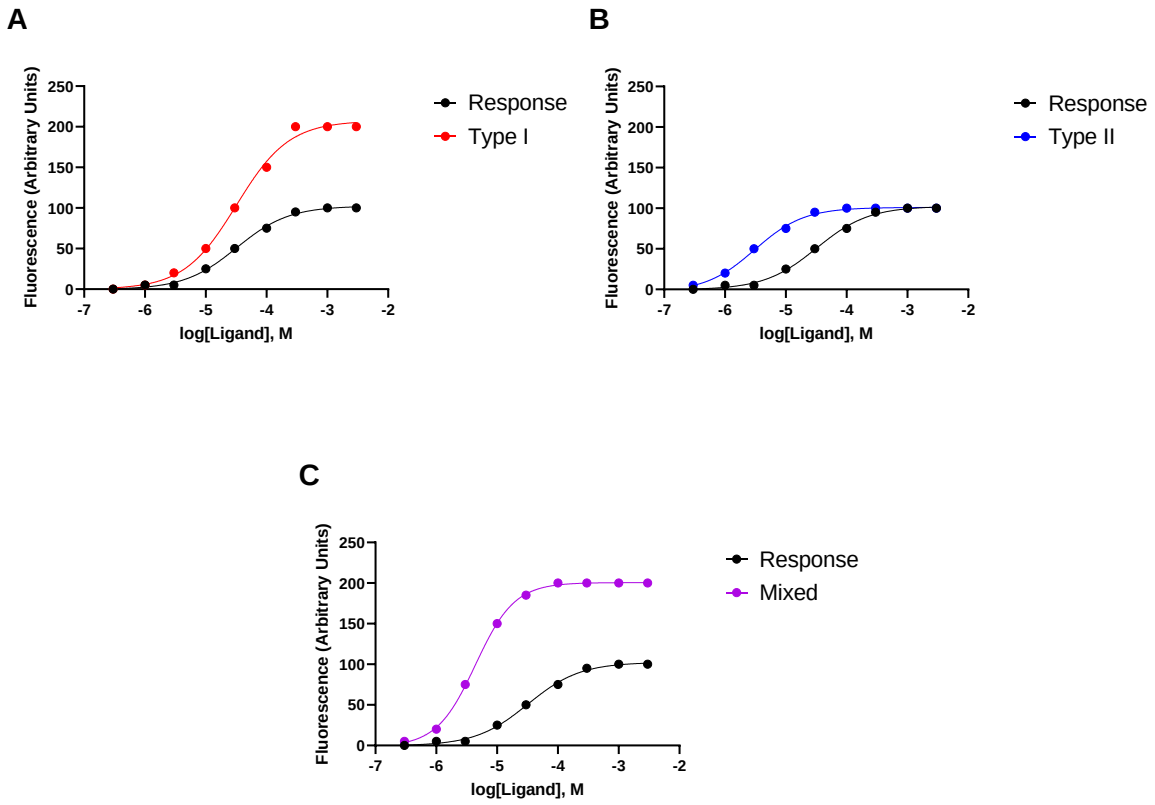

Figure 4.14 – Diagrams showing types of positive allosteric modulation (PAM) on concentration response curves to a ligand. Three types of modulation are outlined: panel **A** shows a Type I response, where the maximum response is increased but the EC_{50} value remains the same; panel **B** shows a Type II response, where there is no increase in the maximum response but there is a decrease in the EC_{50} value (shown by the leftward shift in blue); and panel **C** shows a mixed Type I/II effect, where there is both an increase in the maximum response and a leftward shift in the concentration response curve corresponding to a decrease in the EC_{50} value. Diagrams are for illustrative purposes only and do not represent measured data.

This is the case for both hP2X2a and hP2X4 mutants tested in the membrane potential assay (**Figures 4.4, 4.5,** and **4.8**), despite it being previously shown that a mixed type I/II effect is possible at hP2X4 in dye uptake assays (Dhuna et al., 2019). This suggests that this is likely a feature of the membrane potential assay rather than the receptor itself, especially given that ginsenosides were able to raise the maximum response at hP2X4 in the calcium assay (**Figure 4.10)**. This effect has also been observed

in patch-clamp electrophysiology experiments which measure the current, i.e., the movement of ions, across the cell membrane. For example, ivermectin is known to potentiate P2X4 responses (Priel and Silberberg, 2004), and concentration response curves generated in the presence and absence of ivermectin using patch-clamp electrophysiology also show a type II PAM effect. This phenomenon is not limited to P2X receptors – EU1794-27 displays a type II PAM effect at the NMDA receptor GluN2C, measured using patch-clamp electrophysiology (Perszyk et al., 2018). It is not clear why this is the case: it could depend on the total amount of membrane potential dye able to incorporate between the lipid bilayer, as responses would be limited by this. However, when measuring intracellular calcium ions, it could be possible to modulate the preference for calcium over other ions entering the cell by reducing the movement of other ions, keeping the total charge movement the same. This would mean it is possible to measure both type I and type II PAM effects in the FURA-2AM assay. This is an important consideration for the YO-PRO-1 iodide assay also, as the ceiling limit for this assay would be dependent on the total number of YO-PRO-1 molecules available to intercalate with DNA (or RNA) or the total amount of DNA in a cell, both of which will have high saturation values, and therefore explain why both type I and type II PAM effects can be measured in this assay. Overall, the data in this chapter do not convincingly suggest that the ginsenosides act as positive allosteric modulators of the hP2X2a receptor, although the hP2X2a receptor provides a useful comparison for investigating binding of the ginsenosides at the other P2X receptors. In future, it may be useful to create chimeric receptors of both hP2X4 and hP2X7 with sequences from hP2X2a to validate which residues are important in potentiation, given that hP2X2a shows a lack of potentiation by the ginsenosides compared to hP2X4 and hP2X7.

Chapter 5 – Exploring the Predicted Positive Allosteric Modulator Site in Human P2X7

5.1 Introduction

The first foray into exploring the mechanism of action of the ginsenosides on P2X7 was in 2019, when Bidula *et al* examined via computational docking and subsequent site directed mutagenesis the central vestibule region of the human P2X7 (hP2X7) receptor (Bidula et al., 2019b). In this paper, key single point mutations were found to affect the sensitivity of the receptor to ATP and also the ability of ginsenoside CK to potentiate ATP responses (Bidula et al., 2019b). In particular, mutations of D318 and L320 residues (specifically D320L and L320A) were found to abolish potentiation by ginsenosides CK and Rd in the YO-PRO-1 assay, whilst also yielding smaller YO-PRO-1 uptake responses to ATP and reduced EC_{50} values (Bidula et al., 2019b). Furthermore, fold potentiation by either ginsenoside CK or Rd was reduced in the FURA-2AM assay for both the D318L and L320A mutants, but fold potentiation for the D318A mutant remained similar to the wild type receptor (Bidula et al., 2019b).

Another mutation found to have impacts on the ability of the ginsenosides to potentiate the hP2X7 receptor was S60A (Bidula et al., 2019b). This mutation reduced the fold potentiation by both ginsenoside CK and Rd in YO-PRO-1 dye uptake and intracellular calcium assays, whilst displaying increased sensitivity to ATP and an increased maximum response to ATP in the YO-PRO-1 assay (Bidula et al., 2019b). Interestingly, when measured using the patch clamp assay, S60A continued to produce a larger response to ATP than the wild type receptor; D320L and L320A also produced larger responses to ATP, whereas previously their YO-PRO-1 uptake had been reduced compared to the wild type receptor (Bidula et al., 2019b). Furthermore, the D318L, L320A, and S60A mutants all showed reduced fold potentiation by ginsenoside CK in the patch clamp assay compared to the wild type receptor, whereas the D318A mutant showed slight increased potentiation by CK (Bidula et al., 2019b). **Figure 5.1** summarises the location of these key residues identified by Bidula *et al*, along with the residues that were investigated. Additional residues in this region are indicated and will be explored in this chapter.

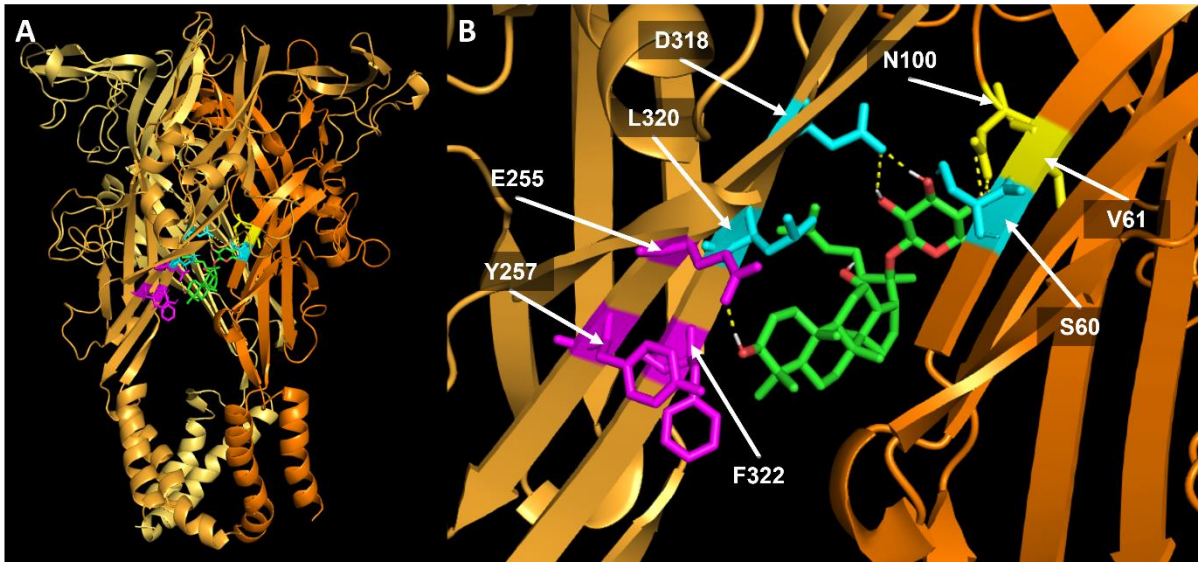

Figure 5.1 – Homology model of human P2X7 showing ginsenoside CK docked to the central vestibule region. Key residues identified by Bidula *et al* are highlighted in cyan, with other mutants examined in this chapter highlighted in magenta. Residues that make polar interactions but were not investigated in this chapter are highlighted in yellow. **A**: Ginsenoside CK (shown in green) docked to the central vestibule region of human P2X7. **B**: Close up of the central vestibule region with ginsenoside CK docked (green) and select residues labelled. The posterior subunit and residues R277 to Y291 on the left subunit (pale orange) have been hidden to allow for better viewing of the central vestibule region. Homology models are based on the crystal structure of zebrafish-P2X4 (PDB: 4DW1) with the human P2X7 sequence overlayed. Docking was performed by Dr Sam Walpole, UEA, using Glide (Schrödinger).

Screening of a series of related glycosides by Piyasirananda *et al* elucidated a structure-activity relationship for the ginsenosides at P2X7, with key regions at carbon 3 and carbon 20, where either a hydroxyl or sugar moiety should be present for activity (**Figure 5.2**) (Piyasirananda et al., 2021). A key finding in this study was that ginsenoside F1 does not show activity at the human P2X7 receptor, despite differing from ginsenoside CK by one single hydroxyl at the carbon 6 position (Piyasirananda et al., 2021). This has also been validated in HEK-hP2X7 in Chapter 3 (**Figure 3.10**) using the membrane potential blue assay. The reason for this lack of activity at hP2X7 is unknown and will be tested in this chapter. It is a possibility that there is steric hindrance from residues bordering the lateral portals preventing PAM activity of ginsenoside F1.

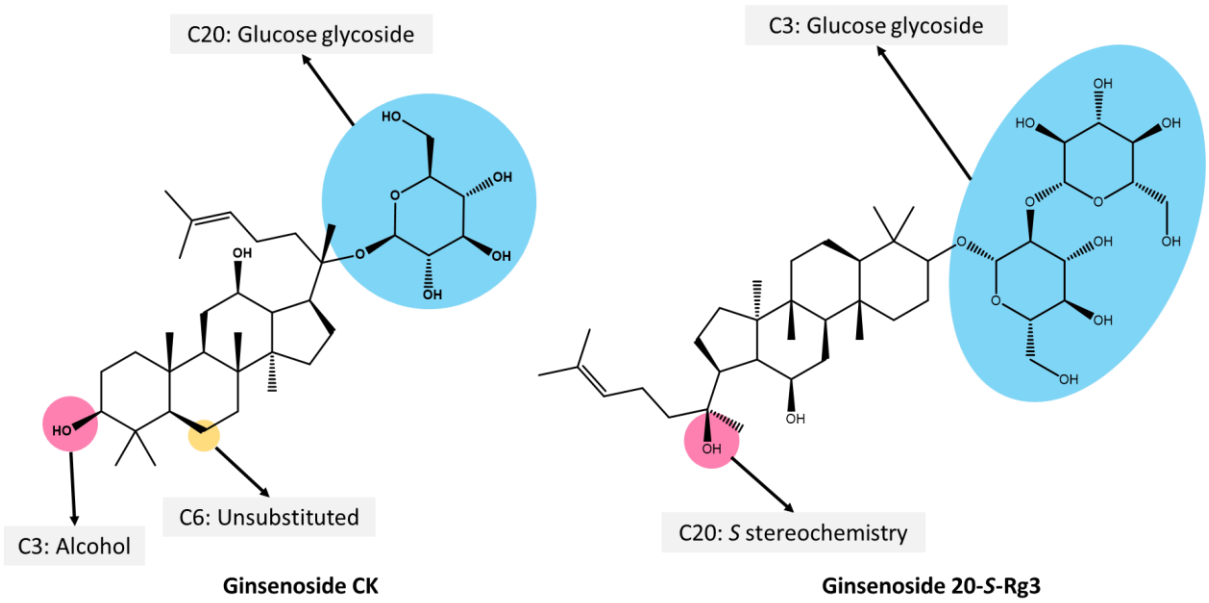

Figure 5.2 – Proposed structure activity relationship for ginsenosides at hP2X7. Residues important for activity include a glucose moiety at carbon 3 or carbon 20, a hydroxyl group at position 3 (if binding in ginsenoside CK orientation) or *S* stereochemistry at carbon 20 (if binding in 20-*S*-Rg3 orientation), and an absence of functional groups at carbon 6. Adapted from Piyasirananda *et al*, 2021 (https://doi.org/10.1124/molpharm.120.000129).

Although mutations have been made to several key residues in the central vestibule region of the human P2X7 receptor, most have been focussed on the apex of the pocket; here, extended mutagenesis along the edge of the central vestibule region was performed to assess the impact of these mutations on the activity of the hP2X7 receptor, given that various single point mutations have been found to affect receptor sensitivity and activity of ginsenoside CK (Bidula et al., 2019b). The aims of this chapter are to expand on the data published by Bidula *et al* , exploring the mutants in this paper and additional mutations to the central vestibule region in detail using the Membrane Potential Blue, FURA-2AM, and dye uptake assays, such as YO-PRO-1 iodide, Ethidium Bromide, and TO-PRO-3. Furthermore, the lack of activity of ginsenoside F1 compared to ginsenoside CK will be reviewed using both computational docking analysis and fluorescence assays.

5.2 Validation of Key Residues in the Central Vestibule Region of Human P2X7 Using the FURA-2AM and YO-PRO-1 Assays

Firstly, key mutants that were found to have an effect by Bidula *et al* were investigated using the FURA-2AM and YO-PRO-1 assays: D318A, L320A, and S60A (Bidula et al., 2019b). Although the effects of these mutations had been investigated at a single concentration of ATP by Bidula *et al*, the effects on the concentration response curve have not been published, and so full concentration response curves were generated here.

Initially, the responses of these transiently transfected hP2X7 mutants were considered using the FURA-2AM intracellular calcium assay, alongside wild type hP2X7 and native HEK-293 cells (**Figure 5.3**). An EC_{50} value could not be determined for the D318A mutant due to the lack of a sigmoidal concentration response curve, although the receptor appears to show increased affinity for ATP compared to the wild type, which is in contrast to what was documented using the YO-PRO-1 assay (Bidula et al., 2019b). In agreement with previously published data, the L320A and S60A mutants were more sensitive to ATP in this assay (Bidula et al., 2019b). EC_{50} values are summarised in **Table 5.1**. In terms of potentiation, both the L320A and S60A mutants were potentiated by ginsenoside CK, although to a lesser extent than the wild type. The D318A mutant displayed increased potentiation compared to the wild type, perhaps due to the fact that the initial ATP concentration response is no bigger than that of the native HEK-293 cells, although the native cells were not potentiated by CK. This increase in potentiation at the D318A mutant is different to what was observed in the YO-PRO-1 assay previously, where the D318A mutant had reduced fold potentiation (Bidula et al., 2019b). In addition, similar to what was observed with the patch clamp assay by Bidula *et al* (Bidula et al., 2019b), the S60A mutant produced a much larger response to ATP compared to the wild type P2X7 receptor. Overall, the D318A mutant appeared to have increased potentiation by ginsenoside CK in the FURA-2AM assay, whereas the L320A and S60A mutations appeared to have reduced potentiation; the L320A mutation reduced both the leftward shift and the increase in the maximum response induced by ginsenoside CK, whereas the S60A mutation reduced mainly the increase in the maximum response.

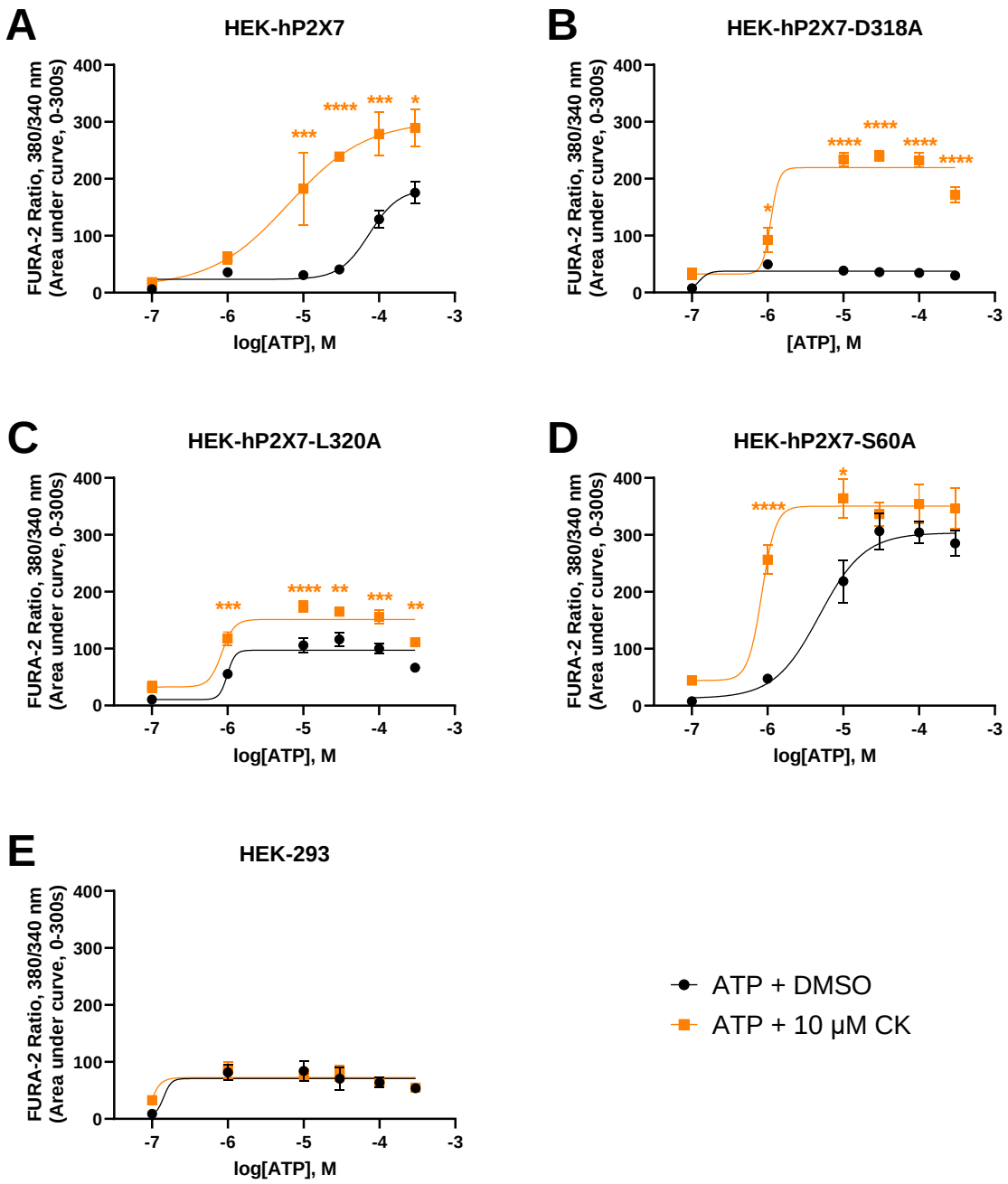

Figure 5.3 – Intracellular calcium measurements on HEK-293 cells transiently transfected with wild type or mutant hP2X7 measured using the FURA-2AM assay. Concentration response to ATP in the presence and absence of 10 µM CK at **A**: wild type hP2X7 **B:** D318A hP2X7 **C:** L320A hP2X7 **D:** S60A hP2X7 and **E:** native HEK-293 cells. Cells were loaded in low divalent cation buffer (ELDV) containing 2 µM FURA-2AM and 250 µM sulfinpyrazone and experiments conducted in low divalent cation buffer (ELDV) containing 250 µM sulfinpyrazone. Graphs are plotted as area under the curve (AUC) values between 0-300 seconds from three independent experiments ± SEM and fitted with a four-parameter non-linear regression curve. Average EC_{50} values ± SD are calculated using individual EC_{50} values from three independent experiments (see **Table 5.1**). *P < 0.05, **P<0.01, ***P<0.001, ****P<0.0001 determined using two-way ANOVA with Šídák's multiple comparisons test.

Table 5.1 – Average EC_{50} values for ATP in the presence and absence of ginsenoside CK in HEK-293 cells transiently transfected wild type or mutant hP2X7 measured using the FURA-2AM assay. Average EC_{50} values are calculated using individual EC_{50} values from three independent experiments. Cells were loaded in low divalent cation buffer (ELDV) containing 2 µM FURA-2AM and 250 µM sulfinpyrazone and experiments conducted in low divalent cation buffer (ELDV) containing 250 µM sulfinpyrazone. *P<0.05, ***P<0.001 determined by unpaired, two-tailed t-test.

Mutant	Compound	Average EC_{50} (µM ± SD)	pEC_{50}	Difference in pEC_{50} ($-pEC_{50}$ ATP + CK – $-pEC_{50}$ ATP)
Wild-type P2X7	**ATP**	74.47 ± 3.78	-4.128	0.993
	ATP + CK	7.57 ± 7.80 ***	-5.121	
HEK-P2X7-L320A	**ATP**	0.98 ± 0.04	-6.008	0.098
	ATP + CK	0.78 ± 0.25	-6.106	
HEK-P2X7-S60A	**ATP**	5.86 ± 3.07	-5.232	0.833
	ATP + CK	0.86 ± 0.03 *	-6.065	

Next, the YO-PRO-1 assay was used to determine full concentration response curves for ATP and ginsenoside CK HEK-293 cells transiently transfected wild type and or mutant hP2X7 receptors (**Figure 5.4**). The S60A mutant is more sensitive to ATP, as was observed previously by Bidula *et al*, however, this was less clear for the D318A and L320A mutants as YO-PRO-1 uptake was poor or absent in these mutants. EC_{50} values are summarised in **Table 5.2**. The S60A mutant was potentiated by ginsenoside CK to a similar degree as the wild type, although there was little difference in the maximum response achieved by ATP alone compared to in the presence of ginsenoside CK. The dramatic increase in the maximum response in the presence of ginsenoside CK in the D318A mutant was not observed to the same extent in the YO-PRO-1 assay as what had been observed in the FURA-2AM assay previously, however, potentiation could still be observed at concentrations of ATP >200 µM. This data is in agreement with published data using the same YO-PRO-1 assay, with D318A having reduced fold potentiation compared to the wild type receptor (Bidula et al., 2019b), highlighting key differences in potentiation between the FURA-2AM and YO-PRO-1 assays. To summarise, the D318A mutant showed reduced potentiation by CK in this dye uptake assay whereas in the FURA-2AM assay potentiation by CK was increased. The S60A mutant behaved in a similar manner in this dye uptake assay to the FURA-2AM assay, with a reduction in the increase in the maximum response with little change to the degree of shift. The L320A mutant did not display dye uptake in the YO-PRO-1 assay, and so the effects of this mutant on potentiation by CK could not be assessed for this assay.

In both the FURA-2AM and YO-PRO-1 iodide assays, mutating residues L320 and S60 to alanine reduced potentiation by ginsenoside CK, although key differences exist between the FURA-2AM and YO-PRO-1 assays: the L320A mutant produces a functional ATP concentration response in the FURA-2AM assay but does not display dye uptake properties in the YO-PRO-1 assay. Overall, this highlights the importance of conducting full concentration response studies on mutants of the hP2X7 receptor in different assays to be sure the effect is not assay-specific.

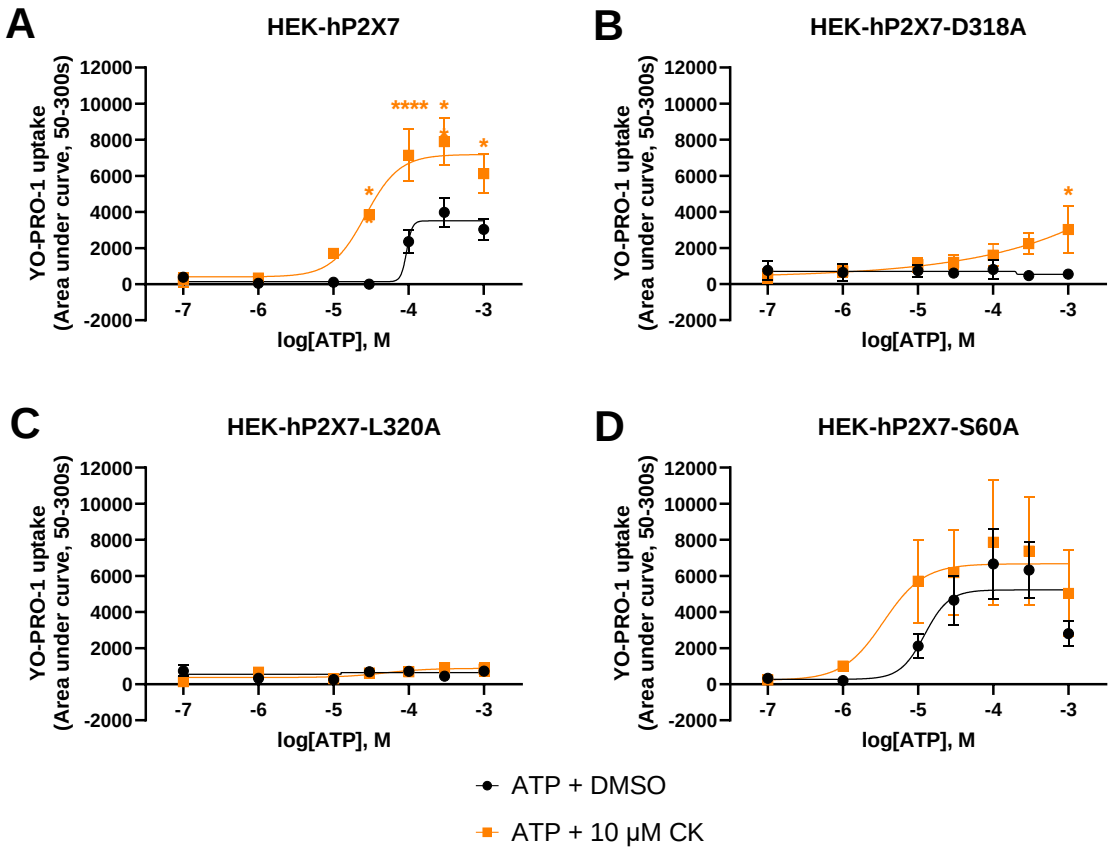

Figure 5.4 – Responses to ATP and ATP + 10 µM CK in HEK-293 cells transiently transfected with either wild-type human P2X7 or mutant human P2X7. The control ATP response is shown in black, whereas ATP with 10 µM ginsenoside CK is shown in orange for **A** wild type hP2X7 **B**: D318A hP2X7 **C:** L320A hP2X7 and **D**: S60A hP2X7 cells. Experiments were conducted in low divalent cation buffer (ELDV). Graphs are plotted as area under the curve (AUC) values between 50-300 seconds from three independent experiments ± SEM and fitted with a four-parameter non-linear regression curve. Average EC_{50} values ± SD are calculated using individual EC_{50} values from three independent experiments (see **Table 5.2**). *P < 0.05, **P<0.01, ***P<0.001, ****P<0.0001 determined using two-way ANOVA with Šídák's multiple comparisons test.

Table 5.2 – Average EC_{50} values for ATP in the presence and absence of ginsenoside CK in HEK-293 cells transiently transfected wild type or mutant hP2X7 measured using the YO-PRO-1 assay. Average EC_{50} values are calculated using individual EC_{50} values from three independent experiments (except for L320A, where an EC_{50} could only be determined in a single experiment). Experiments were conducted in low divalent cation extracellular buffer (ELDV). *P<0.05, ***P<0.001 determined by unpaired, two-tailed t-test.

Mutant	Compound	Average EC_{50} (μM ± SD)	pEC_{50}	Difference in pEC_{50} (-pEC_{50} ATP + CK – -pEC_{50} ATP)
Wild-type P2X7	**ATP**	79.86 ± 21.58	-4.098	0.495
	ATP + CK	25.54 ± 6.39 *	-4.593	
HEK-P2X7-L320A	**ATP**	10.72	-4.970	-0.844
	ATP + CK	74.86	-4.126	
HEK-P2X7-S60A	**ATP**	12.72 ± 1.18	-4.895	0.654
	ATP + CK	2.82 ± 1.43 ***	-5.549	

5.3 Investigating the Inactivity of Ginsenoside F1 at Human P2X7 Receptors Using the Membrane Potential Blue Assay and Site Directed Mutagenesis

A key finding published in 2021 by Piyasirananda *et al* showed that ginsenoside F1, despite being structurally similar to ginsenoside CK, is inactive at the human P2X7 receptor (Piyasirananda et al., 2021). Ginsenoside CK has two crucial functional groups that are thought to be involved in binding of CK to the central vestibule region: a hydroxyl group on carbon 3, and a glucose sugar moiety on carbon 20 (see **Figure 5.1**) (Bidula et al., 2019b). Ginsenoside F1 has both of these functional groups, but also contains an additional hydroxyl group on carbon 6 (**Figure 5.5**). Despite this somewhat minor addition, and the rest of the compound being a comparable structure to ginsenoside CK, ginsenoside F1 is inactive (Piyasirananda et al., 2021).

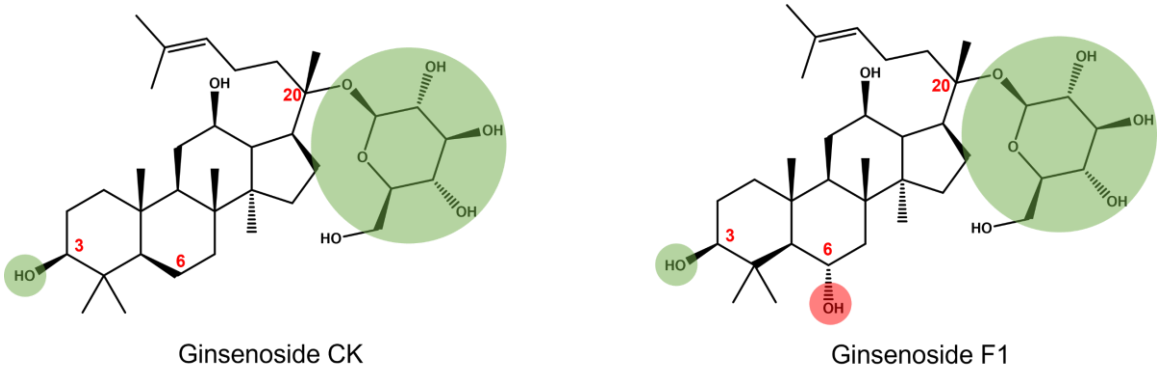

Figure 5.5 – Diagrams of ginsenosides CK and F1 showing key structural components of each. Key functional groups involved in binding to the central vestibule are highlighted in green, whereas the additional hydroxyl group in ginsenoside F1 is highlighted in red. Carbons substituted with key functional groups are numbered accordingly.

To investigate this further, the membrane potential blue assay was used to determine if this effect was mirrored in this assay, which is representative of bulk ion movement across the membrane, compared to a dye uptake assay. **Figure 5.6** outlines the responses to ATP -/+ 10 µM CK or 10 µM F1. Responses to ATP alone and ATP with 10 µM F1 were comparable, but a leftward shift in the concentration response curve was observed in the presence of ginsenoside CK. Neither ginsenoside was able to substantially increase the maximum response from that of ATP alone, with average maximum values of 41196.4 and 37135.4 for ginsenoside CK and F1 respectively compared to 38573.7 for ATP alone.

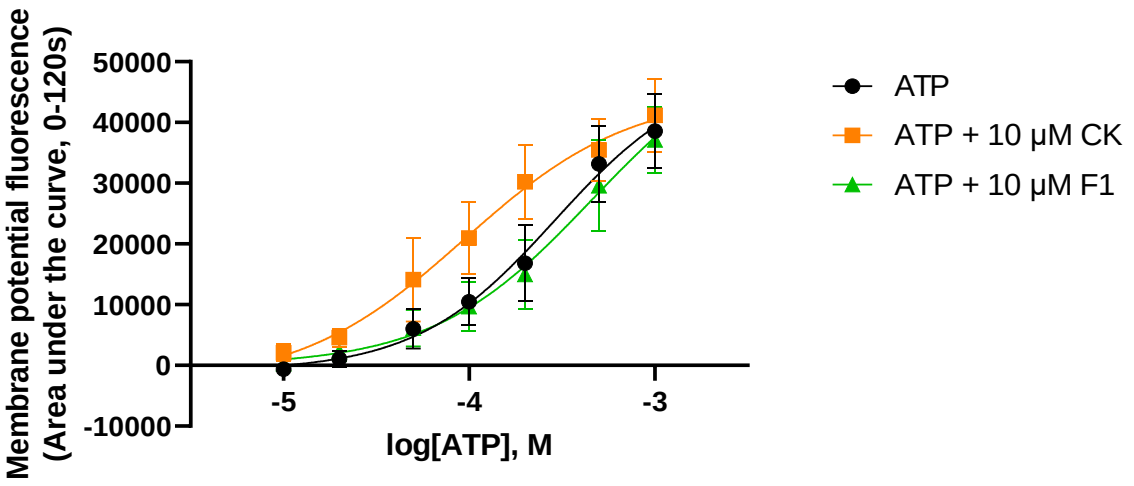

Figure 5.6 – Responses to ATP in the presence and absence of ginsenosides in HEK-293 cells stably expressing the wild-type human P2X7 receptor measured using the membrane potential blue assay. The response to ATP is shown in black, with the responses to ATP + 10 µM CK shown in orange and ATP + 10 µM F1 shown in green. Experiments were conducted in standard divalent cation extracellular buffer (Etotal). Data are plotted as mean area under the curve (AUC) values from three independent experiments ± SEM and fitted with a four-parameter non-linear regression curve. Average EC_{50} values are calculated using individual EC_{50} values from three independent experiments (see **Table 5.3**).

Average EC_{50} values are summarised in **Table 5.3**, with ATP and ATP + 10 µM F1 having similar average EC_{50} values. The average EC_{50} value calculated for CK reflects what is seen in **Figure 5.6**, with an approximately four-fold reduction in the EC_{50} value and therefore an increase in sensitivity of the receptor to ATP.

Table 5.3 – Average EC_{50} values for ATP, ATP + 10 µM CK, and ATP + 10 µM F1 measured at HEK-293 cells stably expressing the human P2X7 receptor using the membrane potential blue assay. Average EC_{50} values are calculated using individual EC_{50} values from three independent experiments. Experiments were conducted in standard extracellular buffer (Etotal). *P<0.05 determined by one-way ANOVA with Dunnett's multiple comparisons test.

Receptor	Compound	Average EC_{50} (nM ± SD)	pEC_{50}	Difference in pEC_{50} (-pEC_{50} ATP + ginsenoside – -pEC_{50} ATP)
Wild-type P2X7	**ATP**	278.93 ± 71.75	-3.555	
	ATP + CK	69.30 ± 31.61 *	-4.159	0.604
	ATP + F1	291.00 ± 119.22	-3.536	-0.019

As ginsenoside F1 has been shown to be ineffective in the membrane potential assay (**Figure 5.6**) in addition to YO-PRO-1 dye uptake (Bidula et al., 2019b), it is important to consider the possible orientation of the CK molecule in relation to neighbouring residues. **Figure 5.7** shows ginsenoside CK (green) docked to the central vestibule region of a human P2X7 homology model (orange).

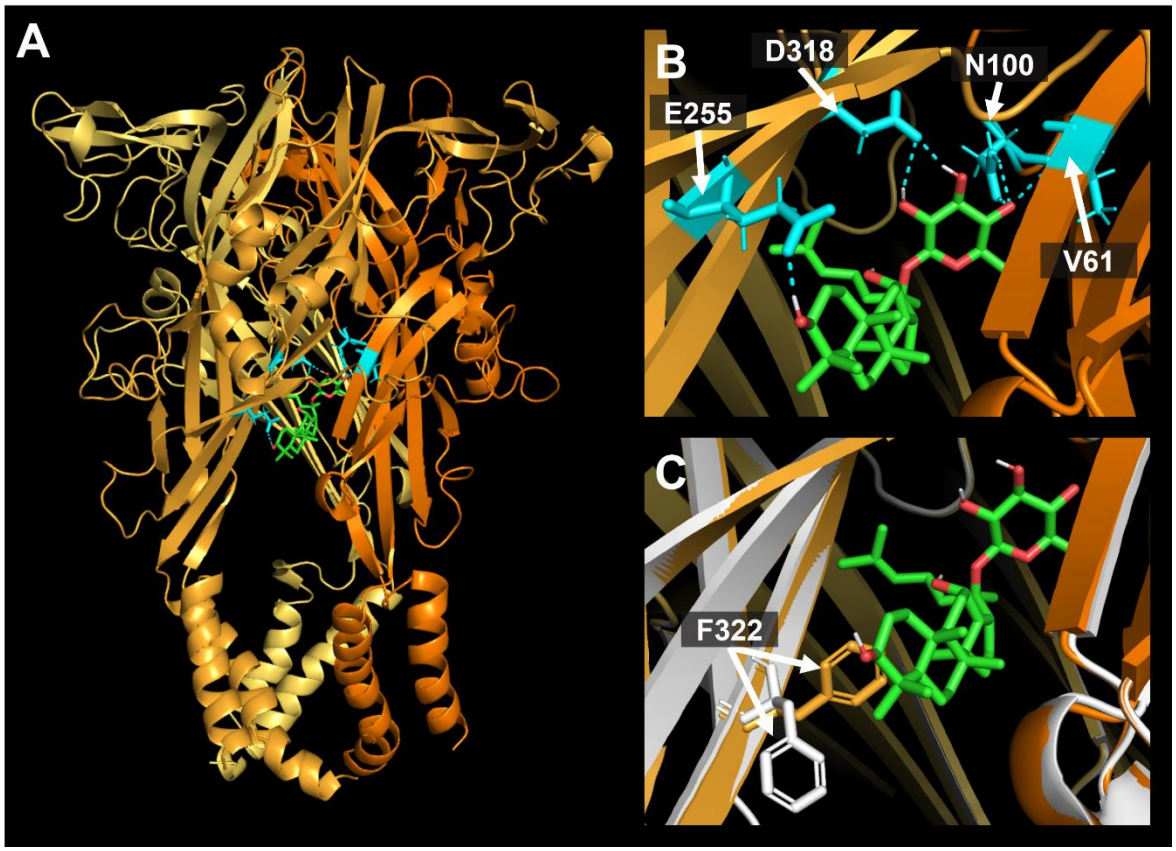

Figure 5.7 – Homology model of human P2X7 showing ginsenoside CK docked to the central vestibule region. **A**: Ginsenoside CK (shown in green) docked to the central vestibule region of human P2X7, with residues that make polar contacts highlighted in cyan. **B**: Close up of the central vestibule region with ginsenoside CK docked (green). Interacting residues are highlighted in cyan and labelled accordingly. **C**: Overlay of homology models showing ATP-bound open-state human P2X7 without CK docked (orange) and with CK docked (white). Note the position change of residue F322 (labelled) between docked and undocked states. Homology models are based on the crystal structure of zebrafish-P2X4 (PDB: 4DW1) with the human P2X7 sequence overlayed. Docking was performed by Dr Sam Walpole, UEA, using Glide (Schrödinger).

Residues that are proposed to make polar interactions with CK are highlighted in cyan (panels **A** and **B**). In panel **A**, CK is predicted to sit high up into the central vestibule region, with the sugar moiety on carbon 20 making interactions with the side chains of D318 and N100 and the main chain of V61 (panel **B**). The steroidal scaffold portion of the CK molecule is proposed to sit further down in the pocket, with the C3 hydroxyl residue interacting with the side chain of residue E255 (panel **B**). When investigating residues that neighbour the lower portion of the molecule (specifically, those close to C3

and C6), it was noted that the side chain of residue F322 does not appear to sit in the same orientation when CK is docked to the central vestibule (panel **C**). In the ATP-bound open state (orange), the side chain of residue F322 appears to point upwards into the central vestibule, whereas when CK is docked to the ATP-bound open state receptor (white), the side chain of F322 residue appears to 'flip' downwards. The movement of this phenylalanine side chain could be key to stabilising the binding and subsequent interactions of the ginsenosides with the central vestibule region of the P2X7 receptor, and so this F322 residue – and others in the surrounding vicinity – were investigated further.

Given that residue F322 lies close to where the C6 hydroxyl group of F1 would sit based on CK docking, it was considered that this hydrophobic residue could be a steric hindrance to ginsenoside F1 binding. To investigate this further, the F322 residue was mutated to alanine to reduce the incidence of steric hindrance and in turn determine whether this would allow ginsenoside F1 to potentiate. HEK-293 cells were transiently transfected with mutant F322A human P2X7 and responses to ATP in the presence and absence of either ginsenoside CK or F1 were measured using the membrane potential assay (**Figure 5.8**). Firstly, it is noted that mutating F322 to alanine increases the sensitivity of the receptor to ATP compared to the wild type by approximately an entire log unit. This is similar to what was observed when mutating neighbouring residues D318A and L320A in the FURA-2AM assay, where sensitivity to ATP appeared to be increased at both (see **Figure 5.3**). Ginsenoside CK is able to induce a leftward shift to the ATP concentration response curve in the F322A mutant, however, F1 remains inactive. **Table 5.4** summarises the average and individual EC_{50} values from each of the three experiments conducted. An EC_{50} value could not be calculated for ATP in the presence of ginsenoside CK as the concentrations of ATP used did not go low enough to produce a sigmoidal concentration response curve. The EC_{50} value would likely be < 10 μM given the shape of the graph. This suggests that mutating this residue alone is not enough to restore activity of ginsenoside F1 to the same level as ginsenoside CK, and that the C6 hydroxyl must be conflicting in more ways with the binding pocket than with residue F322 alone.

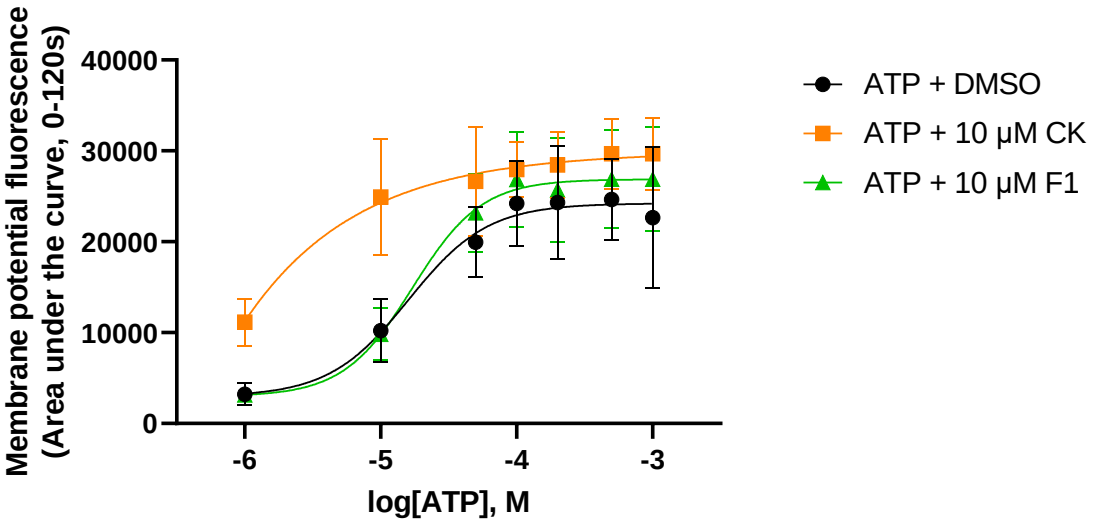

Figure 5.8 – Responses to ATP in the presence and absence of either ginsenoside CK or F1 in HEK-293 cells transiently transfected with F322A mutant hP2X7 measured using the membrane potential blue assay. The response to ATP is shown in black, with the responses to ATP + 10 µM CK shown in orange and ATP + 10 µM F1 shown in green. Experiments were conducted in low divalent cation buffer (ELDV). Data are plotted as area under the curve (AUC) values ± SEM from two independent experiments and fitted with a four-parameter non-linear regression curve. Average EC_{50} values ± SD are calculated using individual EC_{50} values from two independent experiments (see **Table 5.4**).

Table 5.4 – Average EC_{50} values for ATP in the presence and absence of either ginsenoside CK or F1 in HEK-293 cells transiently transfected with F322A mutant hP2X7 measured using the membrane potential blue assay. Average EC_{50} values are calculated using individual EC_{50} values from two independent experiments. Experiments were conducted in low divalent cation extracellular buffer (ELDV).

Receptor	Compound	Average EC_{50} (µM ± SD)	pEC_{50}	Difference in pEC_{50} (-pEC_{50} ATP + ginsenoside – -pEC_{50} ATP)
HEK-hP2X7-F322A	**ATP**	15.80 ± 0.57	-4.801	
	ATP + 10 µM CK	*ND*	*ND*	*ND*
	ATP + 10 µM F1	17.21 ± 1.11	-4.764	-0.037

5.4 Extended Mutagenesis of the Central Vestibule Region of Human P2X7 and Subsequent Effects on Potentiation by Ginsenoside CK Determined Using Multiple Fluorescence Assays

In addition to mutating residue F322, additional alanine mutants were made for residues Y257 and E255. Residue Y257, although not thought to make direct interactions with ginsenoside CK, lies on the β-strand neighbouring residue F322, and therefore could make aromatic ring interactions with residue F322 and alter the conformation of the binding pocket and ease of movement of the transmembrane domain connecting rods on receptor activation (**Figure 5.9**).

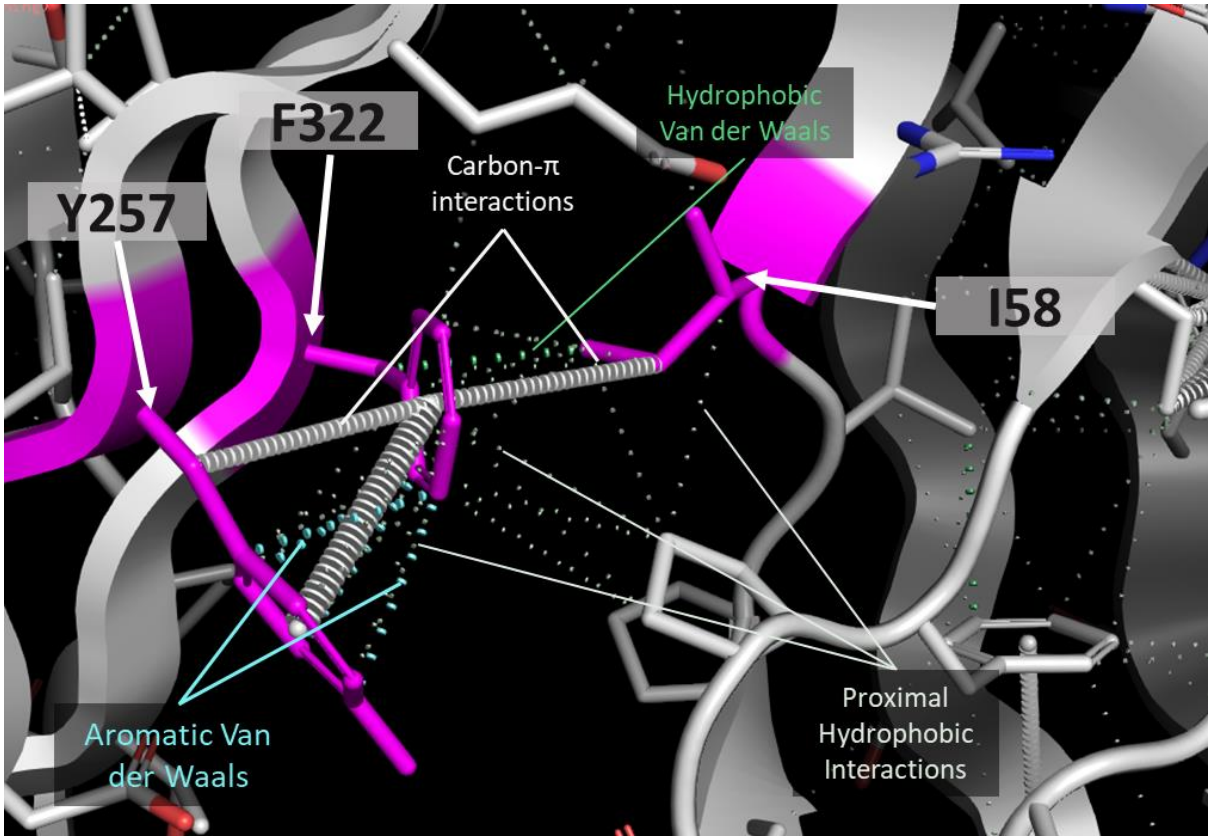

Figure 5.9 – Possible interactions between residue F322 and Y257 and I58. Residues F322, Y257, and I58 are highlighted in magenta. Multiple hydrophobic interactions can be seen between Y257 and F322, including aromatic and pi-pi interactions. There are also interactions between the subunits, with F322 proposed to make hydrophobic interactions with I58 on the neighbouring subunit. Homology models are based on the crystal structure of zebrafish-P2X4 (PDB: 4DW1) with the human P2X7 sequence overlayed. Homology models were produced by Dr Sam Walpole, UEA. Interactions were calculated using Arpeggio (https://biosig.lab.uq.edu.au/arpeggioweb/).

Residue E255 is thought to interact directly with the C3 hydroxyl of ginsenoside CK based on computational docking, and so mutating this residue may destabilise the binding of CK. In addition to these single point mutations in hP2X7, combination mutants were also generated; these were E255A with F322A and Y257A with F322A. **Figure 5.10** shows intracellular calcium measurements conducted on HEK-293 cells transiently transfected with either wild-type human P2X7 or one of the five mutants generated.

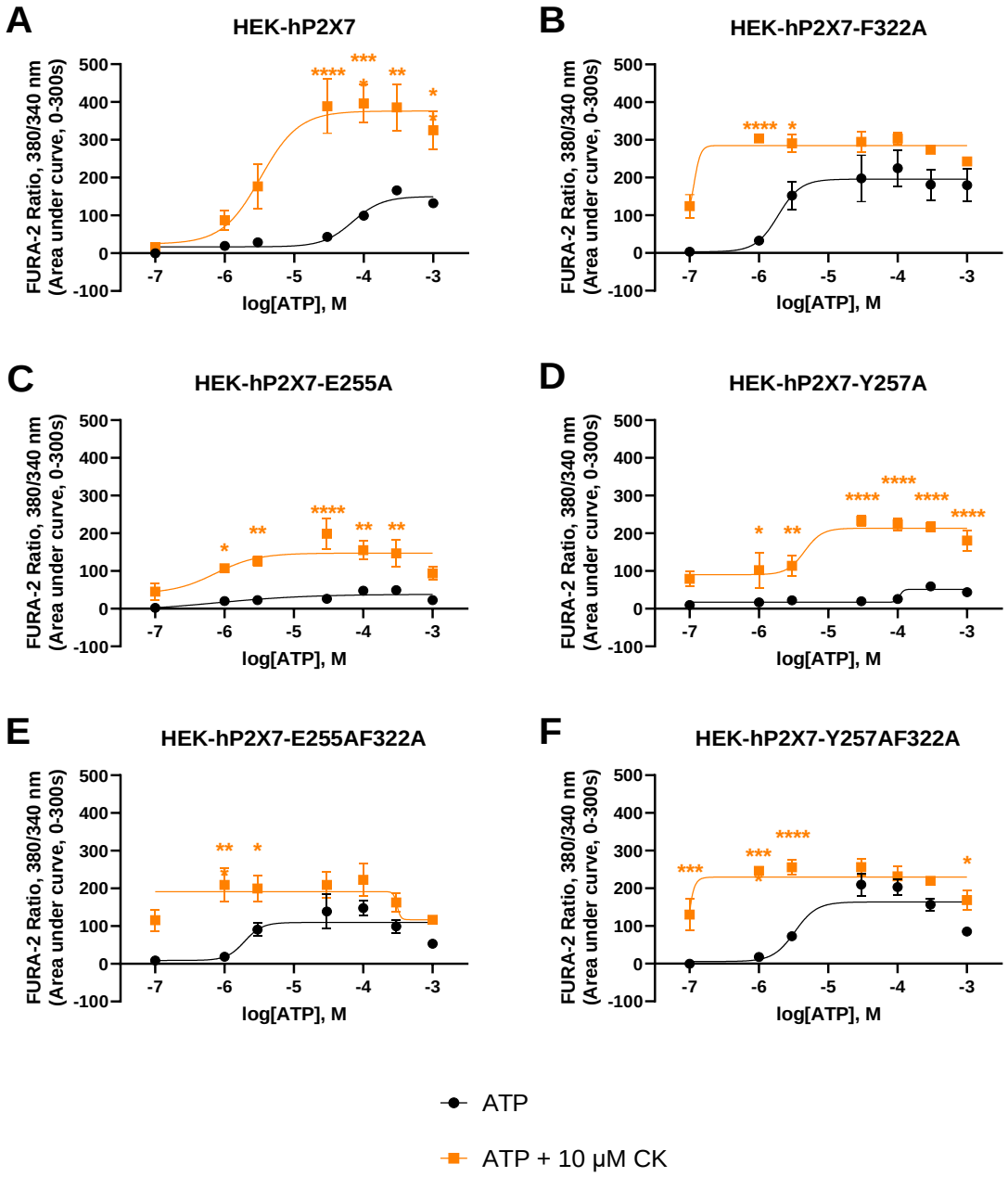

Figure 5.10 – Intracellular calcium measurements on HEK-293 cells transiently transfected with wild-type or mutant P2X7 measured using the FURA-2AM assay. The control response to ATP is shown in black, whereas the response to ATP + 10 µM CK is shown in orange for **A**: wild type hP2X7 **B:** F322A hP2X7 **C**: E255A hP2X7 **D**: Y257A hP2X7 **E:** E255A F322A hP2X7 and **F**: Y257A F322A hP2X7. Cells were loaded in low divalent cation buffer (ELDV) containing 2 µM FURA-2AM and 250 µM sulfinpyrazone and experiments conducted in low divalent cation buffer (ELDV) containing 250 µM sulfinpyrazone. Graphs are plotted as area under the curve (AUC) values between 0-300 seconds from three independent experiments ± SEM and fitted with a four-parameter non-linear regression curve. Average EC_{50} values ± SD are calculated using individual EC_{50} values from three independent experiments (see **Table 5.5**). *P < 0.05, **P<0.01, ***P<0.001, ****P<0.0001 determined using two-way ANOVA with Šídák's multiple comparisons test.

Firstly, there are variations in the sensitivity to ATP of each of the mutants generated when compared to wild-type human P2X7. Mutant F322A is considerably more sensitive to ATP than its wild-type counterpart, whereas the Y257A mutant is less sensitive. The results are less clear for the E255A mutant, as the responses are lower than that observed at the wild-type receptor, but it appears that this mutant is more sensitive to ATP. The combination mutants E255A+F322A and Y257A+F322A appear to follow the trend of the F322A mutant, both being more sensitive to ATP with similar average EC_{50} values as summarised in **Table 5.5**. Maximum responses to ATP tend to be less than that of the wild-type receptor, apart from mutants involving the F322A mutation (F322A, E255A+F322A, and Y257A+F322A), with the single F322A mutant giving a considerably bigger maximum response to ATP than the wild-type receptor (approximately 225 AUC compared to 166 AUC for the wild-type receptor).

At the wild-type human P2X7 receptor, the addition of ginsenoside CK produces a mixed type I/II positive allosteric modulator (PAM) response, resulting in an increase in the maximum measured response and a reduction in the EC_{50} (see **Table 5.5**). A leftward shift in the presence of ginsenoside CK can be observed at each of the mutants tested, suggesting that none of the mutants generated were sufficient to impair the activity of CK. For the single mutants E255A and Y257A, ginsenoside CK remains able to increase the maximum response, although not to the same maximum value as observed at the wild-type receptor. Interestingly, the single mutant F322A does not show as substantial of an increase in the maximum measured response, with the values similar for both CK and ATP alone (304 and 224 respectively, compared to an almost four-fold increase in the response measured for the wild-type receptor and E255A and Y257A mutants). The double mutants containing the F322A mutant also display this same phenomenon, with the maximum values for ATP and ATP + CK being comparable.

Table 5.5 – Average EC_{50} values for ATP and ATP + 10 µM CK measured at HEK-293 cells transiently transfected with wild-type or mutant human P2X7 using the FURA-2AM assay. Average EC_{50} values are calculated using individual EC_{50} values from up to three independent experiments. Cells were loaded in low divalent cation buffer (ELDV) containing 2 µM FURA-2AM and 250 µM sulfinpyrazone and experiments conducted in low divalent cation buffer (ELDV) containing 250 µM sulfinpyrazone. *P<0.05, **P<0.01 determined by one-way ANOVA with Dunnett's multiple comparisons test.

Mutant	Compound	Average EC_{50} (µM ± SD)	pEC_{50}	Difference in pEC_{50} ($-pEC_{50}$ ATP + CK – $-pEC_{50}$ ATP)
Wild-type P2X7	**ATP**	76.50 ± 25.75	-4.116	1.355
	ATP + CK	3.38 ± 1.59 **	-5.471	
HEK-P2X7-F322A	**ATP**	1.85 ± 0.59	-5.732	1.263
	ATP + CK	0.10 ± 0.005 *	-6.995	
HEK-P2X7-E255A	**ATP**	22.55 ± 19.14	-4.647	1.610
	ATP + CK	0.55 ± 0.61	-6.257	
HEK-P2X7-Y257A	**ATP**	327.14 ± 322.67	-3.485	2.080
	ATP + CK	2.726 ± 1.69	-5.565	
HEK-P2X7-E255AF322A	**ATP**	2.08 ± 0.86	-5.683	ND
	ATP + CK	*ND*	*ND*	
HEK-P2X7-Y257AF322A	**ATP**	3.16 ± 0.50	-5.500	1.504
	ATP + CK	0.099 *	-7.004	

Additional mutants were made along the edges of the lateral portal. One of these was R276A, which sits close to the F322 residue and at the top edge of the lateral portal, and the other was D197A, which again sits at the edge of the lateral portal but on the opposite edge to R276 (**Figure 5.11**).

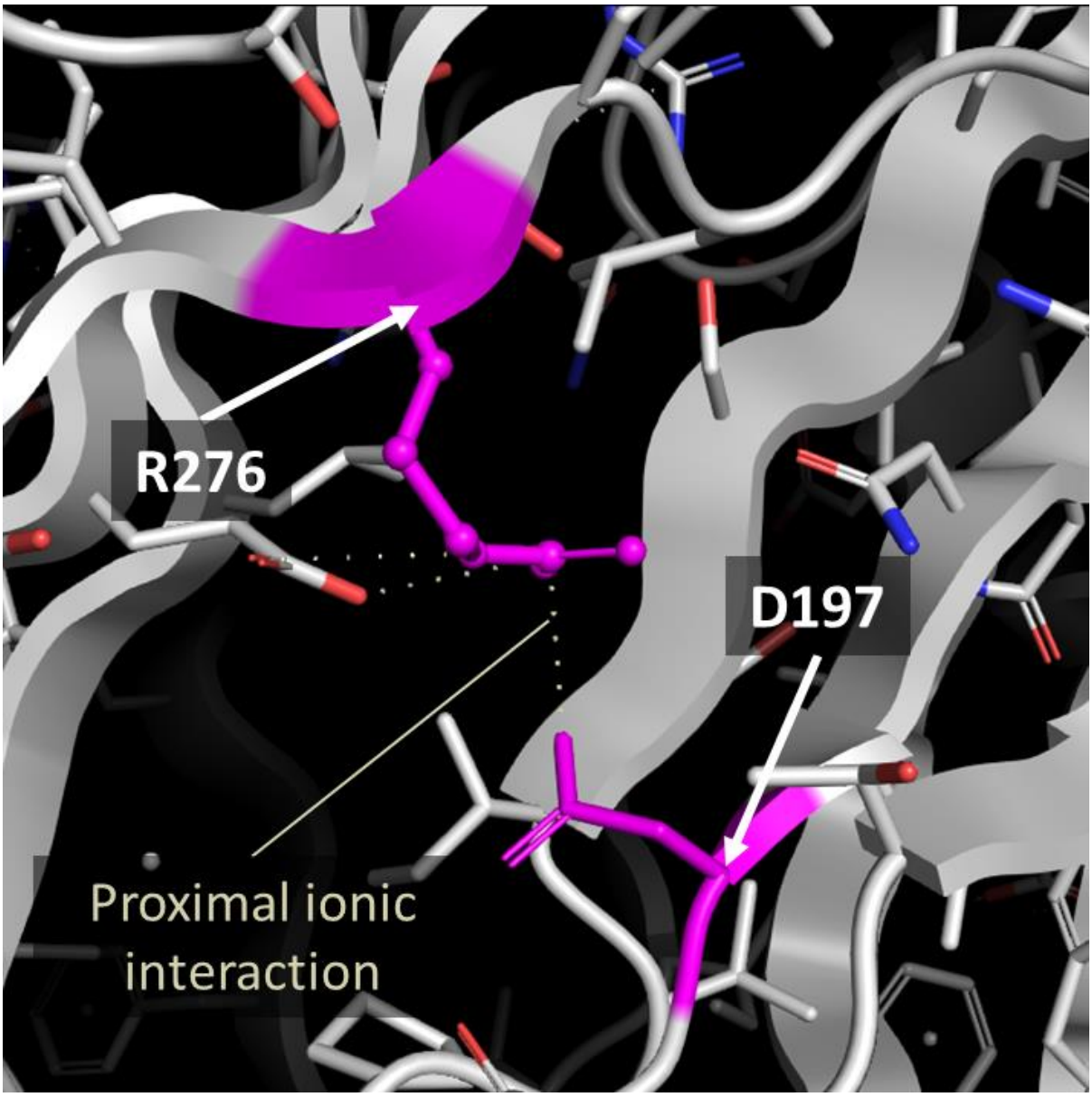

Figure 5.11 – Diagram showing possible ionic interactions between R276 and D197 in hP2X7. Residues R276 and D197 are highlighted in magenta. Proposed ionic interactions can be seen between these two residues. Homology models are based on the crystal structure of zebrafish-P2X4 (PDB: 4DW1) with the human P2X7 sequence overlayed. Homology models were produced by Dr Sam Walpole, UEA. Interactions were calculated using Arpeggio (https://biosig.lab.uq.edu.au/arpeggioweb/).

Using the membrane potential blue assay, ATP concentration responses were measured at HEK-293 cells transiently transfected with wild-type human P2X7, R276A hP2X7, or native HEK-293 cells (**Figure 5.12**). Wild-type human P2X7 had an EC_{50} to ATP of 120.9 µM, whereas the response to ATP in the R276A mutant was similar to the native HEK-293 cells. As a result, it was determined that this receptor was non-functional. Indeed, a single nucleotide polymorphism (SNP) in the human P2X7 population, where residue R276 is mutated to histidine, results in a non-functional receptor (Stokes et al., 2010).

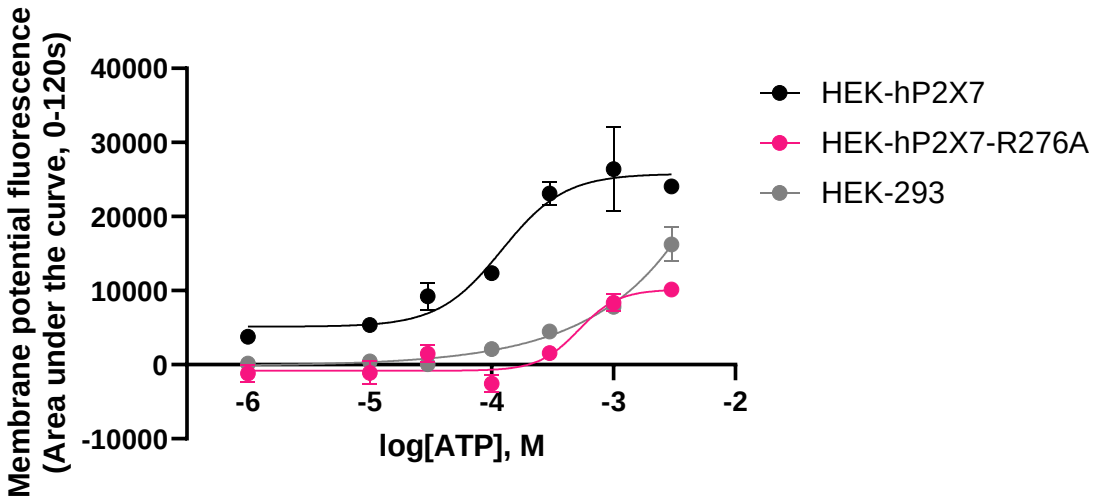

Figure 5.12 – Responses to ATP on HEK-293 cells transiently transfected with wild-type or mutant human P2X7 measured using the membrane potential blue assay. Wild type hP2X7 is shown in black, R276A mutant hP2X7 is shown in pink, and native HEK-293 cells are shown in grey. The experiment was conducted in standard extracellular buffer (Etotal). Data are plotted as mean area under the curve (AUC) values from one independent experiment ± SEM and fitted with a four-parameter non-linear regression curve. EC_{50} values are as follows: HEK-hP2X7 120.9 µM; HEK-hP2X7-R267A 516.9 µM.

The D197A mutant was able to produce a response to ATP in both the FURA-2AM and YO-PRO-1 assays (**Figure 5.13**). In the FURA-2AM assay, the D197A mutant had a lower maximum response to ATP compared to the wild type, but the EC_{50} values were comparable between the WT and mutant (see **Table 5.6**). Both the wild type and mutant receptors were potentiated by ginsenoside CK, although, despite the lower initial response to the ATP control, the D197A mutant achieved a greater maximum response in the presence of 10 µM CK compared to the wild type receptor. This effect was echoed in the YO-PRO-1 dye uptake assay, where both wild type and D197A mutant receptors had similar responses to ATP with comparable EC_{50} and maximum response values, but the D197A mutant displayed a much larger increase in the maximum response compared to the wild type hP2X7 receptor.

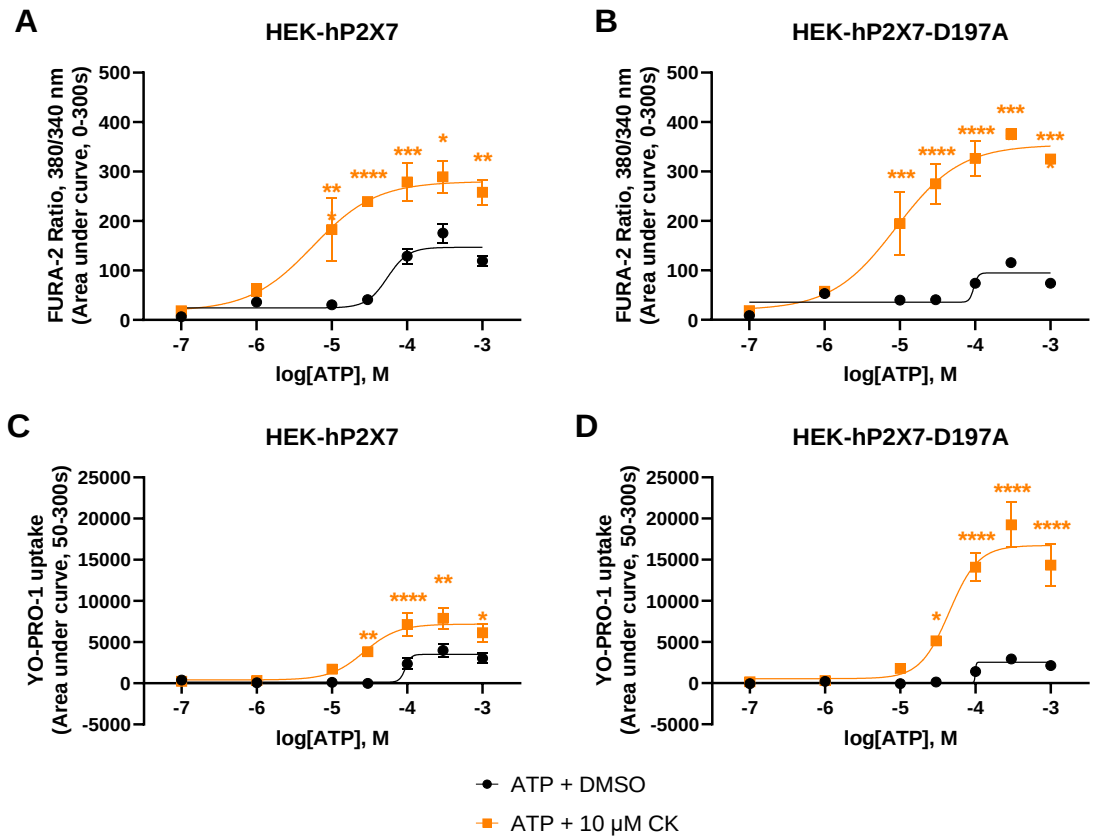

Figure 5.13 – Responses to ATP in the presence and absence of 10 µM ginsenoside CK measured in HEK-293 cells expressing either wild type or D197A mutant hP2X7. Panels **A** and **B** were measured using the FURA-2AM assay on HEK-293 cells transiently transfected with either wild type or mutant hP2X7. Panels **C** and **D** were measured using the YO-PRO-1 assay on G418-selected HEK-293 cells transfected with either wild type or mutant hP2X7. Responses to ATP and ATP + 10 µM CK for **A**, **C**: wild type hP2X7 and **B, D**: D197A mutant hP2X7. For panels **A** and **B**, cells were loaded in low divalent cation buffer (ELDV) containing 2 µM FURA-2AM and 250 µM sulfinpyrazone and experiments conducted in low divalent cation buffer (ELDV) containing 250 µM sulfinpyrazone. For panels **C** and **D**, experiments were conducted in ELDV containing 2 µM YO-PRO-1 iodide. Graphs are plotted as area under the curve (AUC) values between 0-300 seconds (**A** and **B**) or 50-300 seconds (**C** and **D**) from three independent experiments ± SEM and fitted with a four-parameter non-linear regression curve. Average EC_{50} values ± SD are calculated using individual EC_{50} values from three independent experiments (see **Table 5.6**). *P < 0.05, **P<0.01, ***P<0.001, ****P<0.0001 determined using two-way ANOVA with Šídák's multiple comparisons test.

Table 5.6 – Average EC_{50} values for ATP and ATP + 10 µM CK measured in HEK-293 cells expressing wild-type or mutant D197A hP2X7. Responses were measured using two separate assays (FURA-2AM and YO-PRO-1). For the FURA-2AM assay, responses were obtained from HEK-293 cells transiently transfected with either wild type or mutant hP2X7. For the YO-PRO-1 assay, responses were obtained from G418-selected HEK-293 cells transfected with either wild type or mutant hP2X7. Experiments were conducted in low divalent cation buffer (ELDV), with the addition of 250 µM sulfinpyrazone for FURA-2 experiments. Average EC_{50} values are calculated using individual EC_{50} values from up to three independent experiments. *P<0.05, **P<0.01, ***P<0.001 determined by one-way ANOVA with Dunnett's multiple comparisons test.

Assay	Mutant	Compound	Average EC_{50} (µM ± SD)	pEC_{50}	Difference in pEC_{50} ($-pEC_{50}$ ATP + CK – $-pEC_{50}$ ATP)
FURA-2AM	**Wild type hP2X7**	**ATP**	55.34 ± 4.06	-4.257	0.887
		ATP + CK	7.18 ± 7.76 ***	-5.144	
	HEK-hP2X7-D197A	**ATP**	73.46 ± 33.91	-4.134	0.706
		ATP + CK	14.46 ± 16.40	-4.840	
YO-PRO-1	**Wild type hP2X7**	**ATP**	79.86 ± 21.58	-4.098	0.495
		ATP + CK	25.54 ± 6.39 *	-4.593	
	HEK-hP2X7-D197A	**ATP**	98.24 ± 3.83	-4.008	0.347
		ATP + CK	44.19 ± 12.55 **	-4.355	

5.5 Characterisation of the F322A Human P2X7 Mutant using Multiple Fluorescence Assays

Given that ginsenoside CK appeared unable to increase the maximum response in the F322A mutant in both the FURA-2AM and membrane potential blue assays, this effect was explored further using the YO-PRO-1 dye uptake assay. Ginsenosides CK and F1 were tested on HEK-293 cells stably expressing the mutant F322A receptor (HEK-P2X7-F322A) in all three assay types – YO-PRO-1, membrane potential blue, and FURA-2AM – to allow for direct comparison between them (**Figure 5.14**). The F322A mutant was more sensitive to ATP in all assays; moreover, it was not potentiated by CK in the same way as the wildtype receptor. Ginsenoside CK was able to induce a leftward shift in the ATP concentration response at both the wildtype and mutant receptors in all assays, however, it did not increase the maximum response at the F322A mutant. Instead, CK appeared to reduce the maximum response in the YO-PRO-1 dye uptake assay from approximately 2788 for ATP alone to 1845 for ATP in the presence of CK. The maximum responses measured at HEK-P2X7-F322A were similar for ATP and ATP + CK in the membrane potential blue and FURA-2AM assays. Ginsenoside CK was able to increase the maximum response measured at wildtype HEK-P2X7 in the YO-PRO-1 and FURA-2AM assays, but not the membrane potential blue assay. Average EC_{50} values for both wild-type and F322A mutant P2X7 in all three assays are summarised in **Table 5.7**.

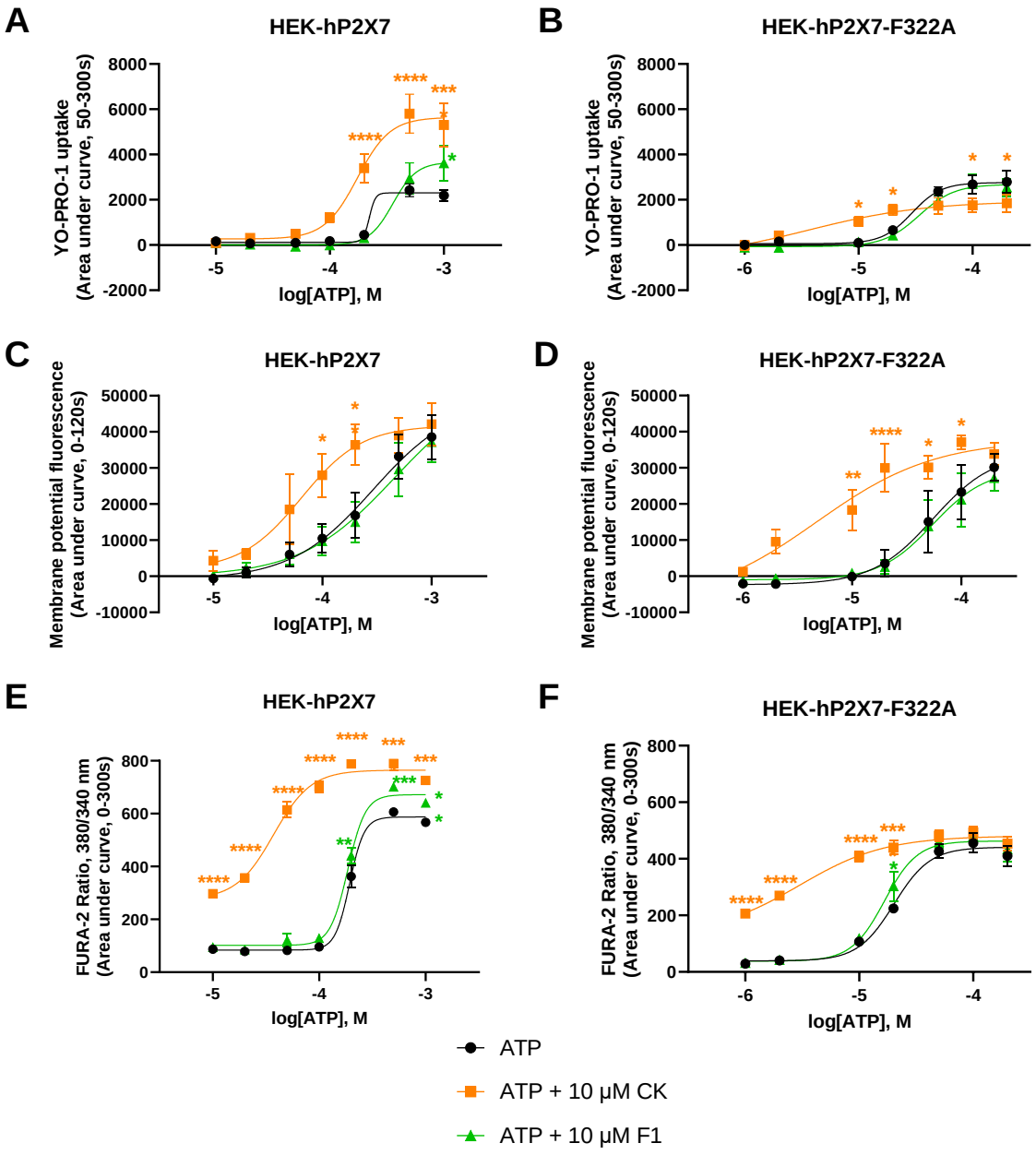

Figure 5.14 – Responses to ATP in the presence and absence of either 10 µM ginsenoside CK or 10 µM ginsenoside F1 in HEK-293 cells stably expressing wild-type human P2X7 or mutant F322A human P2X7. Responses in panels **A** and **B** were measured using the YO-PRO-1 assay, responses in panels **C** and **D** were measured using the Membrane Potential Blue assay, and responses in panels **E** and **F** were measured using the FURA-2AM calcium assay. Responses to ATP, ATP + 10 µM CK, and ATP + 10 µM F1 for **A**, **C, E**: wild type hP2X7 and **B, D, F**: F322A mutant hP2X7. Cells in panels **E** and **F** were loaded in low divalent cation buffer (ELDV) containing 2 µM FURA-2AM and 250 µM sulfinpyrazone. Experiments in all panels were conducted in standard extracellular buffer (Etotal) with the addition of 250 µM sulfinpyrazone for experiments in panels **E** and **F**. Graphs are plotted as area under the curve (AUC) values from three independent experiments ± SEM and fitted with a four-parameter non-linear regression curve. Average EC_{50} values ± SD are calculated using individual EC_{50} values from three independent experiments (see **Table 5.7**). *P < 0.05, **P<0.01, ***P<0.001, ****P<0.0001 determined using two-way ANOVA with Šídák's multiple comparisons test.

Table 5.7 – Average EC_{50} values for ATP, ATP + 10 µM CK, and ATP + 10 µM F1 measured at HEK-293 cells stably expressing wild-type or mutant F322A human P2X7. Responses were measured using three separate assays (YO-PRO-1, Membrane Potential Blue, and FURA-2AM). Average EC_{50} values are calculated using individual EC_{50} values from three independent experiments. Cells in the FURA-2AM experiments were loaded in low divalent cation buffer (ELDV) containing 2 µM FURA-2AM and 250 µM sulfinpyrazone. All experiments were conducted in standard extracellular buffer (Etotal) with the addition of 250 µM sulfinpyrazone for FURA-2 experiments. *P < 0.05, **P<0.01, ****P<0.0001 determined using two-way ANOVA with Šídák's multiple comparisons test.

Assay	Mutant	Compound	Average EC_{50} (µM ± SD)	pEC_{50}	Difference in pEC_{50} (-pEC_{50} ATP + ginsenoside – -pEC_{50} ATP)
YO-PRO-1	Wild-type P2X7	ATP	221.70 ± 2.51	-3.654	
		ATP + CK	174.70 ± 23.97	-3.758	0.104
		ATP + F1	365.37 ± 61.05 **	-3.437	-0.217
	HEK-P2X7-F322A	ATP	28.56 ± 8.13	-4.544	
		ATP + CK	6.86 ± 4.24 *	-5.164	0.620
		ATP + F1	34.18 ± 8.74	-4.466	-0.078
Membrane Potential Blue	Wild-type P2X7	ATP	278.93 ± 71.75	-3.555	
		ATP + CK	69.30 ± 31.61 *	-4.159	0.604
		ATP + F1	291.00 ± 119.22	-3.536	-0.019
	HEK-P2X7-F322A	ATP	51.09 ± 34.58	-4.292	
		ATP + CK	9.31 ± 8.38	-5.031	0.739
		ATP + F1	48.91 ± 25.16	-4.311	0.019
FURA-2AM	Wild-type P2X7	ATP	191.43 ± 17.86	-3.718	
		ATP + CK	38.30 ± 6.36 ****	-4.417	0.699
		ATP + F1	186.27 ± 12.51	-3.730	0.012
	HEK-P2X7-F322A	ATP	20.70 ± 3.42	-4.684	
		ATP + CK	3.67 ± 2.10 **	-5.435	0.751
		ATP + F1	17.22 ± 3.80	-4.764	0.080

To explore whether this phenomenon was specific to the YO-PRO-1 dye uptake assay or to dye uptake assays in general, multiple dyes were tested on HEK-293 or HEK20E6 cells stably expressing either the wildtype human P2X7 receptor or F322A mutant P2X7 receptor. **Figure 5.15** shows responses to ATP in the presence and absence of either 10 µM ginsenoside CK or 10 µM ginsenoside F1 measured using the YO-PRO-1 iodide assay, the TO-PRO-3 dye uptake assay, and the ethidium bromide (EtBr) uptake assay using the Flexstation 3 plate reader. As seen in the YO-PRO-1 iodide assay previously using standard extracellular buffer, similar responses can be observed in both wild-type P2X7 and mutant F322A P2X7 when measured in a low divalent cation buffer (panels **A** and **B**). Ginsenoside CK is able to increase the maximum response and decrease the EC_{50} value to ATP at the wild type receptor, whereas F1 shows little difference in the EC_{50} value and maximum response compared to ATP alone (EC_{50} values are summarised in **Table 5.8**). However, at the F322A mutant, CK is again able to reduce the EC_{50} value, but no potentiation of the maximum response is seen. Instead, the maximum response is significantly reduced from around 8350 AUC for ATP alone to approximately 6112 AUC for ATP with 10 µM CK.

This reduction in the maximum dye uptake response at the HEK-P2X7-F322A mutant was not observed in the TO-PRO-3 assay; ginsenoside CK was able to induce a leftward shift in the concentration response curve at the wildtype P2X7 receptor, but no leftward shift was observed at the F322A mutant (panels **C** and **D**). The F322A mutant was more sensitive to ATP in the TO-PRO-3 assay, as with previously tested assays, but gave a smaller maximum response than the wildtype receptor. This is different to what was seen in the YO-PRO-1 assay; in standard divalent cation extracellular buffer, the maximum responses to ATP in the YO-PRO-1 assay were similar between the wild type and mutant receptors (see **Figure 5.14**). When using low divalent cation buffer, the F322A mutant gave an increased response to ATP in the same assay (see **Figure 5.15**, panel **B**).

The responses in the EtBr assay mirrored that observed with the YO-PRO-1 assay: ginsenoside CK was able to increase the maximum response and increase the sensitivity to ATP in the wildtype receptor, whereas for the F322A mutant only the latter was true (panels **E** and **F**). Again, the F322A mutant was more sensitive to ATP than its wildtype counterpart, with average EC_{50} values similar to that observed in the YO-PRO-1 assay (**Table 5.8**). It is important to note that the EtBr experiments were conducted on HEK20E6 cells stably expressing both wildtype and mutant F322A receptors; these cells are P2Y2-CRISPR KO HEK-293 cells, and so this is unlikely to impact P2X7-dependent dye uptake responses (P2Y2 is not thought to be involved in dye uptake). Ethidium bromide experiments were conducted concurrently with the FURA-2AM assay, and so this cell type was chosen to minimise the effects of the P2Y2 receptor on intracellular calcium measurements.

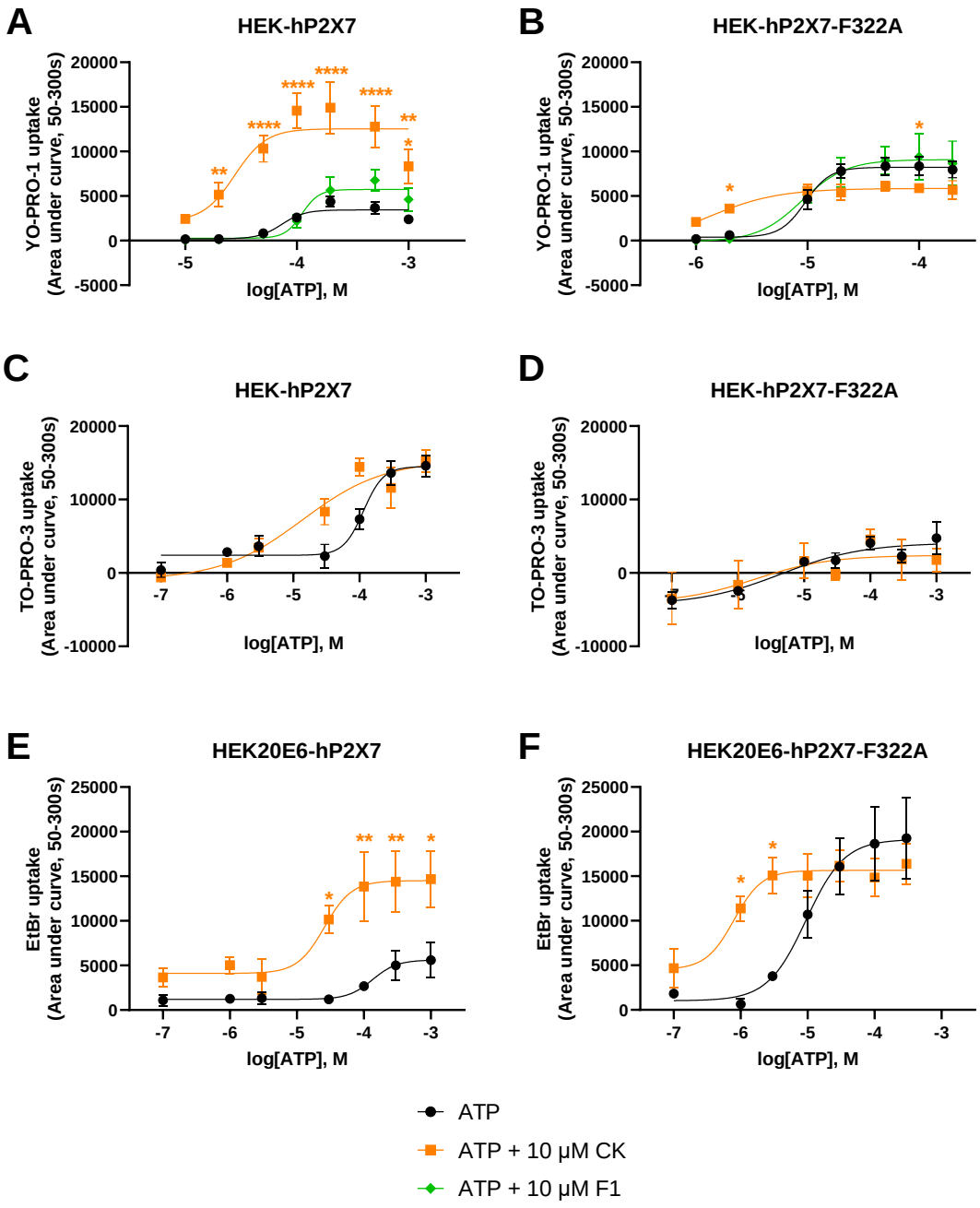

Figure 5.15 – Dye uptake responses to ATP in the presence and absence of either 10 µM ginsenoside CK or 10 µM ginsenoside F1 in HEK-293 cells stably expressing either wild-type human P2X7 or mutant F322A human P2X7. Responses in panels **A** and **B** were measured using the YO-PRO-1 assay, responses in panels **C** and **D** were measured using the TO-PRO-3 assay, and responses in panels **E** and **F** were measured using the ethidium bromide (EtBr) assay. Responses to ATP, ATP + 10 µM CK, and ATP + 10 µM F1 for **A**, **C, E**: wild type hP2X7 and **B, D, F**: F322A mutant hP2X7. **A, B, E, F**: n=3. **C**: n=1. **D**: n=2. HEK20E6 cells are P2Y2-KO HEK-293 cells described in **Chapter 2**. Graphs are plotted as area under the curve (AUC) values ± SEM and fitted with a four-parameter non-linear regression curve. Average EC_{50} values ± SD are calculated using individual EC_{50} values from the specified number of independent experiments (see **Table 5.8**). Experiments in all panels were conducted in low divalent cation buffer (ELDV) with the addition of 250 µM sulfinpyrazone for experiments in panels **E** and **F** as these were run concurrently with FURA-2AM.

Table 5.8 – Average EC_{50} values for ATP, ATP + 10 µM CK, and ATP + 10 µM F1 measured at HEK-293 cells expressing wild-type or mutant F322A human P2X7. Responses were measured using three separate assays (YO-PRO-1, TO-PRO-3, and ethidium bromide (EtBr)). Average EC_{50} values are calculated using individual EC_{50} values from up to three independent experiments. Experiments were conducted in low divalent cation buffer (ELDV) with the addition of 250 µM sulfinpyrazone for EtBr experiments as these were run concurrently with FURA-2. EtBr experiments were conducted on HEK20E6 cells which are P2Y2-KO HEK-293 cells. *P < 0.05, **P<0.01 determined using two-way ANOVA with Šídák's multiple comparisons test.

Assay	Mutant	Compound	Average EC_{50} (µM ± SD)	pEC_{50}	Difference in pEC_{50} (-pEC_{50} ATP + ginsenoside – -pEC_{50} ATP)
YO-PRO-1	Wild-type P2X7	ATP	72.55 ± 3.09	-4.139	
		ATP + CK	30.65 ± 15.43 *	-4.514	0.375
		ATP + F1	112.57 ± 17.52 *	-3.949	-0.190
	HEK-P2X7-F322A	ATP	6.12 ± 2.12	-5.213	
		ATP + CK	2.00 ± 0.50	-5.700	0.487
		ATP + F1	8.74 ± 2.58	-5.058	-0.155
TO-PRO-3	Wild-type P2X7	ATP	114.9	-3.940	0.924
		ATP + CK	13.67	-4.864	
	HEK-P2X7-F322A	ATP	7.54	-5.123	0.366
		ATP + CK	3.25	-5.489	
Ethidium Bromide (EtBr)	Wild-type P2X7	ATP	118.86 ± 74.78	-3.925	0.620
		ATP + CK	28.52 ± 0.87	-4.545	
	HEK-P2X7-F322A	ATP	9.97 ± 1.21	-5.001	0.976
		ATP + CK	1.05 ± 0.13 **	-5.977	

Data obtained for the TO-PRO-3 dye using the Flexstation 3 did not demonstrate as clear effects as with the YO-PRO-1 and ethidium bromide dyes. As a result, TO-PRO-3 uptake was measured using an alternative method: a flow cytometer. TO-PRO-3 fluorescence was measured against a range of concentrations of ATP between 1 μM and 1 mM on stably expressing wild type HEK-hP2X7 and mutant HEK-hP2X7-F322A (**Figure 5.16**). Responses to ATP in both cell lines were dose dependent, with the F322A mutant showing increased sensitivity to ATP compared to the wild type as has been seen in other assays. The addition of 10 μM ginsenoside CK potentiated responses to ATP at the wild type receptor at all concentrations measured, however, potentiation at the F322A mutant was only observed at concentrations ≤ 10 μM ATP. At concentrations of ATP 50 μM and above, the addition of ginsenoside CK reduced responses to ATP, similar to what was observed with other dyes (see **Figure 5.15**).

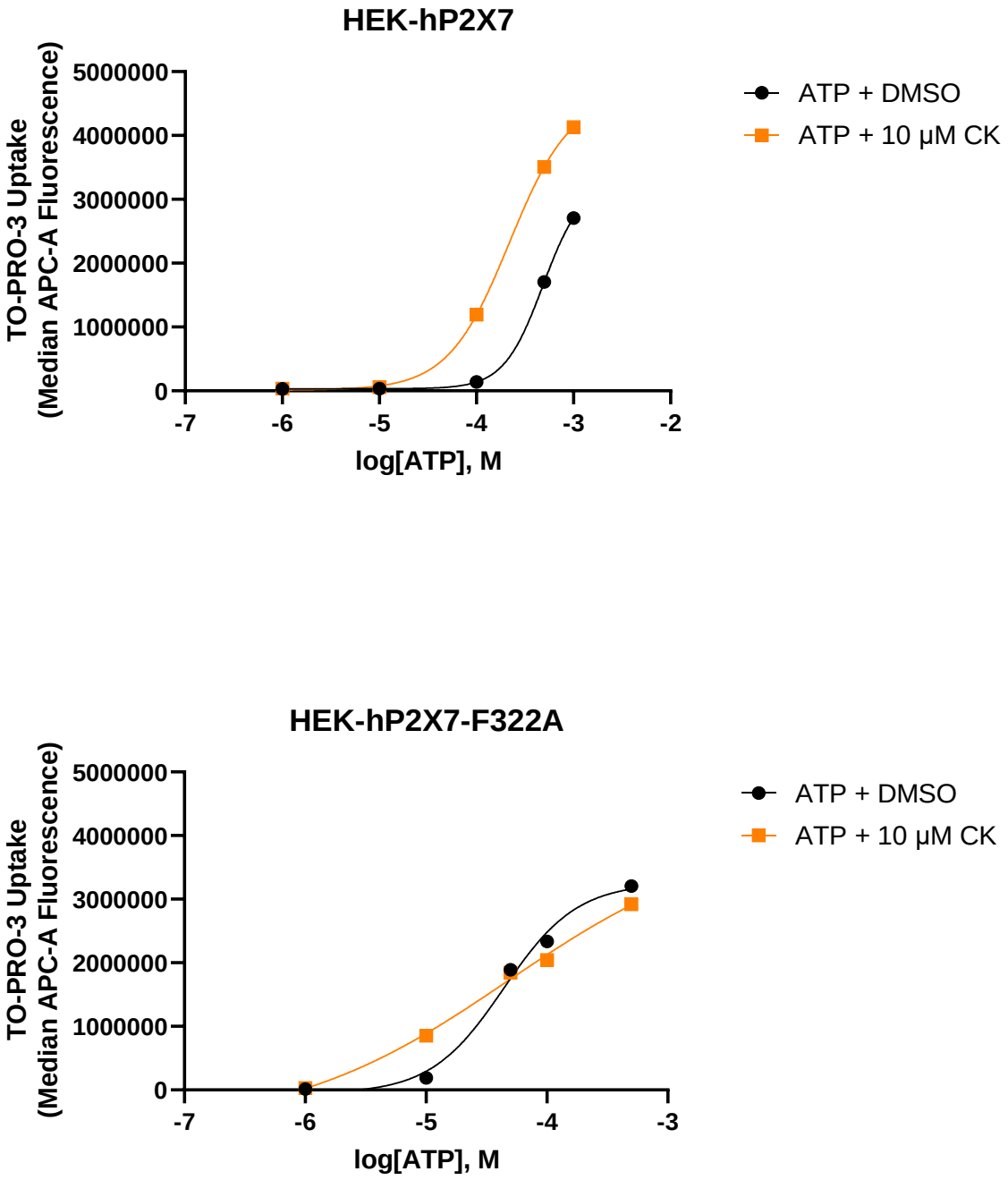

Figure 5.16 – TO-PRO-3 uptake responses measured in HEK-293 cells stably expressing wild type hP2X7 or mutant F322A hP2X7 using flow cytometry. **A**-**C**: Responses measured on wild type HEK-hP2X7 cells. **D**-**F**: Responses measured on mutant HEK-hP2X7-F322A cells. **A**: Concentration response curve to [ATP] between 1 µM and 1 mM in the presence of vehicle (DMSO, black) or 10 µM ginsenoside CK (orange) in wild type HEK-hP2X7 cells. EC_{50} values: ATP + DMSO 485.6 µM, ATP + 10 µM CK 219.3 µM. **B**: Concentration response curve to [ATP] between 1 µM and 500 µM in the presence of vehicle (DMSO, black) or 10 µM ginsenoside CK (orange) in mutant F322A HEK-hP2X7 cells. EC_{50} values: ATP + DMSO 43.9 µM, ATP + CK 48.2 µM. Graphs are plotted as median fluorescence measured using the APC-A channel. Concentration response curves are fitted with a four-parameter non-linear regression curve. Data are the result of one experiment conducted in low divalent cation buffer (ELDV), measured using a Beckmann Coulter CytoFLEX machine and analysed using CytExpert software.

With the reduction of the ATP response in the presence of CK on the F322A mutant confirmed in three different dye uptake assays using two different machines, this effect was explored further using different agonists. The ATP analogue 2'(3')-O-(4-Benzoylbenzoyl)adenosine-5'-triphosphate, or BzATP, is a full agonist at human P2X7 receptors, with increased potency at the wildtype receptor compared to ATP(Syed and Kennedy, 2012). As ATP appears to be a more potent agonist at the F322A mutant compared to the wildtype receptor, this was compared to the responses to BzATP in the YO-PRO-1 dye uptake assay using the Flexstation 3 plate reader (**Figure 5.17**). In addition, ginsenoside CK was tested with both agonists, ATP and BzATP. In **Figure 5.17**, panel **A**, ATP alone (grey) gives the smallest response and is the most right shifted. The addition of 10 µM CK increases the maximum response and the sensitivity to ATP, bringing the response in line with that of BzATP, the full agonist. The response to BzATP in the presence of CK is again left shifted, but the maximum responses to ATP + CK, BzATP, and BzATP + CK are all similar, with the maximum response to BzATP + CK being slightly reduced compared to the response to BzATP alone.

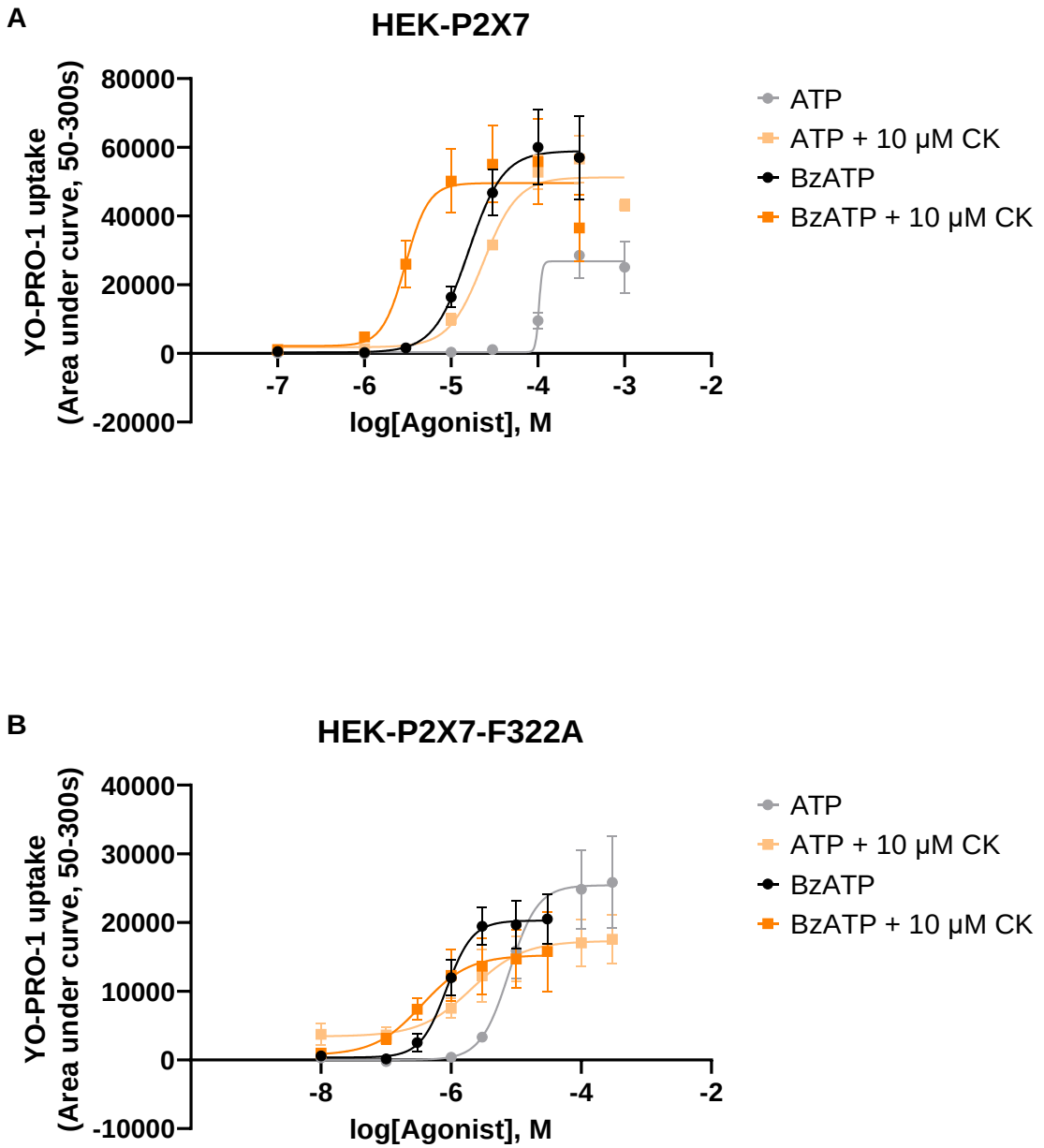

Figure 5.17 – Responses to either ATP or BzATP in the presence and absence of 10 µM CK in HEK-293 cells stably expressing wild-type hP2X7 or mutant F322A hP2X7 measured using the YO-PRO-1 assay. **A:** Concentration response curves showing responses in wild-type HEK-P2X7 cells (n=3). **B:** Concentration response curves showing responses in mutant HEK-P2X7-F322A cells (n=4). Experiments were conducted in low divalent cation buffer (ELDV) containing 2 µM YO-PRO-1 iodide. Graphs are plotted as area under the curve (AUC) values ± SEM and fitted with a four-parameter non-linear regression curve. Average EC_{50} values ± SD are calculated using individual EC_{50} values from the specified number of independent experiments (see **Table 5.9**).

When considering the responses at the F322A mutant, the order of activity is quite different: instead, ATP alone gives the largest maximum response in the YO-PRO-1 assay, although the EC_{50} is the most right shifted. The addition of CK to the ATP concentration response causes a leftward shift, but again decreases the maximum response measured. Interestingly, BzATP has a similar EC_{50} value to ATP + CK but has a slightly increased maximum response. Similar to the wildtype receptor, BzATP + CK gives the most left-shifted response, but again the maximum response is reduced when compared to BzATP alone, with a maximum value like that of ATP + CK. Average EC_{50} values are summarised in **Table 5.9**.

Table 5.9 – Average EC_{50} values for ATP, ATP + 10 µM CK, BzATP, and BzATP + 10 µM CK measured in HEK-293 cells stably expressing wild-type or mutant F322A human P2X7. Responses were measured using the YO-PRO-1 assay. Average EC_{50} values are calculated using individual EC_{50} values from up to four independent experiments. Experiments were conducted in low divalent cation buffer (ELDV) with the addition of 2 µM YO-PRO-1 iodide. *P<0.05, **P<0.01, ****P<0.0001 determined by unpaired, two-tailed t test.

Mutant	Compound	Average EC_{50} (µM ± SD)	pEC_{50}	Difference in pEC_{50} ($-pEC_{50}$ agonist + CK – $-pEC_{50}$ agonist)
Wild-type P2X7	**ATP**	104.17 ± 2.02	-3.983	0.644
	ATP + CK	23.63 ± 5.15 ****	-4.627	
	BzATP	15.75 ± 5.17	-4.803	0.697
	BzATP + CK	3.16 ± 0.50 *	-5.500	
HEK-P2X7-F322A	**ATP**	7.86 ± 0.64	-5.104	0.335
	ATP + CK	3.64 ± 4.08	-5.439	
	BzATP	0.88 ± 0.25	-6.055	0.420
	BzATP + CK	0.34 ± 0.13 **	-6.475	

To see if this effect was specific to dye uptake assays, FURA-2 measurements were performed. ATP responses were not reduced by the addition of CK in HEK-P2X7-F322A cells, but there was not the same degree of increase in the maximum as observed with the wildtype receptor previously (see **Figure 5.14**). Again, both ATP and BzATP were tested in the presence and absence of ginsenoside CK but this time in the FURA-2AM assay (**Figure 5.18**). Similar to the YO-PRO-1 assay, ATP is the most right shifted with the smallest maximum response at the wildtype P2X7 receptor (**Figure 5.18 A**). The addition of CK causes a leftward shift and subsequent decrease in the EC_{50} value but did not increase the maximum response as much as has been previously seen. Interestingly, the response to BzATP was left shifted compared to ATP, but the maximum response with both agonists was similar. Ginsenoside CK was again able to increase the sensitivity of the receptor to BzATP but did not substantially alter the maximum response measured when compared to BzATP alone.

The differences between the responses to ATP and BzATP are not as dramatic in the F322A mutant (**Figure 5.18 B**). Both have a similar EC_{50} value (summarised in **Table 5.10**), with BzATP being slightly more potent at this mutant receptor than ATP. Unlike in the YO-PRO-1 assay, CK is able to increase the maximum response to both ATP and BzATP in the FURA-2AM assay at the HEK-P2X7-F322A mutant. The response to BzATP has a similar maximum to that of ATP + CK, with BzATP + CK giving the highest overall maximum response. The addition of CK to either agonist also increases the sensitivity, however, the degree of this shift is less than that observed at the wildtype receptor. The average EC_{50} values for BzATP + CK are similar at both the wildtype and mutant F322A receptors.

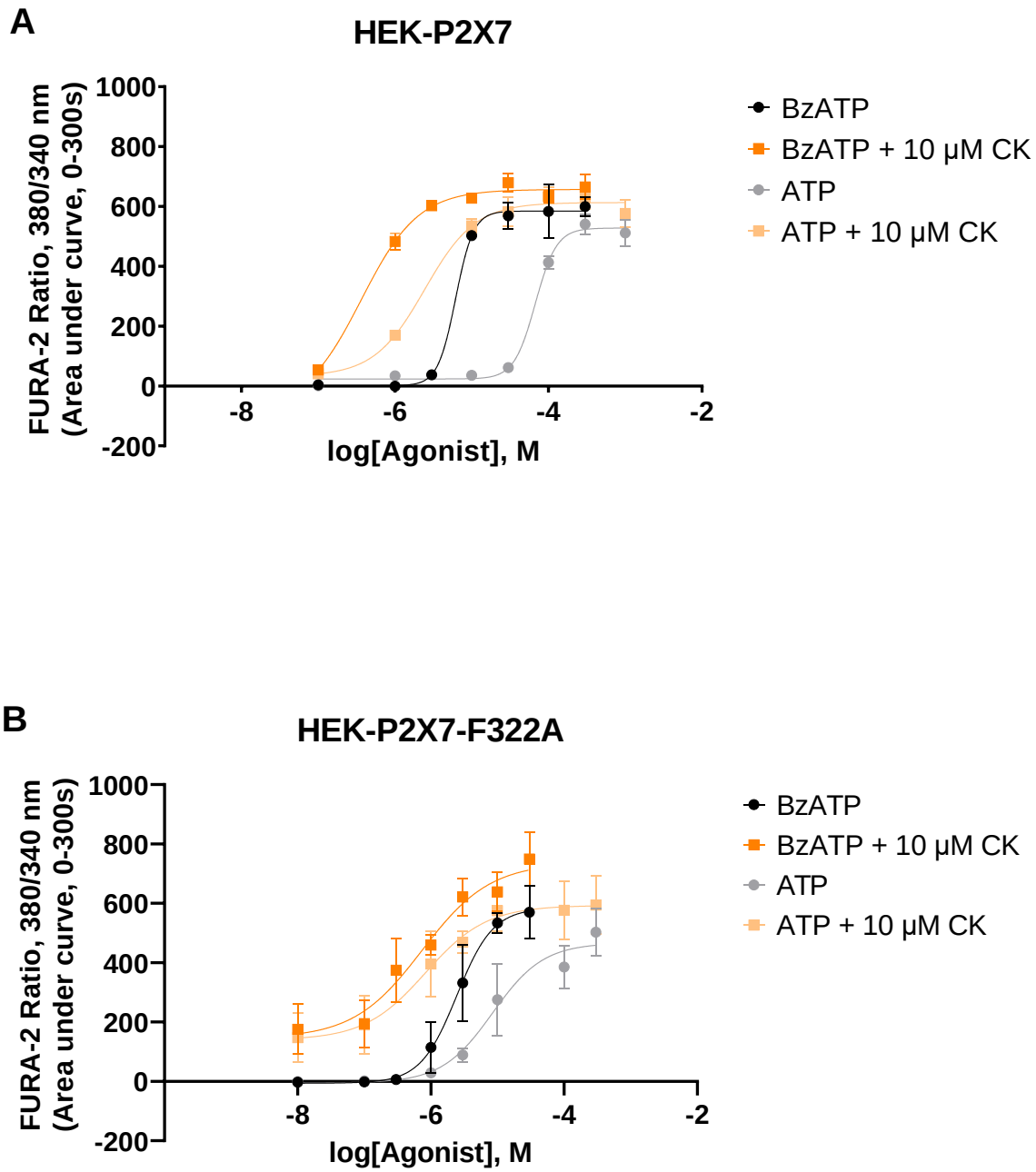

Figure 5.18 – Responses to either ATP or BzATP in the presence and absence of 10 µM CK in HEK-293 cells stably expressing wild-type P2X7 or mutant F322A P2X7. **A:** Concentration response curves showing responses in wild-type HEK-P2X7 cells (n=3). **B:** Concentration response curves showing responses in mutant HEK-P2X7-F322A cells (n=3). Experiments were conducted in low divalent cation buffer (ELDV) containing 250 µM sulfinpyrazone. Graphs are plotted as area under the curve (AUC) values ± SEM and fitted with a four-parameter non-linear regression curve. Average EC_{50} values ± SD are calculated using individual EC_{50} values from three independent experiments (see **Table 5.10**).

Table 5.10 – Average EC_{50} values for ATP, ATP + 10 µM CK, BzATP, and BzATP + 10 µM CK measured in HEK-293 cells expressing wild-type or mutant F322A human P2X7. Responses were measured using the FURA-2AM. Average EC_{50} values are calculated using individual EC_{50} values from three independent experiments. Experiments were conducted in low divalent cation buffer (ELDV) with the addition of 250 µM sulfinpyrazone. *P<0.05, **P<0.01 determined by unpaired, two-tailed t-test.

Mutant	Compound	Average EC_{50} (µM ± SD)	pEC_{50}	Difference in pEC_{50} (-pEC_{50} agonist + CK – -pEC_{50} agonist)
Wild-type P2X7	**ATP**	67.72 ± 15.08	-4.169	1.438
	ATP + CK	2.47 ± 0.91 **	-5.607	
	BzATP	6.17 ± 0.82	-5.210	1.024
	BzATP + CK	0.56 ± 0.13 **	-6.234	
HEK-P2X7-F322A	**ATP**	4.56 ± 0.33	-5.341	0.621
	ATP + CK	1.09 ± 1.60	-5.962	
	BzATP	2.94 ± 2.90	-5.532	0.727
	BzATP + CK	0.55 ± 0.57	-6.259	

5.6 Investigating the F322 Residue using Cysteine Mutagenesis and Methanethiosulfonate Reagents

Next, it was considered that mutating the F322 residue to cysteine would introduce a reactive side chain susceptible to modification by methanethiosulfonate (MTS) reagents. In modifying this mutant with different MTS reagents, the effects on potentiation by CK, and potentially access to the central vestibule region given that this residue lies on the edge of the lateral portals, can be assessed. First, the F322 residue was mutated to cysteine instead of alanine (F322C) and expressed in HEK-293 cells lacking the P2Y2 receptor (HEK20E6) for characterisation. Responses to ATP in the presence and absence of CK were determined using fluorescence assays to assess the similarity of the F322C mutant to the F322A mutant. **Figure 5.19** shows concentration responses to the agonists ATP and BzATP measured using the FURA-2AM calcium assay and the YO-PRO-1 iodide dye uptake assay.

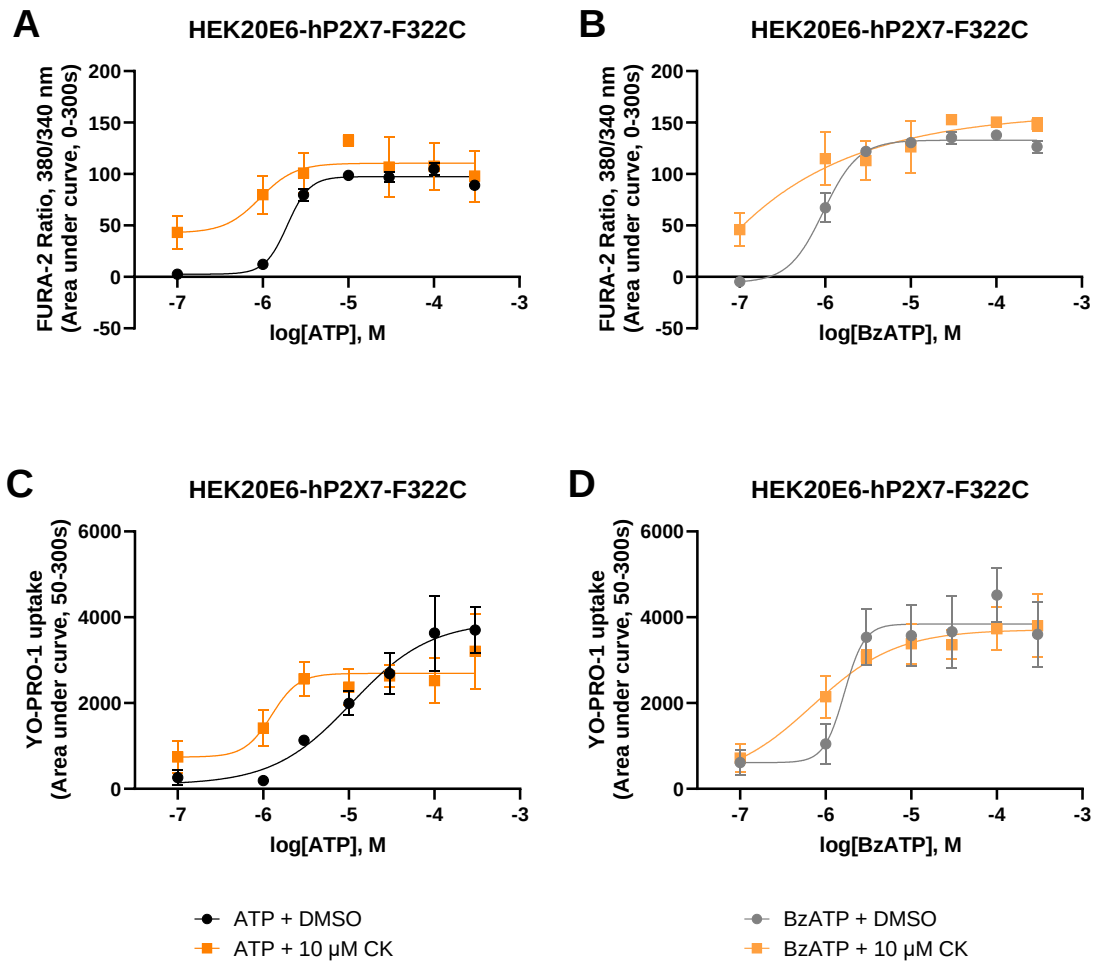

Figure 5.19 – Concentration responses to ATP and BzATP in the presence or absence of 10 µM ginsenoside CK measured in G418-selected HEK20E6 cells expressing the hP2X7-F322C mutant receptor. Responses in panels **A** and **B** were measured using the FURA-2AM assay. Responses in panels **C** and **D** were measured using the YO-PRO-1 assay. **A, C**: Concentration responses to [ATP] between 100 nM and 300 µM in the presence of vehicle (DMSO, black) or 10 µM CK (orange). **B, D**: Concentration responses to [BzATP] between 100 nM and 300 µM in the presence of vehicle (DMSO, grey) or 10 µM CK (pale orange). For **A** and **B**, cells were loaded in low divalent cation buffer (ELDV) containing 2 µM FURA-2AM and 250 µM sulfinpyrazone and experiments were conducted in ELDV in the presence of 250 µM sulfinpyrazone. For **C** and **D,** experiments were conducted in ELDV containing 2 µM YO-PRO-1 iodide. Graphs are plotted as area under the curve (AUC) values ± SEM from three independent experiments and fitted with a four-parameter non-linear regression curve. Average EC_{50} values ± SD are calculated using individual EC_{50} values from the three independent experiments (see **Table 5.11**).

The F322C mutant was more sensitive to ATP than the wild type P2X7 receptor, as was seen earlier with the F322A mutant (see **Figures 5.13** and **5.14**). EC_{50} values for the F322C mutant outlined in **Table 5.11** are comparable to the ones measured for the F322A mutant in **Tables 5.9** and **5.10**, suggesting that the cysteine mutant has similar sensitivity to agonists as the alanine mutant. CK was not able to potentiate the response to ATP at higher concentrations in the YO-PRO-1 assay; instead, responses were reduced at higher concentrations of ATP in the presence of ginsenoside CK compared to ATP alone. In both the FURA-2AM and YO-PRO-1 assays, ginsenoside CK was able to left-shift the concentration response curve to ATP; this effect is less clear with BzATP, as the concentration of agonist did not go low enough to cause the concentration response curves to plateau in the presence of CK.

Table 5.11 – Average EC_{50} values for ATP, ATP + 10 µM CK, BzATP, and BzATP + 10 µM CK measured in G418-selected HEK20E6 cells expressing mutant F322C human P2X7. Responses were measured using either the FURA-2AM assay or YO-PRO-1 assay. Average EC_{50} values are calculated using individual EC_{50} values from up to three independent experiments. For FURA-2AM experiments, cells were loaded in low divalent cation buffer (ELDV) containing 2 µM FURA-2AM and 250 µM sulfinpyrazone and experiments were conducted in low divalent cation buffer (ELDV) in the presence of 250 µM sulfinpyrazone. YO-PRO-1 experiments were conducted in low divalent cation buffer (ELDV) containing 2 µM YO-PRO-1 iodide. *P<0.05 determined by unpaired, two-tailed t test.

Assay	Mutant	Compound	Average EC_{50} (µM ± SD)	pEC_{50}	Difference in pEC_{50} (-pEC_{50} agonist + CK – -pEC_{50} agonist)
FURA-2AM	HEK20E6-hP2X7-F322C	ATP	1.98 ± 0.39	-5.703	0.312
		ATP + CK	0.97 ± 0.47 *	-6.015	
		BzATP	1.01 ± 0.33	-5.996	-1.059
		BzATP + CK	11.56	-4.937	
YO-PRO-1	HEK20E6-hP2X7-F322C	ATP	12.22 ± 0.83	-4.913	1.262
		ATP + CK	0.67	-6.175	
		BzATP	1.79 ± 0.91	-5.747	0.207
		BzATP + CK	1.11 ± 0.12	-5.954	

Given that the F322C mutant responds in a similar fashion to the F322A mutant (i.e., the mutant is more sensitive to ATP than the wild type receptor and CK is unable to increase the maximum response to ATP measured using the YO-PRO-1 assay), it was deemed suitable for continued investigation. Using this cysteine mutant, various methane thiol sulfonate (MTS) reagents were reacted with the residue and the impact on P2X7 receptor function and potentiation by ginsenoside CK was determined. Firstly, responses were measured in HEK20E6-F322C mutant and HEK20E6-hP2X7 wild type cells that had been pre-treated with 3 μM MTS-rhodamine to compare to those that had not been pre-treated (**Figure 5.20**). It was hypothesised that pre-treatment with MTS-rhodamine would allow binding of the MTS reagent to the cysteine mutant, leading to steric blocking of the central vestibule region and possible reduced access of ginsenoside CK to the binding pocket. If ginsenoside CK was unable to reach the proposed binding area in the central vestibule region due to steric hindrance from a bound MTS reagent, then potentiation would be subsequently reduced. The following figures show preliminary data from investigations at this mutant receptor.

Figure 5.20 shows that responses to ATP were reduced in both the wild type and F322C mutant cell lines following exposure to MTS-rhodamine, although EC_{50} values to ATP were similar. Although an EC_{50} value could not be determined for the MTS-rhodamine treated wild type hP2X7 expressing cells, it appears from the graph that the value for ATP is likely to lie between 10 and 100 μM. Pre-treatment with MTS-rhodamine did not appear to substantially affect the potentiation by CK at the F322C mutant, with ginsenoside CK still able to left-shift the response to ATP.

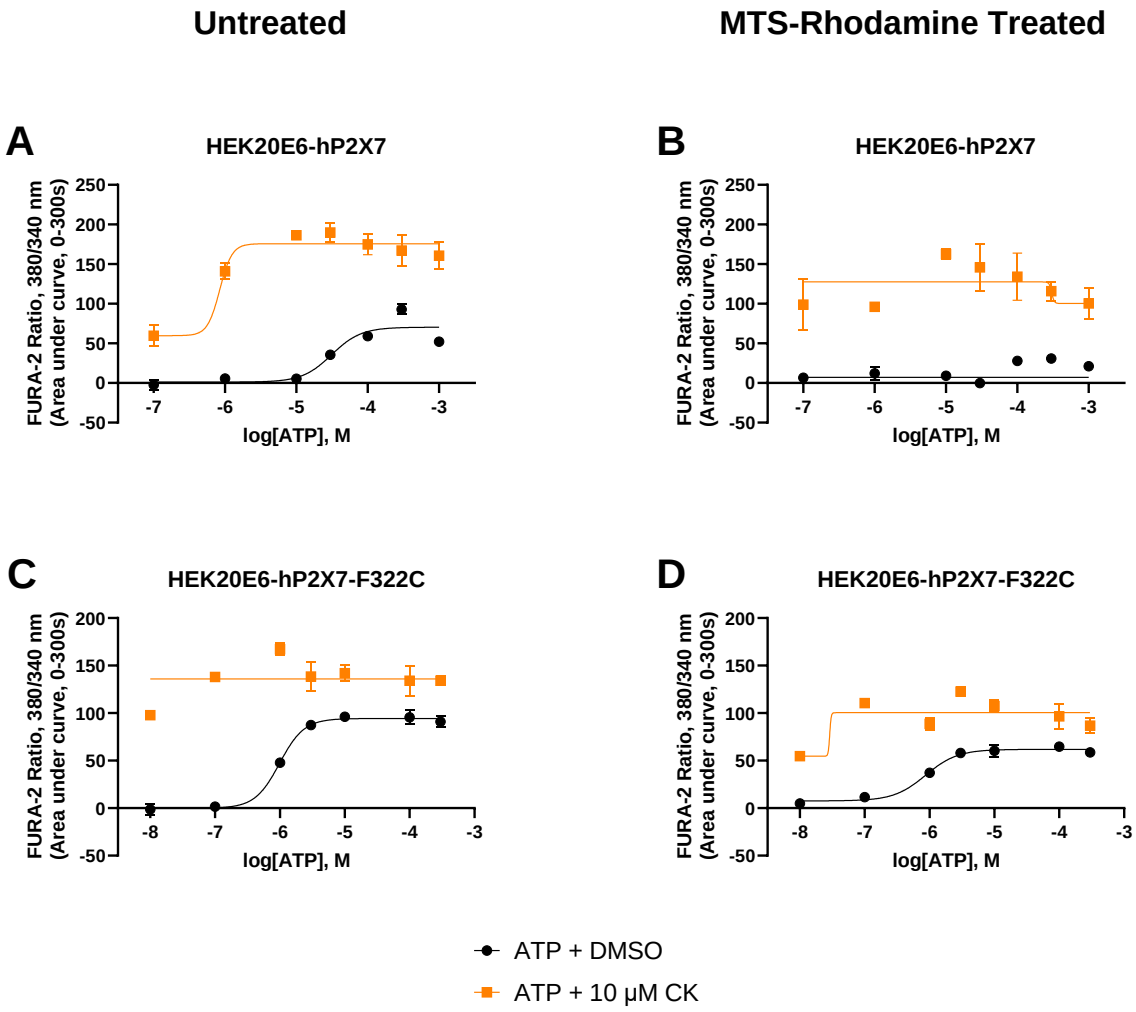

Figure 5.20 – Effects of pre-treatment with 3 µM MTS-rhodamine on intracellular calcium responses to ATP and ATP + 10 µM CK measured in HEK20E6 cells expressing either wild type hP2X7 or F322C mutant hP2X7. **A**: Responses to ATP and ATP + CK in wild type hP2X7 expressing cells (untreated). EC_{50} values: ATP + DMSO 31.3 µM, ATP + CK 845.7 nM. **B**: Responses to ATP and ATP + CK in wild type hP2X7 expressing cells (pre-treated with MTS-rhodamine). EC_{50} values were not determined. **C**: Responses to ATP and ATP + CK in F322C mutant hP2X7 expressing cells (untreated). EC_{50} values: ATP + DMSO 984.9 nM, ATP + CK not determined. **D**: Responses to ATP and ATP + CK in F322C mutant hP2X7 expressing cells (pre-treated with MTS-rhodamine). EC_{50} values: ATP + DMSO 871.1 nM, ATP + CK not determined. The experiment was conducted in low divalent cation buffer (ELDV) containing 250 µM sulfinpyrazone. Graphs are plotted as area under the curve (AUC) values ± SEM and fitted with a four-parameter non-linear regression curve. EC_{50} values are calculated using the individual EC_{50} value from one independent experiment.

A similar experiment was conducted, but this time using a flow cytometer rather than a plate reader. To begin with, labelling of F322C expressing cells with MTS-rhodamine was compared to native HEK20E6 and HEK20E6 cells expressing the wild type hP2X7 receptor (**Figure 5.21**). This was done on closed receptors in the absence of ATP. To do this, $1x10^5$ cells were aliquoted into brown microcentrifuge tubes and 500 µL of low divalent cation buffer (ELDV) containing 3 µM of freshly thawed MTS-rhodamine was added. Cells were incubated at room temperature for 5 minutes before being spun down and resuspended in ELDV to remove excess MTS-rhodamine and fluorescence measured using the flow cytometer. Responses show PE-A fluorescence was enhanced in HEK20E6 cells expressing the F322C mutant compared to those expressing the wild type hP2X7 receptor and native HEK20E6 cells, suggesting increased MTS-rhodamine labelling of these cells.

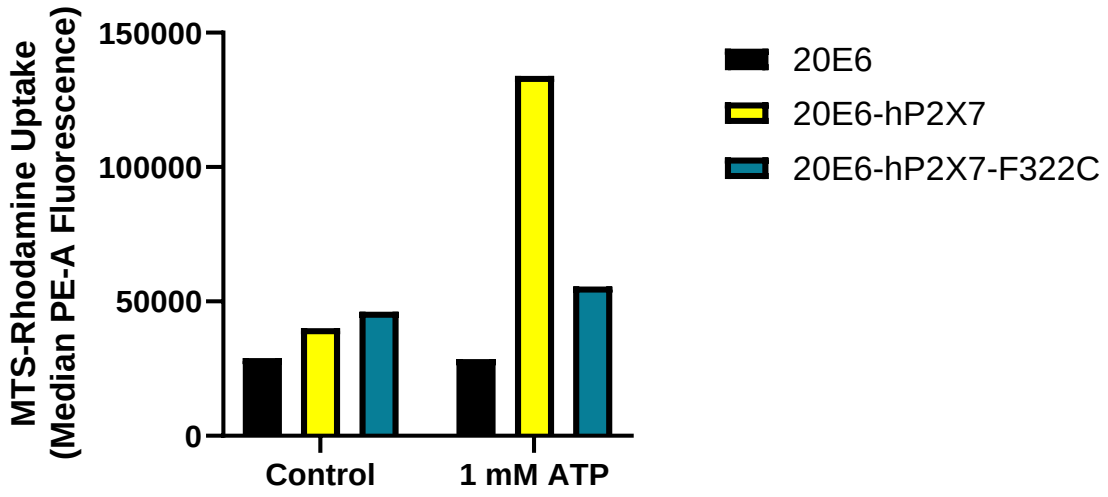

Figure 5.21 – MTS-rhodamine uptake in stable wild type HEK20E6-hP2X7, G418 selected HEK20E6-hP2X7-F322C, and native HEK20E6 cells. Cells were pre-treated for 5 minutes with low divalent cation buffer (ELDV) containing 3 µM MTS-rhodamine alone or 3 µM MTS-rhodamine and 1 mM ATP before being spun down and resuspended in ELDV buffer prior to fluorescence measurements. Graph is plotted as median fluorescence measured using the PE-A channel. Data are the result of one experiment measured using a Beckmann Coulter CytoFLEX machine and analysed using CytExpert software.

The experiment was repeated, but this time in the presence of 1 mM ATP to investigate whether labelling was enhanced with receptors in the open state (**Figure 5.21**). Cells were incubated at room temperature as above, but in ELDV containing 3 µM MTS-rhodamine and 1 mM ATP rather than MTS-rhodamine only, before being spun down and resuspended in ELDV prior to fluorescence measurement. Instead of labelling the F322C mutant, large amounts of fluorescence could be measured in HEK20E6 cells expressing the wild type hP2X7 receptor. This was assumed to be due to

MTS-rhodamine uptake through the P2X7 pore rather than labelling of the receptor itself. Native HEK20E6 cells did not show any increased fluorescence when exposed to 1 mM ATP, whereas both wild type hP2X7 and mutant F322C hP2X7 expressing cells demonstrated increased cell-associated rhodamine fluorescence. Wild type hP2X7 displayed a large increase in fluorescence upon exposure to 1 mM ATP, whereas the F322C mutant only showed a slight increase in fluorescence compared to control.

Labelling with MTS-rhodamine was assessed in native HEK20E6 and HEK20E6-hP2X7-F322C mutant cells by imaging. Cells were exposed to 10 µM MTS-rhodamine for two minutes before being washed twice and resuspended in standard divalent cation extracellular buffer (Etotal) and imaged using a fluorescence microscope (**Figure 5.22**). If MTS-rhodamine was bound to the F322C mutant, it would be expected that concentrated red fluorescence would be seen where this receptor is expressed, i.e., the cell membrane. Little difference can be observed between the native HEK20E6 cells (panels A-C) and those expressing mutant F322C hP2X7 (panels D-E), with some red fluorescence around the edges of each cell type, although cells expressing the F322C mutant receptor in panel E appear to show increased cell surface fluorescence compared to those in the other panels.

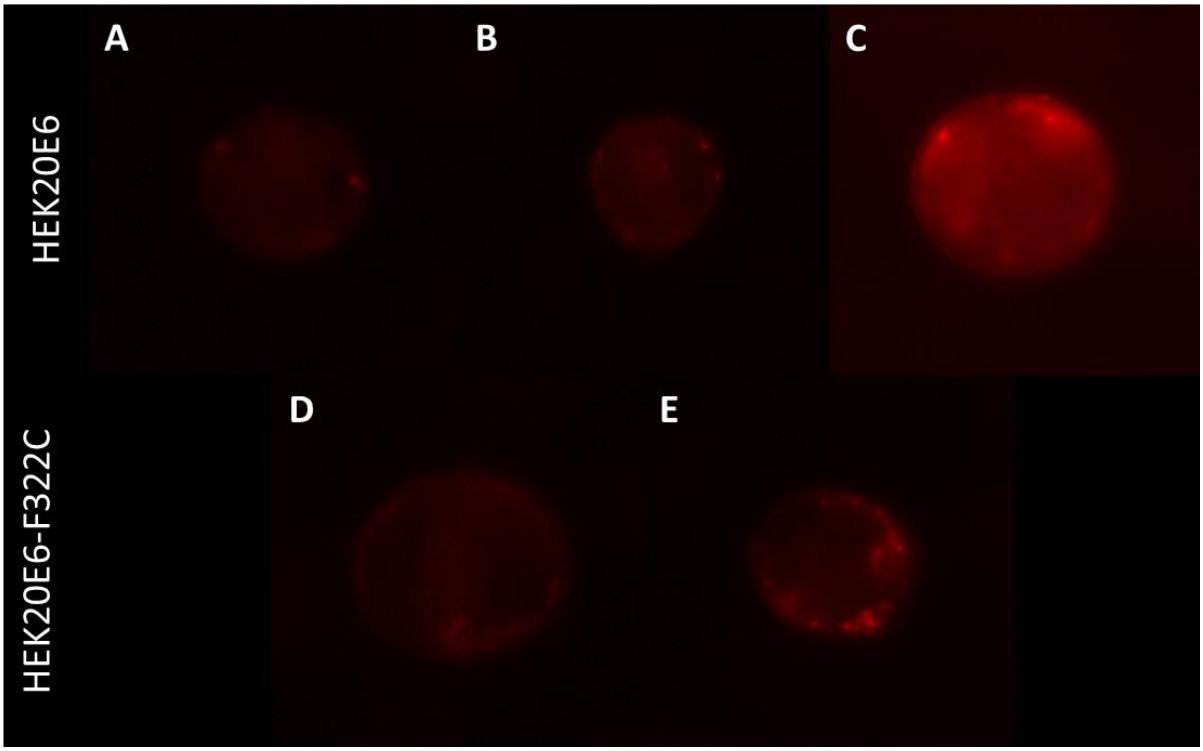

Figure 5.22 – Fluorescence microscopy images of native HEK20E6 cells (A-C) or HEK20E6 cells stably expressing hP2X7-F322C(D-E) exposed to 3 µM MTS-rhodamine for two minutes. Images were obtained following a four second exposure using NIS Elements software.

Next, the effect of labelling the F322C residue with MTSEA-biotin was assessed. MTSEA-biotin is a large, non-fluorescent MTS reagent (unlike MTS-rhodamine, which is fluorescent) and therefore it would not interfere with TO-PRO-3 fluorescence.

Cells were incubated for 5 minutes at 37°C in low divalent cation buffer (ELDV) containing 1 µM TO-PRO-3 and either no MTS reagent or 100 µM MTSEA-biotin. After 5 minutes, buffer controls or ATP +/- 10 µM CK were added, and cells incubated at 37°C for a further 5 minutes. Following this, TO-PRO-3 fluorescence was immediately measured using a flow cytometer (**Figure 5.23**). The MTSEA-biotin concentration was chosen to be close to that used by Roberts *et al* whilst preserving stocks (Roberts et al., 2012), with ATP concentrations chosen as potentiation by CK is seen at the mutant receptor at 1 µM ATP, and only at the wild type receptor at 100 µM ATP (see **Figure 5.19**).

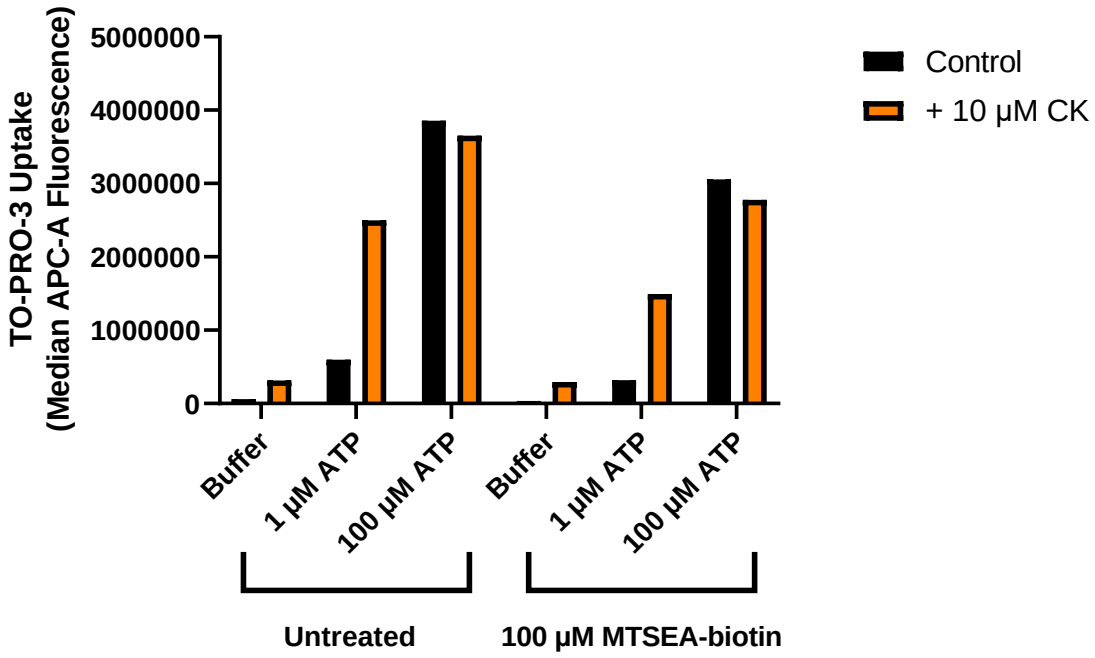

Figure 5.23 – TO-PRO-3 uptake in stably expressing HEK20E6-hP2X7-F322C cells in the presence and absence of 100 µM MTSEA-biotin. Cells were incubated for five minutes in low divalent cation buffer (ELDV) containing 1 µM TO-PRO-3 and either no MTS reagent or 100 µM MTSEA-biotin. Cells were then treated with either ATP alone (black) or ATP with 10 µM ginsenoside CK (orange). Graph is plotted as median fluorescence measured using the APC-A channel. Data are the result of one experiment conducted in low divalent cation buffer (ELDV) and measured using a Beckmann Coulter CytoFLEX machine and analysed using CytExpert software.

Cells that had been treated with MTSEA-biotin had reduced TO-PRO-3 uptake at all concentrations of agonist compared to the control (untreated) cells. HEK20E6-hP2X7-F322C responses to 1 μM ATP were potentiated by ginsenoside CK in both control and MTSEA-biotin treated conditions to a similar extent, with untreated cells being potentiated approximately 4.2-fold and MTSEA-biotin treated cells potentiated by approximately 4.7-fold. At100 μM ATP, TO-PRO-3 uptake was reduced in the presence of ginsenoside CK, with a fold potentiation of 0.95 for untreated cells compared to 0.91 for those exposed to MTSEA-biotin, similar to what has been observed previously (see **Figure 5.16**). This suggests that MTSEA-biotin is unable to alter the activity of ginsenoside CK at the F322C mutant hP2X7 receptor.

5.7 Chapter 5 Discussion

Although previous work has identified key residues in the central vestibule region that impact the activity and potentiation by ginsenosides of human P2X7, full concentration response curves have not been published (Bidula et al., 2019b). Here, the effects of mutating residues D318, L320, and S60 to alanine have been validated in both the FURA-2AM intracellular calcium and YO-PRO-1 dye uptake assays (**Figure 5.3** and **Figure 5.4**). Mutating all three key residues to alanine resulted in receptors that were more sensitive to ATP in the FURA-2AM assay, largely confirming what was seen by Bidula *et al* (except for D318A, which was previously shown to be less sensitive to ATP in YO-PRO-1 studies). At the rat P2X4 receptor, mutating residue D320A has been shown to increase the sensitivity of the receptor to ATP, decreasing the EC_{50} from approximately 3.1 µM to 0.6 µM, whilst decreasing the peak amplitude measured (Yan et al., 2006). At the P2X7 receptor, mutating residues L320 and S60 to cysteine simultaneously almost entirely abolished current induced by BzATP; mutating S60C individually resulted in a receptor with enhanced responses to 300 µM BzATP, whereas L320C had substantially reduced responses (Caseley et al., 2017). Although the effects of mutating these residues on the sensitivity to ATP was not detailed, the results are similar to what was observed for the S60A and L320A mutants by Bidula *et al* in patch clamp studies (Bidula et al., 2019b).

Mutating residue D318 to alanine confirmed a reduction in potentiation by CK in the YO-PRO-1 assay, however, the effect on potentiation by CK in the FURA-2AM assay was less clear. Mutating residues L320 and S60 to alanine both reduced potentiation of the ATP response by CK, validating what had been seen previously (Bidula et al., 2019b). Perhaps unexpected, however, was that dye uptake responses in both the D318A and L320A mutants was poor. Without the full concentration response, it would appear that potentiation by ginsenoside CK has been abolished, however, with testing at multiple concentrations of ATP potentiation by CK can still be observed at the D318A mutant at the 1 mM concentration in the YO-PRO-1 assay, and potentiation can be observed with both the D318A and L320A mutants in the FURA-2AM assay. This data highlights the importance of conducting full concentration responses in multiple assays, particularly at least one based on ion influx and one on dye uptake, in order to fully understand the effects of mutations to the hP2X7 receptor.

Mutating residue F322 to alanine also increased the sensitivity of the receptor to agonists in all three assays used: membrane potential blue, FURA-2AM, and YO-PRO-1 (**Figure 5.14**). This residue is conserved at the rat P2X7 receptor and mutating this residue in the rat P2X7 (rP2X7) receptor yielded similar results. Sensitivity to BzATP was increased by mutating F322A in rP2X7, reducing the EC_{50} for stabilised patch-clamp electrophysiology responses from approximately 20.9 µM to 2.4 µM, with the F322L mutant displaying similar results (Rupert et al., 2020). Interestingly, mutating residue F322 to

either tryptophan or tyrosine, aromatic groups larger than the native phenylalanine, resulted in receptors with comparable EC_{50} values to the wild type receptor (F322W 16.5 μM, F322Y 26 μM) (Rupert et al., 2020). In this chapter, it can be seen that mutating the F322 residue to cysteine also increases the sensitivity of the receptor to ATP similar to what was observed for the F322A and F322L in the rat receptor, suggesting key differences in receptor activity depending on whether an aromatic group is present at this position or not. Rupert *et al* suggested that it was the size and degree of hydrophobicity of the residue present at position 322 that was important, rather than the aromaticity (Rupert et al., 2020). The smaller alanine and leucine mutants increased the sensitivity of the receptor to ATP whereas the larger tyrosine and tryptophan substitutions maintained sensitivity similar to that of the wild type receptor, despite the tryptophan introducing a polar residue when all other substitutions were non-polar (Rupert et al., 2020). Interestingly, mutating F322 to either alanine, leucine, tryptophan, or tyrosine in the rat P2X7 receptor enhanced ethidium bromide uptake in response to BzATP compared to the wild type receptor (Rupert et al., 2020). A similar effect was seen here with ATP, although this phenomenon was not consistent between dye uptake assays used, with the maximum dye uptake response often being lower in the F322A mutant compared to the wild type receptor (**Figure 5.15**).

The reason for this increase in sensitivity to the F322A mutant is unknown; in Figure 5.1, it can be seen that residue Y257, a large aromatic residue, lies very close to residue F322, although on a neighbouring β-strand. Due to their close proximity, it is possible that these two residues could be interacting: the study by Rupert *et al* would agree with this hypothesis; they suggested that there could be interactions between F322 and Y257 (Rupert et al., 2020), although the interaction between subunits of F322 with I58 in the rat P2X7 receptor was suggested to be of greater importance as this interaction is disrupted when considering homology models of closed and open state receptors (Rupert et al., 2020). If the increase in sensitivity of the F322A mutant was due to disruptions in π-π aromatic interactions between F322 and Y257, making it easier for ATP to induce the conformational change necessary to facilitate opening of the receptor, mutating the Y257 residue to alanine should have a similar effect. However, this was not the case: mutating residue Y257 to alanine resulted in a receptor that was less sensitive to ATP than the wild type, although potentiation by CK was still possible (**Figure 5.10**), suggesting that this interaction is not the reason for the increase in sensitivity of the F322A mutant. Although ginsenoside CK was able to potentiate responses to ATP at the F322A mutant, it did not appear able to increase maximum responses like what has been observed for the wild type receptor (**Figure 5.10**). Interestingly, double mutant receptors consisting of the F322A mutation and one other (either Y257A or E255A) also did not display increases in the maximum FURA-2AM response to higher concentrations of ATP with ginsenoside CK, whereas the individual Y257A and E255A mutations did,

suggesting that it is the F322 residue that is key for increases in response to higher concentrations of ATP. The binding of ginsenoside CK to wild type P2X7 appears to result in residue F322 moving from its normal position in the pocket (see **Figure 5.7**) – this could in theory mimic the effects of mutating residue F322 to alanine, as it would move the residue further from I58 on the neighbouring subunit, disrupting the interactions between subunits and making it easier for the receptor to open. This effect is summarised in **Figure 5.24**, where the distance between residues F322 and I58 is increased to 10.9 Å in the open state CK-bound human P2X7 homology model used in **Figure 5.24**, compared to 6.93 Å for the open state rat P2X7 homology model used by Rupert *et al* (Rupert et al., 2020).

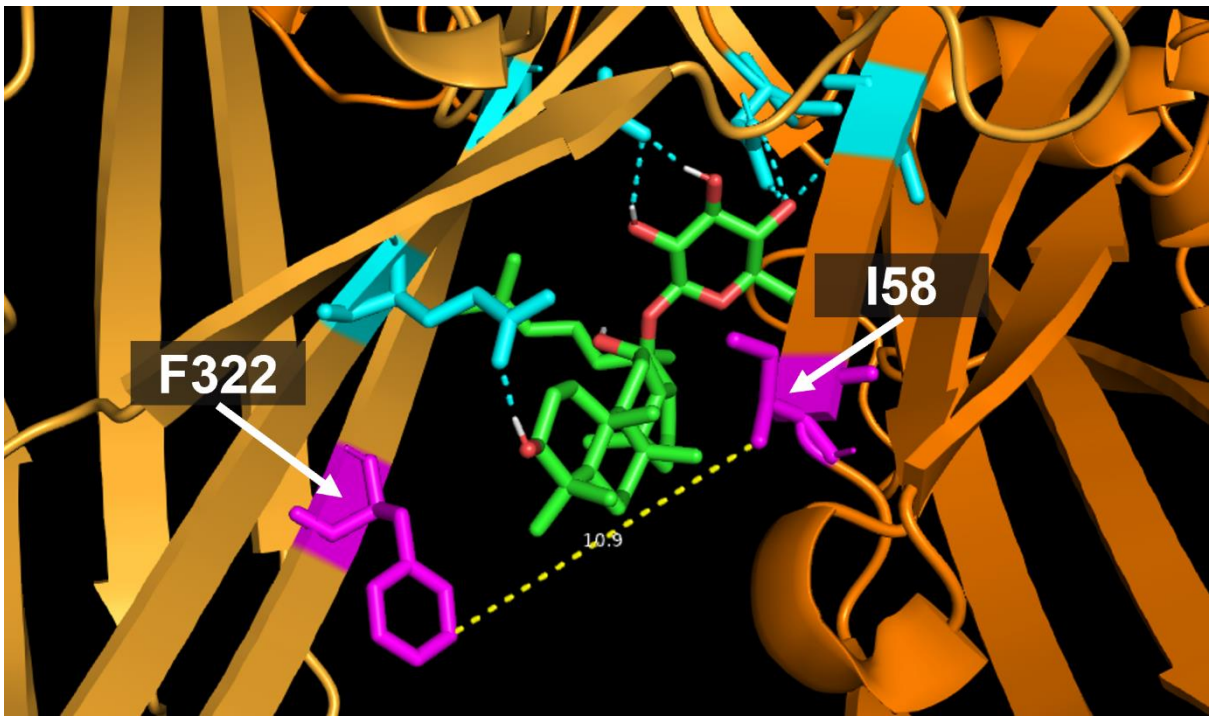

Figure 5.24 – Homology model of human P2X7 showing ginsenoside CK docked to the central vestibule region. Ginsenoside CK, shown in green, is docked to the central vestibule region of human P2X7 (orange), with residues that make polar contacts highlighted in cyan. Residues F322 and I58 are highlighted in magenta with the approximate distance between them highlighted by the yellow dashed line (10.9 Å). Homology models are based on the crystal structure of zebrafish-P2X4 (PDB: 4DW1) with the human P2X7 sequence overlayed. Docking was performed by Dr Sam Walpole, UEA, using Glide (Schrödinger).

The F322 residue lies in close proximity to both D318 and L320, both of which result in a receptor with increased sensitivity to ATP when mutated to alanine. Given this information, it suggests that this region of the P2X7 receptor is key to receptor sensitivity; indeed, these residues lie on the β sheet that connects the ATP binding site with the pore forming transmembrane domains, and so are likely to be important in the conformational changes that occur upon ATP binding that allow the receptor to transition to the open state. It would be interesting to see if mutating I58 to alanine produced a

receptor more sensitive to ATP (like F322A) in the human P2X7 receptor (as this residue is again conserved between species) to assess this possible interaction further. Given that S60 lies in close proximity to I58, and mutating the S60 residue to alanine has been shown to increase the sensitivity of the hP2X7 receptor to ATP both here and in the literature (Bidula et al., 2019b), it could be that mutations along this side of the lateral portal have a similar effect in increasing the sensitivity of the receptor to ATP as has been seen with mutations to the D318, L320, and F322 residues.

Originally, the F322 residue was mutated as it was believed it could be interfering with the hydroxyl group of ginsenoside F1. Based on computational docking studies, residue F322 appears to move position when ginsenoside CK is docked to the central vestibule region (**Figure 5.7**). It is important to bear in mind that induced-fit docking allows for movement of the side chains to better fit docked ligands, and so this effect may be due to that rather than the CK itself causing the movement. Nonetheless, C6 lies close to this residue according to molecular models, and so it could be that the addition of a polar hydroxyl group here clashes with the hydrophobic phenylalanine at position 322. Mutation of this residue to alanine did not impart activity to ginsenoside F1, although ginsenoside CK was able to potentiate responses to ATP at this mutant (**Figure 5.8**). Therefore, it is unlikely that the inactivity of ginsenoside F1 is due to the phenylalanine residue at position 322.

Whilst investigating the effects of ginsenosides CK and F1 at the F322A mutant, it was noted that potentiation by ginsenoside CK in dye uptake assays did not reflect what was seen in assays that measured ion flow (**Figure 5.14**). Responses to ATP did not increase as dramatically in the presence of ginsenoside CK at the F322A mutant compared to the wild type receptor in the FURA-2AM assay; this phenomenon had been observed previously, with mutants containing the F322A mutation not displaying an increase in response (see **Figure 5.10**). Unexpectedly, F322A responses to higher concentrations of ATP (≥ 100 μM) in the YO-PRO-1 assay decreased in the presence of ginsenoside CK, whereas responses at lower concentrations (≤ 20 μM) were potentiated. This effect was confirmed in other dye uptake assays (**Figure 5.15**), although the reduction in response was only significant in the YO-PRO-1 assay. To confirm if this reduction was due to the type of assay (i.e., a plate reader-based assay), the effects of ginsenoside CK at the F322A mutant were also tested using a flow cytometer. Here, it was also confirmed that TO-PRO-3 uptake in response to ATP was reduced in the F322A mutant in the presence of ginsenoside CK, whereas responses to ATP in the wild type receptor were potentiated by CK (**Figure 5.16**). Although this experiment was only performed once, the fact that this effect can be seen in multiple dye uptake assays across different pieces of equipment suggests that this is a genuine effect that needs to be explored further. It is difficult to explain why this effect occurs; the F322A mutant is still capable of dye uptake, unlike the D318A and L320A mutants, producing dose-

dependent ATP responses in multiple dye uptake assays, and ginsenoside CK is still able to potentiate the response to ATP, causing a leftward shift to the concentration response curve and a decrease in the EC_{50}. This suggests that ginsenoside CK is still binding, and therefore still able to exert its effects, although perhaps in a different orientation or conformation, meaning it is unable to make the required change to the protein to increase the rate of dye uptake that is seen at the wild type receptor. The study by Rupert *et al* demonstrates increased ethidium bromide uptake in the F322A mutant rat P2X7 receptor, which is also demonstrated here, but the effects of this mutation on potentiation of the receptor have never been explored until now.

In contrast to the F322A mutant, mutating residue D197 to alanine results in a receptor that is less sensitive to ATP (**Figure 5.13**). The effects of this mutation on potentiation by ginsenoside CK are opposite to that observed with the F322A mutant: whereas F322A abolishes the increase in the maximum response to ATP in the presence of CK, mutating D197A results in an increase in the maximum response greater than what is observed at the wild type. The reduction in the EC_{50} with ginsenoside CK remains comparable to that observed at the wild type hP2X7 receptor. Similar to what was observed here with ATP, the D197A mutant in rat P2X7 was less sensitive to the agonist BzATP, with an EC_{50} of 91.4 μM compared to 18.4 μM for the wild type receptor (Liu et al., 2009). This residue has been shown to be key to a number of functions of the rat P2X7 receptor, with involvement in pH sensitivity and modulation by copper and zinc (Liu et al., 2008, Liu et al., 2009). P2X7 receptors are known to be strongly inhibited by acidic pH; mutating the D197 residue to alanine at the rat receptor almost completely abolished this inhibition, with the receptor now 9-fold less sensitive to inhibition in patch-clamp assays than the wild type (Liu et al., 2009). Similarly, mutating the analogous H197 residue to alanine in the mouse P2X7 receptor reversed inhibition by pH 6.5, resulting in peak currents larger than those observed for the wild type receptor at pH 8 (Liu et al., 2009). Dye uptake assays confirmed the findings in patch-clamp assays, with the D197A mutant displaying increased ethidium bromide dye uptake compared to the wild type in acidic conditions (Liu et al., 2009).

Likewise, this residue has also been shown to be important to modulation by copper and zinc. The rat P2X7 receptor is inhibited by both copper and zinc, although the mouse P2X7 receptor has been shown to be potentiated by zinc at concentrations of 300 μM(Moore and MacKenzie, 2008). Copper consistently inhibits rat, mouse, and human P2X7 receptors, with the human receptor also inhibited by zinc (Fujiwara et al., 2017). Studies investigating the role of the D197 receptor on modulation by copper and zinc showed a reduction in the inhibition by 30 μM zinc on currents evoked by 30 μM BzATP or 1 mM ATP, although currents were still reduced to some extent (Liu et al., 2008). Combining the D197A mutant with the H62A mutant resulted in a near complete abolition of inhibition by zinc of

either agonist response (Liu et al., 2008). Mutating residue S60 to alanine, which lies close to residue D197, reduces potentiation by ginsenoside CK. Mutating residues opposite D197, namely D318 and L320, also reduces potentiation (**see Figure 5.25**). This information, in combination with the knowledge that the D197 mutant plays a key role in regulation of the receptor by external pH and metal ions, highlights the importance of this region in modulation of the receptor. The fact that mutating D197 to alanine results in a receptor that displays almost complete opposite characteristics to the F322A mutant on the opposing subunit is intriguing; it would be interesting to explore this mutant further, perhaps alongside the I58 residue that is proposed to interact with residue F322.

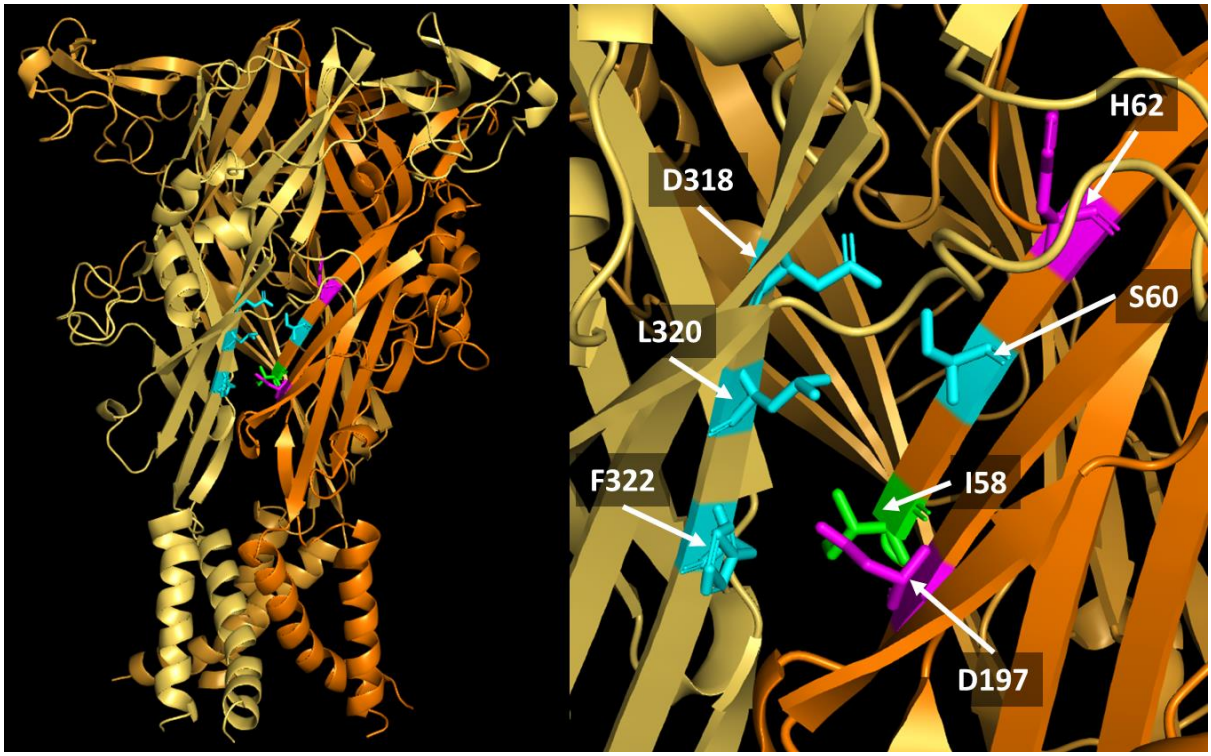

Figure 5.25 – Diagram showing key residues involved in sensitivity of the receptor to ATP or modulation by ginsenoside CK, acidic pH, or metal ions. **Left:** homology model of closed hP2X7 showing key residues highlighted in either cyan, magenta, or green, showing proximity to the lateral portals. **Right:** labelling of key residues found to alter sensitivity of the receptor to agonists and modulation when mutated. Mutations to residues D318, L320, and S60 (cyan) have all been shown to reduce potentiation by ginsenoside CK, whereas mutating residue F322 (cyan) reduces potentiation in the YO-PRO-1 assay only. Residues D197 and H62 (magenta) have been shown to be important to modulation of the receptor by zinc, copper, and protons, whereas residue I58 (green) has been proposed to form intersubunit interactions with F322. Homology models are based on the crystal structure of zebrafish-P2X4 (PDB: 4DW1) with the human P2X7 sequence overlayed. Homology models were produced by Dr Sam Walpole, UEA.

Ginsenoside CK is proposed to bind to the central vestibule region of hP2X7, likely entering through the lateral portals to access its binding site (Bidula et al., 2019b). Given that residue F322 lies directly

at the top of the lateral portal, modifying this residue could affect access to the central vestibule region and therefore potentiation by ginsenoside CK. Cysteine mutagenesis of the F322 residue resulted in a receptor that displayed similar properties to the F322A mutant (**Figure 5.19**). An attempt to label this residue with MTS-reagents using flow cytometry did not yield clear results; labelling by MTS-rhodamine of the closed receptor appears to be increased slightly in the F322C mutant compared to the wild type receptor, although increases in fluorescence upon treatment with ATP resulted in uptake rather than labelling at both the wild type and mutant receptors (**Figure 5.21**). Fluorescence was reduced in the F322C mutant compared to the wild type receptor; it is not clear why, but this could be due to labelling of the F322C residue by MTS-rhodamine, leading to blockage of the lateral portal and a reduction in uptake via the transmembrane pore. TO-PRO-3 uptake at all concentrations of ATP tested was also reduced following incubation of F322C expressing cells with 100 µM MTSEA-biotin (**Figure 5.23**). Cysteine mutants of residues close to F322 have been shown to be accessible to methanethiosulfonate reagents, particularly D58C in P2X4 (Samways et al., 2011) (which lies opposite F322 in this receptor) and I328C in P2X2 (Rassendren et al., 1997a, Egan et al., 1998). Although F322 is not conserved at the P2X2 receptor (it is instead a histidine), I328 is analogous to L320 in P2X7, which neighbours the F322 residue. A reduction in currents following application of 1 mM MTSEA-biotin was seen at both the D58C P2X4 and I328C P2X2 receptors, suggesting that both of these residues are accessible. Given their close proximity to where F322 lies, it is likely that the F322 residue would be capable of being labelled too. Indeed, the analogous F326C mutant in the P2X1 receptor has been shown to be labelled by MTSEA-biotin, with an increase in labelling following application of ATP (Roberts and Evans, 2007). This effect would need to be investigated further to confirm if labelling had occurred at the F322C hP2X7 receptor, as imaging did not provide clear evidence (**Figure 5.22**). Nonetheless, ginsenoside CK displayed similar effects in both MTSEA-biotin treated and untreated cells (**Figure 5.23**), and so if any binding of MTSEA-biotin to the F322C residue had occurred, it was insufficient to prevent ginsenoside CK from accessing its binding pocket. It would be good to repeat this experiment using a higher concentration of MTSEA-biotin (1 mM), as this concentration has been shown to label cysteine mutants of the P2X7 receptor in patch-clamp electrophysiology studies (Browne et al., 2013). In addition, it would be useful to experiment with larger modifications – it may be possible to react streptavidin with the MTSEA-biotin group following labelling, which would give a much larger group that may further reduce access to the lateral portals. There are also larger biotin-labelled MTS-reagents that could be used, such as MTSEA-biotin-X and MTSEA-biotin-XX.

Chapter 6 – Overall Discussion

6.1 Summary

To summarise, this thesis shows that the FLIPR Membrane Potential Blue assay is a useful tool for measuring the pharmacology of ion channels with a range of desensitisation kinetics, from the non-desensitising P2X7 receptor to the quickly desensitising P2X1 and P2X3 receptors. In addition, the FLIPR Membrane Potential Blue assay allows for rapid screening of modulators of ion channels, although the quencher dyes present in the kit may interfere with the efficacy of some modulators. Overall, this assay provides an effective and efficient method of screening compounds of interest to take forward for further investigation in other assays.

In addition, this thesis also demonstrates that the ginsenosides have activity at all P2X receptors investigated, although with a different rank order of potency at each. Ginsenoside CK in particular appears to have activity at all receptors studied in this thesis with the exception of P2X3, with the greatest activity at the P2X4 and P2X7 receptors.

Mutations to the central vestibule region affect the sensitivity of the receptor to ATP, with mutations to D318 and L320 in hP2X7 demonstrating reduced dye uptake compared to the wild type receptor. Mutating one particular aspartic acid, (hP2X2a: D326, hP2X4: D320, hP2X7: D318) reduces potentiation by ginsenoside CK in all three P2X receptors tested. Mutations to residue D197 in hP2X7 reduce the sensitivity of the receptor to ATP and enhance potentiation by ginsenoside CK in both the FURA-2AM and YO-PRO-1 assays, which would be particularly interesting to investigate further. Finally, residue F322 in hP2X7 plays a key role in pore formation and subsequent dye uptake. Modulation by ginsenoside CK is abolished at high concentrations of ATP in hP2X7 receptors with a mutated F322 residue. In summary, the data presented in this thesis suggest a key role for residues of the central vestibule region in receptor gating and activity.

6.2 Chapter 6 Discussion

The properties of each of the P2X receptors differs greatly between subtypes: the P2X7 receptor requires considerably higher concentrations of ATP to activate compared to the other P2X receptors (hundred micromolar range) , but has the largely unique characteristic of being able to form a large, non-specific pore capable of allowing passage of membrane-impermeant dyes, such as NMDG; something only reported to be shared by the P2X4 and P2X2 receptors (Kaczmarek-Hájek et al., 2012). The P2X7 receptor does not appear to desensitise - following the recent cryo-EM structure of the full

rat P2X7 receptor in the open and closed states, this lack of desensitisation is thought to be due to large cysteine rich 'anchors' below the cell membrane, supported by the large c-terminus that acts as a cytoplasmic ballast (McCarthy et al., 2019). The P2X4 and P2X2 receptors are both slowly desensitising, whereas the P2X1 and P2X3 receptors are both rapidly desensitising, making their activity difficult to measure (Kaczmarek-Hájek et al., 2012). Patch-clamp electrophysiology is largely regarded as the gold standard technique for measuring ion channel activity (Di Virgilio et al., 2019), but this technique is difficult to master and time consuming when screening large volumes of compounds.

The FLIPR Membrane Potential Blue assay, a plate reader-based fluorescence assay that measures the movement of ions across the cell membrane, offers a unique method of measuring ion channel activity with multiple conditions in an efficient and accessible way. Here, this assay has been used to reliably measure responses to ATP for all P2X receptors studied, from the rapidly desensitising P2X1 and P2X3 receptors all the way through to the non-desensitising P2X7 receptor. Pharmacology of the human P2X2a receptor has been explored in more detail; although this receptor was first cloned in the 1990s (Brake et al., 1994), with a benchmark study into the pharmacology of both the human P2X2a and P2X2b splice variants in 1999 (Lynch et al., 1999) , there are still no specific antagonists of the human P2X2 receptor. In this thesis, known non-specific antagonists of P2X receptors (PPADS and suramin) were explored in the membrane potential blue and FURA-2AM assays, as was the anthraquinone dye Reactive Blue 4 (Rb4), which has been suggested to inhibit rat P2X2 (Baqi et al., 2011) but its effects on the human receptor were unknown. Here, it was discovered that Rb4 potentiates ATP-induced responses at the hP2X2a receptor. Whilst this effect has not been explored further in this thesis, it may provide a unique starting point for hP2X2 potentiators in the future. This highlights the importance of testing multiple species when developing novel modulators of P2X receptors, especially considering rodent models are often used in research before human studies.

In general, antagonists tested using the membrane potential blue assay tend to yield larger IC_{50} values than reported in the literature. As the membrane potential assays are known to include a coloured quencher dye to reduce background fluorescence, and dyes are known to modulate P2X receptors (Jiang et al., 2000, Baqi et al., 2011), it could be that these quencher dyes are interfering pharmacologically with the activity of the antagonists.

Despite the apparent reduction in sensitivity to antagonists, measurement of positive allosteric modulation of P2X receptors using the membrane potential blue assay remains possible: ginsenosides shown to modulate the P2X7 receptor, namely ginsenosides CK, 20-*S*-Rg3, and F2, have also been shown to increase response to ATP in the membrane potential blue assay. The same can be said for

the P2X4 receptor, where multiple ginsenosides have been shown to potentiate responses to ATP in the membrane potential blue assay, although ginsenoside Rd appears to potentiate to a lesser extent in this assay than has been observed previously (Dhuna et al., 2019). One of the main aims of this thesis was to determine whether the ginsenosides had activity at the other P2X receptors that had not yet been investigated: ginsenosides appeared able to potentiate the responses to 10 μM ATP at the human P2X2a receptor, with ginsenoside CK showing the largest increase, although results were not always statistically significant. Minor potentiation was also able to be measured at the rapidly desensitising receptors P2X1 and P2X3 receptors, but again this was not statistically significant, suggesting that positive allosteric modulation by the ginsenosides is not conserved between all P2X receptors. It is important to note that the rank order of potentiation was also different for each receptor subtype tested: this could suggest differences in the binding pocket, allowing for development of novel potentiators that are selective for one receptor subtype over another. In particular, ginsenoside CK appears to somewhat enhance responses all receptor subtypes tested with the exception of P2X3, which would be interesting to investigate further.

In addition to the ginsenosides, several structurally similar compounds such as the natural product glycosides and steroids, have been reported to potentiate P2X receptors (Piyasirananda et al., 2021, Cario-Toumaniantz et al., 1998, De Roo et al., 2010). Progesterone has been reported as one of the few positive allosteric modulators of the rat P2X2 receptor, although its activity at the human receptor was unknown: here, progesterone can be seen to increase responses to 20 μM ATP in HEK-hP2X2a cells, although some increases in ATP-induced responses were also seen in native HEK-293 cells. It would be interesting to perform full concentration response investigations into the potentiatory effects of this steroid at the human receptor. A specific P2X2 antagonist would be useful in such investigations, as it would be beneficial to observe whether the potentiation could be blocked by such an antagonist and therefore determine if the potentiation is P2X2-receptor specific. Interestingly, this thesis shows that steroids such as 17β-estradiol and testosterone can inhibit P2X7 receptor responses, suggesting that it may be possible for modulation of the receptor by endogenous steroids to occur *in vivo*.

Although potentiation by the ginsenosides has now been confirmed at multiple P2X receptors, it is unclear whether this is due to interaction with a similar binding site as described for the hP2X7 receptor (Bidula et al., 2019b). Comparison of the amino acid sequences in the central vestibule region confirm that there is some conservation between the receptor subtypes, particularly with the DXXV motif between residues 318-321 (hP2X7 numbering). Key differences exist though, with variation in residues towards the top of the central vestibule region (residues 96-101, hP2X7 numbering). The hP2X2 receptor varies the most from the hP2X7 and hP2X4 receptors; it still contains the DXXV motif,

however, the other regions thought to be involved in ginsenoside CK binding at the human P2X7 receptor differ greatly at the hP2X2a receptor, which may go some way in explaining why effects at the hP2X2a receptor are limited.

Potentiation by ginsenoside CK, along with several other ginsenosides, had been observed at the hP2X2a receptor using the membrane potential blue assay and a fixed concentration of ATP in Chapter 3, however, potentiation was minor and the effects on the full concentration response curve were not fully understood. In Chapter 4, a slight shift in the EC_{50} value can be observed using the membrane potential blue assay, with some statistical significance, although the degree of shift is smaller than has been observed at the hP2X4 and hP2X7 receptors using different assays (Dhuna et al., 2019, Helliwell et al., 2015). Interestingly, the degree of shift with known potentiators of the rat P2X2 receptor is also small: for example, testosterone butyrate was able to shift the EC_{50} value to ATP at the rat P2X2 receptor to a similar extent as what was seen for ginsenoside CK at the human P2X2 receptor (Sivcev et al., 2019), and previous studies on progesterone at the rat P2X2 receptor also show a small decrease in the EC_{50} value (De Roo et al., 2010). It could be that this receptor is only able to display a small degree of potentiation compared to the other P2X receptors, as the shift observed with ginsenosides CK and Rb1 is comparable to that seen with other potentiators.

Using the membrane potential blue assay, the D326A mutant in hP2X2a gave similar outcomes to the analogous mutation in hP2X7, D318A (Bidula et al., 2019b): although the receptor was more sensitive to ATP (more like the D318L mutant in hP2X7), potentiation by CK was reduced, comparable to what had been observed at hP2X7. In addition, the S77A mutant (analogous to the S60A mutation in hP2X7) increased sensitivity to ATP and reduced potentiation by ginsenoside CK: both the same as what had been seen for the analogous mutation at hP2X7 (Bidula et al., 2019b). Finally, the I328A mutation, analogous to the L320A mutant in hP2X7, reduced potentiation by CK in a similar fashion (Bidula et al., 2019b). All this suggests that there may be some overlap in the binding pocket, given that potentiation was reduced by the same mutations in both hP2X2a and hP2X7. Interestingly, mutating S76 to alanine resulted in a receptor that was better potentiated by ginsenoside CK. This mutation in hP2X7 (S59A) did not result in the same effect, instead resulting in a P2X7 receptor that had a lower fold potentiation by CK in both YO-PRO-1 and calcium responses compared to the wild-type receptor (Bidula et al., 2019b). This again highlights a key difference between the two receptor subtypes; something that could be exploited further to develop specific modulators. Further investigations would be needed, however, as results were not always corroborated in the FURA-2AM assay. Repeats of these experiments using the same buffer in both the membrane potential and FURA-2AM assays would minimise changes to conditions.

Mutating the D320 residue to leucine in the hP2X4 receptor also appeared to minimise potentiation by ginsenoside CK, akin to what was seen for D326A in hP2X2a and D318A/D318L in hP2X7 (Bidula et al., 2019b). Given that this residue is one of the only key residues in the binding pocket conserved between all three receptors investigated in Chapter 4, it is interesting that the effects of mutating this residue are also conserved between the receptor subtypes. It would be especially useful to have full concentration responses for ginsenoside CK in particular at key mutants of hP2X7 to allow direct comparison between them, as published data for the activity of ginsenoside on mutants of hP2X7 focuses on single concentrations of ATP. Given that these mutants change the sensitivity of the receptor to ATP, it is unwise to test the effects of potentiation on only one concentration; this may be approximately EC_{50} for the wild type, but maximal at a mutant receptor, and therefore shifts in the concentration response curve would not be readily apparent.

With both the hP2X4 and hP2X2a receptors providing inconclusive results, investigations moved onto the hP2X7 receptor and further investigation of the central vestibule region. As mentioned previously, activity of ginsenoside CK at mutants of hP2X7 had been largely determined using a smaller range of concentrations of ATP. This did not fully demonstrate the effects mutating the receptor had on activity of the ginsenosides, and so full concentration responses were conducted in both the FURA-2AM and YO-PRO-1 assays. Data obtained from these full concentration response curves confirmed a lot of what had been previously published, although key differences arose: the D318A mutant reduced potentiation by CK of the response to 200 μM ATP (Bidula et al., 2019b), but here, potentiation of the maximum response is greatly increased. Whilst the S60A mutant has decreased potentiation by ginsenoside CK, it has not completely abolished potentiation as was seen in the FURA-2AM and YO-PRO-1 assays when using a single concentration of ATP (Bidula et al., 2019b) . Interestingly, the D318A and L320A mutants had poor YO-PRO-1 responses, suggesting that these mutants disrupt the dye uptake pathway of the P2X7 receptor. As a result, this assay is not appropriate to be used at these mutants for measuring changes in potentiation compared to the wild type, as the mutants are not able to allow for dye uptake in a similar way to the wild type receptor.

Extended mutagenesis of the binding pocket, particularly to residues E255 and Y257, did not reveal any additional residues that were likely to be involved in ginsenoside binding. Mutating either E255 or Y257 to alanine did not substantially change the fold potentiation by CK, suggesting that these are not necessary for ginsenoside CK to bind to the receptor and exert its effects. This is interesting given that E255 is proposed to interact with the lower potion (C3) of ginsenoside CK, although stabilising interactions with the sugar moiety may be sufficient to overcome the lack of binding towards the bottom of the central vestibule region. Another key mutant, D197A, resulted in a dramatic increase in the response to ATP in the presence of ginsenoside CK. Although the difference in the pEC_{50} was

comparable in both the FURA-2AM and YO-PRO-1 assays between the wild type and D197A hP2X7 receptors, the increase in the maximum response in the D197A mutant was increased. Residues R276 and D197 are close enough to interact, and it is entirely possible that they are able to form an ionic interaction across the central vestibule region. By mutating D197 to alanine, this could make it easier for ginsenoside CK to navigate to the central vestibule region and exert its potentiatory effects, perhaps by accelerating its onset of action and thus increasing the maximum response observed. This would be interesting for future investigation by the Stokes lab.

Expanding on key findings by Piyasirananda *et al* (Piyasirananda et al., 2021), the lack of activity of ginsenoside F1 compared to ginsenoside CK was explored further. From viewing homology models with ginsenoside CK docked, it was proposed that residue F322 may be conflicting with the additional hydroxyl present on C6 in ginsenoside F1. Mutation of F322 to alanine did not confer activity to ginsenoside F1, suggesting that this was not the reason for F1's lack of activity, however, it did reveal some interesting differences in potentiation. One such difference was that the maximum response to ATP could not be increased by ginsenoside CK in the FURA-2AM assay, unlike what was seen for the wild-type receptor. Double mutant receptors that also contained the F322A mutant also displayed a similar phenomenon, whereas individual mutations without the F322A mutation did not. Potentiation by ginsenoside CK was observed at the F322A mutant in both the membrane potential and FURA-2AM assays, both of which are interpretations of ion influx, but dye uptake assays revealed something else: potentiation could be seen by ginsenoside CK at lower concentrations of ATP, but at higher concentrations responses were significantly reduced in the presence of ginsenoside CK. This was the case in multiple dye uptake assays measured using different equipment, suggesting that this effect is indeed genuine.

Although the F322A mutant has been shown to have reduced potentiation by ginsenoside CK at higher concentrations of ATP, even perhaps inhibiting the dye uptake response to some extent, the mechanism of this is not yet understood. The effect appears comparable to that of BzATP with CK at the wild type receptor; ATP appears to act as a full agonist at the F322A mutant, much like BzATP at the wild type receptor. At the wild type receptor, responses to BzATP with ginsenoside CK decrease the maximum dye uptake responses compared to BzATP alone, although fold potentiation of the EC_{50} remains consistent. Dye uptake responses to supramaximal concentrations of ATP (>1 mM) are often lower than that of those below 1 mM concentrations, with maximum responses often around 300 – 500 μM; the addition of ginsenoside CK to a full agonist appears to mimic this effect, but at lower concentrations of ATP.

Cysteine mutagenesis of hP2X7 aimed to explore the mechanism of potentiation by ginsenoside CK further, challenging accessibility of the central vestibule region to potentiators by the addition of bulky MTS-reagents at the entrance to the lateral portals. Mutating residue F322 to cysteine resulted in a receptor that had similar pharmacology to the F322A receptor, with a similar decrease in the dye uptake response to ATP in the presence of ginsenoside CK, meaning that the effects measured with ginsenoside CK at the F322A mutant was not being altered by changing this residue to cysteine. Reaction with MTS reagents did not reveal any convincing evidence that the F322C residue was indeed able to be labelled, with non-transfected cells showing similar fluorescence labelling. When measuring ATP-induced dye uptake responses between MTS-rhodamine or MTS-biotin treated and non-treated F322C cells, there was no difference. A good place to continue investigating this phenomenon would be to use confocal microscopy to assess labelling of MTS-rhodamine, perhaps alongside a GFP-tagged F322C mutant P2X7 receptor. Background fluorescence due to the presence of abundant free cysteines on the cell surface would likely always be a contributing factor, despite the presence of additional free cysteines on the over expressed F322C mutant hP2X7 receptor; another way to assess labelling would be to perform a Western blot analysis using streptavidin-HRP to evaluate MTSEA-biotin labelling.

It is not clear whether this reduction in the dye uptake response is due to reduced access of dye molecules to the channel pore in the presence of CK, perhaps due to steric hindrance or repulsion from CK binding. Alternatively, activation of the P2X7 receptor with such a potent modulator plus a supramaximal concentration of full agonist confers a different activation state to the receptor, a desensitised state. Given that the F322 residue lies on the β14 strand that connects the ATP site to transmembrane domain 2 that is directly linked to the cysteine rich palmitoylation anchor domain, it could be that mutating this residue affects the ability of the C-cys anchor to prevent desensitisation of the receptor (McCarthy et al., 2019). Nonetheless, this highlights that it may be possible to differentially modulate ion influx and large molecule movement through the P2X7 receptor. This knowledge will be of importance in development of novel modulators of the P2X7 receptor, and it will be interesting to determine the consequences of modulating one such property over another on downstream receptor function.

Appendices

Appendix 1 – Structures of Ginsenosides

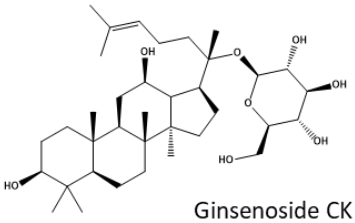

Ginsenoside CK

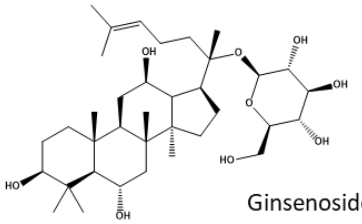

Ginsenoside F1

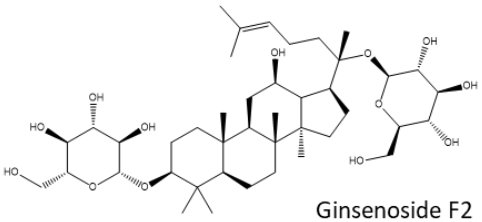

Ginsenoside F2

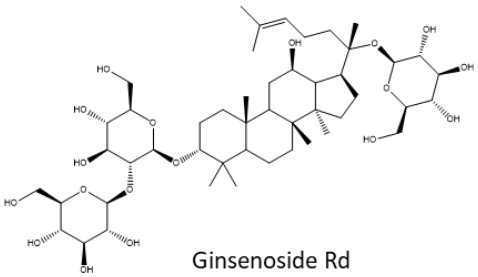

Ginsenoside Rd

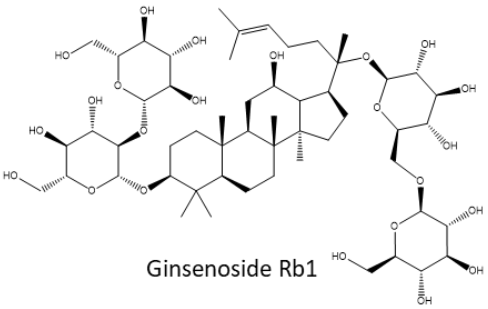

Ginsenoside Rb1

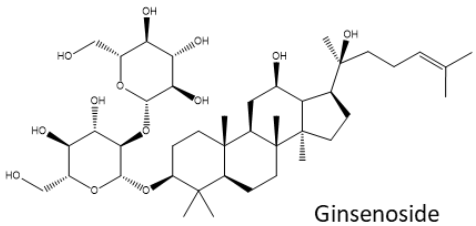

Ginsenoside
20-*S*-Rg3

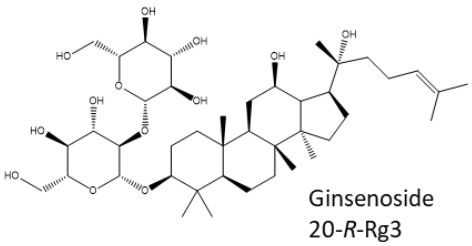

Ginsenoside
20-*R*-Rg3

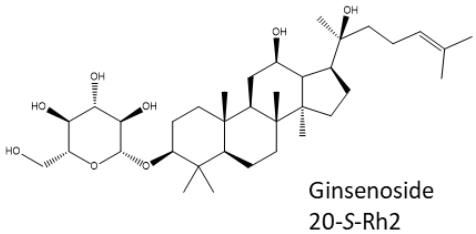

Ginsenoside
20-*S*-Rh2

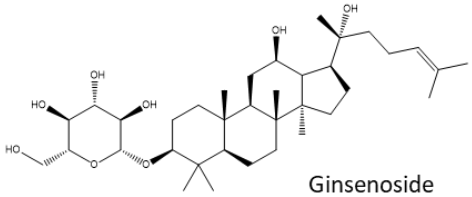

Ginsenoside
20-*R*-Rh2

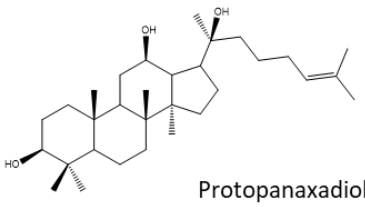

Protopanaxadiol

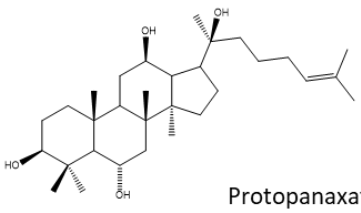

Protopanaxatriol

Appendix 2 – Structures of Glycosides and Related Compounds

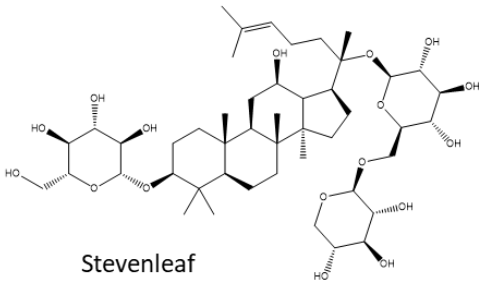

Stevenleaf

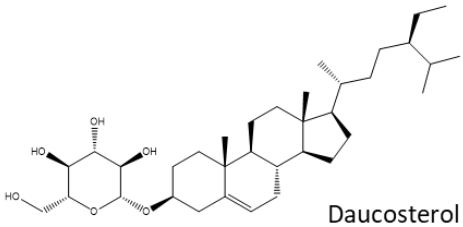

Daucosterol

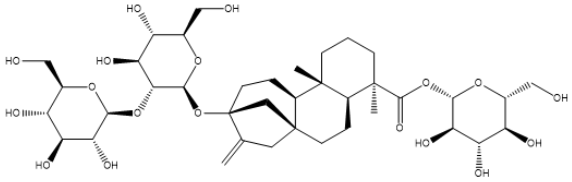

Stevioside

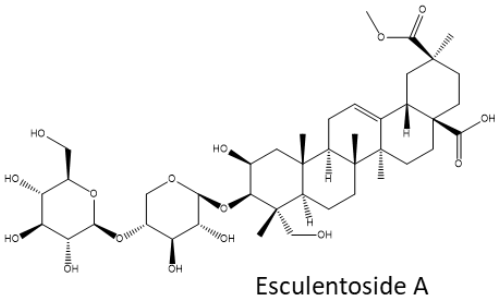

Esculentoside A

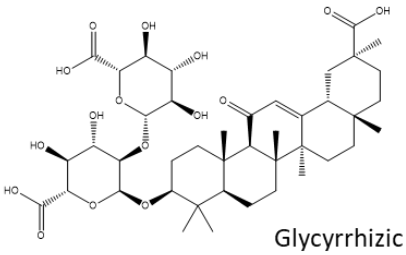

Glycyrrhizic Acid

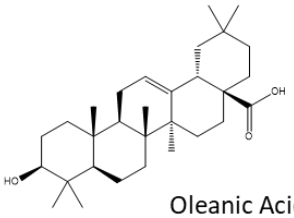

Oleanic Acid

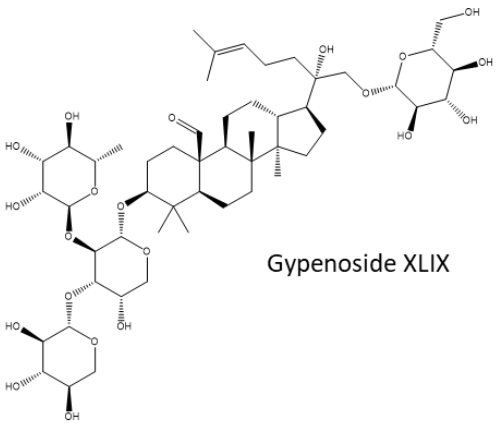

Gypenoside XLIX

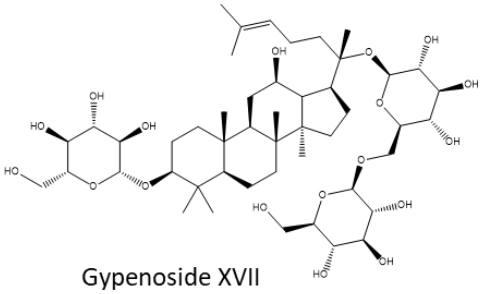

Gypenoside XVII

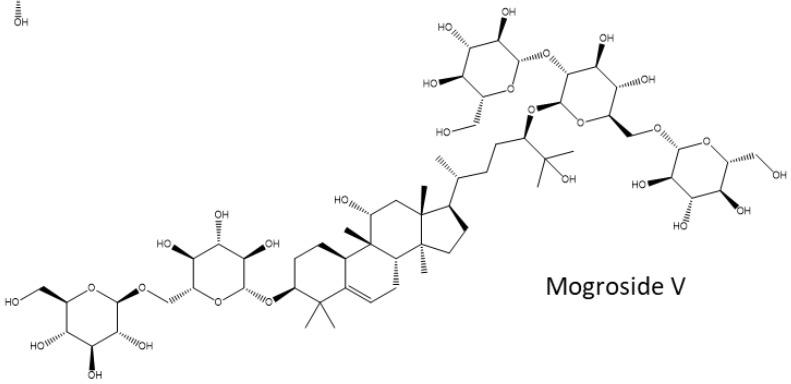

Mogroside V

Appendix 3 – Structures of Steroids

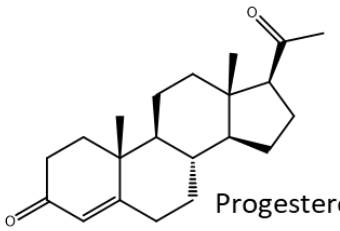

Progesterone

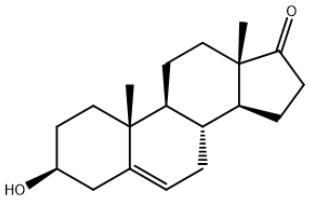

Dehydroepiandrosterone (DHEA)

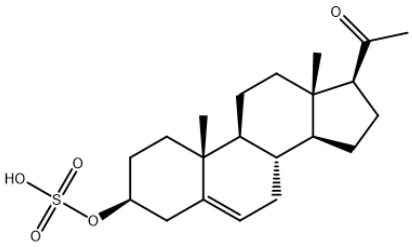

PregnEnolone Sulfate

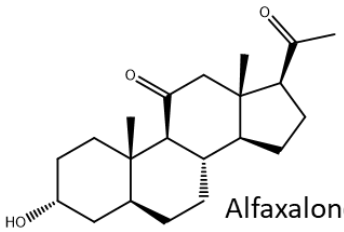

Alfaxalone

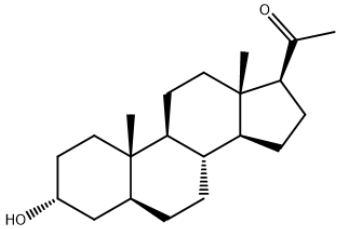

Allopregnanolone

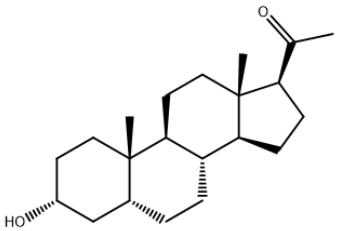

PregnAnolone

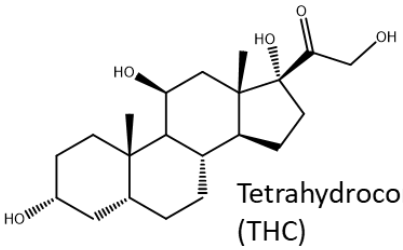

Tetrahydrocortisol (THC)

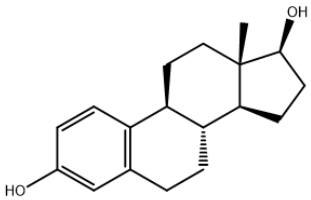

17β-estradiol

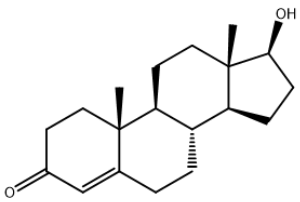

Testosterone

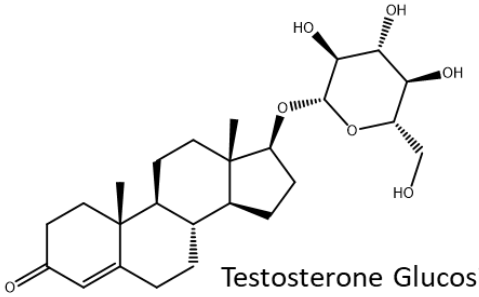

Testosterone Glucoside (AB1)

Appendix 4 – Effects of Quencher Dyes on Responses to ATP

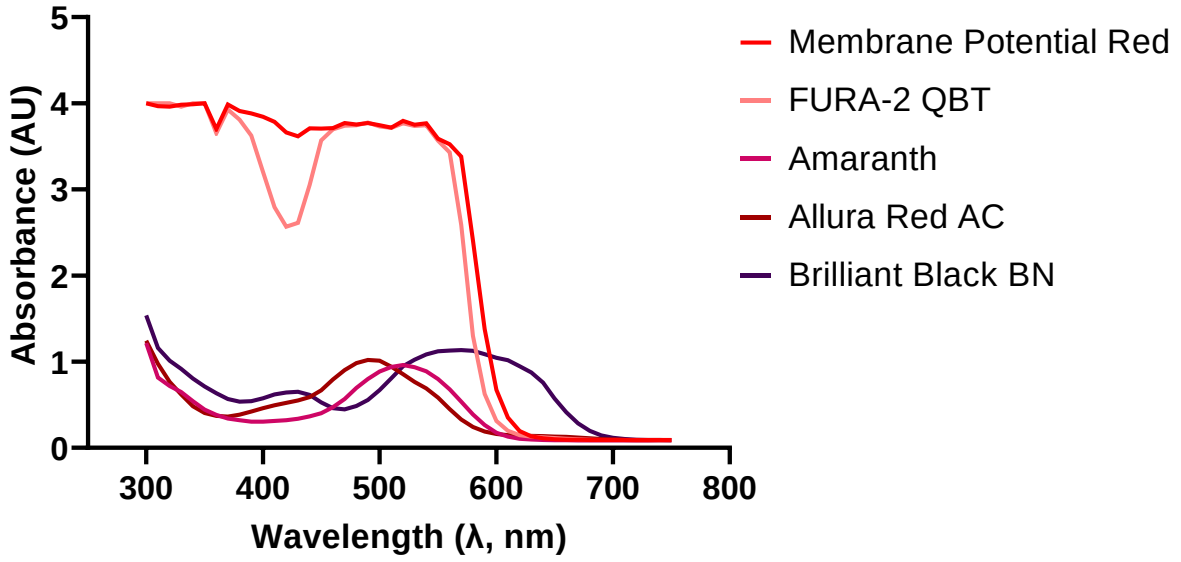

Figure A0.1 – Absorbance spectra for a range of quencher dyes used in fluorometric assays. Brilliant Black BN is believed to be the quencher dye used in the FLIPR Membrane Potential Blue assay (see US patent number US 6,420,183 B1). Red coloured quencher dyes investigated include Amaranth and Allura Red AC. The absorbance spectra of FURA-2 QBT and the FLIPR Membrane Potential Red assay were compared as both contain a red quencher dye.

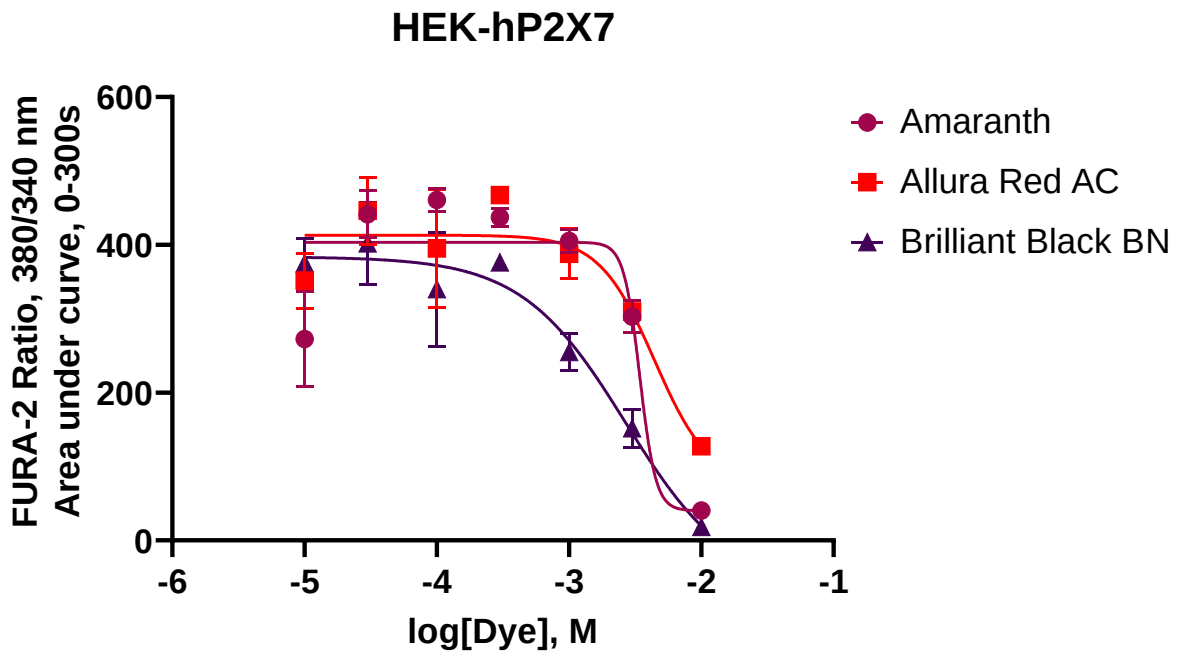

Figure A0.2 – Inhibition of HEK-hP2X7 responses to 500 µM ATP by dyes measured using the FURA-2AM assay. IC_{50} values are as follows: Amaranth 3.4 mM; Allura Red AC 4.4 mM; Brilliant Black BN 2.7 mM. Cells exposed to 10 mM of these dyes appeared more similar to the controls compared to those that had been treated with 500 µM ATP alone, suggesting that inhibition had occurred (data not shown).

List of Abbreviations

αβ-MeATP	αβ-methylene ATP
βγ-MeATP	L-βγ methylene ATP
2-MeSATP	2-Methylthio ATP
ADP	Adenosine 5’-diphosphate
AMP	Adenosine 5’-monophosphate
ANOVA	Analysis of Variance
ATP	Adenosine 5’-triphosphate
BBG	Brilliant Blue G
BDNF	Brain Derived Neurotrophic Factor
BzATP	2'(3')-O-(4-Benzoylbenzoyl)adenosine-5'-triphosphate
cDNA	Complementary Deoxyribonucleic Acid
CFA	Complete Freund’s Adjuvant
CHO-K1	Chinese Hamster Ovary K1 Cells
CRISPR	Clustered Regularly Interspaced Short Palindromic Repeats
CTP	Cytidine 5’-triphosphate
DMEM	Dulbecco's Modified Eagle's Medium
DMSO	Dimethyl Sulfoxide
DNA	Deoxyribonucleic Acid
EtBr	Ethidium Bromide
FBS	Foetal Bovine Serum
GFP	Green Fluorescent Protein
GPCR	G-Protein Coupled Receptor
HBSS	Hanks' Balanced Salt Solution
HEK-293	Human Embryonic Kidney 293 Cells
HEK20E6	P2Y2-knockout HEK-293 cells
KO	Knockout
LPS	Lipopolysaccharide
MPB	Membrane Potential Blue
mRNA	Messenger Ribonucleic Acid
MTS	Methanethiosulfonate
MTSEA-Biotin-X	2-((6-((biotinoyl)amino)hexanoyl)amino)ethylmethanethiosulfonate
MTSEA-Biotin-XX	2-((6-((6-((biotinoyl)amino)hexanoyl)amino)hexanoyl)amino)ethylmethanethiosulfonate
PDL	Poly-D-Lysine
PPADS	Pyridoxal phosphate-6-azo(benzene-2,4-disulfonic acid)
Rb4	Reactive Blue 4
RNA	Ribonucleic Acid
siRNA	Small Interfering Ribonucleic Acid
SNP	Single Nucleotide Polymorphism
TO-PRO-3	3-methyl-2-(3-[1-(3-[trimethylammonio]propyl)quinolin-4(1H)-ylidene]prop-1-en-1-yl)-1,3-benzothiazol-3-ium diiodide
UDP	Uridine 5’-diphosphate
UTP	Uridine 5’-triphosphate

YO-PRO-1	4-[(3-methyl-1,3-benzoxazol-2(3H)-ylidene)methyl]-1-[3-(trimethylammonio)propyl]quinolinium diiodide

References

ABBRACCHIO, M. P. & BURNSTOCK, G. 1994. Purinoceptors: are there families of P2X and P2Y purinoceptors? *Pharmacol Ther,* 64**,** 445-75.

ABDULQAWI, R., DOCKRY, R., HOLT, K., LAYTON, G., MCCARTHY, B. G., FORD, A. P. & SMITH, J. A. 2015. P2X3 receptor antagonist (AF-219) in refractory chronic cough: a randomised, double-blind, placebo-controlled phase 2 study. *Lancet,* 385**,** 1198-205.

ACUNA-CASTILLO, C., MORALES, B. & HUIDOBRO-TORO, J. P. 2000. Zinc and copper modulate differentially the P2X4 receptor. *J Neurochem,* 74**,** 1529-37.

ADINOLFI, E., CIRILLO, M., WOLTERSDORF, R., FALZONI, S., CHIOZZI, P., PELLEGATTI, P., CALLEGARI, M. G., SANDONA, D., MARKWARDT, F., SCHMALZING, G. & DI VIRGILIO, F. 2010. Trophic activity of a naturally occurring truncated isoform of the P2X7 receptor. *Faseb j,* 24**,** 3393-404.

ADINOLFI, E., GIULIANI, A. L., DE MARCHI, E., PEGORARO, A., ORIOLI, E. & DI VIRGILIO, F. 2018. The P2X7 receptor: A main player in inflammation. *Biochemical Pharmacology,* 151**,** 234-244.

ADINOLFI, E., RAFFAGHELLO, L., GIULIANI, A. L., CAVAZZINI, L., CAPECE, M. & CHIOZZI, P. 2012. Expression of P2X7 receptor increases in vivo tumor growth. *Cancer Res,* 72.

ALEXANDER, K., NIFORATOS, W., BIANCHI, B., BURGARD, E. C., LYNCH, K. J., KOWALUK, E. A., JARVIS, M. F. & VAN BIESEN, T. 1999. Allosteric Modulation and Accelerated Resensitization of Human P2X₃ Receptors by Cibacron Blue. *Journal of Pharmacology and Experimental Therapeutics,* 291**,** 1135.

ALLSOPP, R. C., DAYL, S., SCHMID, R. & EVANS, R. J. 2017. Unique residues in the ATP gated human P2X7 receptor define a novel allosteric binding pocket for the selective antagonist AZ10606120. *Scientific Reports,* 7**,** 725.

ARMSTRONG, A. 2022. *Merck plans to count coughs and months until gefapixant is back in FDA hands* [Online]. https://www.fiercebiotech.com/biotech/merck-plans-count-coughs-and-months-until-gefapixant-back-fda-hands: Fierce Biotech. Available: https://www.fiercebiotech.com/biotech/merck-plans-count-coughs-and-months-until-gefapixant-back-fda-hands [Accessed 04/11 2022].

ASATRYAN, L., YARDLEY, M. M., KHOJA, S., TRUDELL, J. R., HYUNH, N., LOUIE, S. G., PETASIS, N. A., ALKANA, R. L. & DAVIES, D. L. 2014. Avermectins differentially affect ethanol intake and receptor function: implications for developing new therapeutics for alcohol use disorders. *International Journal of Neuropsychopharmacology,* 17**,** 907-916.

ASE, A. R., HONSON, N. S., ZAGHDANE, H., PFEIFER, T. A. & SÉGUÉLA, P. 2015. Identification and characterization of a selective allosteric antagonist of human P2X4 receptor channels. *Mol Pharmacol,* 87**,** 606-16.

BAE, E.-A., HAN, M. J., SHIN, Y.-W. & KIM, D.-H. 2006. Inhibitory Effects of Korean Red Ginseng and Its Genuine Constituents Ginsenosides Rg3, Rf, and Rh2 in Mouse Passive Cutaneous Anaphylaxis Reaction and Contact Dermatitis Models. *Biological and Pharmaceutical Bulletin,* 29**,** 1862-1867.

BAEG, I. H. & SO, S. H. 2013. The world ginseng market and the ginseng (Korea). *J Ginseng Res,* 37**,** 1-7.

BALLERINI, P., RATHBONE, M. P., IORIO, P. D., RENZETTI, A., GIULIANI, P., D'ALIMONTE, L., TRUBIANI, O., CACIAGLI, F. & CICCARELLI, R. 1996. Rat astroglial P2Z (P2X7) receptors regulate intracellular calcium and purine release. *NeuroReport,* 7.

BALÁZS, B., DANKÓ, T., KOVÁCS, G., KÖLES, L., HEDIGER, M. A. & ZSEMBERY, A. 2013. Investigation of the inhibitory effects of the benzodiazepine derivative, 5-BDBD on P2X4 purinergic receptors by two complementary methods. *Cell Physiol Biochem,* 32**,** 11-24.

BANKS, F. C., KNIGHT, G. E., CALVERT, R. C., TURMAINE, M., THOMPSON, C. S., MIKHAILIDIS, D. P., MORGAN, R. J. & BURNSTOCK, G. 2006. Smooth muscle and purinergic contraction of the human, rabbit, rat, and mouse testicular capsule. *Biol Reprod,* 74**,** 473-80.

BAQI, Y., HAUSMANN, R., ROSEFORT, C., RETTINGER, J., SCHMALZING, G. & MÜLLER, C. E. 2011. Discovery of potent competitive antagonists and positive modulators of the P2X2 receptor. *J Med Chem,* 54**,** 817-30.

BARCZYK, A., BAUDERLIQUE-LE ROY, H., JOUY, N., RENAULT, N., HOTTIN, A., MILLET, R., VOURET-CRAVIARI, V., ADRIOUCH, S., IDZIOREK, T. & DEZITTER, X. 2021. Flow cytometry: An accurate tool for screening P2RX7 modulators. *Cytometry Part A,* 99**,** 793-806.

BELLUSHEALTH. 2022. *About Us: Our Company* [Online]. https://bellushealth.com/about-us/our-company/: BellusHealth. [Accessed 04/11 2022].

BENNETT, M. R. 2007. Synaptic P2X7 Receptor Regenerative-Loop Hypothesis for Depression. *Australian & New Zealand Journal of Psychiatry,* 41**,** 563-571.

BENNETTS, F. M., MOBBS, J. I., VENTURA, S. & THAL, D. M. 2022. The P2X1 receptor as a therapeutic target. *Purinergic Signalling*.

BERNIER, L. P., ASE, A. R., BOUÉ-GRABOT, E. & SÉGUÉLA, P. 2012. P2X4 receptor channels form large noncytolytic pores in resting and activated microglia. *Glia,* 60**,** 728-37.

BERTIN, E., MARTINEZ, A., FAYOUX, A., CARVALHO, K., CARRACEDO, S., FERNAGUT, P. O., KOCH-NOLTE, F., BLUM, D., BERTRAND, S. S. & BOUÉ-GRABOT, E. 2022. Increased surface P2X4 receptors by mutant SOD1 proteins contribute to ALS pathogenesis in SOD1-G93A mice. *Cell Mol Life Sci,* 79**,** 431.

BHATTACHARYA, A. 2018. Recent Advances in CNS P2X7 Physiology and Pharmacology: Focus on Neuropsychiatric Disorders. *Frontiers in Pharmacology,* 9.

BIANCHI, B. R., LYNCH, K. J., TOUMA, E., NIFORATOS, W., BURGARD, E. C., ALEXANDER, K. M., PARK, H. S., YU, H., METZGER, R., KOWALUK, E., JARVIS, M. F. & VAN BIESEN, T. 1999. Pharmacological characterization of recombinant human and rat P2X receptor subtypes. *European Journal of Pharmacology,* 376**,** 127-138.

BIBIC, L., HERZIG, V., KING, G. F. & STOKES, L. 2019. Development of High-Throughput Fluorescent-Based Screens to Accelerate Discovery of P2X Inhibitors from Animal Venoms. *Journal of Natural Products,* 82**,** 2559-2567.

BIDULA, S., DHUNA, K., HELLIWELL, R. & STOKES, L. 2019a. Positive allosteric modulation of P2X7 promotes apoptotic cell death over lytic cell death responses in macrophages. *Cell Death & Disease,* 10**,** 882.

BIDULA, S. M., CROMER, B. A., WALPOLE, S., ANGULO, J. & STOKES, L. 2019b. Mapping a novel positive allosteric modulator binding site in the central vestibule region of human P2X7. *Sci Rep,* 9**,** 3231.

BIRRING, S. S., SMITH, J. A., MORICE, A., PAVORD, I., DICPINIGAITIS, P. V., MCGARVEY, L., TZONTCHEVA, A., LI, Q., MARTIN NGUYEN, A., SCHELFHOUT, J., MUCCINO, D. & LA ROSA, C. 2021a. The Cough Severity Diary in a pooled analysis of two, phase 3 trials of gefapixant in chronic cough. *European Respiratory Journal,* 58**,** OA4060.

BIRRING, S. S., SMITH, J. A., MORICE, A. H., SHER, M., HULL, J. H., GOLDSOBEL, A. B., LANOUETTE, S., LI, E., HARVEY, L. & BONUCCELLI, C. M. 2021b. Improvements in cough severity and cough-related quality of life in a phase 2 trial (RELIEF) with the P2X3 antagonist BLU-5937 in refractory chronic cough (RCC). *European Respiratory Journal,* 58**,** OA1199.

BO, X., ALAVI, A., XIANG, Z., OGLESBY, I., FORD, A. & BURNSTOCK, G. 1999. Localization of ATP-gated P2X2 and P2X3 receptor immunoreactive nerves in rat taste buds. *Neuroreport,* 10**,** 1107-11.

BO, X., JIANG, L. H., WILSON, H. L., KIM, M., BURNSTOCK, G., SURPRENANT, A. & NORTH, R. A. 2003a. Pharmacological and biophysical properties of the human P2X5 receptor. *Mol Pharmacol,* 63**,** 1407-16.

BO, X., KIM, M., NORI, S. L., SCHOEPFER, R., BURNSTOCK, G. & NORTH, R. A. 2003b. Tissue distribution of P2X4 receptors studied with an ectodomain antibody. *Cell Tissue Res,* 313**,** 159-65.

BO, X., ZHANG, Y., NASSAR, M., BURNSTOCK, G. & SCHOEPFER, R. 1995. A P2X purinoceptor cDNA conferring a novel pharmacological profile. *FEBS Lett,* 375**,** 129-33.

BOGDANOV, Y., RUBINO, A. & BURNSTOCK, G. 1998. Characterisation of subtypes of the P2X and P2Y families of ATP receptors in the foetal human heart. *Life Sci,* 62**,** 697-703.

BOUÉ-GRABOT, E., AKIMENKO, M. A. & SÉGUÉLA, P. 2000. Unique functional properties of a sensory neuronal P2X ATP-gated channel from zebrafish. *J Neurochem,* 75**,** 1600-7.

BOWLER, J. W., BAILEY, R. J., NORTH, R. A. & SURPRENANT, A. 2003. P2X4, P2Y1 and P2Y2 receptors on rat alveolar macrophages. *Br J Pharmacol,* 140**,** 567-75.

BRAKE, A. J., WAGENBACH, M. J. & JULIUS, D. 1994. New structural motif for ligand-gated ion channels defined by an ionotropic ATP receptor. *Nature,* 371**,** 519-23.

BRAUN, K., RETTINGER, J., GANSO, M., KASSACK, M., HILDEBRANDT, C., ULLMANN, H., NICKEL, P., SCHMALZING, G. & LAMBRECHT, G. 2001. NF449: a subnanomolar potency antagonist at recombinant rat P2X1 receptors. *Naunyn Schmiedebergs Arch Pharmacol,* 364**,** 285-90.

BROTHERTON-PLEISS, C. E., DILLON, M. P., FORD, A. P., GEVER, J. R., CARTER, D. S., GLEASON, S. K., LIN, C. J., MOORE, A. G., THOMPSON, A. W., VILLA, M. & ZHAI, Y. 2010. Discovery and optimization of RO-85, a novel drug-like, potent, and selective P2X3 receptor antagonist. *Bioorg Med Chem Lett,* 20**,** 1031-6.

BROWNE, L. E., COMPAN, V., BRAGG, L. & NORTH, R. A. 2013. P2X7 receptor channels allow direct permeation of nanometer-sized dyes. *J Neurosci,* 33**,** 3557-66.

BRÄNDLE, U., GUENTHER, E., IRRLE, C. & WHEELER-SCHILLING, T. H. 1998. Gene expression of the P2X receptors in the rat retina. *Brain Res Mol Brain Res,* 59**,** 269-72.

BRÄNDLE, U., SPIELMANNS, P., OSTEROTH, R., SIM, J., SURPRENANT, A., BUELL, G., RUPPERSBERG, J. P., PLINKERT, P. K., ZENNER, H. P. & GLOWATZKI, E. 1997. Desensitization of the P2X(2) receptor controlled by alternative splicing. *FEBS Lett,* 404**,** 294-8.

BUELL, G., LEWIS, C., COLLO, G., NORTH, R. A. & SURPRENANT, A. 1996a. An antagonist-insensitive P2X receptor expressed in epithelia and brain. *Embo j,* 15**,** 55-62.

BUELL, G., MICHEL, A. D., LEWIS, C., COLLO, G., HUMPHREY, P. P. & SURPRENANT, A. 1996b. P2X1 receptor activation in HL60 cells. *Blood,* 87**,** 2659-64.

BURNSTOCK, G. 1971. Neural Nomenclature. *Nature,* 229**,** 282-283.

BURNSTOCK, G. 1976. Purinergic receptors. *J Theor Biol,* 62**,** 491-503.

BURNSTOCK, G. 2004. Introduction: P2 receptors. *Curr Top Med Chem,* 4**,** 793-803.

BURNSTOCK, G. 2007. Purine and pyrimidine receptors. *Cell Mol Life Sci,* 64**,** 1471-83.

BURNSTOCK, G. 2014. Purinergic signalling in the reproductive system in health and disease. *Purinergic Signalling,* 10**,** 157-187.

BURNSTOCK, G. 2018. The therapeutic potential of purinergic signalling. *Biochem Pharmacol,* 151**,** 157-165.

BURNSTOCK, G., CAMPBELL, G., BENNETT, M. & HOLMAN, M. E. 1964. INNERVATION OF THE GUINEA-PIG TAENIA COLI: ARE THERE INTRINSIC INHIBITORY NERVES WHICH ARE DISTINCT FROM SYMPATHETIC NERVES? *Int J Neuropharmacol,* 3**,** 163-6.

BURNSTOCK, G., CAMPBELL, G. & RAND, M. J. 1966. The inhibitory innervation of the taenia of the guinea-pig caecum. *J Physiol,* 182**,** 504-26.

CAO, X., LI, L.-P., WANG, Q., WU, Q., HU, H.-H., ZHANG, M., FANG, Y.-Y., ZHANG, J., LI, S.-J., XIONG, W.-C., YAN, H.-C., GAO, Y.-B., LIU, J.-H., LI, X.-W., SUN, L.-R., ZENG, Y.-N., ZHU, X.-H. & GAO, T.-M. 2013. Astrocyte-derived ATP modulates depressive-like behaviors. *Nature Medicine,* 19**,** 773-777.

CARIO-TOUMANIANTZ, C., LOIRAND, G., FERRIER, L. & PACAUD, P. 1998. Non-genomic inhibition of human P2X7 purinoceptor by 17beta-oestradiol. *The Journal of physiology,* 508 (Pt 3)**,** 659-666.

CASELEY, E. A., MUENCH, S. P. & JIANG, L.-H. 2017. Conformational changes during human P2X7 receptor activation examined by structural modelling and cysteine-based cross-linking studies. *Purinergic Signalling,* 13**,** 135-141.

CHAE, S., KANG, K. A., CHANG, W. Y., KIM, M. J., LEE, S. J., LEE, Y. S., KIM, H. S., KIM, D. H. & HYUN, J. W. 2009. Effect of Compound K, a Metabolite of Ginseng Saponin, Combined with γ-Ray Radiation in Human Lung Cancer Cells in Vitro and in Vivo. *Journal of Agricultural and Food Chemistry,* 57**,** 5777-5782.

CHAN, C. M., UNWIN, R. J., BARDINI, M., OGLESBY, I. B., FORD, A. P., TOWNSEND-NICHOLSON, A. & BURNSTOCK, G. 1998. Localization of P2X1 purinoceptors by autoradiography and immunohistochemistry in rat kidneys. *Am J Physiol,* 274**,** F799-804.

CHAVES, S. P., TORRES-SANTOS, E. C., MARQUES, C., FIGLIUOLO, V. R., PERSECHINI, P. M., COUTINHO-SILVA, R. & ROSSI-BERGMANN, B. 2009. Modulation of P2X(7) purinergic receptor in macrophages by Leishmania amazonensis and its role in parasite elimination. *Microbes Infect,* 11**,** 842-9.

CHEEWATRAKOOLPONG, B., GILCHREST, H., ANTHES, J. C. & GREENFEDER, S. 2005. Identification and characterization of splice variants of the human P2X7 ATP channel. *Biochemical and Biophysical Research Communications,* 332**,** 17-27.

CHEN, C. C., AKOPIAN, A. N., SIVILOTTI, L., COLQUHOUN, D., BURNSTOCK, G. & WOOD, J. N. 1995. A P2X purinoceptor expressed by a subset of sensory neurons. *Nature,* 377**,** 428-31.

CHEN, K., LIU, J., JI, R., CHEN, T., ZHOU, X., YANG, J., TONG, Y., JIANG, C., ZHOU, J., ZHAO, Y., JIN, Y., YUAN, Y. & HUANG, L. 2018. Biogenic Synthesis and Spatial Distribution of Endogenous Phytohormones and Ginsenosides Provide Insights on Their Intrinsic Relevance in Panax ginseng. *Front Plant Sci,* 9**,** 1951.

CHESSELL, I. P., HATCHER, J. P., BOUNTRA, C., MICHEL, A. D., HUGHES, J. P., GREEN, P., EGERTON, J., MURFIN, M., RICHARDSON, J., PECK, W. L., GRAHAMES, C. B., CASULA, M. A., YIANGOU, Y., BIRCH, R., ANAND, P. & BUELL, G. N. 2005. Disruption of the P2X7 purinoceptor gene abolishes chronic inflammatory and neuropathic pain. *Pain,* 114**,** 386-96.

CHESSELL, I. P., MICHEL, A. D. & HUMPHREY, P. P. A. 1998. Effects of antagonists at the human recombinant P2X7 receptor. *British Journal of Pharmacology,* 124**,** 1314-1320.

CHO, J. Y., YOO, E. S., BAIK, K. U., PARK, M. H. & HAN, B. H. 2001. In vitro inhibitory effect of protopanaxadiol ginsenosides on tumor necrosis factor (TNF)-alpha production and its modulation by known TNF-alpha antagonists. *Planta Med,* 67**,** 213-8.

CHOI, S. H., KIM, H. J., KIM, B. R., SHIN, T. J., HWANG, S. H., LEE, B. H., LEE, S. M., RHIM, H. & NAH, S. Y. 2013. Gintonin, a ginseng-derived lysophosphatidic acid receptor ligand, potentiates ATP-gated $P2X_1$ receptor channel currents. *Mol Cells,* 35**,** 142-50.

CLARKE, C. E., BENHAM, C. D., BRIDGES, A., GEORGE, A. R. & MEADOWS, H. J. 2000. Mutation of histidine 286 of the human P2X4 purinoceptor removes extracellular pH sensitivity. *J Physiol,* 523 Pt 3**,** 697-703.

CLIFFORD, E. E., PARKER, K., HUMPHREYS, B. D., KERTESY, S. B. & DUBYAK, G. R. 1998. The P2X1 receptor, an adenosine triphosphate-gated cation channel, is expressed in human platelets but not in human blood leukocytes. *Blood,* 91**,** 3172-81.

CLINICALTRIALS.GOV. 2021. *Evaluation of the Efficacy and*

Safety of BLU-5937 in Adults With Refractory Chronic Cough (SOOTHE) [Online]. https://clinicaltrials.gov/ct2/show/NCT04678206. [Accessed 04.11 2022].

COCKCROFT, S. & GOMPERTS, B. D. 1979. Activation and inhibition of calcium-dependent histamine secretion by ATP ions applied to rat mast cells. *J Physiol,* 296**,** 229-43.

CODDOU, C., LORCA, R. A., ACUÑA-CASTILLO, C., GRAUSO, M., RASSENDREN, F. & HUIDOBRO-TORO, J. P. 2005. Heavy metals modulate the activity of the purinergic P2X4 receptor. *Toxicol Appl Pharmacol,* 202**,** 121-31.

CODOCEDO, J. F., RODRÍGUEZ, F. E. & HUIDOBRO-TORO, J. P. 2009. Neurosteroids differentially modulate P2X ATP-gated channels through non-genomic interactions. *J Neurochem,* 110**,** 734-44.

COLLO, G., NEIDHART, S., KAWASHIMA, E., KOSCO-VILBOIS, M., NORTH, R. A. & BUELL, G. 1997. Tissue distribution of the P2X7 receptor. *Neuropharmacology,* 36**,** 1277-83.

COLLO, G., NORTH, R. A., KAWASHIMA, E., MERLO-PICH, E., NEIDHART, S., SURPRENANT, A. & BUELL, G. 1996. Cloning OF P2X5 and P2X6 receptors and the distribution and properties of an extended family of ATP-gated ion channels. *J Neurosci,* 16**,** 2495-507.

COOK, S. P., RODLAND, K. D. & MCCLESKEY, E. W. 1998. A Memory for Extracellular Ca²⁺ by Speeding Recovery of P2X Receptors from Desensitization. *The Journal of Neuroscience,* 18**,** 9238.

COOK, S. P., VULCHANOVA, L., HARGREAVES, K. M., ELDE, R. & MCCLESKEY, E. W. 1997. Distinct ATP receptors on pain-sensing and stretch-sensing neurons. *Nature,* 387**,** 505-8.

CORRÊA, G., MARQUES DA SILVA, C., DE ABREU MOREIRA-SOUZA, A. C., VOMMARO, R. C. & COUTINHO-SILVA, R. 2010. Activation of the P2X(7) receptor triggers the elimination of Toxoplasma gondii tachyzoites from infected macrophages. *Microbes Infect,* 12**,** 497-504.

COULL, J. A., BEGGS, S., BOUDREAU, D., BOIVIN, D., TSUDA, M., INOUE, K., GRAVEL, C., SALTER, M. W. & DE KONINCK, Y. 2005. BDNF from microglia causes the shift in neuronal anion gradient underlying neuropathic pain. *Nature,* 438**,** 1017-21.

COUTINHO-SILVA, R., PERFETTINI, J. L., PERSECHINI, P. M., DAUTRY-VARSAT, A. & OJCIUS, D. M. 2001. Modulation of P2Z/P2X(7) receptor activity in macrophages infected with Chlamydia psittaci. *Am J Physiol Cell Physiol,* 280**,** C81-9.

COUTINHO-SILVA, R., PERSECHINI, P. M., BISAGGIO, R. D., PERFETTINI, J. L., NETO, A. C., KANELLOPOULOS, J. M., MOTTA-LY, I., DAUTRY-VARSAT, A. & OJCIUS, D. M. 1999. P2Z/P2X7 receptor-dependent apoptosis of dendritic cells. *Am J Physiol,* 276**,** C1139-47.

DARVILLE, T., WELTER-STAHL, L., CRUZ, C., SATER, A. A., ANDREWS, C. W., JR. & OJCIUS, D. M. 2007. Effect of the purinergic receptor P2X7 on Chlamydia infection in cervical epithelial cells and vaginally infected mice. *J Immunol,* 179**,** 3707-14.

DASGEB, B., KORNREICH, D., MCGUINN, K., OKON, L., BROWNELL, I. & SACKETT, D. L. 2018. Colchicine: an ancient drug with novel applications. *Br J Dermatol,* 178**,** 350-356.

DAVENPORT, A. J., NEAGOE, I., BRÄUER, N., KOCH, M., ROTGERI, A., NAGEL, J., LAUX-BIEHLMANN, A., MACHET, F., COELHO, A. M., BOYCE, S., CARTY, N., GEMKOW, M. J., HESS, S. D., ZOLLNER, T. M. & FISCHER, O. M. 2021. Eliapixant is a selective P2X3 receptor antagonist for the treatment of disorders associated with hypersensitive nerve fibers. *Sci Rep,* 11**,** 19877.

DAVIES, D. L., KOCHEGAROV, A. A., KUO, S. T., KULKARNI, A. A., WOODWARD, J. J., KING, B. F. & ALKANA, R. L. 2005. Ethanol differentially affects ATP-gated P2X3 and P2X4 receptor subtypes expressed in Xenopus oocytes. *Neuropharmacology,* 49**,** 243-253.

DE ROO, M., BOUÉ-GRABOT, E. & SCHLICHTER, R. 2010. Selective potentiation of homomeric P2X2 ionotropic ATP receptors by a fast non-genomic action of progesterone. *Neuropharmacology,* 58**,** 569-77.

DE ROO, M., RODEAU, J. L. & SCHLICHTER, R. 2003. Dehydroepiandrosterone potentiates native ionotropic ATP receptors containing the P2X2 subunit in rat sensory neurones. *J Physiol,* 552**,** 59-71.

DELL'ANTONIO, G., QUATTRINI, A., DAL CIN, E., FULGENZI, A. & FERRERO, M. E. 2002. Antinociceptive effect of a new P(2Z)/P2X7 antagonist, oxidized ATP, in arthritic rats. *Neurosci Lett,* 327**,** 87-90.

DEMAIN, A. L. & VAISHNAV, P. 2011. Natural products for cancer chemotherapy. *Microb Biotechnol,* 4**,** 687-99.

DESBOROUGH, M. J. R. & KEELING, D. M. 2017. The aspirin story – from willow to wonder drug. *British Journal of Haematology,* 177**,** 674-683.

DHULIPALA, P. D., WANG, Y. X. & KOTLIKOFF, M. I. 1998. The human P2X4 receptor gene is alternatively spliced. *Gene,* 207**,** 259-66.
DHUNA, K., FELGATE, M., BIDULA, S. M., WALPOLE, S., BIBIC, L., CROMER, B. A., ANGULO, J., SANDERSON, J., STEBBING, M. J. & STOKES, L. 2019. Ginsenosides Act As Positive Modulators of P2X4 Receptors. *Molecular pharmacology,* 95**,** 210-221.
DI VIRGILIO, F., JIANG, L.-H., ROGER, S., FALZONI, S., SARTI, A. C., VULTAGGIO-POMA, V., CHIOZZI, P. & ADINOLFI, E. 2019. Chapter Eight - Structure, function and techniques of investigation of the P2X7 receptor (P2X7R) in mammalian cells. *In:* GALLUZZI, L. & RUDQVIST, N.-P. (eds.) *Methods in Enzymology.* Academic Press.
DI VIRGILIO, F., SCHMALZING, G. & MARKWARDT, F. 2018. The Elusive P2X7 Macropore. *Trends in Cell Biology,* 28**,** 392-404.
DIAS, D. A., URBAN, S. & ROESSNER, U. 2012. A historical overview of natural products in drug discovery. *Metabolites,* 2**,** 303-36.
DICPINIGAITIS, P. V., MCGARVEY, L. P. & CANNING, B. J. 2020. P2X3-Receptor Antagonists as Potential Antitussives: Summary of Current Clinical Trials in Chronic Cough. *Lung,* 198**,** 609-616.
DING, S. & SACHS, F. 2000. Inactivation of P2X2 purinoceptors by divalent cations. *J Physiol,* 522 Pt 2**,** 199-214.
DONG, W.-W., XUAN, F.-L., ZHONG, F.-L., JIANG, J., WU, S., LI, D. & QUAN, L.-H. 2017. Comparative Analysis of the Rats' Gut Microbiota Composition in Animals with Different Ginsenosides Metabolizing Activity. *Journal of Agricultural and Food Chemistry,* 65**,** 327-337.
DONNELLY-ROBERTS, D. L., NAMOVIC, M. T., HAN, P. & JARVIS, M. F. 2009a. Mammalian P2X7 receptor pharmacology: comparison of recombinant mouse, rat and human P2X7 receptors. *British Journal of Pharmacology,* 157**,** 1203-1214.
DONNELLY-ROBERTS, D. L., NAMOVIC, M. T., SURBER, B., VAIDYANATHAN, S. X., PEREZ-MEDRANO, A., WANG, Y., CARROLL, W. A. & JARVIS, M. F. 2009b. [3H]A-804598 ([3H]2-cyano-1-[(1S)-1-phenylethyl]-3-quinolin-5-ylguanidine) is a novel, potent, and selective antagonist radioligand for P2X7 receptors. *Neuropharmacology,* 56**,** 223-229.
DOUGUET, L., JANHO DIT HREICH, S., BENZAQUEN, J., SEGUIN, L., JUHEL, T., DEZITTER, X., DURANTON, C., RYFFEL, B., KANELLOPOULOS, J., DELARASSE, C., RENAULT, N., FURMAN, C., HOMERIN, G., FÉRAL, C., CHERFILS-VICINI, J., MILLET, R., ADRIOUCH, S., GHINET, A., HOFMAN, P. & VOURET-CRAVIARI, V. 2021. A small-molecule P2RX7 activator promotes anti-tumor immune responses and sensitizes lung tumor to immunotherapy. *Nat Commun,* 12**,** 653.
DRURY, A. N. & SZENT-GYÖRGYI, A. 1929. The physiological activity of adenine compounds with especial reference to their action upon the mammalian heart1. *The Journal of Physiology,* 68**,** 213-237.
DUNN, P. M. & BLAKELEY, A. G. 1988. Suramin: a reversible P2-purinoceptor antagonist in the mouse vas deferens. *Br J Pharmacol,* 93**,** 243-5.
EGAN, T. M., HAINES, W. R. & VOIGT, M. M. 1998. A Domain Contributing to the Ion Channel of ATP-Gated P2X₂ Receptors Identified by the Substituted Cysteine Accessibility Method. *The Journal of Neuroscience,* 18**,** 2350.
EISE, N. T., SIMPSON, J. S., THOMPSON, P. E. & VENTURA, S. 2022. Aqueous extracts of Urtica dioica (stinging nettle) leaf contain a P2-purinoceptor antagonist-Implications for male fertility. *PLoS One,* 17**,** e0271735.
EVANS, R. J., LEWIS, C., VIRGINIO, C., LUNDSTROM, K., BUELL, G., SURPRENANT, A. & NORTH, R. A. 1996. Ionic permeability of, and divalent cation effects on, two ATP-gated cation channels (P2X receptors) expressed in mammalian cells. *J Physiol,* 497 (Pt 2)**,** 413-22.
EVOTEC. 2022. *Ad hoc: Evotec SE - Bayer discontinues clinical development candidate eliapixant (BAY1817080); Evotec regains the rights to all P2X3 assets* [Online]. https://www.evotec.com/en/investor-relations/news/p/ad-hoc-evotec-se---bayer-

discontinues-clinical-development-candidate-eliapixant-bay1817080-evotec-regains-the-rights-to-all-p2x3-assets-6141: Evotec. [Accessed 04/11 2022].
FAIRBAIRN, I. P., STOBER, C. B., KUMARARATNE, D. S. & LAMMAS, D. A. 2001. ATP-mediated killing of intracellular mycobacteria by macrophages is a P2X(7)-dependent process inducing bacterial death by phagosome-lysosome fusion. *J Immunol,* 167**,** 3300-7.
FALETRA, F., GIROTTO, G., D'ADAMO, A. P., VOZZI, D., MORGAN, A. & GASPARINI, P. 2014. A novel P2RX2 mutation in an Italian family affected by autosomal dominant nonsyndromic hearing loss. *Gene,* 534**,** 236-9.
FERRARI, D., CHIOZZI, P., FALZONI, S., DAL SUSINO, M., MELCHIORRI, L., BARICORDI, O. R. & DI VIRGILIO, F. 1997a. Extracellular ATP triggers IL-1 beta release by activating the purinergic P2Z receptor of human macrophages. *J Immunol,* 159**,** 1451-8.
FERRARI, D., CHIOZZI, P., FALZONI, S., HANAU, S. & DI VIRGILIO, F. 1997b. Purinergic modulation of interleukin-1 beta release from microglial cells stimulated with bacterial endotoxin. *J Exp Med,* 185**,** 579-82.
FERRARI, D., LOS, M., BAUER, M. K., VANDENABEELE, P., WESSELBORG, S. & SCHULZE-OSTHOFF, K. 1999. P2Z purinoreceptor ligation induces activation of caspases with distinct roles in apoptotic and necrotic alterations of cell death. *FEBS Lett,* 447**,** 71-5.
FERRARI, D., PIZZIRANI, C., ADINOLFI, E., FORCHAP, S., SITTA, B., TURCHET, L., FALZONI, S., MINELLI, M., BARICORDI, R. & DI VIRGILIO, F. 2004. The antibiotic polymyxin B modulates P2X7 receptor function. *J Immunol,* 173**,** 4652-60.
FERRARI, D., VILLALBA, M., CHIOZZI, P., FALZONI, S., RICCIARDI-CASTAGNOLI, P. & DI VIRGILIO, F. 1996. Mouse microglial cells express a plasma membrane pore gated by extracellular ATP. *J Immunol,* 156**,** 1531-9.
FINGER, T. E., DANILOVA, V., BARROWS, J., BARTEL, D. L., VIGERS, A. J., STONE, L., HELLEKANT, G. & KINNAMON, S. C. 2005. ATP signaling is crucial for communication from taste buds to gustatory nerves. *Science,* 310**,** 1495-9.
FISCHER, W., URBAN, N., IMMIG, K., FRANKE, H. & SCHAEFER, M. 2014. Natural compounds with P2X7 receptor-modulating properties. *Purinergic Signalling,* 10**,** 313-326.
FLITTIGER, B., KLAPPERSTÜCK, M., SCHMALZING, G. & MARKWARDT, F. 2010. Effects of protons on macroscopic and single-channel currents mediated by the human P2X7 receptor. *Biochimica et Biophysica Acta (BBA) - Biomembranes,* 1798**,** 947-957.
FORD, A. P. D. W., GEVER, J. R., NUNN, P. A., ZHONG, Y., CEFALU, J. S., DILLON, M. P. & COCKAYNE, D. A. 2006. Purinoceptors as therapeutic targets for lower urinary tract dysfunction. *British Journal of Pharmacology,* 147**,** S132-S143.
FORD, R., LEROUX, F. & STOCKS, M. 2003. *Novel adamantane derivatives*. 02/10/2003.
FRANCESCHINI, A., CAPECE, M., CHIOZZI, P., FALZONI, S., SANZ, J. M., SARTI, A. C., BONORA, M., PINTON, P. & DI VIRGILIO, F. 2015. The P2X7 receptor directly interacts with the NLRP3 inflammasome scaffold protein. *The FASEB Journal,* 29**,** 2450-2461.
FRANKLIN, K. M., ASATRYAN, L., JAKOWEC, M. W., TRUDELL, J. R., BELL, R. L. & DAVIES, D. L. 2014. P2X4 receptors (P2X4Rs) represent a novel target for the development of drugs to prevent and/or treat alcohol use disorders. *Frontiers in Neuroscience,* 8.
FRANKLIN, K. M., HAUSER, S. R., LASEK, A. W., BELL, R. L. & MCBRIDE, W. J. 2015. Involvement of Purinergic P2X4 Receptors in Alcohol Intake of High-Alcohol-Drinking (HAD) Rats. *Alcoholism: Clinical and Experimental Research,* 39**,** 2022-2031.
FREDHOLM, B. B., AP, I. J., JACOBSON, K. A., KLOTZ, K. N. & LINDEN, J. 2001. International Union of Pharmacology. XXV. Nomenclature and classification of adenosine receptors. *Pharmacol Rev,* 53**,** 527-52.
FRIEDRICH, C., FRANCKE, K., GASHAW, I., SCHEERANS, C., KLEIN, S., FELS, L., SMITH, J. A., HUMMEL, T. & MORICE, A. 2022. Safety, Pharmacodynamics, and Pharmacokinetics of P2X3 Receptor Antagonist Eliapixant (BAY 1817080) in Healthy Subjects: Double-Blind Randomized Study. *Clin Pharmacokinet,* 61**,** 1143-1156.

FUJIWARA, M., OHBORI, K., OHISHI, A., NISHIDA, K., UOZUMI, Y. & NAGASAWA, K. 2017. Species Difference in Sensitivity of Human and Mouse P2X7 Receptors to Inhibitory Effects of Divalent Metal Cations. *Biol Pharm Bull,* 40**,** 375-380.

GARCEAU, D. & CHAURET, N. 2019a. BLU-5937: A selective P2X3 antagonist with potent anti-tussive effect and no taste alteration. *Pulm Pharmacol Ther,* 56**,** 56-62.

GARCEAU, D. & CHAURET, N. 2019b. BLU-5937: A selective P2X3 antagonist with potent anti-tussive effect and no taste alteration. *Pulmonary Pharmacology & Therapeutics,* 56**,** 56-62.

GARCIA-GUZMAN, M., SOTO, F., GOMEZ-HERNANDEZ, J. M., LUND, P. E. & STÜHMER, W. 1997a. Characterization of recombinant human P2X4 receptor reveals pharmacological differences to the rat homologue. *Mol Pharmacol,* 51**,** 109-18.

GARCIA-GUZMAN, M., STÜHMER, W. & SOTO, F. 1997b. Molecular characterization and pharmacological properties of the human P2X3 purinoceptor. *Molecular Brain Research,* 47**,** 59-66.

GARGETT, C. E., CORNISH, J. E. & WILEY, J. S. 1997. ATP, a partial agonist for the P2Z receptor of human lymphocytes. *Br J Pharmacol,* 122**,** 911-7.

GARGETT, C. E. & WILEY, J. S. 1997. The isoquinoline derivative KN-62 a potent antagonist of the P2Z-receptor of human lymphocytes. *Br J Pharmacol,* 120**,** 1483-90.

GARTLAND, A., HIPSKIND, R. A., GALLAGHER, J. A. & BOWLER, W. B. 2001. Expression of a P2X7 receptor by a subpopulation of human osteoblasts. *J Bone Miner Res,* 16**,** 846-56.

GARTLAND, A., SKARRATT, K. K., HOCKING, L. J., PARSONS, C., STOKES, L., JØRGENSEN, N. R., FRASER, W. D., REID, D. M., GALLAGHER, J. A. & WILEY, J. S. 2012. Polymorphisms in the P2X7 receptor gene are associated with low lumbar spine bone mineral density and accelerated bone loss in post-menopausal women. *Eur J Hum Genet,* 20**,** 559-64.

GENNARI, C., CARCANO, M., DONGHI, M., MONGELLI, N., VANOTTI, E. & VULPETTI, A. 1997. Taxol Semisynthesis: A Highly Enantio- and Diastereoselective Synthesis of the Side Chain and a New Method for Ester Formation at C-13 Using Thioesters. *The Journal of Organic Chemistry,* 62**,** 4746-4755.

GEVER, J. R., COCKAYNE, D. A., DILLON, M. P., BURNSTOCK, G. & FORD, A. P. 2006. Pharmacology of P2X channels. *Pflugers Arch,* 452**,** 513-37.

GEVER, J. R., SOTO, R., HENNINGSEN, R. A., MARTIN, R. S., HACKOS, D. H., PANICKER, S., RUBAS, W., OGLESBY, I. B., DILLON, M. P., MILLA, M. E., BURNSTOCK, G. & FORD, A. P. 2010. AF-353, a novel, potent and orally bioavailable P2X3/P2X2/3 receptor antagonist. *Br J Pharmacol,* 160**,** 1387-98.

GIANNUZZO, A., PEDERSEN, S. F. & NOVAK, I. 2015. The P2X7 receptor regulates cell survival, migration and invasion of pancreatic ductal adenocarcinoma cells. *Molecular Cancer,* 14**,** 203.

GILBERT, S. M., GIDLEY BAIRD, A., GLAZER, S., BARDEN, J. A., GLAZER, A., TEH, L. C. & KING, J. 2017. A phase I clinical trial demonstrates that nfP2X(7) -targeted antibodies provide a novel, safe and tolerable topical therapy for basal cell carcinoma. *Br J Dermatol,* 177**,** 117-124.

GILBERT, S. M., OLIPHANT, C. J., HASSAN, S., PEILLE, A. L., BRONSERT, P., FALZONI, S., DI VIRGILIO, F., MCNULTY, S. & LARA, R. 2019. ATP in the tumour microenvironment drives expression of nfP2X7, a key mediator of cancer cell survival. *Oncogene,* 38**,** 194-208.

GIULIANI, A. L., COLOGNESI, D., RICCO, T., RONCATO, C., CAPECE, M., AMOROSO, F., WANG, Q. G., DE MARCHI, E., GARTLAND, A., DI VIRGILIO, F. & ADINOLFI, E. 2014. Trophic Activity of Human P2X7 Receptor Isoforms A and B in Osteosarcoma. *PLOS ONE,* 9**,** e107224.

GOODMAN, J., WALSH, V. & WALSH, P. I. M. M. B. S. V. 2001. *The Story of Taxol: Nature and Politics in the Pursuit of an Anti-Cancer Drug*, Cambridge University Press.

GORDON, J. L. 1986. Extracellular ATP: effects, sources and fate. *Biochem J,* 233**,** 309-19.

GREENWOOD, D., YAO, W. P. & HOUSLEY, G. D. 1997. Expression of the P2X2 receptor subunit of the ATP-gated ion channel in the retina. *Neuroreport,* 8**,** 1083-8.

GUBERT, C., FRIES, G. R., PFAFFENSELLER, B., FERRARI, P., COUTINHO-SILVA, R., MORRONE, F. B., KAPCZINSKI, F. & BATTASTINI, A. M. O. 2016. Role of P2X7 Receptor in an Animal Model of Mania Induced by D-Amphetamine. *Molecular Neurobiology,* 53**,** 611-620.

HARKAT, M., PEVERINI, L., CERDAN, A. H., DUNNING, K., BEUDEZ, J., MARTZ, A., CALIMET, N., SPECHT, A., CECCHINI, M., CHATAIGNEAU, T. & GRUTTER, T. 2017. On the permeation of large organic cations through the pore of ATP-gated P2X receptors. *Proceedings of the National Academy of Sciences,* 114**,** E3786-E3795.

HARTZELL, C., PUTZIER, I. & ARREOLA, J. 2004. CALCIUM-ACTIVATED CHLORIDE CHANNELS. *Annual Review of Physiology,* 67**,** 719-758.

HATTORI, M. & GOUAUX, E. 2012. Molecular mechanism of ATP binding and ion channel activation in P2X receptors. *Nature,* 485**,** 207-12.

HAUSMANN, R., RETTINGER, J., GEREVICH, Z., MEIS, S., KASSACK, M. U., ILLES, P., LAMBRECHT, G. & SCHMALZING, G. 2006. The suramin analog NF110 potently blocks P2X3 receptors: subtype selectivity is determined by location of sulfonic acid groups. *Molecular Pharmacology*.

HE, B. & SODERLUND, D. M. 2010. Human embryonic kidney (HEK293) cells express endogenous voltage-gated sodium currents and Na v 1.7 sodium channels. *Neurosci Lett,* 469**,** 268-72.

HE, M.-L., ZEMKOVA, H., KOSHIMIZU, T.-A., TOMIĆ, M. & STOJILKOVIC, S. S. 2003. Intracellular calcium measurements as a method in studies on activity of purinergic P2X receptor channels. *American Journal of Physiology-Cell Physiology,* 285**,** C467-C479.

HECHLER, B., LENAIN, N., MARCHESE, P., VIAL, C., HEIM, V., FREUND, M., CAZENAVE, J. P., CATTANEO, M., RUGGERI, Z. M., EVANS, R. & GACHET, C. 2003. A role of the fast ATP-gated P2X1 cation channel in thrombosis of small arteries in vivo. *J Exp Med,* 198**,** 661-7.

HECHLER, B., MAGNENAT, S., ZIGHETTI, M. L., KASSACK, M. U., ULLMANN, H., CAZENAVE, J. P., EVANS, R., CATTANEO, M. & GACHET, C. 2005. Inhibition of platelet functions and thrombosis through selective or nonselective inhibition of the platelet P2 receptors with increasing doses of NF449 [4,4',4'',4'''-(carbonylbis(imino-5,1,3-benzenetriylbis-(carbonylimino)))tetrakis-benzene-1,3-disulfonic acid octasodium salt]. *J Pharmacol Exp Ther,* 314**,** 232-43.

HELLIWELL, R. M., SHIOUKHUEY, C. O., DHUNA, K., MOLERO, J. C., YE, J. M., XUE, C. C. & STOKES, L. 2015. Selected ginsenosides of the protopanaxdiol series are novel positive allosteric modulators of P2X7 receptors. *Br J Pharmacol,* 172**,** 3326-40.

HERNANDEZ-OLMOS, V., ABDELRAHMAN, A., EL-TAYEB, A., FREUDENDAHL, D., WEINHAUSEN, S. & MULLER, C. E. 2012. N-substituted phenoxazine and acridone derivatives: structure-activity relationships of potent P2X4 receptor antagonists. *J Med Chem,* 55**,** 9576-88.

HOEBERTZ, A., TOWNSEND-NICHOLSON, A., GLASS, R., BURNSTOCK, G. & ARNETT, T. R. 2000. Expression of P2 receptors in bone and cultured bone cells. *Bone,* 27**,** 503-10.

HONORE, P., DONNELLY-ROBERTS, D., NAMOVIC, M., ZHONG, C., WADE, C., CHANDRAN, P., ZHU, C., CARROLL, W., PEREZ-MEDRANO, A., IWAKURA, Y. & JARVIS, M. F. 2009. The antihyperalgesic activity of a selective P2X7 receptor antagonist, A-839977, is lost in IL-1alphabeta knockout mice. *Behav Brain Res,* 204**,** 77-81.

HONORE, P., DONNELLY-ROBERTS, D., NAMOVIC, M. T., HSIEH, G., ZHU, C. Z., MIKUSA, J. P., HERNANDEZ, G., ZHONG, C., GAUVIN, D. M., CHANDRAN, P., HARRIS, R., MEDRANO, A. P., CARROLL, W., MARSH, K., SULLIVAN, J. P., FALTYNEK, C. R. & JARVIS, M. F. 2006. A-740003 [N-(1-{[(Cyanoimino)(5-quinolinylamino) methyl]amino}-2,2-dimethylpropyl)-2-(3,4-dimethoxyphenyl)acetamide], a Novel and Selective P2X₇ Receptor Antagonist, Dose-Dependently Reduces Neuropathic Pain in the Rat. *Journal of Pharmacology and Experimental Therapeutics,* 319**,** 1376.

HOU, M., WANG, R., ZHAO, S. & WANG, Z. 2021. Ginsenosides in Panax genus and their biosynthesis. *Acta Pharm Sin B,* 11**,** 1813-1834.

HOULT, R. 1979. Cell membrane receptors for drugs and hormones: A multidisciplinary approach. *FEBS Letters,* 103**,** 375-375.

HOURANI, S. M. O. 1996. Purinoceptors and platelet aggregation. *Journal of Autonomic Pharmacology,* 16**,** 349-352.

HOUSLEY, G. D., JAGGER, D. J., GREENWOOD, D., RAYBOULD, N. P., SALIH, S. G., JÄRLEBARK, L. E., VLAJKOVIC, S. M., KANJHAN, R., NIKOLIC, P., MUÑOZ, D. J. M. & THORNE, P. R. 2002. Purinergic Regulation of Sound Transduction and Auditory Neurotransmission. *Audiology and Neurotology,* 7**,** 55-61.

HOUSLEY, G. D., KANJHAN, R., RAYBOULD, N. P., GREENWOOD, D., SALIH, S. G., JÄRLEBARK, L., BURTON, L. D., SETZ, V. C., CANNELL, M. B., SOELLER, C., CHRISTIE, D. L., USAMI, S., MATSUBARA, A., YOSHIE, H., RYAN, A. F. & THORNE, P. R. 1999. Expression of the P2X(2) receptor subunit of the ATP-gated ion channel in the cochlea: implications for sound transduction and auditory neurotransmission. *J Neurosci,* 19**,** 8377-88.

HU, B., MEI, Q. B., YAO, X. J., SMITH, E., BARRY, W. H. & LIANG, B. T. 2001. A novel contractile phenotype with cardiac transgenic expression of the human P2X4 receptor. *Faseb j,* 15**,** 2739-41.

HÜLSMANN, M., NICKEL, P., KASSACK, M., SCHMALZING, G., LAMBRECHT, G. & MARKWARDT, F. 2003. NF449, a novel picomolar potency antagonist at human P2X1 receptors. *Eur J Pharmacol,* 470**,** 1-7.

IARC 2016. *Some Drugs and Herbal Products.,* Lyon, France, International Agency for Research on Cancer.

ILLES, P., MÜLLER, C. E., JACOBSON, K. A., GRUTTER, T., NICKE, A., FOUNTAIN, S. J., KENNEDY, C., SCHMALZING, G., JARVIS, M. F., STOJILKOVIC, S. S., KING, B. F. & DI VIRGILIO, F. 2021. Update of P2X receptor properties and their pharmacology: IUPHAR Review 30. *British Journal of Pharmacology,* 178**,** 489-514.

ILYASKIN, A. V., SURE, F., NESTEROV, V., HAERTEIS, S. & KORBMACHER, C. 2019. Bile acids inhibit human purinergic receptor P2X4 in a heterologous expression system. *Journal of General Physiology,* 151**,** 820-833.

IMMADISETTY, K., ALENCIKS, J. & KEKENES-HUSKEY, P. 2021. Modulation of P2X4 pore closure by magnesium, potassium, and ATP. *bioRxiv***,** 2021.05.16.444323.

IMMADISETTY, K., ALENCIKS, J. & KEKENES-HUSKEY, P. M. 2022. Modulation of P2X4 pore closure by magnesium, potassium, and ATP. *Biophysical Journal,* 121**,** 1134-1142.

INSCHO, E. W., COOK, A. K., IMIG, J. D., VIAL, C. & EVANS, R. J. 2003. Physiological role for P2X1 receptors in renal microvascular autoregulatory behavior. *J Clin Invest,* 112**,** 1895-905.

INSCHO, E. W., COOK, A. K., IMIG, J. D., VIAL, C. & EVANS, R. J. 2004. Renal autoregulation in P2X1 knockout mice. *Acta Physiol Scand,* 181**,** 445-53.

JACOBSON, K. A., KIM, Y.-C., WILDMAN, S. S., MOHANRAM, A., HARDEN, T. K., BOYER, J. L., KING, B. F. & BURNSTOCK, G. 1998. A Pyridoxine Cyclic Phosphate and Its 6-Azoaryl Derivative Selectively Potentiate and Antagonize Activation of P2X1 Receptors. *Journal of Medicinal Chemistry,* 41**,** 2201-2206.

JAIME-FIGUEROA, S., GREENHOUSE, R., PADILLA, F., DILLON, M. P., GEVER, J. R. & FORD, A. P. D. W. 2005. Discovery and synthesis of a novel and selective drug-like P2X1 antagonist. *Bioorganic & Medicinal Chemistry Letters,* 15**,** 3292-3295.

JARVIS, M. F., BURGARD, E. C., MCGARAUGHTY, S., HONORE, P., LYNCH, K., BRENNAN, T. J., SUBIETA, A., VAN BIESEN, T., CARTMELL, J., BIANCHI, B., NIFORATOS, W., KAGE, K., YU, H., MIKUSA, J., WISMER, C. T., ZHU, C. Z., CHU, K., LEE, C. H., STEWART, A. O., POLAKOWSKI, J., COX, B. F., KOWALUK, E., WILLIAMS, M., SULLIVAN, J. & FALTYNEK, C. 2002. A-317491, a novel potent and selective non-nucleotide antagonist of P2X3 and P2X2/3 receptors, reduces chronic inflammatory and neuropathic pain in the rat. *Proc Natl Acad Sci U S A,* 99**,** 17179-84.

JARVIS, M. F. & KHAKH, B. S. 2009. ATP-gated P2X cation-channels. *Neuropharmacology,* 56**,** 208-215.

JIANG, L.-H., MACKENZIE, A. B., NORTH, R. A. & SURPRENANT, A. 2000. Brilliant Blue G Selectively Blocks ATP-Gated Rat P2X₇ Receptors. *Molecular Pharmacology,* 58**,** 82.

JIANG, L.-H. & ROGER, S. 2020. Heterologous Expression and Patch-Clamp Recording of P2X Receptors in HEK293 Cells. *In:* PELEGRÍN, P. (ed.) *Purinergic Signaling: Methods and Protocols.* New York, NY: Springer New York.

JIANG, L. H. 2009. Inhibition of P2X(7) receptors by divalent cations: old action and new insight. *Eur Biophys J,* 38**,** 339-46.

JOH, E.-H., LEE, I.-A., JUNG, I.-H. & KIM, D.-H. 2011. Ginsenoside Rb1 and its metabolite compound K inhibit IRAK-1 activation—The key step of inflammation. *Biochemical Pharmacology,* 82**,** 278-286.

JONES, C. A., CHESSELL, I. P., SIMON, J., BARNARD, E. A., MILLER, K. J., MICHEL, A. D. & HUMPHREY, P. P. 2000. Functional characterization of the P2X(4) receptor orthologues. *British journal of pharmacology,* 129**,** 388-394.

JUNG, K. Y., MOON, H. D., LEE, G. E., LIM, H. H., PARK, C. S. & KIM, Y. C. 2007. Structure-activity relationship studies of spinorphin as a potent and selective human P2X(3) receptor antagonist. *J Med Chem,* 50**,** 4543-7.

JØRGENSEN, N. R., HENRIKSEN, Z., SØRENSEN, O. H., ERIKSEN, E. F., CIVITELLI, R. & STEINBERG, T. H. 2002. Intercellular calcium signaling occurs between human osteoblasts and osteoclasts and requires activation of osteoclast P2X7 receptors. *J Biol Chem,* 277**,** 7574-80.

KACZMAREK-HÁJEK, K., LÖRINCZI, E., HAUSMANN, R. & NICKE, A. 2012. Molecular and functional properties of P2X receptors--recent progress and persisting challenges. *Purinergic Signal,* 8.

KANJHAN, R., HOUSLEY, G. D., THORNE, P. R., CHRISTIE, D. L., PALMER, D. J., LUO, L. & RYAN, A. F. 1996. Localization of ATP-gated ion channels in cerebellum using P2x2R subunit-specific antisera. *Neuroreport,* 7**,** 2665-9.

KARASAWA, A., MICHALSKI, K., MIKHELZON, P. & KAWATE, T. 2017. The P2X7 receptor forms a dye-permeable pore independent of its intracellular domain but dependent on membrane lipid composition. *Elife,* 6.

KASUYA, G., YAMAURA, T., MA, X.-B., NAKAMURA, R., TAKEMOTO, M., NAGUMO, H., TANAKA, E., DOHMAE, N., NAKANE, T., YU, Y., ISHITANI, R., MATSUZAKI, O., HATTORI, M. & NUREKI, O. 2017. Structural insights into the competitive inhibition of the ATP-gated P2X receptor channel. *Nature Communications,* 8**,** 876.

KE, H. Z., QI, H., WEIDEMA, A. F., ZHANG, Q., PANUPINTHU, N., CRAWFORD, D. T., GRASSER, W. A., PARALKAR, V. M., LI, M., AUDOLY, L. P., GABEL, C. A., JEE, W. S., DIXON, S. J., SIMS, S. M. & THOMPSON, D. D. 2003. Deletion of the P2X7 nucleotide receptor reveals its regulatory roles in bone formation and resorption. *Mol Endocrinol,* 17**,** 1356-67.

KENNEDY, C. 2007. MRS2159. *In:* ENNA, S. J. & BYLUND, D. B. (eds.) *xPharm: The Comprehensive Pharmacology Reference.* New York: Elsevier.

KHAKH, B. S., BAO, X. R., LABARCA, C. & LESTER, H. A. 1999a. Neuronal P2X transmitter-gated cation channels change their ion selectivity in seconds. *Nat Neurosci,* 2**,** 322-30.

KHAKH, B. S., PROCTOR, W. R., DUNWIDDIE, T. V., LABARCA, C. & LESTER, H. A. 1999b. Allosteric control of gating and kinetics at P2X(4) receptor channels. *J Neurosci,* 19**,** 7289-99.

KHOJA, S., HUYNH, N., ASATRYAN, L., JAKOWEC, M. W. & DAVIES, D. L. 2018a. Reduced expression of purinergic P2X4 receptors increases voluntary ethanol intake in C57BL/6J mice. *Alcohol,* 68**,** 63-70.

KHOJA, S., HUYNH, N., WARNECKE, A. M. P., ASATRYAN, L., JAKOWEC, M. W. & DAVIES, D. L. 2018b. Preclinical evaluation of avermectins as novel therapeutic agents for alcohol use disorders. *Psychopharmacology (Berl),* 235**,** 1697-1709.

KIM, H., PARK, C. W. & CHO, S. H. 2018. The Beneficial Effect of Korean Red Ginseng Extract on Atopic Dermatitis Patients: An 8 Weeks Open, Noncomparative Clinical Study. *Ann Dermatol,* 30**,** 304-308.

KIM, J. H., YI, Y. S., KIM, M. Y. & CHO, J. Y. 2017. Role of ginsenosides, the main active components of Panax ginseng, in inflammatory responses and diseases. *J Ginseng Res,* 41**,** 435-443.

KIM, N. D., KIM, E. M., KANG, K. W., CHO, M. K., CHOI, S. Y. & KIM, S. G. 2003. Ginsenoside Rg3 inhibits phenylephrine-induced vascular contraction through induction of nitric oxide synthase. *Br J Pharmacol,* 140**,** 661-70.

KING, B. F. 2022. Rehabilitation of the P2X5 receptor: a re-evaluation of structure and function. *Purinergic Signalling*.

KING, B. F., WILDMAN, S. S., ZIGANSHINA, L. E., PINTOR, J. & BURNSTOCK, G. 1997. Effects of extracellular pH on agonism and antagonism at a recombinant P2X2 receptor. *Br J Pharmacol,* 121**,** 1445-53.

KLEIN, S., GASHAW, I., BAUMANN, S., CHANG, X., HUMMEL, T., THUß, U. & FRIEDRICH, C. 2022. First-in-human study of eliapixant (BAY 1817080), a highly selective P2X3 receptor antagonist: Tolerability, safety and pharmacokinetics. *Br J Clin Pharmacol,* 88**,** 4552-4564.

KOH, E., JANG, O.-H., HWANG, K.-H., AN, Y.-N. & MOON, B. 2015. Effects of Steaming and Air-Drying on Ginsenoside Composition of Korean Ginseng (Panax ginseng C.A. Meyer). *Journal of Food Processing and Preservation,* 39**,** 207-213.

KOSHIMIZU, T., KOSHIMIZU, M. & STOJILKOVIC, S. S. 1999. Contributions of the C-terminal domain to the control of P2X receptor desensitization. *J Biol Chem,* 274**,** 37651-7.

KOSHLUKOVA, S. E., ARAUJO, M. W., BAEV, D. & EDGERTON, M. 2000. Released ATP is an extracellular cytotoxic mediator in salivary histatin 5-induced killing of Candida albicans. *Infect Immun,* 68**,** 6848-56.

KOTNIS, S., BINGHAM, B., VASILYEV, D. V., MILLER, S. W., BAI, Y., YEOLA, S., CHANDA, P. K., BOWLBY, M. R., KAFTAN, E. J., SAMAD, T. A. & WHITESIDE, G. T. 2010. Genetic and functional analysis of human P2X5 reveals a distinct pattern of exon 10 polymorphism with predominant expression of the nonfunctional receptor isoform. *Mol Pharmacol,* 77**,** 953-60.

KUANG, X. J., ZHANG, C. Y., YAN, B. Y., CAI, W. Z., LU, C. L., XIE, L. J., LI, S. J., KONG, P. L., FAN, J., PAN, S. M., GUO, T. & CAO, X. 2022. P2X2 receptors in pyramidal neurons are critical for regulating vulnerability to chronic stress. *Theranostics,* 12**,** 3703-3718.

LAMMAS, D. A., STOBER, C., HARVEY, C. J., KENDRICK, N., PANCHALINGAM, S. & KUMARARATNE, D. S. 1997. ATP-Induced Killing of Mycobacteria by Human Macrophages Is Mediated by Purinergic P2Z(P2X₇) Receptors. *Immunity,* 7**,** 433-444.

LARA, R., ADINOLFI, E., HARWOOD, C. A., PHILPOTT, M., BARDEN, J. A., DI VIRGILIO, F. & MCNULTY, S. 2020. P2X7 in Cancer: From Molecular Mechanisms to Therapeutics. *Frontiers in Pharmacology,* 11.

LE FEUVRE, R. A., BROUGH, D., IWAKURA, Y., TAKEDA, K. & ROTHWELL, N. J. 2002. Priming of macrophages with lipopolysaccharide potentiates P2X7-mediated cell death via a caspase-1-dependent mechanism, independently of cytokine production. *J Biol Chem,* 277**,** 3210-8.

LEE, I. A., HYAM, S. R., JANG, S. E., HAN, M. J. & KIM, D. H. 2012. Ginsenoside Re ameliorates inflammation by inhibiting the binding of lipopolysaccharide to TLR4 on macrophages. *J Agric Food Chem,* 60**,** 9595-602.

LEE, J. H., CHIBA, T. & MARCUS, D. C. 2001. P2X₂ Receptor Mediates Stimulation of Parasensory Cation Absorption by Cochlear Outer Sulcus Cells and Vestibular Transitional Cells. *The Journal of Neuroscience,* 21**,** 9168.

LETAVIC, M. A., SAVALL, B. M., ALLISON, B. D., ALUISIO, L., ANDRES, J. I., DE ANGELIS, M., AO, H., BEAUCHAMP, D. A., BONAVENTURE, P., BRYANT, S., CARRUTHERS, N. I., CEUSTERS, M., COE, K. J., DVORAK, C. A., FRASER, I. C., GELIN, C. F., KOUDRIAKOVA, T., LIANG, J., LORD, B., LOVENBERG, T. W., OTIENO, M. A., SCHOETENS, F., SWANSON, D. M., WANG, Q., WICKENDEN, A. D. & BHATTACHARYA, A. 2017. 4-Methyl-6,7-dihydro-4H-triazolo[4,5-c]pyridine-Based P2X7 Receptor Antagonists: Optimization of Pharmacokinetic Properties Leading to the Identification of a Clinical Candidate. *Journal of Medicinal Chemistry,* 60**,** 4559-4572.

LEUNG, K. W. & WONG, A. S. 2010. Pharmacology of ginsenosides: a literature review. *Chin Med,* 5**,** 20.

LEWIS, C., NEIDHART, S., HOLY, C., NORTH, R. A., BUELL, G. & SURPRENANT, A. 1995. Coexpression of P2X2 and P2X3 receptor subunits can account for ATP-gated currents in sensory neurons. *Nature,* 377**,** 432-5.

LEWIS, C. J., ENNION, S. J. & EVANS, R. J. 2000. P2 purinoceptor-mediated control of rat cerebral (pial) microvasculature; contribution of P2X and P2Y receptors. *The Journal of Physiology,* 527**,** 315-324.

LI, L., ZOU, Y., LIU, B., YANG, R., YANG, J., SUN, M., LI, Z., XU, X., LI, G., LIU, S., GREFFRATH, W., TREEDE, R.-D., LI, G. & LIANG, S. 2020. Contribution of the P2X4 Receptor in Rat Hippocampus to the Comorbidity of Chronic Pain and Depression. *ACS Chemical Neuroscience,* 11**,** 4387-4397.

LI, M., WANG, Y., BANERJEE, R., MARINELLI, F., SILBERBERG, S., FARALDO-GÓMEZ, J. D., HATTORI, M. & SWARTZ, K. J. 2019. Molecular mechanisms of human P2X3 receptor channel activation and modulation by divalent cation bound ATP. *Elife,* 8.

LI, S. & CHAN, Z. 2018. Evaluation of antifatigue effects of 20(S)-ginsenoside Rg3 in forced swimming mice. *Indian Journal of Pharmaceutical Sciences,* 80**,** 510-515.

LI, S. & ZHANG, W. 2014. Ethnobotany of Camptotheca Decaisne: New Discoveries of Old Medicinal Uses. *Pharmaceutical Crops,* 5**,** 140-145.

LIN, S., HUANG, L., LUO, Z. C., LI, X., JIN, S. Y., DU, Z. J., WU, D. Y., XIONG, W. C., LUO, Z. Y., SONG, Y. L., WANG, Q., LIU, X. W., MA, R. J., WANG, M. L., REN, C. R., YANG, J. M. & GAO, T. M. 2022. The ATP Level in the Medial Prefrontal Cortex Regulates Depressive-like Behavior via the Medial Prefrontal Cortex-Lateral Habenula Pathway. *Biol Psychiatry,* 92**,** 179-192.

LIU, X., MA, W., SURPRENANT, A. & JIANG, L. H. 2009. Identification of the amino acid residues in the extracellular domain of rat P2X(7) receptor involved in functional inhibition by acidic pH. *Br J Pharmacol,* 156**,** 135-42.

LIU, X., SURPRENANT, A., MAO, H. J., ROGER, S., XIA, R., BRADLEY, H. & JIANG, L. H. 2008. Identification of key residues coordinating functional inhibition of P2X7 receptors by zinc and copper. *Mol Pharmacol,* 73**,** 252-9.

LIÑÁN-RICO, A., WUNDERLICH, J. E., ENNEKING, J. T., TSO, D. R., GRANTS, I., WILLIAMS, K. C., OTEY, A., MICHEL, K., SCHEMANN, M., NEEDLEMAN, B., HARZMAN, A. & CHRISTOFI, F. L. 2015. Neuropharmacology of purinergic receptors in human submucous plexus: Involvement of P2X1, P2X2, P2X3 channels, P2Y and A3 metabotropic receptors in neurotransmission. *Neuropharmacology,* 95**,** 83-99.

LOESCH, A. & BURNSTOCK, G. 1998. Electron-immunocytochemical localization of P2X1 receptors in the rat cerebellum. *Cell Tissue Res,* 294**,** 253-60.

LONGHURST, P. A., SCHWEGEL, T., FOLANDER, K. & SWANSON, R. 1996. The human P2x1 receptor: molecular cloning, tissue distribution, and localization to chromosome 17. *Biochim Biophys Acta,* 1308**,** 185-8.

LORZ, L. R., KIM, M. Y. & CHO, J. Y. 2020. Medicinal potential of Panax ginseng and its ginsenosides in atopic dermatitis treatment. *J Ginseng Res,* 44**,** 8-13.

LUSTIG, K. D., SHIAU, A. K., BRAKE, A. J. & JULIUS, D. 1993. Expression cloning of an ATP receptor from mouse neuroblastoma cells. *Proc Natl Acad Sci U S A,* 90**,** 5113-7.

LYNCH, K. J., TOUMA, E., NIFORATOS, W., KAGE, K. L., BURGARD, E. C., VAN BIESEN, T., KOWALUK, E. A. & JARVIS, M. F. 1999. Molecular and functional characterization of human P2X(2) receptors. *Mol Pharmacol,* 56**,** 1171-81.

MACKENZIE, A. B., MAHAUT-SMITH, M. P. & SAGE, S. O. 1996. Activation of receptor-operated cation channels via P2X1 not P2T purinoceptors in human platelets. *J Biol Chem,* 271**,** 2879-81.

MAHAUT-SMITH, M. P., ENNION, S. J., ROLF, M. G. & EVANS, R. J. 2000. ADP is not an agonist at P2X(1) receptors: evidence for separate receptors stimulated by ATP and ADP on human platelets. *Br J Pharmacol,* 131**,** 108-14.

MANCUSO, C. & SANTANGELO, R. 2017. Panax ginseng and Panax quinquefolius: From pharmacology to toxicology. *Food and Chemical Toxicology,* 107**,** 362-372.

MARKHAM, A. 2022. Gefapixant: First Approval. *Drugs,* 82**,** 691-695.
MARQUES-DA-SILVA, C., CHAVES, M. M., CASTRO, N. G., COUTINHO-SILVA, R. & GUIMARAES, M. Z. P. 2011. Colchicine inhibits cationic dye uptake induced by ATP in P2X2 and P2X7 receptor-expressing cells: implications for its therapeutic action. *British Journal of Pharmacology,* 163**,** 912-926.
MARTÍNEZ, M., MARTÍNEZ, N. A. & SILVA, W. I. 2017. Measurement of the Intracellular Calcium Concentration with Fura-2 AM Using a Fluorescence Plate Reader. *Bio Protoc,* 7**,** e2411.
MARUCCI, G., DAL BEN, D., BUCCIONI, M., MARTÍ NAVIA, A., SPINACI, A., VOLPINI, R. & LAMBERTUCCI, C. 2019. Update on novel purinergic P2X3 and P2X2/3 receptor antagonists and their potential therapeutic applications. *Expert Opin Ther Pat,* 29**,** 943-963.
MATSUMURA, Y., YAMASHITA, T., SASAKI, A., NAKATA, E., KOHNO, K., MASUDA, T., TOZAKI-SAITOH, H., IMAI, T., KURAISHI, Y., TSUDA, M. & INOUE, K. 2016. A novel P2X4 receptor-selective antagonist produces anti-allodynic effect in a mouse model of herpetic pain. *Scientific Reports,* 6**,** 32461.
MCCARTHY, A. E., YOSHIOKA, C. & MANSOOR, S. E. 2019. Full-Length P2X(7) Structures Reveal How Palmitoylation Prevents Channel Desensitization. *Cell,* 179**,** 659-670.e13.
MCGARAUGHTY, S., WISMER, C. T., ZHU, C. Z., MIKUSA, J., HONORE, P., CHU, K. L., LEE, C. H., FALTYNEK, C. R. & JARVIS, M. F. 2003. Effects of A-317491, a novel and selective P2X3/P2X2/3 receptor antagonist, on neuropathic, inflammatory and chemogenic nociception following intrathecal and intraplantar administration. *Br J Pharmacol,* 140**,** 1381-8.
MCGARVEY, L., BIRRING, S., MORICE, A., DICPINIGAITIS, P., PAVORD, I., SCHELFHOUT, J., MARTIN NGUYEN, A., LI, Q., TZONTCHEVA, A., ISKOLD, B., GREEN, S., LA ROSA, C., MUCCINO, D. & SMITH, J. 2020. Late Breaking Abstract - Two Phase 3 Randomized Clinical Trials of Gefapixant, a P2X3 Receptor Antagonist, in Refractory or Unexplained Chronic Cough (COUGH-1 and COUGH-2). *European Respiratory Journal,* 56**,** 3800.
MCGARVEY, L. P., BIRRING, S. S., MORICE, A. H., DICPINIGAITIS, P. V., PAVORD, I. D., SCHELFHOUT, J., NGUYEN, A. M., LI, Q., TZONTCHEVA, A., ISKOLD, B., GREEN, S. A., ROSA, C., MUCCINO, D. R. & SMITH, J. A. 2022. Efficacy and safety of gefapixant, a P2X(3) receptor antagonist, in refractory chronic cough and unexplained chronic cough (COUGH-1 and COUGH-2): results from two double-blind, randomised, parallel-group, placebo-controlled, phase 3 trials. *Lancet,* 399**,** 909-923.
MELNIK, S., WRIGHT, M., TANNER, J. A., TSINTSADZE, T., TSINTSADZE, V., MILLER, A. D. & LOZOVAYA, N. 2006. Diadenosine Polyphosphate Analog Controls Postsynaptic Excitation in CA3-CA1 Synapses via a Nitric Oxide-Dependent Mechanism. *Journal of Pharmacology and Experimental Therapeutics,* 318**,** 579.
MENG, F. & LOWELL, C. A. 1997. Lipopolysaccharide (LPS)-induced macrophage activation and signal transduction in the absence of Src-family kinases Hck, Fgr, and Lyn. *J Exp Med,* 185**,** 1661-70.
MERCK. 2022. *Merck Provides U.S. and Japan Regulatory Update for Gefapixant* [Online]. Merck. Available: https://www.merck.com/news/merck-provides-u-s-and-japan-regulatory-update-for-gefapixant/ [Accessed 15/11 2022].
MICHEL, A. D., CHAMBERS, L. J. & WALTER, D. S. 2008. Negative and positive allosteric modulators of the P2X(7) receptor. *British journal of pharmacology,* 153**,** 737-750.
MILLER, K. J., MICHEL, A. D., CHESSELL, I. P. & HUMPHREY, P. P. A. 1998. Cibacron blue allosterically modulates the rat P2X4 receptor. *Neuropharmacology,* 37**,** 1579-1586.
MOLECULAR DEVICES. 2023. *Technology of FLIPR Membrane Potential Assay Kits* [Online]. https://www.moleculardevices.com/products/assay-kits/ion-channel/flipr-membrane-potential#Technology. Available: https://www.moleculardevices.com/products/assay-kits/ion-channel/flipr-membrane-potential#Technology [Accessed 19/06 2023].
MOLNÁR, K., NÓGRÁDI, B., KRISTÓF, R., MÉSZÁROS, Á., PAJER, K., SIKLÓS, L., NÓGRÁDI, A., WILHELM, I. & KRIZBAI, I. A. 2022. Motoneuronal inflammasome activation triggers excessive

neuroinflammation and impedes regeneration after sciatic nerve injury. *J Neuroinflammation,* 19**,** 68.
MOORE, S. F. & MACKENZIE, A. B. 2008. Species and agonist dependent zinc modulation of endogenous and recombinant ATP-gated P2X7 receptors. *Biochemical Pharmacology,* 76**,** 1740-1747.
MORICE, A., DICPINIGAITIS, P., MCGARVEY, L. & BIRRING, S. S. 2021a. Chronic cough: new insights and future prospects. *European Respiratory Review,* 30**,** 210127.
MORICE, A., SMITH, J. A., MCGARVEY, L., BIRRING, S. S., PARKER, S. M., TURNER, A., HUMMEL, T., GASHAW, I., FELS, L., KLEIN, S., FRANCKE, K. & FRIEDRICH, C. 2021b. Eliapixant (BAY 1817080), a P2X3 receptor antagonist, in refractory chronic cough: a randomised, placebo-controlled, crossover phase 2a study. *Eur Respir J,* 58.
MOTEKI, H., AZAIEZ, H., BOOTH, K. T., HATTORI, M., SATO, A., SATO, Y., MOTOBAYASHI, M., SLOAN, C. M., KOLBE, D. L., SHEARER, A. E., SMITH, R. J. & USAMI, S. 2015. Hearing loss caused by a P2RX2 mutation identified in a MELAS family with a coexisting mitochondrial 3243AG mutation. *Ann Otol Rhinol Laryngol,* 124 Suppl 1**,** 177s-83s.
MULRYAN, K., GITTERMAN, D. P., LEWIS, C. J., VIAL, C., LECKIE, B. J., COBB, A. L., BROWN, J. E., CONLEY, E. C., BUELL, G., PRITCHARD, C. A. & EVANS, R. J. 2000. Reduced vas deferens contraction and male infertility in mice lacking P2X1 receptors. *Nature,* 403**,** 86-9.
MURGIA, M., HANAU, S., PIZZO, P., RIPPA, M. & DI VIRGILIO, F. 1993. Oxidized ATP. An irreversible inhibitor of the macrophage purinergic P2Z receptor. *J Biol Chem,* 268**,** 8199-203.
MUÑOZ, D. J., KENDRICK, I. S., RASSAM, M. & THORNE, P. R. 2001. Vesicular storage of adenosine triphosphate in the guinea-pig cochlear lateral wall and concentrations of ATP in the endolymph during sound exposure and hypoxia. *Acta Otolaryngol,* 121**,** 10-5.
MUÑOZ, D. J., THORNE, P. R., HOUSLEY, G. D. & BILLETT, T. E. 1995. Adenosine 5'-triphosphate (ATP) concentrations in the endolymph and perilymph of the guinea-pig cochlea. *Hear Res,* 90**,** 119-25.
NAKAZAWA, K. & OHNO, Y. 1997. Effects of neuroamines and divalent cations on cloned and mutated ATP-gated channels. *European Journal of Pharmacology,* 325**,** 101-108.
NEELANDS, T. R., BURGARD, E. C., UCHIC, M. E., MCDONALD, H. A., NIFORATOS, W., FALTYNEK, C. R., LYNCH, K. J. & JARVIS, M. F. 2003. 2', 3'-O-(2,4,6,trinitrophenyl)-ATP and A-317491 are competitive antagonists at a slowly desensitizing chimeric human P2X3 receptor. *Br J Pharmacol,* 140**,** 202-10.
NELSON, D. W., GREGG, R. J., KORT, M. E., PEREZ-MEDRANO, A., VOIGHT, E. A., WANG, Y., GRAYSON, G., NAMOVIC, M. T., DONNELLY-ROBERTS, D. L., NIFORATOS, W., HONORE, P., JARVIS, M. F., FALTYNEK, C. R. & CARROLL, W. A. 2006. Structure-activity relationship studies on a series of novel, substituted 1-benzyl-5-phenyltetrazole P2X7 antagonists. *J Med Chem,* 49**,** 3659-66.
NESSELHUT, J., BARDEN, J., MARX, D., CILLIEN, N., GOEBEL, W., HERRMANN, M., CHANG, R. Y. & NESSELHUT, T. 2013. NfP2X7, a novel target for immune therapeutic approaches in cancer treatment. *Journal of Clinical Oncology,* 31**,** 3094-3094.
NICOL, R. W., TRAQUAIR, J. A. & BERNARDS, M. A. 2002. Ginsenosides as host resistance factors in American ginseng (Panax quinquefolius). *Canadian Journal of Botany,* 80**,** 557-562.
NIIMI, A., SAGARA, H., KIKUCHI, M., ARANO, I., SATO, A., SHIRAKAWA, M., LA ROSA, C. & MUCCINO, D. 2022. A phase 3, randomized, double-blind, clinical study to evaluate the long-term safety and efficacy of gefapixant in Japanese adult participants with refractory or unexplained chronic cough. *Allergol Int,* 71**,** 498-504.
NORTH, R. A. 2002. Molecular physiology of P2X receptors. *Physiol Rev,* 82**,** 1013-67.
NÖRENBERG, W., HEMPEL, C., URBAN, N., SOBOTTKA, H., ILLES, P. & SCHAEFER, M. 2011. Clemastine potentiates the human P2X7 receptor by sensitizing it to lower ATP concentrations. *The Journal of biological chemistry,* 286**,** 11067-11081.
NÖRENBERG, W. & ILLES, P. 2000. Neuronal P2X receptors: localisation and functional properties. *Naunyn Schmiedebergs Arch Pharmacol,* 362**,** 324-39.

NÖRENBERG, W., SOBOTTKA, H., HEMPEL, C., PLÖTZ, T., FISCHER, W., SCHMALZING, G. & SCHAEFER, M. 2012. Positive allosteric modulation by ivermectin of human but not murine P2X7 receptors. *British journal of pharmacology,* 167**,** 48-66.

OSBOURN, A. E. 1996. Preformed Antimicrobial Compounds and Plant Defense against Fungal Attack. *Plant Cell,* 8**,** 1821-1831.

OSMOND, D. A. & INSCHO, E. W. 2010. P2X(1) receptor blockade inhibits whole kidney autoregulation of renal blood flow in vivo. *Am J Physiol Renal Physiol,* 298**,** F1360-8.

OURY, C., KUIJPERS, M. J., TOTH-ZSAMBOKI, E., BONNEFOY, A., DANLOY, S., VREYS, I., FEIJGE, M. A., DE VOS, R., VERMYLEN, J., HEEMSKERK, J. W. & HOYLAERTS, M. F. 2003. Overexpression of the platelet P2X1 ion channel in transgenic mice generates a novel prothrombotic phenotype. *Blood,* 101**,** 3969-76.

PANUPINTHU, N., ROGERS, J. T., ZHAO, L., SOLANO-FLORES, L. P., POSSMAYER, F., SIMS, S. M. & DIXON, S. J. 2008. P2X7 receptors on osteoblasts couple to production of lysophosphatidic acid: a signaling axis promoting osteogenesis. *Journal of Cell Biology,* 181**,** 859-871.

PARKER, K. E. 1998. Modulation of ATP-gated non-selective cation channel (P2X1 receptor) activation and desensitization by the actin cytoskeleton. *The Journal of Physiology,* 510**,** 19-25.

PASQUALETTO, G., BRANCALE, A. & YOUNG, M. T. 2018. The Molecular Determinants of Small-Molecule Ligand Binding at P2X Receptors. *Front Pharmacol,* 9**,** 58.

PELLEGATTI, P., RAFFAGHELLO, L., BIANCHI, G., PICCARDI, F., PISTOIA, V. & DI VIRGILIO, F. 2008. Increased Level of Extracellular ATP at Tumor Sites: In Vivo Imaging with Plasma Membrane Luciferase. *PLoS ONE,* 3**,** e2599.

PERSZYK, R., KATZMAN, B. M., KUSUMOTO, H., KELL, S. A., EPPLIN, M. P., TAHIROVIC, Y. A., MOORE, R. L., MENALDINO, D., BURGER, P., LIOTTA, D. C. & TRAYNELIS, S. F. 2018. An NMDAR positive and negative allosteric modulator series share a binding site and are interconverted by methyl groups. *eLife,* 7**,** e34711.

PEVERINI, L., BEUDEZ, J., DUNNING, K., CHATAIGNEAU, T. & GRUTTER, T. 2018. New Insights Into Permeation of Large Cations Through ATP-Gated P2X Receptors. *Frontiers in Molecular Neuroscience,* 11.

PHILLIPS, J. K., MCLEAN, A. J. & HILL, C. E. 1998. Receptors involved in nerve-mediated vasoconstriction in small arteries of the rat hepatic mesentery. *British Journal of Pharmacology,* 124**,** 1403-1412.

PIYASIRANANDA, W., BEEKMAN, A., GANESAN, A., BIDULA, S. & STOKES, L. 2021. Insights into the Structure-Activity Relationship of Glycosides as Positive Allosteric Modulators Acting on P2X7 Receptors. *Molecular pharmacology,* 99**,** 163-174.

PRATT, E. B., BRINK, T. S., BERGSON, P., VOIGT, M. M. & COOK, S. P. 2005. Use-Dependent Inhibition of P2X₃ Receptors by Nanomolar Agonist. *The Journal of Neuroscience,* 25**,** 7359.

PRIEL, A. & SILBERBERG, S. D. 2004. Mechanism of ivermectin facilitation of human P2X4 receptor channels. *J Gen Physiol,* 123**,** 281-93.

PUNTHAMBAKER, S., BLUM, J. A. & HUME, R. I. 2012. High potency zinc modulation of human P2X2 receptors and low potency zinc modulation of rat P2X2 receptors share a common molecular mechanism. *J Biol Chem,* 287**,** 22099-111.

PUNTHAMBAKER, S. & HUME, R. I. 2014. Potent and long-lasting inhibition of human P2X2 receptors by copper. *Neuropharmacology,* 77**,** 167-76.

RAE, M. G., ROWAN, E. G. & KENNEDY, C. 1998. Pharmacological properties of P2X3-receptors present in neurones of the rat dorsal root ganglia. *British Journal of Pharmacology,* 124**,** 176-180.

RASSENDREN, F., BUELL, G., NEWBOLT, A., NORTH, R. A. & SURPRENANT, A. 1997a. Identification of amino acid residues contributing to the pore of a P2X receptor. *The EMBO Journal,* 16**,** 3446-3454.

RASSENDREN, F., BUELL, G. N., VIRGINIO, C., COLLO, G., NORTH, R. A. & SURPRENANT, A. 1997b. The permeabilizing ATP receptor, P2X7. Cloning and expression of a human cDNA. *J Biol Chem,* 272**,** 5482-6.

RATAN, Z. A., HAIDERE, M. F., HONG, Y. H., PARK, S. H., LEE, J.-O., LEE, J. & CHO, J. Y. 2021. Pharmacological potential of ginseng and its major component ginsenosides. *Journal of Ginseng Research,* 45**,** 199-210.

RECOURT, K., VAN DER AART, J., JACOBS, G., DE KAM, M., DREVETS, W., VAN NUETEN, L., KANHAI, K., SIEBENGA, P., ZUIKER, R., RAVENSTIJN, P., TIMMERS, M., VAN GERVEN, J. & DE BOER, P. 2020. Characterisation of the pharmacodynamic effects of the P2X7 receptor antagonist JNJ-54175446 using an oral dexamphetamine challenge model in healthy males in a randomised, double-blind, placebo-controlled, multiple ascending dose trial. *J Psychopharmacol,* 34**,** 1030-1042.

REN, W. J. & ILLES, P. 2022. Involvement of P2X7 receptors in chronic pain disorders. *Purinergic Signal,* 18**,** 83-92.

RETTINGER, J., BRAUN, K., HOCHMANN, H., KASSACK, M. U., ULLMANN, H., NICKEL, P., SCHMALZING, G. & LAMBRECHT, G. 2005. Profiling at recombinant homomeric and heteromeric rat P2X receptors identifies the suramin analogue NF449 as a highly potent P2X1 receptor antagonist. *Neuropharmacology,* 48**,** 461-468.

RETTINGER, J., SCHMALZING, G., DAMER, S., MÜLLER, G., NICKEL, P. & LAMBRECHT, G. 2000. The suramin analogue NF279 is a novel and potent antagonist selective for the P2X1 receptor. *Neuropharmacology,* 39**,** 2044-2053.

REYNOLDS, S. M., MACKENZIE, A. J., SPINA, D. & PAGE, C. P. 2004. The pharmacology of cough. *Trends in Pharmacological Sciences,* 25**,** 569-576.

RIBEIRO, C., NEIVA, R., SILVA, D., CORREIA-DE-SÁ, P. & FONTES-SOUSA, A. P. 2022. REDUCTION OF HEART RATE VIA P2X4 RECEPTOR ACTIVATION AS A PROMISING TREATMENT STRATEGY IN PULMONARY ARTERIAL HYPERTENSION. *Journal of Hypertension,* 40**,** e232-e233.

ROBERTS, J. A., ALLSOPP, R. C., EL AJOUZ, S., VIAL, C., SCHMID, R., YOUNG, M. T. & EVANS, R. J. 2012. Agonist binding evokes extensive conformational changes in the extracellular domain of the ATP-gated human P2X1 receptor ion channel. *Proceedings of the National Academy of Sciences,* 109**,** 4663-4667.

ROBERTS, J. A. & EVANS, R. J. 2004. ATP Binding at Human P2X1 Receptors: CONTRIBUTION OF AROMATIC AND BASIC AMINO ACIDS REVEALED USING MUTAGENESIS AND PARTIAL AGONISTS. *Journal of Biological Chemistry,* 279**,** 9043-9055.

ROBERTS, J. A. & EVANS, R. J. 2007. Cysteine substitution mutants give structural insight and identify ATP binding and activation sites at P2X receptors. *J Neurosci,* 27**,** 4072-82.

RUEPP, M.-D., BROZIK, J. A., DE ESCH, I. J. P., FARNDALE, R. W., MURRELL-LAGNADO, R. D. & THOMPSON, A. J. 2015. A fluorescent approach for identifying P2X1 ligands. *Neuropharmacology,* 98**,** 13-21.

RUPERT, M., BHATTACHARYA, A., STILLEROVA, V. T., JINDRICHOVA, M., MOKDAD, A., BOUÉ-GRABOT, E. & ZEMKOVA, H. 2020. Role of Conserved Residues and F322 in the Extracellular Vestibule of the Rat P2X7 Receptor in Its Expression, Function and Dye Uptake Ability. *Int J Mol Sci,* 21.

SAKAMURU, S., ATTENE-RAMOS, M. S. & XIA, M. 2016. Mitochondrial Membrane Potential Assay. *In:* ZHU, H. & XIA, M. (eds.) *High-Throughput Screening Assays in Toxicology.* New York, NY: Springer New York.

SAMWAYS, D. S., KHAKH, B. S., DUTERTRE, S. & EGAN, T. M. 2011. Preferential use of unobstructed lateral portals as the access route to the pore of human ATP-gated ion channels (P2X receptors). *Proc Natl Acad Sci U S A,* 108**,** 13800-5.

SANZ, J. M., CHIOZZI, P. & DI VIRGILIO, F. 1998. Tenidap enhances P2Z/P2X7 receptor signalling in macrophages. *Eur J Pharmacol,* 355**,** 235-44.

SAUNDERS, B. M., FERNANDO, S. L., SLUYTER, R., BRITTON, W. J. & WILEY, J. S. 2003. A loss-of-function polymorphism in the human P2X7 receptor abolishes ATP-mediated killing of mycobacteria. *J Immunol,* 171**,** 5442-6.

SAVI, P., BORNIA, J., SALEL, V., DELFAUD, M. & HERBERT, J. M. 1997. Characterization of P2x1 purinoreceptors on rat platelets: effect of clopidogrel. *Br J Haematol,* 98**,** 880-6.

SAVIO, L. E. B., DE ANDRADE MELLO, P., DA SILVA, C. G. & COUTINHO-SILVA, R. 2018. The P2X7 Receptor in Inflammatory Diseases: Angel or Demon? *Frontiers in Pharmacology,* 9.

SCASE, T. J., HEATH, M. F., ALLEN, J. M., SAGE, S. O. & EVANS, R. J. 1998. Identification of a P2X1 purinoceptor expressed on human platelets. *Biochem Biophys Res Commun,* 242**,** 525-8.

SCHILLER, I. C., JACOBSON, K. A., WEN, Z., MALISETTY, A., SCHMALZING, G. & MARKWARDT, F. 2022. Dihydropyridines Potentiate ATP-Induced Currents Mediated by the Full-Length Human P2X5 Receptor. *Molecules* [Online], 27.

SCHMIDT, A., JOUSSEN, S., HAUSMANN, R., GRÜNDER, S. & WIEMUTH, D. 2019. Bile acids are potent inhibitors of rat P2X2 receptors. *Purinergic Signalling,* 15**,** 213-221.

SCHNEIDER, R., LEVEN, P., GLOWKA, T., KUZMANOV, I., LYSSON, M., SCHNEIKER, B., MIESEN, A., BAQI, Y., SPANIER, C., GRANTS, I., MAZZOTTA, E., VILLALOBOS-HERNANDEZ, E., KALFF, J. C., MÜLLER, C. E., CHRISTOFI, F. L. & WEHNER, S. 2021. A novel P2X2-dependent purinergic mechanism of enteric gliosis in intestinal inflammation. *EMBO Molecular Medicine,* 13**,** e12724.

SEARS, J. E. & BOGER, D. L. 2015. Total synthesis of vinblastine, related natural products, and key analogues and development of inspired methodology suitable for the systematic study of their structure-function properties. *Acc Chem Res,* 48**,** 653-62.

SHARMA, A. & LEE, H.-J. 2020. Ginsenoside Compound K: Insights into Recent Studies on Pharmacokinetics and Health-Promoting Activities. *Biomolecules* [Online], 10.

SHIPTON, E. A., SHIPTON, E. E. & SHIPTON, A. J. 2018. A Review of the Opioid Epidemic: What Do We Do About It? *Pain and Therapy,* 7**,** 23-36.

SIVCEV, S., SLAVIKOVA, B., IVETIC, M., KNEZU, M., KUDOVA, E. & ZEMKOVA, H. 2020. Lithocholic acid inhibits P2X2 and potentiates P2X4 receptor channel gating. *The Journal of Steroid Biochemistry and Molecular Biology,* 202**,** 105725.

SIVCEV, S., SLAVIKOVA, B., RUPERT, M., IVETIC, M., NEKARDOVA, M., KUDOVA, E. & ZEMKOVA, H. 2019. Synthetic testosterone derivatives modulate rat P2X2 and P2X4 receptor channel gating. *Journal of Neurochemistry,* 150**,** 28-43.

SMITH, J. A., KITT, M. M., MORICE, A. H., BIRRING, S. S., MCGARVEY, L. P., SHER, M. R., LI, Y.-P., WU, W.-C., XU, Z. J., MUCCINO, D. R., FORD, A. P., SMITH, J., MCGARVEY, L., BIRRING, S., HULL, J., CARR, W. W., GOLDSOBEL, A. B., GROSS, G. N., HOLCOMB, J. R., HUSSAIN, I., SHER, M., SPANGENTHAL, S., STORMS, W., MORICE, A., ELKAYAM, D., STEVEN, G. C., KRAINSON, J., FAKIH, F. A., MATZ, J., BROOKS, G. D., CASALE, T., BERMAN, G. D., CONDEMI, J. J., GREOS, L. S., GOGATE, S. U., SHER, E. R., FRIESEN, J. H., SCHENKEL, E. J., BERNSTEIN, D. I., CORREN, J., SUNDAR, K., GOTFRIED, M. H., MONTANARO, A., LUMRY, W. R., AMAR, N. J., KAPLAN, M. S., PRENNER, B. M., MURPHY, T. R., GOOD, J. S., PARKER, S., HARRISON, T., PAVORD, I., BRIGHTLING, C., DJUKANOVIC, R., MCQUAID, D., DENENBERG, M., ETTINGER, N. A. & IYER, V. 2020. Gefapixant, a P2X3 receptor antagonist, for the treatment of refractory or unexplained chronic cough: a randomised, double-blind, controlled, parallel-group, phase 2b trial. *The Lancet Respiratory Medicine,* 8**,** 775-785.

SOTO, F., LAMBRECHT, G., NICKEL, P., STÜHMER, W. & BUSCH, A. E. 1999. Antagonistic properties of the suramin analogue NF023 at heterologously expressed P2X receptors. *Neuropharmacology,* 38**,** 141-149.

STOCK, T. C., BLOOM, B. J., WEI, N., ISHAQ, S., PARK, W., WANG, X., GUPTA, P. & MEBUS, C. A. 2012. Efficacy and safety of CE-224,535, an antagonist of P2X7 receptor, in treatment of patients with rheumatoid arthritis inadequately controlled by methotrexate. *J Rheumatol,* 39**,** 720-7.

STOKES, L., BIDULA, S., BIBIČ, L. & ALLUM, E. 2020. To Inhibit or Enhance? Is There a Benefit to Positive Allosteric Modulation of P2X Receptors? *Frontiers in Pharmacology,* 11**,** 627.

STOKES, L., FULLER, S. J., SLUYTER, R., SKARRATT, K. K., GU, B. J. & WILEY, J. S. 2010. Two haplotypes of the P2X(7) receptor containing the Ala-348 to Thr polymorphism exhibit a gain-of-function effect and enhanced interleukin-1beta secretion. *Faseb j,* 24**,** 2916-27.

STOKES, L., JIANG, L. H., ALCARAZ, L., BENT, J., BOWERS, K., FAGURA, M., FURBER, M., MORTIMORE, M., LAWSON, M., THEAKER, J., LAURENT, C., BRADDOCK, M. & SURPRENANT, A. 2006a. Characterization of a selective and potent antagonist of human P2X7 receptors, AZ11645373. *British Journal of Pharmacology,* 149**,** 880-887.

STOKES, L., JIANG, L. H., ALCARAZ, L., BENT, J., BOWERS, K., FAGURA, M., FURBER, M., MORTIMORE, M., LAWSON, M., THEAKER, J., LAURENT, C., BRADDOCK, M. & SURPRENANT, A. 2006b. Characterization of a selective and potent antagonist of human P2X(7) receptors, AZ11645373. *British journal of pharmacology,* 149**,** 880-887.

STOKES, L., LAYHADI, J. A., BIBIC, L., DHUNA, K. & FOUNTAIN, S. J. 2017. P2X4 Receptor Function in the Nervous System and Current Breakthroughs in Pharmacology. *Frontiers in Pharmacology,* 8.

STOKES, L., SCURRAH, K., ELLIS, J. A., CROMER, B. A., SKARRATT, K. K., GU, B. J., HARRAP, S. B. & WILEY, J. S. 2011. A loss-of-function polymorphism in the human P2X4 receptor is associated with increased pulse pressure. *Hypertension,* 58**,** 1086-92.

STONE, E. 1763. XXXII. An account of the success of the bark of the willow in the cure of agues. In a letter to the Right Honourable George Earl of Macclesfield, President of R. S. from the Rev. Mr. Edward Stone, of Chipping-Norton in Oxfordshire. *Philosophical Transactions of the Royal Society of London,* 53**,** 195-200.

STOOP, R., SURPRENANT, A. & NORTH, R. A. 1997. Different sensitivities to pH of ATP-induced currents at four cloned P2X receptors. *J Neurophysiol,* 78**,** 1837-40.

SUN, D., JUNGER, W. G., YUAN, C., ZHANG, W., BAO, Y., QIN, D., WANG, C., TAN, L., QI, B., ZHU, D., ZHANG, X. & YU, T. 2013. Shockwaves Induce Osteogenic Differentiation of Human Mesenchymal Stem Cells Through ATP Release and Activation of P2X7 Receptors. *Stem Cells,* 31**,** 1170-1180.

SUNG, W. S. & LEE, D. G. 2008. In Vitro Candidacidal Action of Korean Red Ginseng Saponins against Candida albicans. *Biological and Pharmaceutical Bulletin,* 31**,** 139-142.

SURPRENANT, A., RASSENDREN, F., KAWASHIMA, E., NORTH, R. A. & BUELL, G. 1996. The cytolytic P2Z receptor for extracellular ATP identified as a P2X receptor (P2X7). *Science,* 272**,** 735-8.

SYED, M. B. & PONNUSAMY, T. 2018. Bioconversion of mevastatin to pravastatin by various microorganisms and its applications – A review. *Biocatalysis and Agricultural Biotechnology,* 13**,** 62-74.

SYED, N.-I.-H. & KENNEDY, C. 2012. Pharmacology of P2X receptors. *Wiley Interdisciplinary Reviews: Membrane Transport and Signaling,* 1**,** 16-30.

SÉGUÉLA, P., HAGHIGHI, A., SOGHOMONIAN, J. J. & COOPER, E. 1996. A novel neuronal P2x ATP receptor ion channel with widespread distribution in the brain. *J Neurosci,* 16**,** 448-55.

TAKIMOTO, Y., ISHIDA, Y., KONDO, M., IMAI, T., HANADA, Y., OZONO, Y., KAMAKURA, T., INOHARA, H. & SHIMADA, S. 2018. P2X2 Receptor Deficiency in Mouse Vestibular End Organs Attenuates Vestibular Function. *Neuroscience,* 386**,** 41-50.

TELANG, R. S., PARAMANANTHASIVAM, V., VLAJKOVIC, S. M., MUNOZ, D. J., HOUSLEY, G. D. & THORNE, P. R. 2010. Reduced P2x(2) receptor-mediated regulation of endocochlear potential in the ageing mouse cochlea. *Purinergic Signal,* 6**,** 263-72.

THORNE, P. R., MUÑOZ, D. J. B. & HOUSLEY, G. D. 2004. Purinergic Modulation of Cochlear Partition Resistance and Its Effect on the Endocochlear Potential in the Guinea Pig. *Journal of the Association for Research in Otolaryngology,* 5**,** 58-65.

TIAN, M., ABDELRAHMAN, A., BAQI, Y., FUENTES, E., AZAZNA, D., SPANIER, C., DENSBORN, S., HINZ, S., SCHMID, R. & MÜLLER, C. E. 2020. Discovery and Structure Relationships of Salicylanilide

Derivatives as Potent, Non-acidic P2X1 Receptor Antagonists. *Journal of Medicinal Chemistry,* 63**,** 6164-6178.
TITTLE, R. K. & HUME, R. I. 2008. Opposite effects of zinc on human and rat P2X2 receptors. *J Neurosci,* 28**,** 11131-40.
TORRES, G. E., EGAN, T. M. & VOIGT, M. M. 1999. Hetero-oligomeric assembly of P2X receptor subunits. Specificities exist with regard to possible partners. *J Biol Chem,* 274**,** 6653-9.
TREZISE, D. J., MICHEL, A. D., GRAHAMES, C. B. A., KHAKH, B. S., SURPRENANT, A. & HUMPHREY, P. P. A. 1995. The selective P2X purinoceptor agonist, β,γ-methylene-L-adenosine 5'-triphosphate, discriminates between smooth muscle and neuronal P2X purinoceptors. *Naunyn-Schmiedeberg's Archives of Pharmacology,* 351**,** 603-609.
TSUDA, M., KUBOYAMA, K., INOUE, T., NAGATA, K., TOZAKI-SAITOH, H. & INOUE, K. 2009. Behavioral phenotypes of mice lacking purinergic P2X4 receptors in acute and chronic pain assays. *Mol Pain,* 5**,** 28.
TSUDA, M., SHIGEMOTO-MOGAMI, Y., KOIZUMI, S., MIZOKOSHI, A., KOHSAKA, S., SALTER, M. W. & INOUE, K. 2003. P2X4 receptors induced in spinal microglia gate tactile allodynia after nerve injury. *Nature,* 424**,** 778-83.
ULMANN, L., HATCHER, J. P., HUGHES, J. P., CHAUMONT, S., GREEN, P. J., CONQUET, F., BUELL, G. N., REEVE, A. J., CHESSELL, I. P. & RASSENDREN, F. 2008. Up-regulation of P2X4 receptors in spinal microglia after peripheral nerve injury mediates BDNF release and neuropathic pain. *J Neurosci,* 28**,** 11263-8.
URBANEK, E., NICKEL, P. & SCHLICKER, E. 1990. Antagonistic properties of four suramin-related compounds at vascular purine P2X receptors in the pithed rat. *European Journal of Pharmacology,* 175**,** 207-210.
USDA, SERVICE, A. R. & SYSTEM, N. P. G. 2023a. *Panax ginseng*. National Germplasm Resources Laboratory, Beltsville, Maryland.: Germplasm Resources Information Network (GRIN Taxonomy). .
USDA, SERVICE, A. R. & SYSTEM, N. P. G. 2023b. *Panax notoginseng*. National Germplasm Resources Laboratory, Beltsville, Maryland.: Germplasm Resources Information Network (GRIN Taxonomy).
VALERA, S., HUSSY, N., EVANS, R. J., ADAMI, N., NORTH, R. A., SURPRENANT, A. & BUELL, G. 1994. A new class of ligand-gated ion channel defined by P2x receptor for extracellular ATP. *Nature,* 371**,** 516-9.
VAN DER GIET, M., CINKILIC, O., JANKOWSKI, J., TEPEL, M., ZIDEK, W. & SCHLÜTER, H. 1999. Evidence for two different P2X-receptors mediating vasoconstriction of Ap5A and Ap6A in the isolated perfused rat kidney. *Br J Pharmacol,* 127**,** 1463-9.
VANDENBEUCH, A., LARSON, E. D., ANDERSON, C. B., SMITH, S. A., FORD, A. P., FINGER, T. E. & KINNAMON, S. C. 2015. Postsynaptic P2X3-containing receptors in gustatory nerve fibres mediate responses to all taste qualities in mice. *The Journal of Physiology,* 593**,** 1113-1125.
VELASQUEZ, S. & EUGENIN, E. 2014. Role of Pannexin-1 hemichannels and purinergic receptors in the pathogenesis of human diseases. *Frontiers in Physiology,* 5.
VIAL, C., HECHLER, B., LÉON, C., CAZENAVE, J. P. & GACHET, C. 1997. Presence of P2X1 purinoceptors in human platelets and megakaryoblastic cell lines. *Thromb Haemost,* 78**,** 1500-4.
VIRGINIO, C., CHURCH, D., NORTH, R. A. & SURPRENANT, A. 1997. Effects of divalent cations, protons and calmidazolium at the rat P2X7 receptor. *Neuropharmacology,* 36**,** 1285-94.
VIRGINIO, C., MACKENZIE, A., RASSENDREN, F. A., NORTH, R. A. & SURPRENANT, A. 1999. Pore dilation of neuronal P2X receptor channels. *Nat Neurosci,* 2**,** 315-21.
VIRGINIO, C., NORTH, R. A. & SURPRENANT, A. 1998a. Calcium permeability and block at homomeric and heteromeric P2X2 and P2X3 receptors, and P2X receptors in rat nodose neurones. *J Physiol,* 510 (Pt 1)**,** 27-35.

VIRGINIO, C., ROBERTSON, G., SURPRENANT, A. & NORTH, R. A. 1998b. Trinitrophenyl-Substituted Nucleotides Are Potent Antagonists Selective for P2X₁, P2X₃, and Heteromeric P2X_{2/3} Receptors. *Molecular Pharmacology,* 53**,** 969.

VISOVATTI, S. H., HYMAN, M. C., GOONEWARDENA, S. N., ANYANWU, A. C., KANTHI, Y., ROBICHAUD, P., WANG, J., PETROVIC-DJERGOVIC, D., RATTAN, R., BURANT, C. F. & PINSKY, D. J. 2016. Purinergic dysregulation in pulmonary hypertension. *Am J Physiol Heart Circ Physiol,* 311**,** H286-98.

VON ALBERTINI, M., PALMETSHOFER, A., KACZMAREK, E., KOZIAK, K., STROKA, D., GREY, S. T., STUHLMEIER, K. M. & ROBSON, S. C. 1998. Extracellular ATP and ADP Activate Transcription Factor NF-κB and Induce Endothelial Cell Apoptosis. *Biochemical and Biophysical Research Communications,* 248**,** 822-829.

VON KÜGELGEN, I. 2019. Pharmacology of P2Y receptors. *Brain Research Bulletin,* 151**,** 12-24.

VULCHANOVA, L., ARVIDSSON, U., RIEDL, M., WANG, J., BUELL, G., SURPRENANT, A., NORTH, R. A. & ELDE, R. 1996. Differential distribution of two ATP-gated channels (P2X receptors) determined by immunocytochemistry. *Proc Natl Acad Sci U S A,* 93**,** 8063-7.

WALL, M. E. & WANI, M. C. 1996. Camptothecin and taxol: from discovery to clinic. *Journal of Ethnopharmacology,* 51**,** 239-254.

WAN, Y., LIU, D., XIA, J., XU, J.-F., ZHANG, L., YANG, Y., WU, J.-J. & AO, H. 2022. Ginsenoside CK, rather than Rb1, possesses potential chemopreventive activities in human gastric cancer via regulating PI3K/AKT/NF-κB signal pathway. *Frontiers in Pharmacology,* 13.

WANG, C.-Z., NAMBA, N., GONOI, T., INAGAKI, N. & SEINO, S. 1996. Cloning and Pharmacological Characterization of a Fourth P2X Receptor Subtype Widely Expressed in Brain and Peripheral Tissues Including Various Endocrine Tissues. *Biochemical and Biophysical Research Communications,* 220**,** 196-202.

WANG, C. Z., DU, G. J., ZHANG, Z., WEN, X. D., CALWAY, T., ZHEN, Z., MUSCH, M. W., BISSONNETTE, M., CHANG, E. B. & YUAN, C. S. 2012. Ginsenoside compound K, not Rb1, possesses potential chemopreventive activities in human colorectal cancer. *Int J Oncol,* 40**,** 1970-6.

WANG, J. C., RAYBOULD, N. P., LUO, L., RYAN, A. F., CANNELL, M. B., THORNE, P. R. & HOUSLEY, G. D. 2003. Noise induces up-regulation of P2X2 receptor subunit of ATP-gated ion channels in the rat cochlea. *Neuroreport,* 14**,** 817-23.

WANG, N., AGRAWAL, A., JØRGENSEN, N. R. & GARTLAND, A. 2018. P2X7 receptor regulates osteoclast function and bone loss in a mouse model of osteoporosis. *Sci Rep,* 8**,** 3507.

WEBB, T. E., SIMON, J., KRISHEK, B. J., BATESON, A. N., SMART, T. G., KING, B. F., BURNSTOCK, G. & BARNARD, E. A. 1993. Cloning and functional expression of a brain G-protein-coupled ATP receptor. *FEBS Lett,* 324**,** 219-25.

WEE, J. J., MEE PARK, K. & CHUNG, A. S. 2011. Biological Activities of Ginseng and Its Application to Human Health. *In:* BENZIE, I. F. F. & WACHTEL-GALOR, S. (eds.) *Herbal Medicine: Biomolecular and Clinical Aspects.* Boca Raton (FL): CRC Press/Taylor & Francis

WEI, L., CASELEY, E., LI, D. & JIANG, L.-H. 2016. ATP-induced P2X Receptor-Dependent Large Pore Formation: How Much Do We Know? *Frontiers in Pharmacology,* 7**,** 5.

WESSELIUS, A., BOURS, M. J., HENRIKSEN, Z., SYBERG, S., PETERSEN, S., SCHWARZ, P., JØRGENSEN, N. R., VAN HELDEN, S. & DAGNELIE, P. C. 2013. Association of P2X7 receptor polymorphisms with bone mineral density and osteoporosis risk in a cohort of Dutch fracture patients. *Osteoporos Int,* 24**,** 1235-46.

WETSMAN, N. 2017. Inflammatory illness: Why the next wave of antidepressants may target the immune system. *Nature Medicine,* 23**,** 1009-1011.

WHITE, C. W., CHOONG, Y. T., SHORT, J. L., EXINTARIS, B., MALONE, D. T., ALLEN, A. M., EVANS, R. J. & VENTURA, S. 2013. Male contraception via simultaneous knockout of α1A-adrenoceptors and P2X1-purinoceptors in mice. *Proc Natl Acad Sci U S A,* 110**,** 20825-30.

WILDMAN, S. S., KING, B. F. & BURNSTOCK, G. 1999. Modulatory activity of extracellular H+ and Zn2+ on ATP-responses at rP2X1 and rP2X3 receptors. *British Journal of Pharmacology,* 128**,** 486-492.

WYATT, L. R., FINN, D. A., KHOJA, S., YARDLEY, M. M., ASATRYAN, L., ALKANA, R. L. & DAVIES, D. L. 2014. Contribution of P2X4 receptors to ethanol intake in male C57BL/6 mice. *Neurochemical research,* 39**,** 1127-1139.

WÉRA, O., LECUT, C., SERVAIS, L., HEGO, A., DELIERNEUX, C., JIANG, Z., KEUTGENS, A., EVANS, R. J., DELVENNE, P., LANCELLOTTI, P. & OURY, C. 2020. P2X1 ion channel deficiency causes massive bleeding in inflamed intestine and increases thrombosis. *Journal of Thrombosis and Haemostasis,* 18**,** 44-56.

XIA, G. Q., CAI, J. N., WU, X., FANG, Q., ZHAO, N. & LV, X. W. 2022. The mechanism by which ATP regulates alcoholic steatohepatitis through P2X4 and CD39. *Eur J Pharmacol,* 916**,** 174729.

XIANG, Y. Z., SHANG, H. C., GAO, X. M. & ZHANG, B. L. 2008. A comparison of the ancient use of ginseng in traditional Chinese medicine with modern pharmacological experiments and clinical trials. *Phytotherapy Research,* 22**,** 851-858.

XIONG, K., LI, C. & WEIGHT, F. F. 2000. Inhibition by ethanol of rat P2X(4) receptors expressed in Xenopus oocytes. *British journal of pharmacology,* 130**,** 1394-1398.

YAN, D., ZHU, Y., WALSH, T., XIE, D., YUAN, H., SIRMACI, A., FUJIKAWA, T., WONG, A. C. Y., LOH, T. L., DU, L., GRATI, M. H., VLAJKOVIC, S. M., BLANTON, S., RYAN, A. F., CHEN, Z.-Y., THORNE, P. R., KACHAR, B., TEKIN, M., ZHAO, H.-B., HOUSLEY, G. D., KING, M.-C. & LIU, X. Z. 2013. Mutation of the ATP-gated P2X(2) receptor leads to progressive hearing loss and increased susceptibility to noise. *Proceedings of the National Academy of Sciences of the United States of America,* 110**,** 2228-2233.

YAN, X., FAN, Y., WEI, W., WANG, P., LIU, Q., WEI, Y., ZHANG, L., ZHAO, G., YUE, J. & ZHOU, Z. 2014. Production of bioactive ginsenoside compound K in metabolically engineered yeast. *Cell Res.*

YAN, Z., LIANG, Z., OBSIL, T. & STOJILKOVIC, S. S. 2006. Participation of the Lys³¹³-Ile³³³ Sequence of the Purinergic P2X₄ Receptor in Agonist Binding and Transduction of Signals to the Channel Gate *. *Journal of Biological Chemistry,* 281**,** 32649-32659.

YANG, J.-L., HU, Z.-F., ZHANG, T.-T., GU, A.-D., GONG, T. & ZHU, P. 2018. Progress on the Studies of the Key Enzymes of Ginsenoside Biosynthesis. *Molecules* [Online], 23.

YANG, T., SHEN, J. B., YANG, R., REDDEN, J., DODGE-KAFKA, K., GRADY, J., JACOBSON, K. A. & LIANG, B. T. 2014. Novel protective role of endogenous cardiac myocyte P2X4 receptors in heart failure. *Circ Heart Fail,* 7**,** 510-8.

YARDLEY, M., WYATT, L., KHOJA, S., ASATRYAN, L., RAMAKER, M., FINN, D., ALKANA, R., HUYNH, N., LOUIE, S., PETASIS, N., BORTOLATO, M. & DAVIES, D. 2012. Ivermectin reduces alcohol intake and preference in mice. *Neuropharmacology,* 63**,** 190-201.

YILMAZ, O., YAO, L., MAEDA, K., ROSE, T. M., LEWIS, E. L., DUMAN, M., LAMONT, R. J. & OJCIUS, D. M. 2008. ATP scavenging by the intracellular pathogen Porphyromonas gingivalis inhibits P2X7-mediated host-cell apoptosis. *Cell Microbiol,* 10**,** 863-75.

YIN, Q., CHEN, H., MA, R.-H., ZHANG, Y.-Y., LIU, M.-M., THAKUR, K., ZHANG, J.-G. & WEI, Z.-J. 2021. Ginsenoside CK induces apoptosis of human cervical cancer HeLa cells by regulating autophagy and endoplasmic reticulum stress. *Food & Function,* 12**,** 5301-5316.

ZABORINA, O., MISRA, N., KOSTAL, J., KAMATH, S., KAPATRAL, V., EL-IDRISSI, M. E., PRABHAKAR, B. S. & CHAKRABARTY, A. M. 1999. P2Z-Independent and P2Z receptor-mediated macrophage killing by Pseudomonas aeruginosa isolated from cystic fibrosis patients. *Infect Immun,* 67**,** 5231-42.

ZHANG, B., FU, R., DUAN, Z., SHEN, S., ZHU, C. & FAN, D. 2022. Ginsenoside CK induces apoptosis in triple-negative breast cancer cells by targeting glutamine metabolism. *Biochemical Pharmacology,* 202**,** 115101.

ZHANG, H., ZHOU, Q. M., LI, X. D., XIE, Y., DUAN, X., MIN, F. L., LIU, B. & YUAN, Z. G. 2006. Ginsenoside R(e) increases fertile and asthenozoospermic infertile human sperm motility by induction of nitric oxide synthase. *Arch Pharm Res,* 29**,** 145-51.

ZHANG, X., WANG, J., GAO, J. Z., ZHANG, X. N., DOU, K. X., SHI, W. D. & XIE, A. M. 2021. P2X4 receptor participates in autophagy regulation in Parkinson's disease. *Neural Regen Res,* 16**,** 2505-2511.

ZHONG, Y., DUNN, P. M., XIANG, Z., BO, X. & BURNSTOCK, G. 1998. Pharmacological and molecular characterization of P2X receptors in rat pelvic ganglion neurons. *Br J Pharmacol,* 125**,** 771-81.

ZHOU, X. & GALLIGAN, J. J. 1996. P2X purinoceptors in cultured myenteric neurons of guinea-pig small intestine. *J Physiol,* 496 (Pt 3)**,** 719-29.

ZHUANG, C.-L., MAO, X.-Y., LIU, S., CHEN, W.-Z., HUANG, D.-D., ZHANG, C.-J., CHEN, B.-C., SHEN, X. & YU, Z. 2014. Ginsenoside Rb1 improves postoperative fatigue syndrome by reducing skeletal muscle oxidative stress through activation of the PI3K/Akt/Nrf2 pathway in aged rats. *European Journal of Pharmacology,* 740**,** 480-487.

ZIMMERMANN, H., ZEBISCH, M. & STRÄTER, N. 2012. Cellular function and molecular structure of ecto-nucleotidases. *Purinergic Signal,* 8**,** 437-502.